AD NUMBER

AD473864

LIMITATION CHANGES

TO:

Approved for public release; distribution is unlimited.

FROM:

Distribution authorized to U.S. Gov't. agencies only; Administrative/Operational Use; SEP 1965. Other requests shall be referred to Office of Naval Research, Washington, DC 20360.

AUTHORITY

ONR ltr 4 May 1977

SECURITY MARKING

The classified or limited status of this report applies to each page, unless otherwise marked.
Separate page printouts MUST be marked accordingly.

HUGHES TOOL COMPANY · AIRCRAFT DIVISION
Culver City, California

HTC-AD 65-15

Volume II

APPENDIXES A, B, C, D, E, AND F TO SUMMARY TECHNICAL REPORT ROTOR/WING CONCEPT STUDY

September 1965

Prepared by Robert E. Head

Contract Number: Nonr-4588(00)
Authority: NR 212-162/12-8-64

An Experimental Research Program sponsored by Air Programs, Office of Naval Research, and Airframe Design Division, Bureau of Naval Weapons, U. S. Navy

HUGHES TOOL COMPANY -- AIRCRAFT DIVISION
Culver City, California

FOREWORD

This report presents the results of whirlstand and wind tunnel tests of a one-sixth scale model of the Rotor/Wing high-speed VTOL aircraft. The main body of the report presented as Volume I, discusses highlights of the test results, includes a discussion of the application of the test results to full-scale, and describes the characteristics of such an aircraft. Volume II, which includes Appendixes A through F, contains detailed analyses and test data from the model research program. Volume III, which includes Appendixes G and H, contains a collection of the detailed drawings of the model and the stress analysis used in the design.

TABLE OF CONTENTS

LIST OF ILLUSTRATIONS

APPENDIX A

NATURAL FREQUENCY ANALYSIS

APPENDIX A

NATURAL FREQUENCY ANALYSIS

A major consideration in the investigation of the Rotor/Wing concept is the measurement of airloads on the rotor during conversion. This particular model is extremely rigid compared with a normal rotary wing model, and it is possible to measure rotor rolling and pitching moments by means of strain gages on the rotor shaft — a scheme that would not work ordinarily because of resonances, phase shifts, and so forth, that would completely obscure the airload data. The Rotor/Wing model operates at rotor speeds enough lower than the three-per-rev resonance frequency of the rotor that the moments may be read directly.

Preliminary analyses showed that the model mounted on the tandem struts in the wind tunnel would have a natural frequency much too low for significant testing. A three-legged pyramidal brace system from the tip of the main support strut to the wind tunnel balance frame, as shown in Figure A-1, will stiffen the system sufficiently to obtain meaningful data.

Figure A-2 is a schematic drawing of the support strut-fuselage-Rotor/Wing system used in the analyses. Figure A-3 is a frequency diagram showing the calculated characteristics of the Rotor/Wing model on its support in the wind tunnel.

NATURAL FREQUENCY CALCULATIONS

FORCES & MOMENTS (Refer to Figure A.2)

for $\ell_1 > x > 0$

$$S = S_0$$

$$M = M_0 + S_0 x$$

for $\ell_2 > x > \ell_1$

$$S = -\left(\frac{S_0 \ell_1 + M_0}{\ell_2 - \ell_1}\right)$$

$$M = \left(\frac{S_0 \ell_1 + M_0}{\ell_2 - \ell_1}\right)(\ell_2 - x)$$

for $\ell_3 > x > \ell_2$

$$S = S_0$$

$$M = M_0 + S_0 x$$

for $\ell_4 > x > \ell_3$

$$S = S_0$$

$$M = M_0 + S_0 x$$

STRAIN ENERGY

$$V = \tfrac{1}{2}\int_0^{\ell_4}\left(\frac{1}{EI} M^2 + \frac{1}{KAG} S^2\right) dx$$

CASTIGLIANO'S THEOREM

$$y_0 = \frac{\partial V}{\partial S_0} = \int_0^{\ell_4}\left(\frac{M}{EI}\frac{\partial M}{\partial S_0} + \frac{S}{KAG}\frac{\partial S}{\partial S_0}\right) dx$$

$$\theta_0 = \frac{\partial V}{\partial M_0} = \int_0^{\ell_4}\left(\frac{M}{EI}\frac{\partial M}{\partial M_0} + \frac{S}{KAG}\frac{\partial S}{\partial M_0}\right) dx$$

	$\left(\frac{\partial M}{\partial S_0}\right)$	$\left(\frac{\partial S}{\partial S_0}\right)$	$\left(\frac{\partial M}{\partial M_0}\right)$	$\left(\frac{\partial S}{\partial M_0}\right)$
$\ell_1 > x > 0$	X	1	1	0
$\ell_2 > x > \ell_1$	$\frac{\ell_1(\ell_2 - x)}{\ell_2 - \ell_1}$	$-\left(\frac{\ell_1}{\ell_2 - \ell_1}\right)$	$\frac{\ell_2 - x}{\ell_2 - \ell_1}$	$-\left(\frac{1}{\ell_2 - \ell_1}\right)$
$\ell_3 > x > \ell_2$	X	1	1	0
$\ell_4 > x > \ell_3$	X	1	1	0

$$y_o = \frac{1}{EI_1}\int_0^{l_1}(M_o + S_o x)\,x\,dx + \frac{1}{KA_1G}\int_0^{l} S_o\,dx$$
$$+ \frac{1}{EI_2}\int_{l_1}^{l_2}\left(\frac{S_o l_1 + M_o}{l_2 - l_1}\right)(l_2 - x)^2\left(\frac{l_1}{l_2 - l_1}\right)dx + \frac{1}{KA_2G}\int_{l_1}^{l_2}\left(\frac{S_o l_1 + M_o}{l_2 - l_1}\right)\left(\frac{l_1}{l_2 - l_1}\right)dx$$
$$+ \frac{1}{EI_3}\int_{l_2}^{l_3}(M_o + S_o x)\,x\,dx + \frac{1}{KA_3G}\int_{l_2}^{l_3} S_o\,dx$$
$$+ \frac{1}{EI_4}\int_{l_3}^{l_4}(M_o + S_o x)\,x\,dx + \frac{1}{KA_4G}\int_{l_3}^{l_1} S_o\,dx$$

$$\theta_o = \frac{1}{EI_1}\int_0^{l_1}(M_o + S_o x)\,dx + \frac{1}{KA_1G}\int_0^{l_1} 0$$
$$+ \frac{1}{EI_2}\int_{l_1}^{l_2}\left(\frac{S_o l_1 + M_o}{l_2 - l_1}\right)(l_2 - x)^2\left(\frac{1}{l_2 - l_1}\right)dx + \frac{1}{KA_2G}\int_{l_1}^{l_2}\left(\frac{S_o l_1 + M_o}{l_2 - l_1}\right)\left(\frac{1}{l_2 - l_1}\right)dx$$
$$+ \frac{1}{EI_3}\int_{l_2}^{l_3}(M_o + S_o x)\,dx + \frac{1}{KA_3G}\int_{l_2}^{l_3} 0$$
$$+ \frac{1}{EI_4}\int_{l_3}^{l_4}(M_o + S_o x)\,dx + \frac{1}{KA_4G}\int_{l_3}^{l_4} 0$$

$$y_o = \frac{1}{EI_1}\left[\frac{M_o l_1^2}{2} + \frac{S_o l_1^3}{3}\right] + \frac{1}{KA_1G}\left[S_o l_1\right]$$
$$+ \frac{1}{EI_2}\left[\frac{(S_o l_1 + M_o) l_1}{(l_2 - l_1)^2} \times \frac{(l_2 - l_1)^3}{3}\right] + \frac{1}{KA_2G}\left[\frac{(S_o l_1 + M_o) l_1}{(l_2 - l_1)}\right]$$
$$+ \frac{1}{EI_3}\left[\frac{M_o(l_3^2 - l_2^2)}{2} + \frac{S_o(l_3^3 - l_2^3)}{3}\right] + \frac{1}{KA_3G}\left[S_o(l_3 - l_2)\right]$$
$$+ \frac{1}{EI_4}\left[\frac{M_o(l_4^2 - l_3^2)}{2} + \frac{S_o(l_4^3 - l_3^3)}{3}\right] + \frac{1}{KA_4G}\left[S_o(l_4 - l_3)\right]$$

$$\theta_o = \frac{1}{EI_1}\left[M_o l_1 + \frac{S_o l_1^2}{2}\right] + \frac{1}{EI_2}\left[\frac{(S_o l_1 + M_o)}{(l_2 - l_1)^2} \times \frac{(l_2 - l_1)^3}{3}\right] + \frac{1}{KA_2G}\left[\frac{S_o l_1 + M_o}{l_2 - l_1}\right] + \frac{1}{EI_3}\left[M_o(l_3 - l_2) + \frac{S_o}{2}(l_3^2 - l_2^2)\right] + \frac{1}{EI_4}\left[M_o(l_4 - l_3) + \frac{S_o}{2}(l_4^2 - l_3^2)\right]$$

$$y_o = S_o\left[\frac{l_1^3}{3EI_1} + \frac{l_1}{KA_1G} + \frac{l^2(l_2 - l_1)}{3EI_2} + \frac{l_1^2}{KA_2G(l_2 - l_1)} + \frac{l_3^3 - l_2^3}{3EI_3} + \frac{l_3 - l_2}{KA_3G} + \frac{l_4^3 - l_3^3}{3EI_4} + \frac{l_4 - l_3}{KA_4G}\right] + M_o\left[\frac{l_1^2}{2EI_1} + \frac{l_1(l_2 - l_1)}{3EI_2} + \frac{l_1}{KA_2G(l_2 - l_1)} + \frac{l_3^2 - l_2^2}{2EI_3} + \frac{l_4^2 - l_3^2}{2EI_4}\right]$$

$$\theta_o = S_o\left[\frac{l_1^2}{2EI_1} + \frac{l_1(l_2 - l_1)}{3EI_2} + \frac{l_1}{KA_2G(l_2 - l_1)} + \frac{l_3^2 - l_2^2}{2EI_3} + \frac{l_4^2 - l_3^2}{2EI_4}\right] + M_o\left[\frac{l_1}{EI_1} + \frac{l_2 - l_1}{3EI_2} + \frac{1}{KA_2G(l_2 - l_1)} + \frac{l_3 - l_2}{EI_3} + \frac{l_4 - l_3}{EI_4}\right]$$

$\ell_1 = 7.75$

$\ell_2 = 14.00$

$\ell_3 = 27.00$

$\ell_4 = 53.00$

$(\ell_2 - \ell_1) = 6.25$

$$EI = \frac{\pi E}{64}\left(D_o^4 - D_i^4\right)$$

$$KAG = \frac{\pi G}{8}\left(D_o^2 - D_i^2\right)$$

$EI_1 = 30 \times 10^6 \times .0491\left(2.26^4 - 1.84^4\right) = 21.54 \times 10^6$

$KA_1G = 11.5 \times 10^6 \times .393\left(2.26^2 - 1.84^2\right) = 7.78 \times 10^6$

$EI_2 = 30 \times 10^6 \times .0491\left(1.98^4 - 0.75^4\right) = 22.17 \times 10^6$

$KA_2G = 11.5 \times 10^6 \times .393\left(1.98^2 - 0.75^2\right) = 15.16 \times 10^6$

$EI_3 = 30 \times 10^6 \times .0491\left(3.00^4 - 1.50^4\right) = 111.86 \times 10^6$

$KA_3G = 11.5 \times 10^6 \times .393\left(3.00^2 - 1.50^2\right) = 30.48 \times 10^6$

$EI_4 = 30 \times 10^6 \times .0491\left(3.00^4 - 1.63^4\right) = 108.91 \times 10^6$

$KA_4G = 11.5 \times 10^6 \times .393\left(3.00^2 - 1.63^2\right) = 28.64 \times 10^6$

$$\left(Y_o/S_o\right) \times 10^6 = \left[\frac{7.75}{3 \times 21.54} + \frac{7.75}{7.78} + \frac{7.75^2 \times 6.25}{3 \times 22.17} + \frac{7.75^2}{15.16 \times 6.25} + \frac{27^3 - 14^3}{3 \times 111.86}\right.$$
$$\left. + \frac{13.00}{30.48} + \frac{53^3 - 27^3}{3 \times 108.91} + \frac{26.00}{28.64}\right] = \underline{461.70}$$

$$\left(Y_o/M_o\right) \times 10^6 = \left[\frac{7.75^2}{2 \times 21.54} + \frac{7.75 \times 6.25}{3 \times 22.17} + \frac{7.75}{15.16 \times 6.25} + \frac{27^2 - 14^2}{2 \times 111.86}\right.$$
$$\left. + \frac{53^2 - 27^2}{2 \times 108.91}\right] = \underline{14.14}$$

$$\left(\theta_o/M_o\right)\times 10^6 = \left[\frac{7.75}{21.54} + \frac{6.25}{3\times 22.17} + \frac{1}{15.16\times 6.25} + \frac{13.00}{111.86} + \frac{26.00}{108.91}\right]$$

$$= \underline{0.82}$$

STIFFNESS MATRIX

$$\begin{bmatrix} K_{yy} & K_{y\theta} \\ K_{\theta y} & K_{\theta\theta} \end{bmatrix} = \begin{bmatrix} 461.70 & 14.14 \\ 14.14 & 0.82 \end{bmatrix}^{-1} \times 10^6 = \frac{10^6}{178.66}\begin{bmatrix} .82 & -14.14 \\ -14.14 & 461.70 \end{bmatrix}$$

$$= \begin{bmatrix} .00459 & -.0791 \\ -.0791 & 2.5841 \end{bmatrix} \times 10^6$$

For a conservative frequency estimate, assume the mass of the hub and fuselage is concentrated at the hub center. The inertia of the fuselage is small and is neglected.

$$W_{fus+hub} + \tfrac{1}{3} W_{strut} = 200 + \frac{56}{3} = 219 \text{ lb.}$$

$$M = 219 \times \frac{1}{386} = 0.567 \text{ lb sec}^2/\text{in}$$

$$I_{o_{hub}} = 13{,}300 \text{ lb in}^2$$

$$I = \tfrac{1}{2} \times 13{,}300 \times \frac{1}{386} = 17.20 \text{ lb sec}^2 \text{ in}$$

FREQUENCY EQUATION COEFFICIENTS

$$MI = .567 \times 17.20 = 9.75$$

$$IK_{yy} + MK_{\theta\theta} = \left[17.20 \times .00459 + .567 \times 2.5841\right] \times 10^6 = 1.544 \times 10^6$$

$$K_{yy}K_{\theta\theta} - K_{y\theta}^2 = \left[.00459 \times 2.5841 - (.0791)^2\right] \times 10^{12} = .00521 \times 10^{12}$$

FREQUENCY EQUATION

$$MI\omega^4 - (IK_{yy} + MK_{\theta\theta})\omega^2 + (K_{yy}K_{\theta\theta} - K_{y\theta}^2) = 0$$

$$9.75\,\omega^4 - 1.544 \times 10^6 \omega^2 + .00561 \times 10^{12} = 0$$

$$\omega^2 = \left[\frac{1.544}{2 \times 9.75} \pm \sqrt{\left(\frac{1.544}{2 \times 9.75}\right)^2 - \frac{.00561}{9.75}}\right] \times 10^6$$

$$= \left[.0790 \pm \sqrt{.006244 - .000575}\right] \times 10^6$$

$$= \left[.0790 \pm \sqrt{.005669}\right] \times 10^6$$

$$= \left[.0790 \pm .0753\right] \times 10^6$$

$$= .00370 \times 10^6 \;,\; .1543 \times 10^6$$

$$\omega = 60.8 \;,\; 392.8 \text{ rad/sec}$$

$$\underline{f = 581,\ 3760 \text{ cpm}}$$

IF M = 0

$$\omega^2 = \frac{K_{yy}K_{\theta\theta} - K_{y\theta}^2}{K_{yy}\,I} = \frac{.00561 \times 10^6}{.00459 \times 17.20} = .0711 \times 10^6$$

$$\omega = 266.7 \text{ rad/sec}$$

IF I = 0

$$\omega^2 = \frac{K_{yy}K_{\theta\theta} - K_{y\theta}^2}{K_{\theta\theta}\,M} = \frac{.00561 \times 10^6}{2.584 \times .567} = .00383 \times 10^6$$

$$\omega = 61.9 \text{ rad/sec}$$

The low frequency of 581 cpm is too low to permit the testing required, so add stiffening braces to the support strut to make it essentially rigid. Then:

$$(Y_0/S_0)\times 10^6 = \left[\frac{7.75^3}{3\times 21.54} + \frac{7.75}{7.78} + \frac{7.75^2\times 6.25}{3\times 22.17} + \frac{7.75^2}{15.16\times 6.25}\right] = 14.477$$

$$(Y_0/M_0)\times 10^6 = \left[\frac{7.75^2}{2\times 21.54} + \frac{7.75\times 6.25}{3\times 22.17} + \frac{7.75}{15.16\times 6.25}\right] = 2.204$$

$$(\theta_0/M_0)\times 10^6 = \left[\frac{7.75}{21.54} + \frac{6.25}{3\times 22.17} + \frac{1}{15.16\times 6.25}\right] = 0.465$$

STIFFNESS MATRIX

$$\begin{bmatrix} K_{yy} & K_{y\theta} \\ K_{\theta y} & K_{\theta\theta} \end{bmatrix} = \begin{bmatrix} 14.477 & 2.204 \\ 2.204 & .465 \end{bmatrix}^{-1}\times 10^6 = \frac{10^6}{1.874}\begin{bmatrix} .465 & -2.204 \\ -2.204 & 14.477 \end{bmatrix}$$

$$= \begin{bmatrix} .248 & -1.176 \\ -1.176 & 7.725 \end{bmatrix}\times 10^6$$

$W_{hub} = 84$ lb

$M = 84 \times \frac{1}{386} = .217$ lb sec^2/in

$I = 17.20$ lb sec^2 in

$MI = 17.20 \times .217 = 3.732$

$(IK_{yy} + MK_{\theta\theta}) = (17.20\times .248 + .217\times 7.725)\times 10^6 = 5.942\times 10^6$

$(K_{yy}K_{\theta\theta} - K_{y\theta}^2) = (.248\times 7.725 - (1.176)^2)\times 10^6 = .533\times 10^6$

$$3.732\,\omega^4 - 5.942\,\omega^2\times 10^6 + .533\times 10^{12} = 0$$

$$\omega^2 = \left[\frac{5.942}{2\times 3.732} \pm \sqrt{\left(\frac{5.942}{2\times 3.732}\right)^2 - \frac{.533}{3.732}}\right]\times 10^6$$

$$= \left[.7961 \pm \sqrt{.6337 - .1428}\right]\times 10^6$$

$$= \left[.7961 \pm \sqrt{.4909}\right]\times 10^6$$

$$\omega^2 = [.7961 \pm .7006] \times 10^6$$

$$= .0955 \times 10^6,\ 1.4967 \times 10^6$$

$$\omega = 309,\ 1222 \text{ rad/sec}$$

$$f = 3236,\ 12{,}795 \text{ cpm}$$

If $M = 0$

$$\omega^2 = \frac{K_{yy} K_{\theta\theta} - K_{y\theta}^2}{K_{yy} I} = \frac{.533 \times 10^6}{.248 \times 1720} = .1398 \times 10^6$$

$$\omega = 374 \text{ rad/sec}$$

$$f = 3916 \text{ cpm}$$

The effect of M on the lower mode is about 25 percent and should be a second order effect. So include the gyroscopic couple with $M = a$

$$\omega = \Omega \pm \sqrt{\Omega^2 + \left(\frac{K_{yy} K_{\theta\theta} - K_{y\theta}^2}{K_{yy} I}\right)^2}$$

$$= \Omega \pm \sqrt{\Omega^2 + .1398 \times 10^6}$$

Calculate frequency at $\Omega = 1000$ rpm $= 104.8$ rad/sec

$$\Omega^2 = .0110 \times 10^6$$

$$\omega = 104.8 \pm \sqrt{(.0110 + .1398) \times 10^6} = 104.8 \pm \sqrt{.1508 \times 10^6}$$

$$= 104.8 \pm 388.2$$

$$= 283.4,\ 493.0 \text{ rad/sec}$$

Approximate Correction For Mass

Lower Mode

$K^*_{yy} = K_{yy} - M\omega^2$

for $\omega = 283.4$ $\quad \omega^2 = .0803 \times 10^6$

$K^*_{yy} = .248 \times 10^6 - .217 \times .0803 \times 10^6 = .2306 \times 10^6$

$$\omega = -104.8 + \sqrt{\left[.0110 + \frac{.2306 \times 7.725 - 1.176^2}{17.20 \times .2306}\right] \times 10^6}$$

$$= -104.8 + \sqrt{[.0110 + .1005] \times 10^6}$$

$$= -104.8 + \sqrt{.1115 \times 10^6}$$

$$= -104.8 + 333.9$$

$$= 229.1 \text{ rad/sec}$$

Second Iteration

Estimate $\omega = 240$ rad/sec

$\omega^2 = .0576 \times 10^6$

$K^*_{yy} = .248 \times 10^6 - .217 \times .0576 \times 10^6 = .2355 \times 10^6$

$$\omega = -104.8 + \sqrt{\left[.0110 + \frac{.2355 \times 7.725 - 1.176^2}{17.20 \times .2306}\right] \times 10^6}$$

$$= -104.8 + \sqrt{[.0110 + .1077] \times 10^6}$$

$$= -104.8 + \sqrt{.1187 \times 10^6}$$

$$= -104.8 + 344.5$$

$$= 239.7 \text{ rad/sec}$$

$f = 2510$ cpm

Higher Mode

Estimate $\omega = 396$ rad/sec

$\omega^2 = .1568 \times 10^6$

$K_{yy}^{*} = (.248 - .217 \times .1568) \times 10^{6} = .2140 \times 10^{6}$

$$\omega = 104.8 + \sqrt{\left[.0110 + \frac{.2140 \times 7.725 - 1.176^{2}}{1720 \times .2140}\right] \times 10^{6}}$$

$$= 104.8 + \sqrt{[.0110 + .0734] \times 10^{6}}$$

$$= 104.8 + \sqrt{.0844 \times 10^{6}}$$

$$= 104.8 + 290.5$$

$$= 395.3 \text{ rad/sec}$$

$f = 4139$ cpm

Calculate frequency at $\Omega = 700$ rpm $= 73.3$ rad/sec

Lower Mode

$\Omega^{2} = .00537 \times 10^{6}$

Estimate $\omega = 258$ rad/sec

$\omega^{2} = .0665 \times 10^{6}$

$K_{yy}^{*} = (.248 - .217 \times .0665) \times 10^{6} = .2336 \times 10^{6}$

$$\omega = -73.3 + \sqrt{\left[.00537 + \frac{.2336 \times 7.725 - 1.176^{2}}{.2336 \times 17.20}\right] \times 10^{6}}$$

$$= -73.3 + \sqrt{[.00537 + .10446] \times 10^{6}}$$

$$= -73.3 + \sqrt{.10983 \times 10^{6}}$$

$$= -73.3 + 331.4$$

$$= 258.1 \text{ rad/sec}$$

$f = 2703$ cpm

Higher Mode

Estimate $\omega = 367$ rad/sec

$\omega^{2} = .1347 \times 10^{6}$

$$K^*_{yy} = (.248 - .217 \times .1347) \times 10^6 = .2188 \times 10^6$$

$$\omega = 73.3 + \sqrt{\left(.00537 + \frac{.2188 \times 2.725 - 1.176^2}{.2188 \times 17.20}\right) \times 10^6}$$

$$= 73.3 + \sqrt{(.00537 + .08163) \times 10^6}$$

$$= 73.3 + \sqrt{.08700 \times 10^6}$$

$$= 73.3 + 294.9$$

$$= 368.2 \text{ rad/sec}$$

$$f = 3855 \text{ cpm}$$

Frequency Summary

Ω	ω		f	
rpm	rad/sec		cpm	
	low	high	low	high
0	309	309	3236	3236
700	258	368	2703	3855
1000	240	395	2510	4139

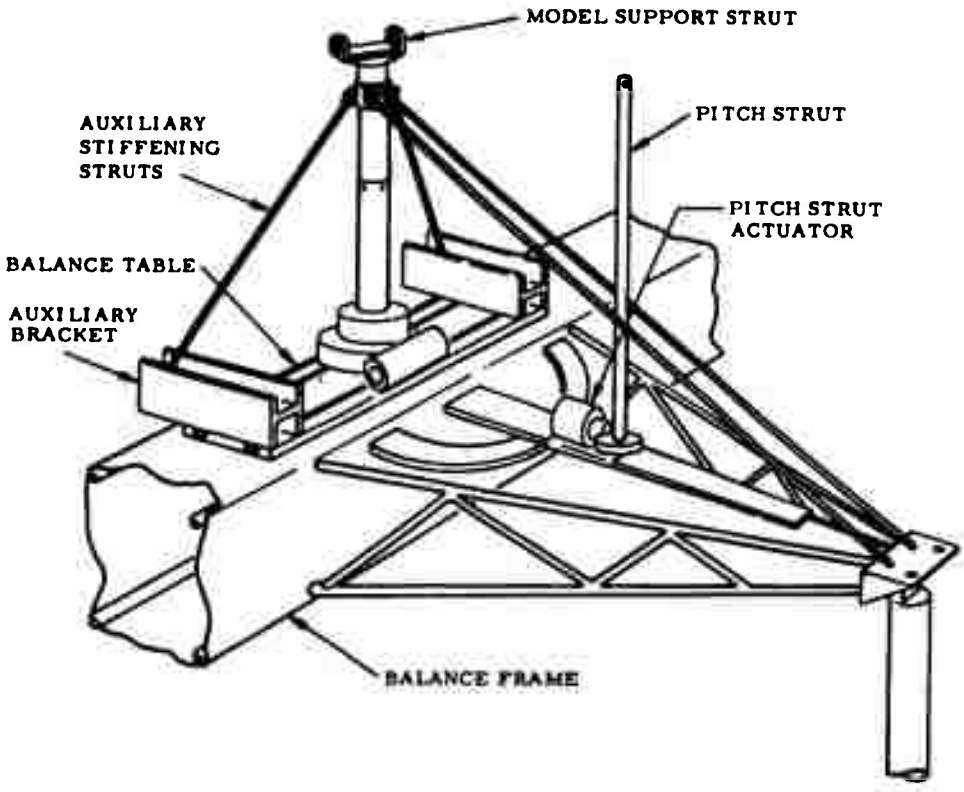

Figure A-1. Schematic of Model Mounting System

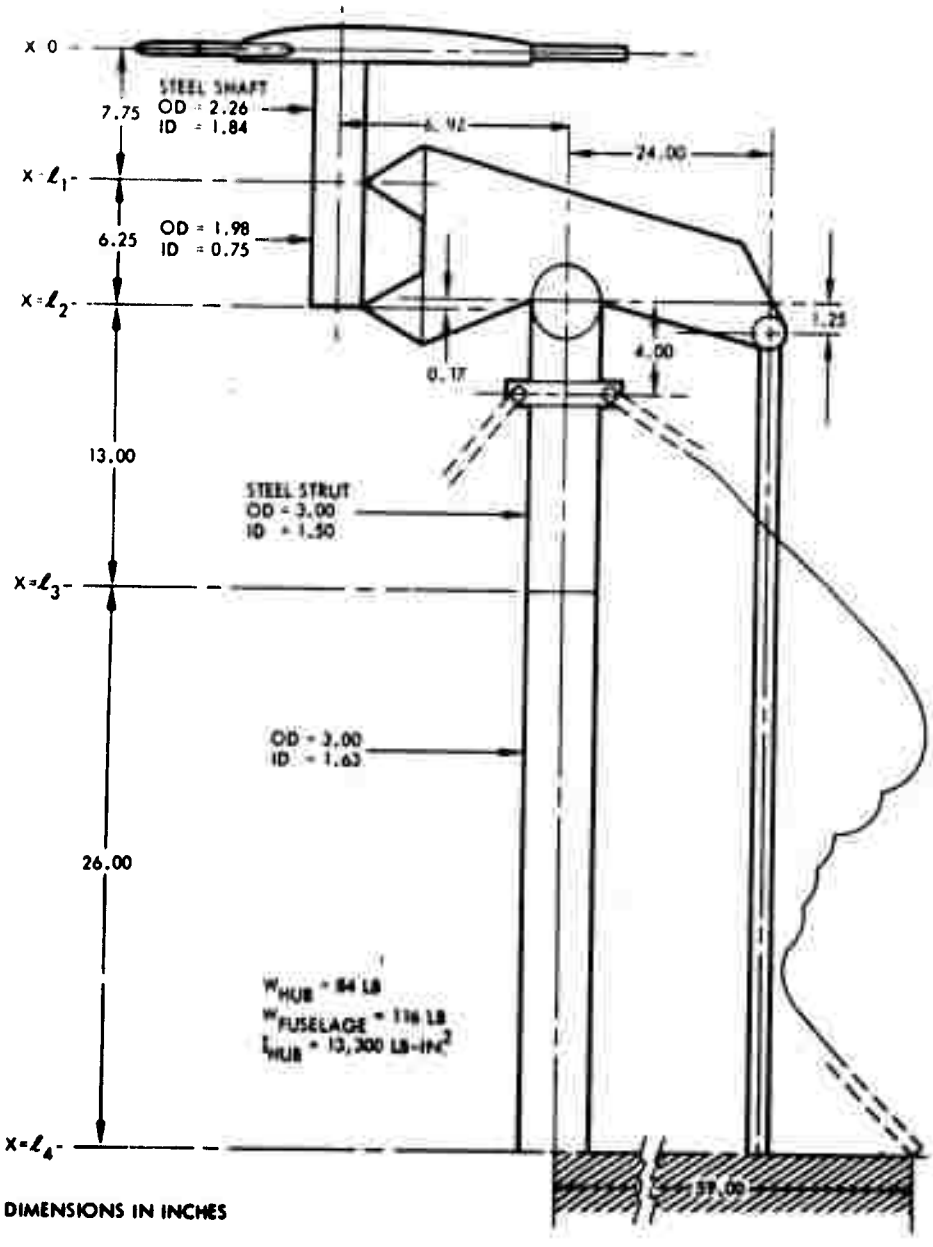

Figure A-2. Schematic of Rotor/Wing Mount

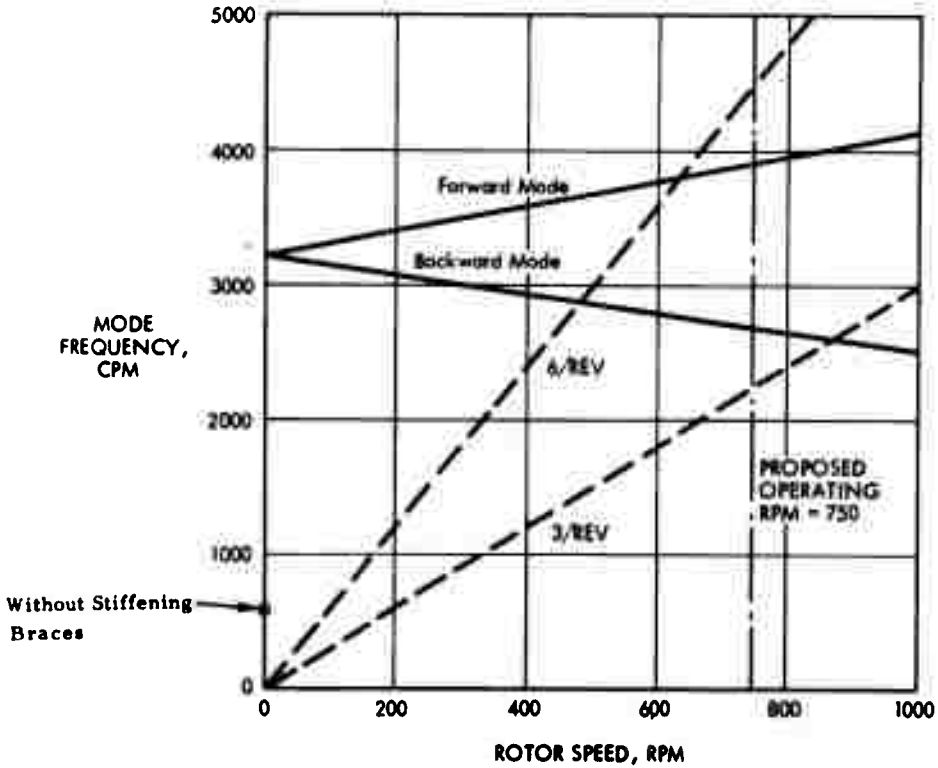

Figure A-3. Rotor/Wing Model Vibration Mode Frequencies in Nonrotating System

APPENDIX B

FLUTTER ANALYSIS

APPENDIX B

FLUTTER ANALYSIS

A flutter analysis program that was originally programmed for the IBM 7094 computer for conventional helicopter rotors was revised to account for the rigid blades and nontilting hub of the Rotor/Wing. The mass and stiffness characteristics of the blades and control system used in this program are given in Figure B-1 and Table B-1.

The model was checked for flutter for maximum airspeed at maximum rotational speed and maximum airspeed at one-half rotational speed; these are two of the cases investigated in the conversion analysis of Appendix C. The computer program used numerical integration and three degrees of freedom. The degrees of freedom are: first mode bending and first and second mode twisting. The higher bending modes were neglected, because the frequencies of these modes are very high; also, since the blades are cantilevered and very stiff in the flapping direction, there would be little deflection in these higher modes. The control system is quite soft compared with the twisting stiffness of the blades (90 percent of the twisting is in the control system). This results in blade twist angles of ± 0.4 degree in the first mode and ± 0.1 degree in the second mode for both of the cases investigated. The computer program includes negative damping at angles of attack of from 11 to 21 degrees. This negative damping was deduced from NASA wind tunnel tests of an oscillating airfoil. The exact angles for negative damping of the circular arc airfoil used on the Rotor/Wing model are not known, so the values for a standard airfoil are assumed applicable.

The full-rpm case is unstable at 270-degree blade azimuth because of the negative damping during stall. The half-rpm case is unstable at both 0-degree and 180-degree azimuth, again because of negative damping during stall, while the 270-degree azimuth is stable because the angle of attack is above the negative damping region. In both cases, there is a large enough stable region on the rotor to damp out the effect of the small unstable regions, and the rotor as a whole is stable.

For the full-rpm case, the blade root bending moment is predicted to be 8 $\pm$10 in.-lb, and the root torque due to twisting is prediced to be 26 $\pm$22 in.-lb. The moment and torque predicted for the half-rpm cases are lower, and are 2 $\pm$7 in.-lb and 6 $\pm$20 in.-lb, respectively.

A flutter analysis was performed on the nonrotating rotor blade. Because these blades are of constant section from root to tip, a two-dimensional analysis could be used. The method used for this analysis is that presented in Reference 7 using the C_L and C_M curves for the circular arc airfoil. In this case, a second twisting mode was added.

The speed for torsional divergence was calculated to be approximately 1400 feet per second. The highest tunnel speed contemplated corresponds to a dynamic pressure of 30 pounds per square foot, or a velocity of approximately 160 feet per second, so torsional divergence should not occur. A quasistatic flutter analysis indicated the flutter speed to be about 400 fps. Since this is more than twice as high as the tunnel speed, it was felt that a complete flutter analysis using oscillatory aerodynamic coefficients was unnecessary.

The dynamic pressure for torsional divergence, nonrotating, is given by equation 6-11, Reference 8:

$$q_D = \frac{K_\theta}{Se\left(\frac{dC_L}{d\alpha}\right)}$$

Where K_θ = twisting spring constant

S = airfoil area

e = distance aerodynamic center to shear center

and $\left(\frac{dC_L}{d\alpha}\right)$ = lift curve slope.

From page 393 of Reference 8, sweep raises the flutter speed by approximately $\frac{1}{\sqrt{\cos}}$, therefore, $q = \frac{q_D}{\cos 30^\circ}$ for this case.

The quasistatic flutter analysis equations for the bending and twisting mode in the nonrotating case are given by the following equations:

$$m\ddot{h} + K_h h + S_\theta \ddot{\theta} = \left(\frac{\partial C_L}{\partial \alpha}\right)\theta qS$$

$$I_\theta \ddot{\theta} + K_\theta \theta + S_\theta \ddot{h} = \left(\frac{\partial C_L}{\partial \alpha}\right)\theta qSe$$

where K_h is the bending stiffness and S_θ represents the offset of the cg and shear center in the case of $S_\theta = 0$. Using the above equations, the velocity at flutter is the forward speed at which the two natural frequencies coalesce, and $V_{flutter} = \frac{V_{coalescence}}{\sqrt{\cos 30^\circ}}$ due to the effect of sweep.

TABLE B-1

ROTOR/WING STIFFNESS AND INERTIA CHARACTERISTICS

Blade Spar	
Flexural stiffness per unit length, EI	366,000 lb.-in.^{2}
Torsional stiffness per unit length, GJ	292,800 lb.-in.^{2}
Torsional moment of inertia, J	0.02445 in.^{4}
Weight, W	2.77 lb
Blade Airfoil	
Torsional moment of inertia, J	9.40 in.^{4}
Weight, W	1.36 lb
Complete Blade	
Flapping moment of inertia about ℄ rotor, I_1	0.612 slug-feet^2
Control System	
Spring constant (at pitch arm), K	54,300 lb.-in./rad
Inertia (rotating system), I	0.001793 slug-ft^2
Inertia (nonrotating system), I	0.002078 slug-ft^2

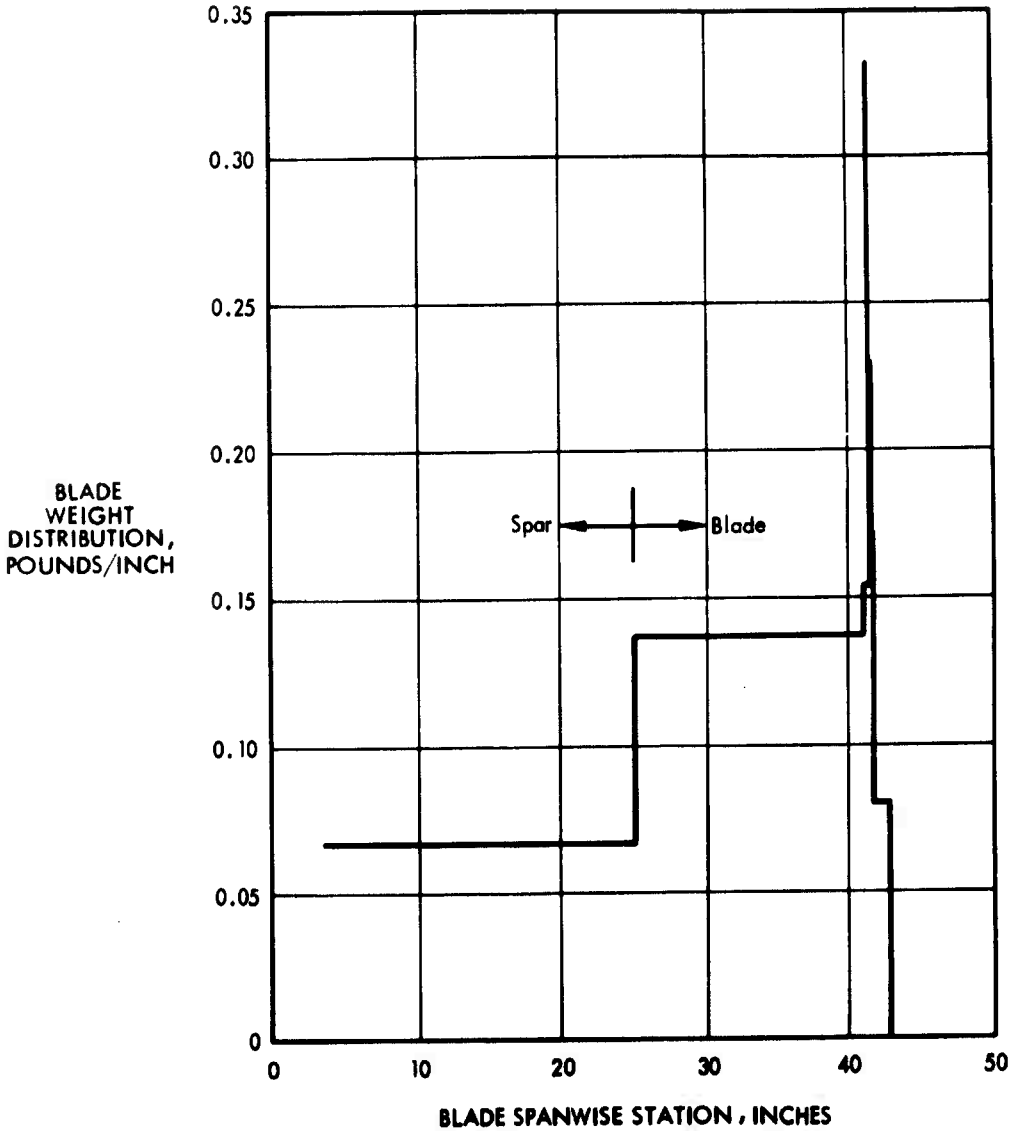

Figure B-1. Rotor/Wing Blade Mass Distribution

APPENDIX C

CONVERSION ANALYSIS

APPENDIX C

CONVERSION ANALYSIS

During conversion from the running-rotor mode to the stopped-rotor mode of the Rotor/Wing, or vice versa, a number of conditions must be satisfied concurrently: the Rotor/Wing must provide enough lift to support the aircraft, a decelerating or accelerating torque must be developed to stop or start the rotor, steady-state rolling and pitching moments must be zero, and the oscillating rolling and pitching moments should be minimal. An analytical procedure has been programmed for the IBM 7094 computer for solving this problem. A conventional swashplate assembly is used to control the pitch angles of the individual blades; a more sophisticated two- or three-per-rev type of swashplate is not considered.

For these calculations, the rotor is considered to be in a steady state for one revolution, and the combination of first harmonic cyclic stick positions necessary to remove the first harmonic rolling moments on the shaft is computed. In this calculation, the steady pitching moment is not cancelled by the cyclic control, the feeling being that the horizontal tail can perform this function. After the stick positions are determined, the lift, torque, drag, and side force on the blades are determined. When these are added to the hub lift and drag, the total forces on the model are determined. The inputs to this computer program are rpm, hub angle of attack, and collective pitch. To determine the correct flight condition, the following procedure must be used.

For each rpm, a value of collective pitch is selected, and then the hub angle of attack is varied until the desired total lift is determined; the torque (accelerating or decelerating) is noted at this condition. This process is carried out for various values of collective pitch until conditions for both maximum accelerating and decelerating torques are determined. Then a schedule of cyclic and collective stick positions and hub angle can be made as a function of rpm for accelerating or decelerating the rotor. In addition, (Δ rpm/Δ t) can be determined from the rotor inertia and the torque.

The aerodynamic forces on the blade are computed by numerically integrating the lift and drag along the blade. Figure C-1 is a plot of airfoil section aerodynamic characteristics for the circular arc blade used on the Rotor/Wing.

The moment about the centerline of the hub provided by the blade is computed using the following equations*:

$$M_{\mathit{CL}\ \text{hub}} = M_T - M_W \qquad (1)$$

$$M_W = \int_C^R mgrdr = \text{weight moment of blade}$$

$$\text{and } M_T = \text{thrust moment of blade} = 1/2\ \rho\, C\, \Omega^2 R^4 \int_{x_c}^{1} u^2 x(C_\ell \cos\phi + C_d \sin\phi)\, dx$$

Because the rotor system is rigid, the flapping angle, β, is zero.

*See Table C-1 for a definition of the symbols used in these equations.

The thrust moment is computed as follows:

$$C_\ell = a\,\alpha_r = a(\theta_o - A_1\cos\psi - B_1\sin\psi + \phi_r) \tag{2}$$

where $\phi_r = \tan^{-1}\left(u_{P_r}/u_{T_r}\right)$

$$u_{T_r} = x + \mu\sin\psi$$

and $u_{P_r} = \lambda$

The contribution of the hub is given by:

$C_{m_h}\cos\psi$ and $C_{\ell_h}\sin\psi$

where C_{m_h} = hub pitching moment

and C_{ℓ_h} = hub rolling moment. These are given in Figure C-2.

The total moment about the centerline of the hub is then given by:

$$C_M = \frac{C}{2\pi R}\int_{x_c}^{R} u^2 x(\theta_o + \phi_r)(a\cos\phi + C_d/a_h\sin\phi)\,dx - \frac{\int_{x_c}^{1} mgr\,dr}{\rho\pi R^3(\Omega R)^2} - C_{m_h}\cos\psi - C_{\ell_h}\sin\psi - A_1\left(\frac{C\cos\psi}{2\pi R}\right)\int_{x_c}^{1} u^2 x a_1\,dx - B_1\left(\frac{C\sin\psi}{2\pi R}\right)\int_{x_c}^{1} u^2 x a_k\,dx \tag{3}$$

where $a_1 = a\cos\phi + C_d/a_h\sin\phi$

The equation for C_M is computed in terms of the unknowns, A_1 and B_1, for constant increments of ψ. Summing the roll component ($C_M \sin \psi$) and pitch component ($C_M \cos \psi$) and setting these equations equal to zero gives two equations in two unknowns that are solved for A and B_1.

In order to account for stall, an iteration must be performed on the above computation. The first time through, a constant value of lift curve slope is assumed. After that, as A_1 and B_1 have converged, they are used to compute the aerodynamic forces on the blade. For that computation the following equations are used:

$$C_T = \int_{x_c}^{1} 1/2\, \sigma u^2 (C_{d_o} \sin \phi + C_\ell \cos \phi)\, dx$$

$$C_Q = \int_{x_c}^{1} 1/2\, \sigma u^2 (C_{d_o} \cos \phi - C_\ell \sin \phi)\, dx$$

$$C_H = \int_{x_c}^{1} 1/2\, \sigma u^2 (C_\ell\, (-\sin \phi \sin \psi) + C_{d_o}\, (\cos \phi \sin \psi))\, dx$$

$$C_y = \int_{x_c}^{1} 1/2\, \sigma u^2 (C_\ell\, (\sin \phi \cos \psi) + C_{d_o}\, (-\cos \phi \cos \psi))\, dx$$

The value of C_M is again computed from Equation 3. Using numerical integration, the above computation is made for each value of ψ, and the average value is determined. A Fourier analysis is made of the above terms. This is especially important for the moment coefficient, as this determines the higher harmonic moments expected on the mode. In making these computations, nine spanwise blade stations and azimuth intervals of 30 degrees are used.

It should be noted that the harmonic analyses of the moments, drag, and side force are in the rotating field. Thus, they represent harmonic moments on the rotating shaft - moments that will be measured by strain gages on the shaft of the wind tunnel model.

Figure C-3 is a plot of the control positions calculated for stopping and starting the rotor, and Table C-2 lists the accompanying moments and forces.

The data given in the Table C-2 represents the model using aerodynamic torque only for accelerating or decelerating the rotor. These probably represent the worst condition with respect to oscillating rolling and pitching moments that may be expected, for two main reasons: first, the blade lift curve for this low Reynolds number range has a $C_{L_{max}}$ of only 0.8, which results in early stall and consequent rough operation; and, second, only aerodynamic torque of the blades was used to accelerate or decelerate the rotor.

Full-scale blades will have high enough Reynolds numbers that $C_{L_{max}}$ will be on the order of thirty percent higher, with an attendant decrease in stall and roughness of operation. A major source of the higher harmonic rolling and pitching moments can be traced to the torque requirement superimposed on the lift and zero first harmonic moment requirements. A braking device (reversed tip-jets, spoilers, or mechanical brake) may be used on a full-scale Rotor/Wing to relieve the blades of the necessity of providing all the braking torque, and the use of rotor power for accelerating the rotor will again relieve the blades of this function. During the wind tunnel tests, this effect of providing other than aerodynamic torque can be demonstrated by using the hydraulic motor as a drive or brake system during conversion.

The conversion control programming device that accomplishes the results calculated here is a servo unit that senses rotor rpm and positions a set of potentiometers as a function of that rotor speed. The potentiometers act as shaped function generators that are connected to the rotor pitch control actuators and control position feedback potentiometers to make the rotor controls move in the manner prescribed to automatically start or stop the rotor while maintaining constant lift and zero rolling moment. Figure C-4 is a photograph of the device, and Figures C-5 and C-6 are wiring diagrams.

TABLE C-1

SYMBOLS

A_1	lateral cyclic pitch, deg
a	lift curve slope, per deg
B_1	longitudinal cyclic pitch, deg
C_{d_o}	blade section drag coefficient
C_H	drag force coefficient
C_l	blade section lift coefficient
C_{l_h}	hub rolling moment coefficient, positive right roll
C_m	moment of blade about centerline
C_{M_h}	hub pitching moment coefficient, positive nose-up
C_y	side force coefficient
C	blade chord, ft
g	acceleration of gravity, ft/sec^2
I_h	mass moment of inertia of blade about hub centerline, $slug\text{-}ft^2$
$M_{\text{℄ hub}}$	total moment of blade about hub centerline, lb-ft
M_T	thrust moment of blade about hub centerline, lb-ft
M_W	weight moment of blade about hub centerline, lb-ft
m	mass of blade per foot of radius, slugs/ft
R	blade radius, ft
r	distance measured along blade from axis of rotation to blade element, ft
u	resultant velocity perpendicular to blade span axis at blade element, ft
u_p	component at blade element of resultant velocity perpendicular to blade-span axis and u_T divided by tip speed
u_T	component at blade element of resultant velocity perpendicular to blade span axis and to shaft axis divided by tip speed

TABLE C-1 (Continued)

v	inflow velocity, fps
V_F	forward speed, fps
x	ratio of blade element radius to rotor-blade radius
a_{hub}	angle of attack of hub positive nose-up, deg
β	blade flapping angle, rad
θ_o	collective-pitch angle, deg
λ	inflow ratio $\left(\frac{V_F \sin a_{hub} - v}{\Omega R}\right)$
μ	tip speed ratio
ρ	mass density of air, slugs/ft^3
σ	rotor solidity
φ	inflow angle at blade element in-plane perpendicular to blade span axis, deg
ψ	blade azimuth angle measured from downwind position in direction of rotation , deg
Ω	rotor angular velocity, rad/sec

Subscripts

c	radius of root of blade
r	function of r

STICK POSITION

V_T	α_{hub}	θ_o	A_1	B_1	T_{hub}	T_{rotor}	T_{total}	Q	1st harmonic Moment Rot. sin/cos	2nd harmonic Moment Rot. sin/cos	3r Mo si
ft/sec	deg	deg	deg	deg	lbs	lbs	lbs	ft-lb	ft-lbs	ft-lbs	
					ROTOR DECELERATION						
280	7.7	6	0	5.24	41.0	50.0	91.0	10.8	-1.06/-2.89	6.94/11.68	2.
210	13.0	5	0	8.10	68.9	24.5	93.4	6.8	-1.47/-3.18	7.90/14.89	4.
140	15.0	8	0	14.64	81.0	10.1	91.1	6.1	-1.18/-.91	4.12/11.23	7.
70	16.5	5.8	0	15.00	91.0	3.6	94.6	1.3	-.61/-.24	2.07/6.26	5.
35	16.5	2.0	0	12.06	91.0	2.8	93.8	.21	.08/1.10	-.96/.16	3.
					ROTOR ACCELERATION						
35	16.5	-10.0	0	-4.27	91.0	6.4	97.4	-5.10	.47/2.07	-4.07/-5.85	
70	16.5	-10.0	0	-3.28	91.0	3.5	94.5	-1.77	-.11/.87	-1.74/-2.16	
140	15.5	-4.0	0	.78	85.0	6.1	91.1	-.46	-.07/-.13	.59/1.06	
210	14.0	-1.0	0	1.48	74.4	16.7	91.1	-.63	-.09/-.25	.98/1.60	

TABLE C-2

STICK POSITION AND AERODYNAMIC FORCES FOR DECELERATION AND ACCELERATION

V_{tunnel} = 98 fps

...onic ...ot.	2nd harmonic Moment Rot. sin/cos	3rd harmonic Moment Rot. sin/cos	Rotor H Steady	1st harmonic H rotating sin/cos	2nd harmonic H rotating sin/cos	3rd harmonic H rotating sin/cos	H hub	H total	Y stea... post. r...
	ft-lbs	ft-lbs	lbs	lbs	lbs	lbs	lbs	lbs	lbs
.89	6.94/11.68	2.41/.56	-.94	3.74/-1.13	.82/.55	.15/.16	4.13	3.19	0
18	7.90/14.89	4.25/-1.22	-1.08	2.54/-.77	.44/.19	-.06/.03	9.65	8.57	0
91	4.12/11.23	7.69/-3.88	-.55	1.61/-.35	-.12/-.47	-.25/-.09	13.32	12.77	0
24	2.07/6.26	5.19/-2.49	-.08	.62/-.14	-.10/-.52	-.50/.23	17.92	17.84	0
10	-.94/.16	3.52/-1.33	-.03	.28/-.07	-.13/-.46	-.42/.12	17.92	17.89	0
07	-4.07/-5.85	.85/-1.10	.98	-2.46/.96	-1.03/-.89	.01/-.48	17.92	18.90	0
7	-1.76/-2.16	.56/-.81	.34	-.60/.28	-.39/-.42	-.03/-.21	17.92	18.26	0
3	.58/1.06	.68/.04	.18	.29/-.08	.02/-.19	-.21/.18	14.70	14.88	0
5	.98/1.60	.75/.26	.44	.06/.04	-.12/-.34	-.18/.13	11.49	11.93	0

H hub	H total	steady post. right	1st harmonic Y rotating sin/cos	2nd harmonic Y rotating sin/cos	3rd harmonic Y rotating sin/cos	$\ddot{\Omega}$	Pitching Moment
lbs	lbs	lbs	lbs	lbs	lbs	rad/sec^2	ft-lbs
.13	3.19	0	-3.61/-10.02	2.33/-2.18	.71/.04	-3.76	6.43
.65	8.5	0	-.69/-1.32	1.17/-.87	.44/.41	-2.36	11.48
.32	12.77	0	-.08/-1.69	1.32/-.46	-.35/-.20	-2.19	13.10
.92	17.84	0	-.12/-.09	.57/-.12	-.11/-.06	-.45	16.56
.92	17.89	0	0 /.24	.43/-.12	.04/.03	-.07	16.56
.92	18.90	0	.35/1.00	-.27/.51	-.60/-.26	+1.78	16.56
.92	18.26	0	.17/.61	-.10/.03	-.08/.21	+.62	16.56
4.70	14.88	0	.17/.50	-.22/0	.28/.26	+.16	13.55
1.49	11.93	0	.19/.41	-.41/.17	.10/.15	+.22	12.61

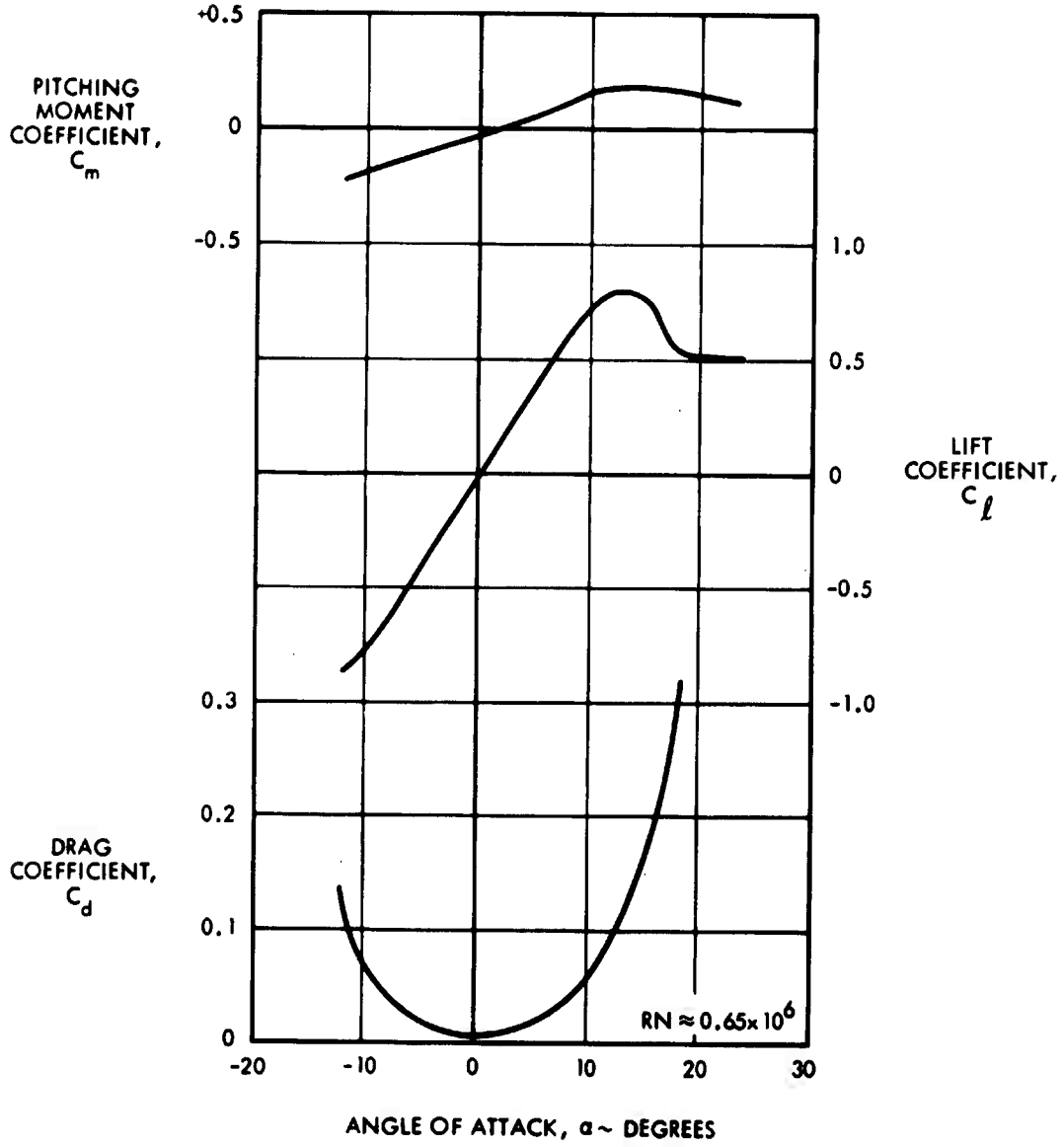

Figure C-1. Rotor Blade Section Aerodynamic Characteristics (Modified Circular Arc Blade)

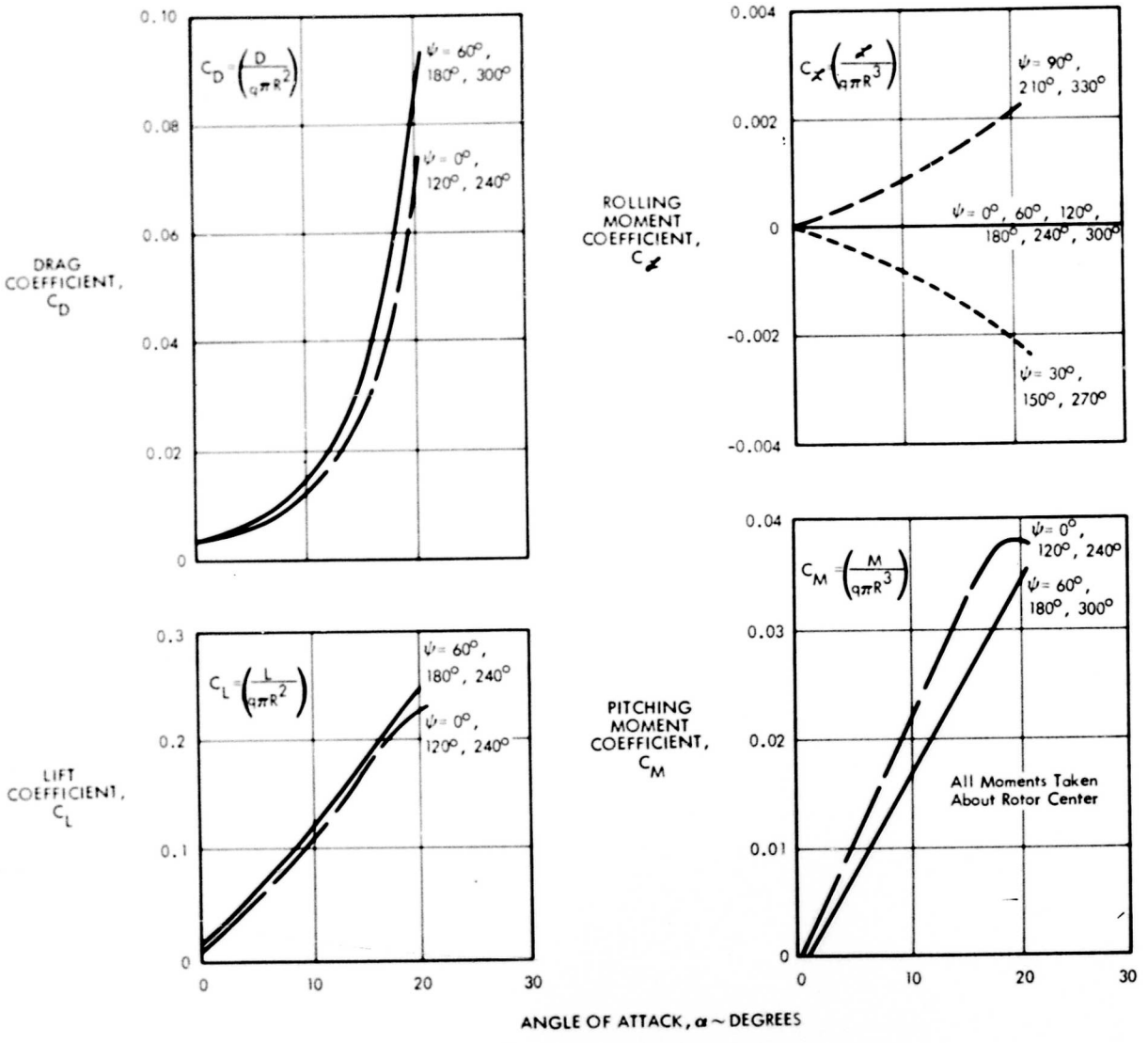

NOTE: FOR OTHER ψ VALUES, FAIR 3/REV SINUSOIDAL CURVE THROUGH GIVEN DATA

Figure C-2. Trisector Rotor Hub Aerodynamic Characteristics

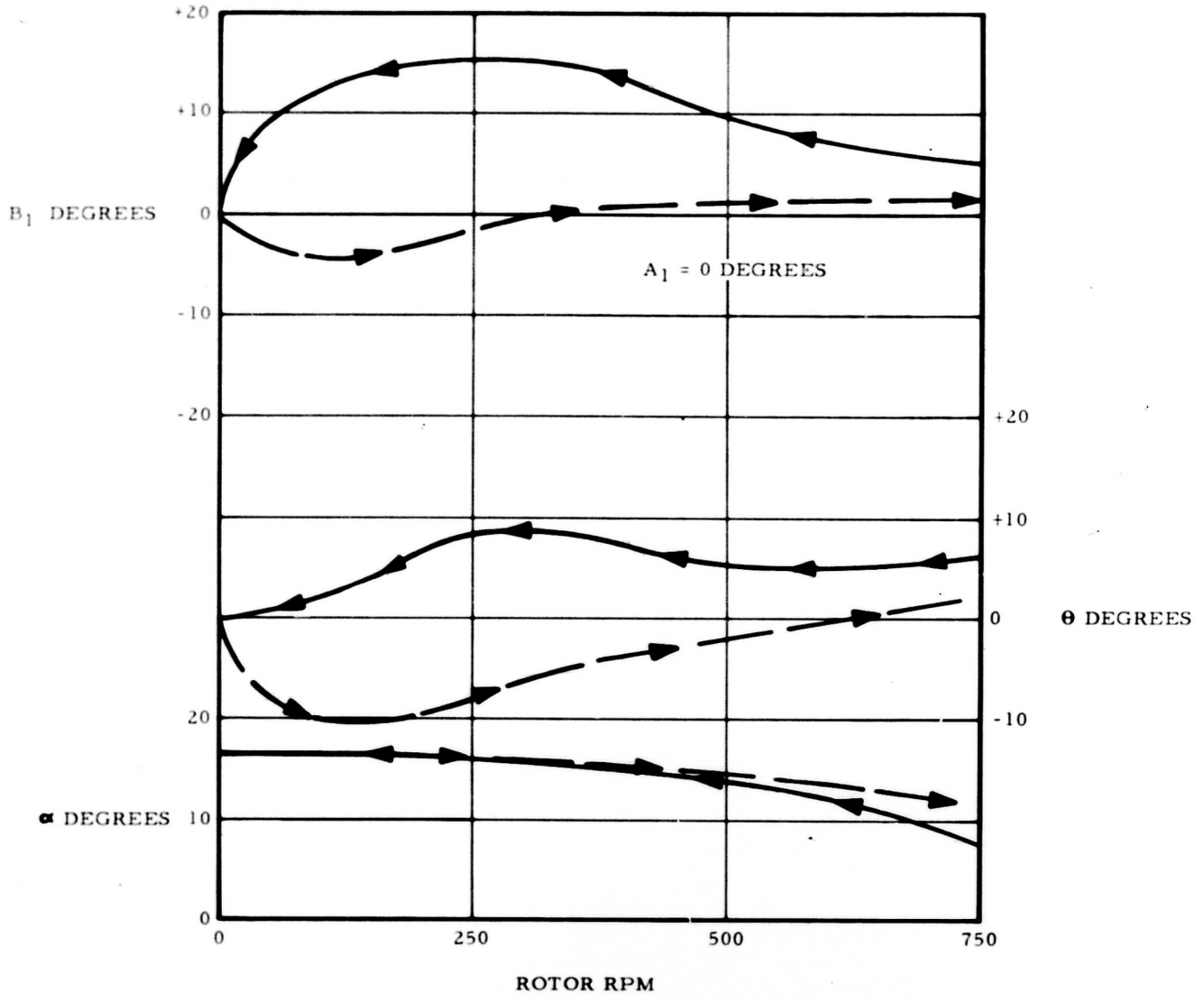

Figure C-3. Conversion Control Program

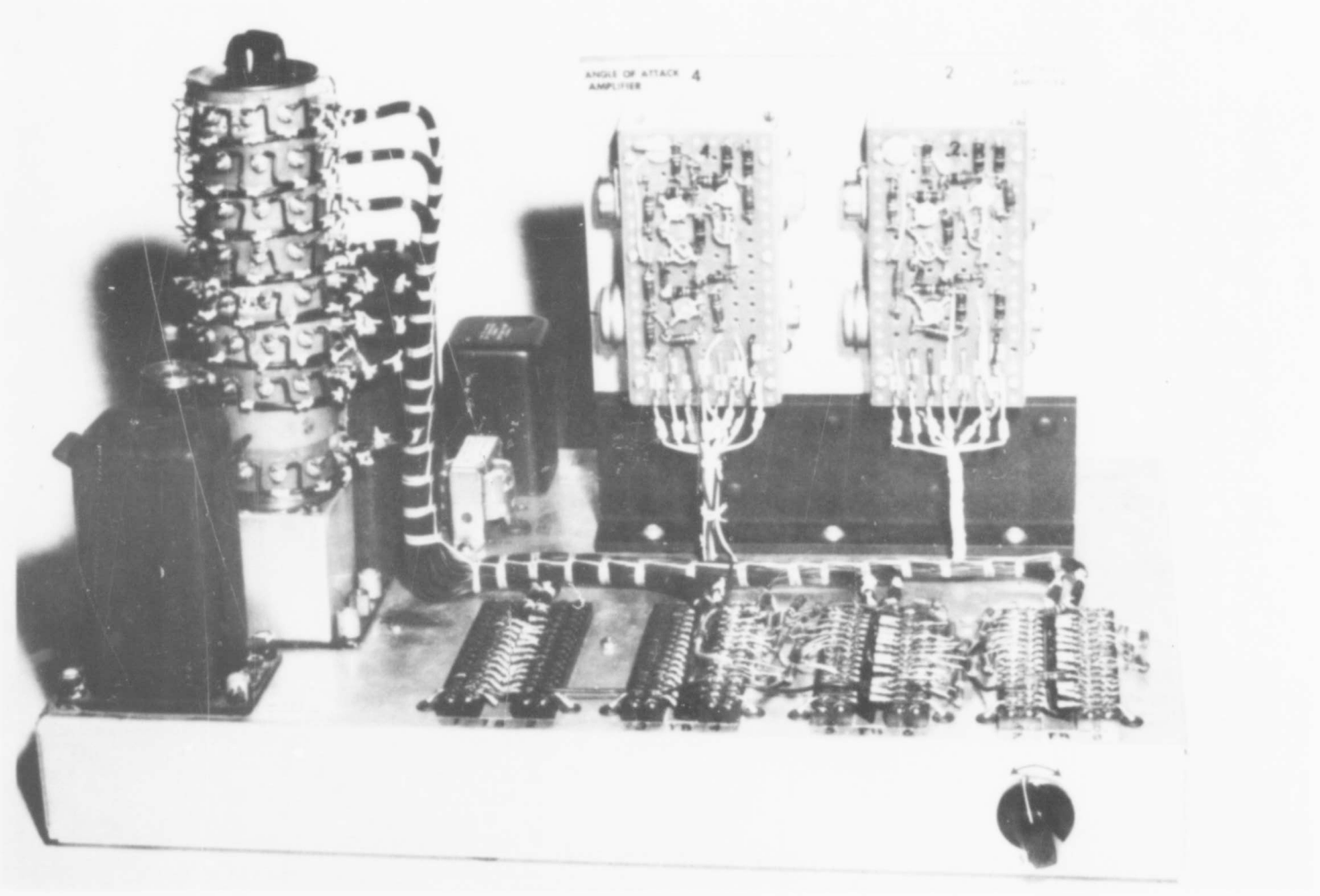

Figure C-4. Conversion Control Programmer

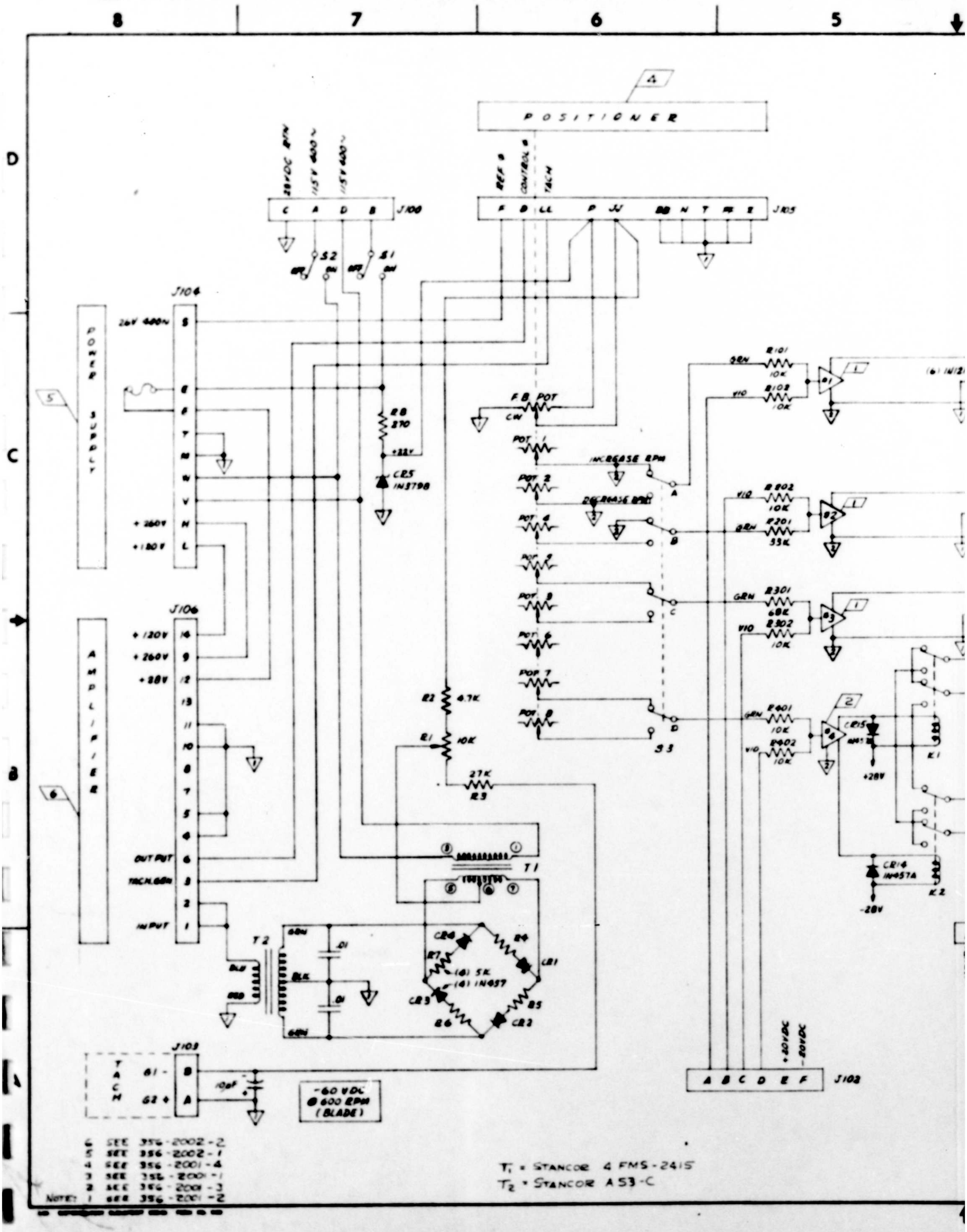
8
7
6
5
D
C
B
POSITIONER
REF Ø
CONTROL Ø
TACH
28 VDC RTN
115 V 400~
115 V 400~
C A D B J100
F D LL P JJ BB N T R Z J105
S2
S1
OFF ON
OFF ON
J104
POWER SUPPLY
26V 400~ S
E
F
T
M
W
V
+260V H
+120V L
R8 270
+28V
CR5 1N3798
F.B. POT
CW
POT 1
POT 2
POT 4
POT 3
POT 5
POT 6
POT 7
POT 8
INCREASE RPM
DECREASE RPM
A
B
C
D
S3
GRN R101 10K
VIO R102 10K
GRN R201 33K
VIO R202 10K
GRN R301 68K
VIO R302 10K
GRN R401 10K
VIO R402 10K
A1
A2
A3
A4
CR15
+28V
K1
CR14 1N457A
-28V
K2
J106
AMPLIFIER
+120V 14
+260V 9
+28V 12
13
11
10
8
7
5
4
OUTPUT 6
TACH GEN 3
2
INPUT 1
R2 4.7K
R1 10K
27K R3
T1
T2
BLU
RED
GRN
BLK
.01
.01
CR4
R4
R7
CR1
(8) 5K
(4) 1N457
CR3
R5
R6
CR2
J103
TACH
G1 - B
G2 + A
10µF
-60 VDC @ 600 RPM (BLADE)
+20VDC
-20VDC
A B C D E F J102
6 SEE 356-2002-2
5 SEE 356-2002-1
4 SEE 356-2001-4
3 SEE 356-2001-1
2 SEE 356-2001-3
NOTE: 1 SEE 356-2001-2
T1 = STANCOR 4 FMS-2415
T2 = STANCOR A53-C

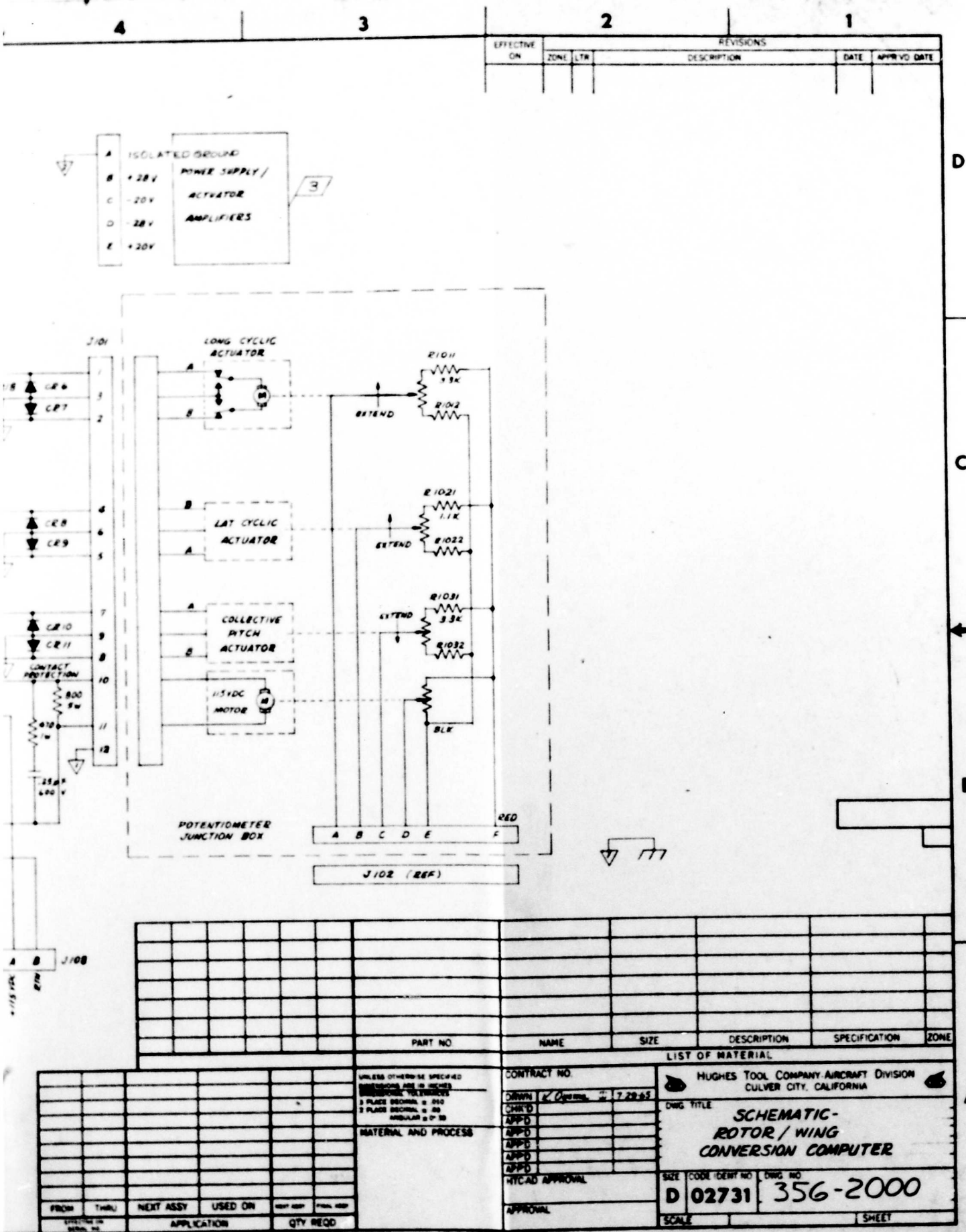

Figure C-5. Wiring Diagram of Conversion Programmer

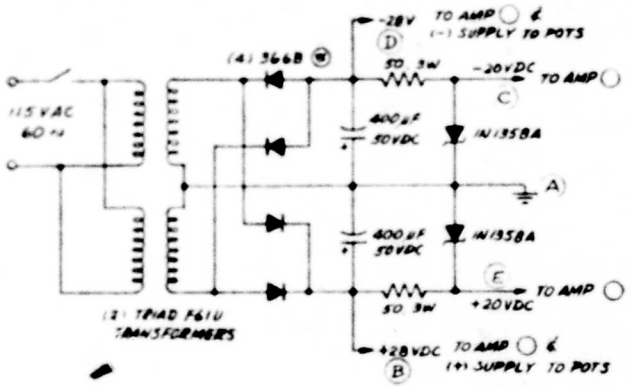

POWER SUPPLY
AMPLIFIER/ACTUATOR

(-1)

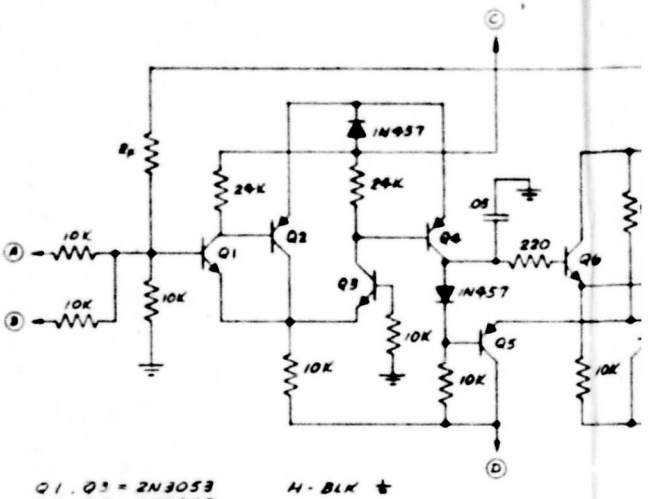

Q1, Q3 = 2N3053
Q2, Q4 = 2N3092
Q5 = 2N1375
Q6 = 2N3054
Q7 = 2N2869
Q8 = 2N3055
Q9 = 2N443

H - BLK
A - FUNCTION POT ARM GRN
B - ACTUATOR POT ARM VIO
C - (+) 20VDC BRN
D - (-) 20VDC ORN
E - (+) 28VDC RED
F - ACTUATOR MOTOR BLUE
G - (-) 28VDC YEL

AMPL
ACTUA

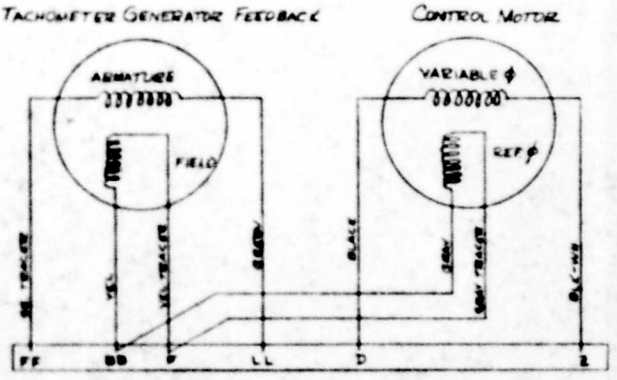

POSITIONER SERVO DRIVE

(-4)

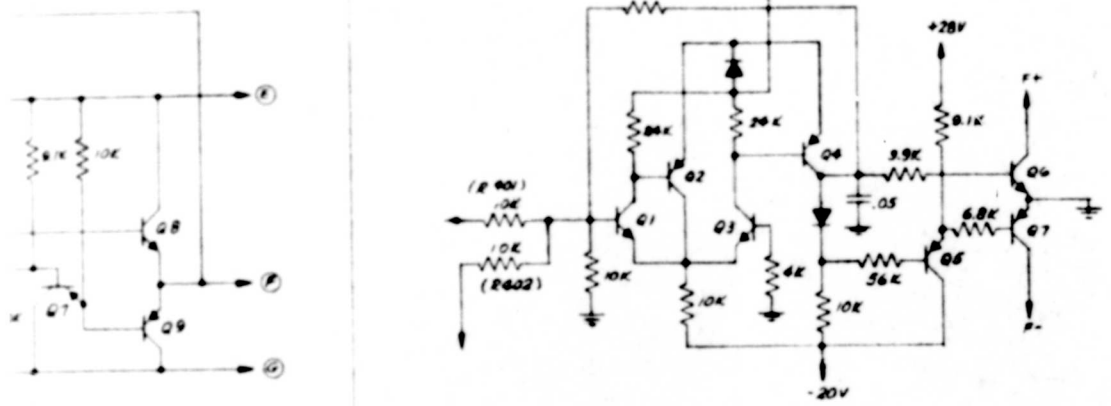

AMPLIFIER, 115 VDC
MOTOR #4

(-3)

MPLIFIER 24 V.D.C.
TUATOR 1, 2, & 3

(-2)

PART NO.	NAME	SIZE	DESCRIPTION	SPECIFICATION	ZONE

LIST OF MATERIAL

UNLESS OTHERWISE SPECIFIED
3 PLACE DECIMAL ± .010
2 PLACE DECIMAL ± .02
ANGULAR ± 0° 30'

MATERIAL AND PROCESS

CONTRACT NO.

DRWN	K OTAMA	7-30-65
CHK'D		
APP'D		
APP'D		
APP'D		
APP'D		
APP'D		

HTC AD APPROVAL

APPROVAL

HUGHES TOOL COMPANY AIRCRAFT DIVISION
CULVER CITY, CALIFORNIA

DWG. TITLE
SCHEMATIC - POWER SUPPLY AND AMPLIFIER 1, 2, 3 & 4

SIZE	CODE IDENT NO	DWG. NO.
D	02731	356-2001

SCALE | SHEET

FROM	THRU	NEXT ASSY	USED ON	NEXT ASSY	FINAL ASSY
		APPLICATION		QTY REQD	

Figure C-6. Wiring Diagram of Power Supply and Amplifiers for Conversion Programmer

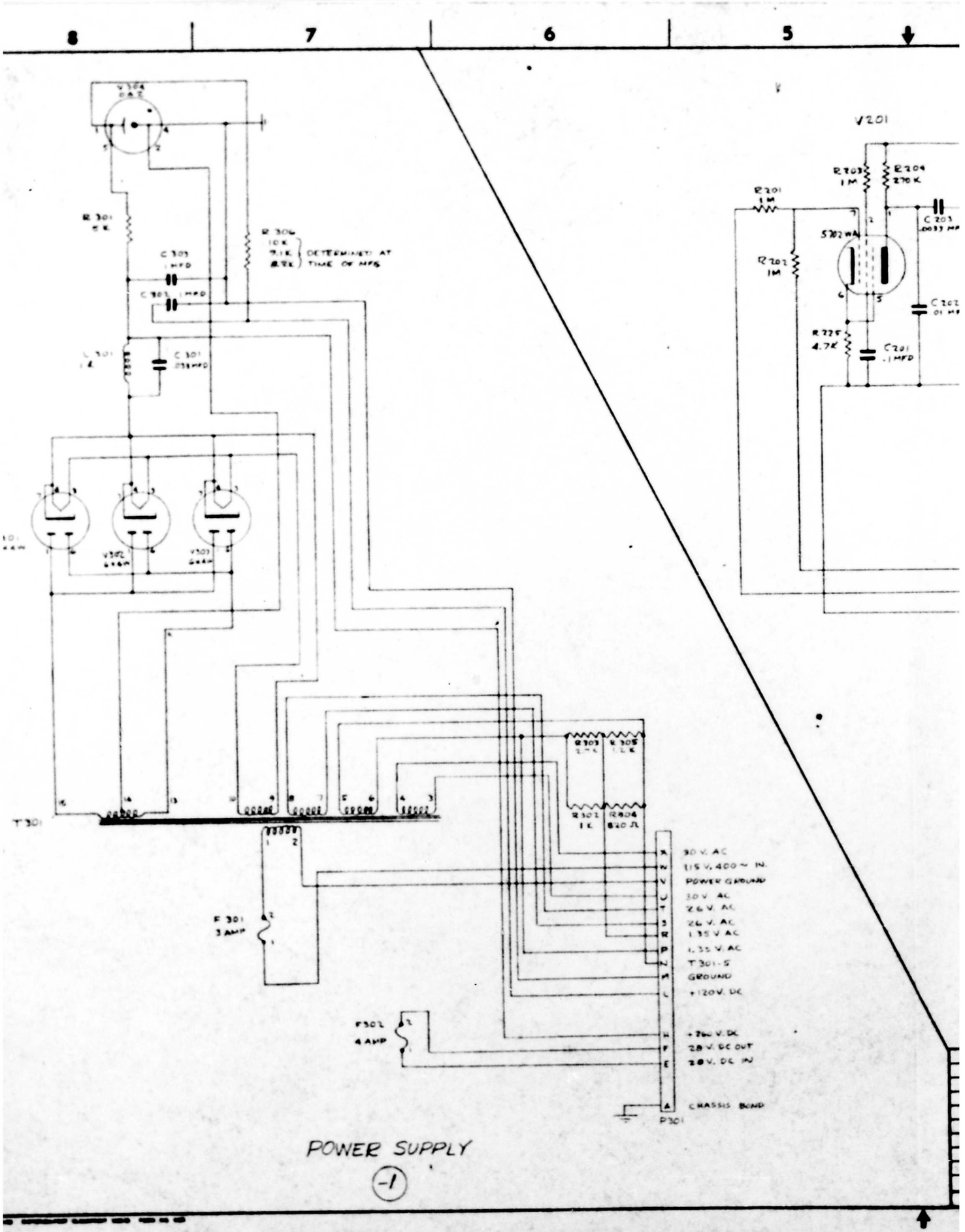

POWER SUPPLY

(-1)

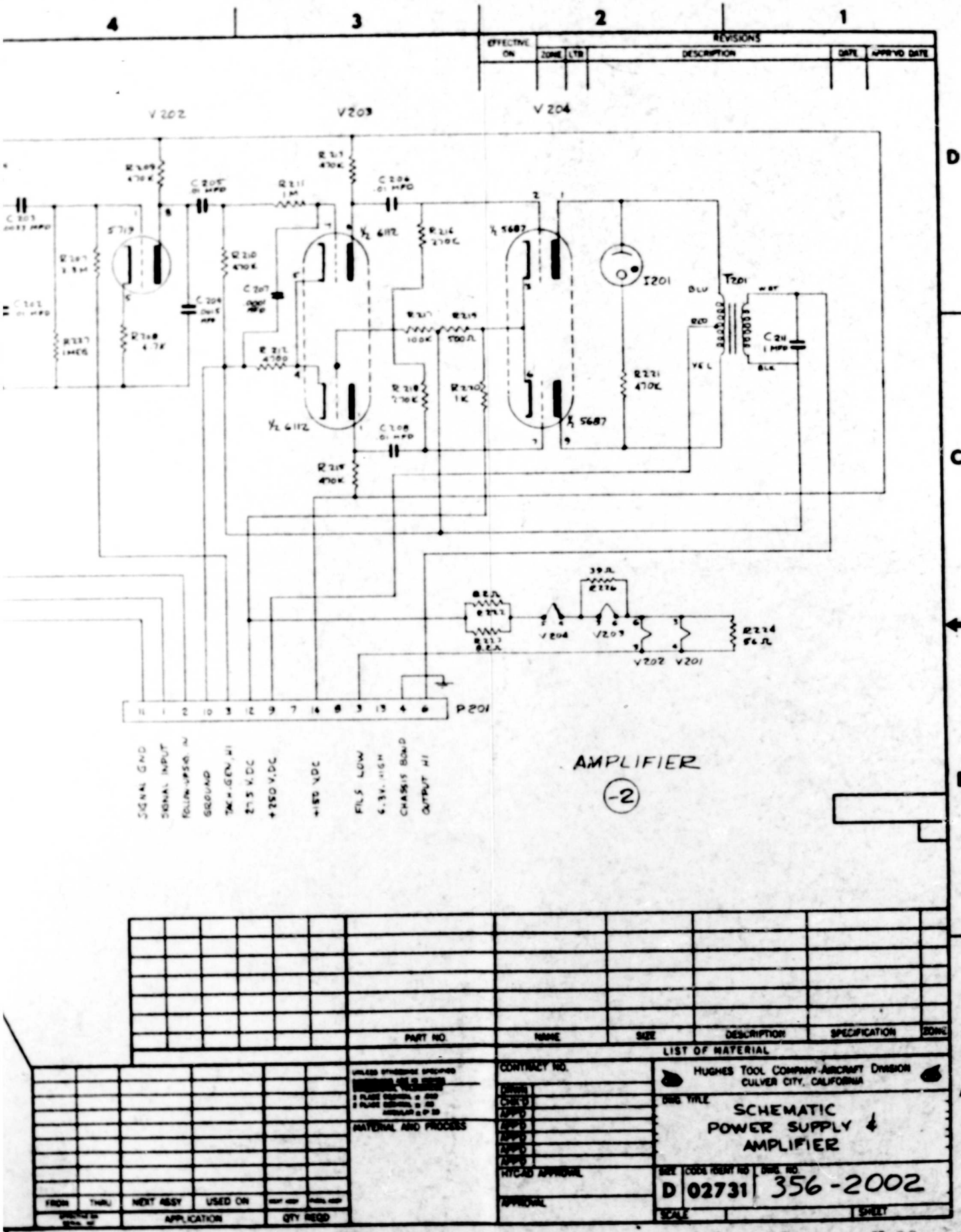

Figure C-7. Schematic-Power Supply and Amplifier

2

APPENDIX D

WHIRLSTAND TEST RESULTS

APPENDIX D

WHIRLSTAND TEST RESULTS

The first purpose of the model tests was to determine the hovering efficiency of the rotor with a large centerbody and to find if an optimum centerbody planform shape exists. The second purpose was to investigate the efficiency of symmetrical (fore and aft) blade airfoil sections, since in the stopped-rotor flight one blade is in reversed flow (compared with helicopter flight) and symmetry of configuration was thought necessary. The third purpose was to investigate the effect of the ratio of centerbody area to rotor disc area. The fourth purpose of the tests was to determine the ground effect for hovering near the ground.

The model was powered by a pneumatic drive, using compressed air to simulate the tip-jet effects on the rotor performance. Three centerbodies of the relative size and shape shown in Figure D-2 were built for these tests. A rotor diameter of 80 inches was established, so that the model could be used later in a low-speed wind tunnel. Each hub had the same planform area (11.9 square feet); thus all occupied a fixed percentage of the rotor disc area. In the latter period of the tests, it was desired to find the effect of changing the hub area-to-disc area ratio. This was done on the trisector hub by using both its normal blades and the blades intended for the circular hub; the rotor diameter increased from 80 to 85.9 inches, and the disc-area-to-hub-area ratio increased from 3.03 to 3.38. A number of blade airfoil sections, all of 15 percent thickness ratio and 6.66 inch chord,

were tested with each hub: NACA 0015, circular arc with parabolic leading and trailing edges, elliptical, and elliptical with camber.

The test facility setup for the hovering Rotor/Wing tests shown in Figure D-1 was out of doors and enclosed in a double chain-link fence. The model was mounted on the top of a pole approximately 10 feet above the ground. A work platform could be raised and lowered inside the fence for ground effect tests. A standard or reference rotor of conventional geometry was tested along with the Rotor/Wing configurations so a comparison could be made with conventional helicopter performance. The outline of the reference rotor is compared with the Rotor/Wing models in Figure D-2.

The first comparison made during the tests, Figure D-3, related the thrust-torque characteristics of the Rotor/Wing with differently shaped centerbodies, all with NACA 0015 blades, to the reference rotor characteristics. At the lower thrust coefficients corresponding to the maximum thrust-to-torque ratio, the trisector hub exhibits slighly more thrust than the circular centerbody. At the larger thrust coefficients, which are of more interest, the thrust for a given torque depends on the actual blade length. The circular hub, with the longest blades, has the most thrust; the triangular hub, with the least amount of blade span, has the least thrust. Note that in this comparison and all that follow, the thrust and torque coefficients are based on the total disc area of the rotor. If based on the annulus swept out of the blades, all the curves would nearly coincide.

Figure D-4 shows a comparison of the various blade sections on the trisector hub; the reference rotor with NACA 0015 blades is shown for comparison. The NACA 0015 blades are better than the double-ended sections by 3 or 4 percent in the high thrust region. This test is not conclusive as to optimum airfoil shape, but an optimum double-ended airfoil should not be far from the circular arc section tested.

Preliminary analysis indicated the possibility of an adverse ground effect caused by evacuating air from the bottom side of the centerbody, and perhaps a hysteresis with ground plane height that is, different augmentation effects depending on whether the Rotor/Wing was approaching or leaving the ground. The effect of ground plane height is shown in Figure D-5. These data were reduced to a common torque coefficient, and plotted as the ratio of thrust in ground effect to thrust out of ground effect. No hysteresis occurred between ground plane moving up and ground plane moving down, and the Rotor/Wing exhibits the usual ground effect experienced by conventional helicopter rotors.

The reduction and analysis of the test data has led to a method of predicting Rotor/Wing hover performance for other combinations of geometry. This method involves adding up the profile torque of the hub (which includes interference), the profile torque of the blades, and the induced torque of the blades. The key geometric parameter for this method is the ratio of blade root radius to blade tip radius called "A". The lower left-hand graph of Figure D-6 shows that the circular hub exhibits more torque required because more of its surface is in the high velocity region. The lower right-hand figure shows that the torque required by the various blade sections follows the prediction that the NACA 0015 would have the least profile torque and the fuller elliptical section would have the most torque required. The upper left-hand figure depicts the induced torque requirements. The parameters plotted are no more than integrated lift and drag coefficients of the blades, based on the annulus the blades sweep out and corrected to the complete disc area and radius.

The hovering efficiency can be summarized by Figure D-7 which shows that the optimum Rotor/Wing (trisector hub; circular arc blades) has approximately

an 18-percent performance degradation compared with the reference rotor — an acceptable price to pay for a VTOL vehicle that has downwash velocities on a par with helicopters and high subsonic cruise speeds.

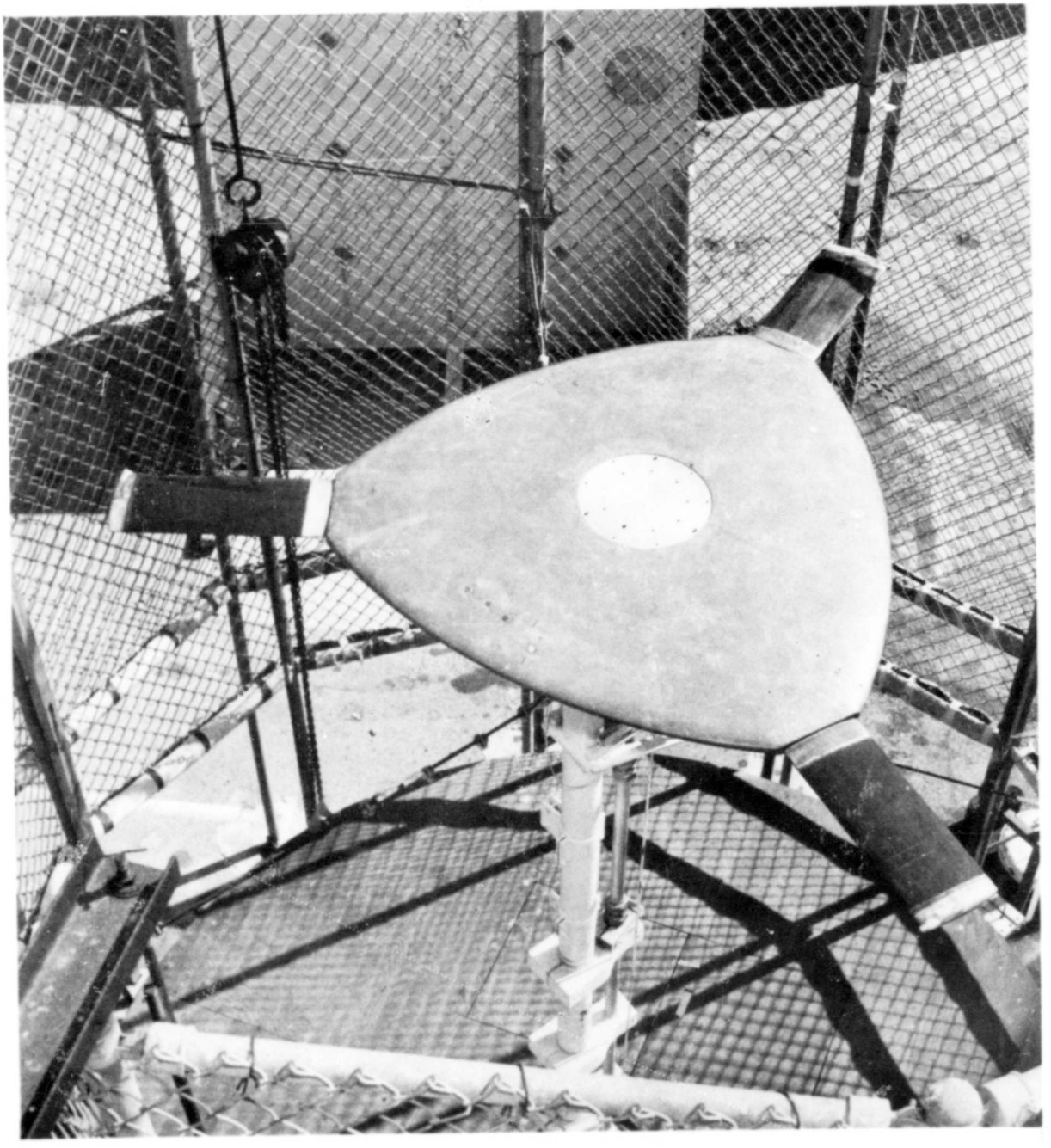

Figure D-1. Rotor/Wing Model Whirlstand

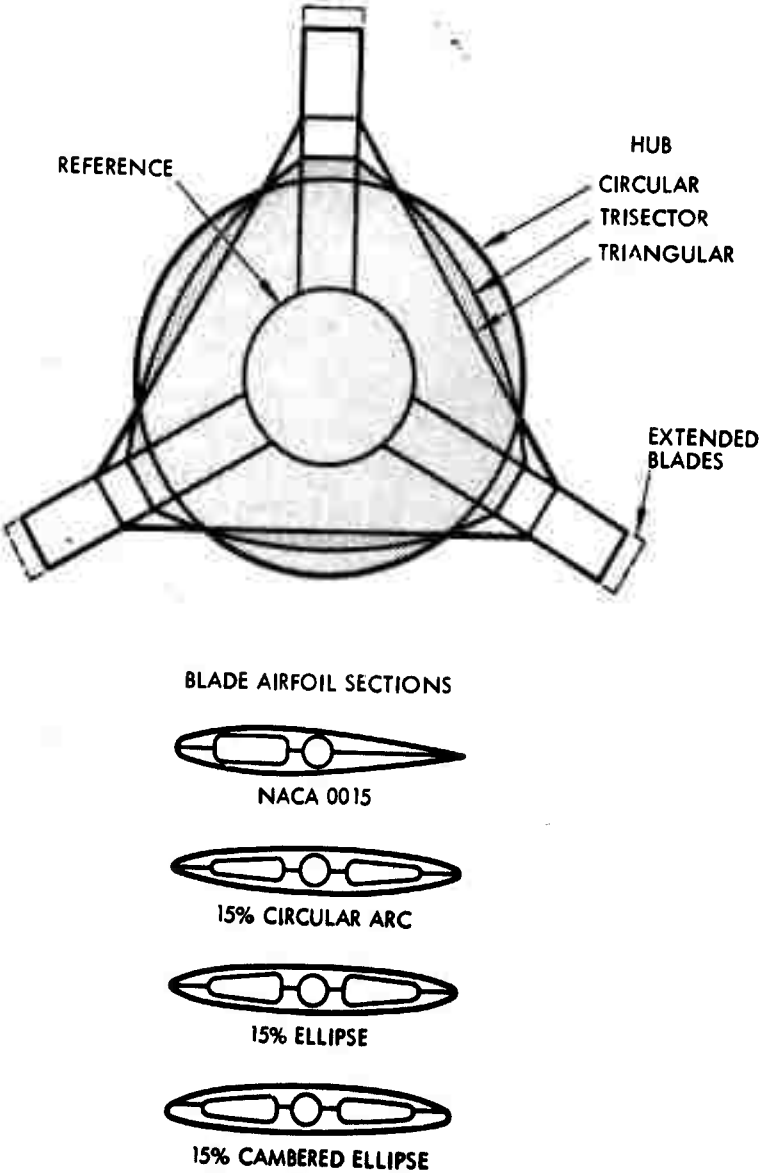

Figure D-2. Rotor/Wing Model Configurations

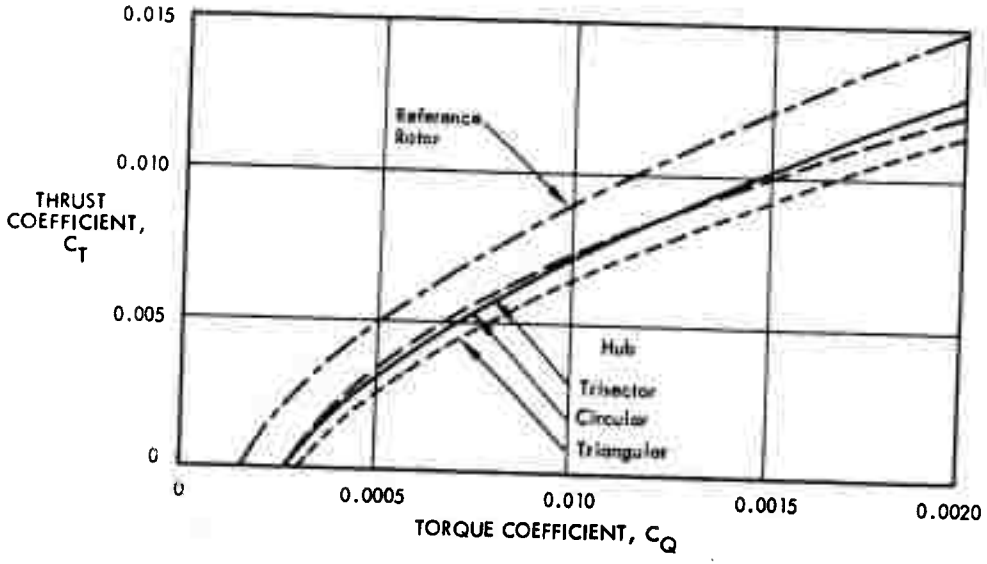

Figure D-3. Centerbody Performance Comparison with NACA 0015 Blades

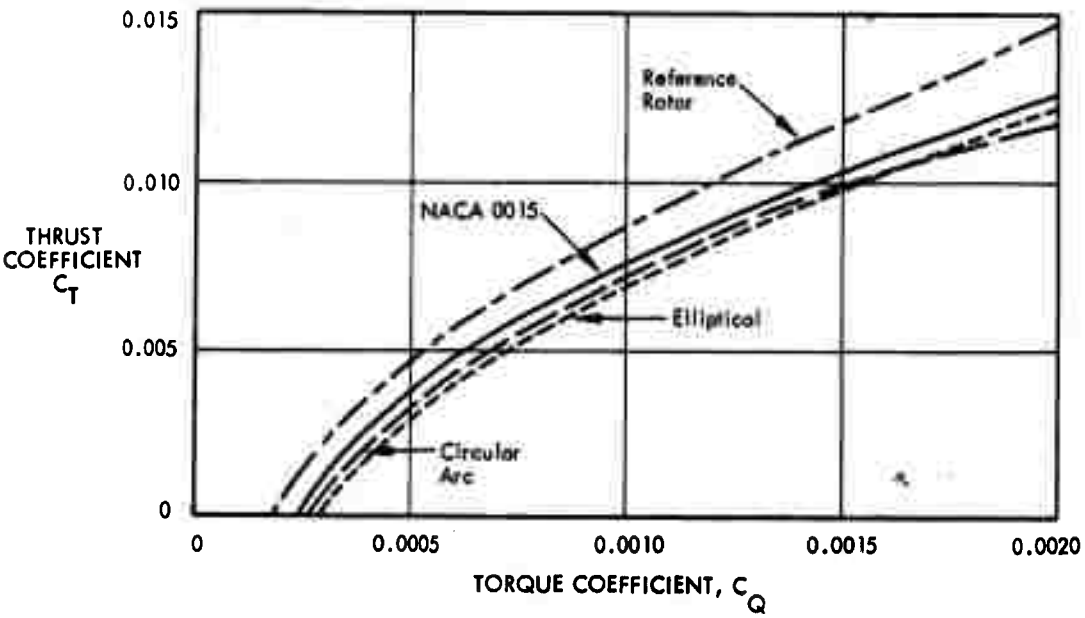

Figure D-4. Blade Section Performance Comparison on Trisector Hub

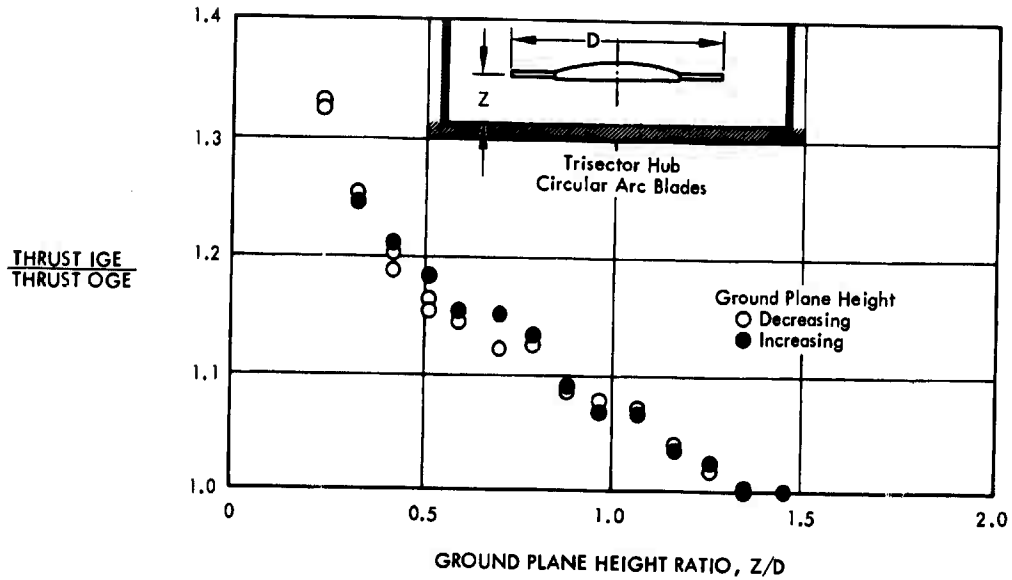

Figure D-5. Rotor/Wing Ground Effect

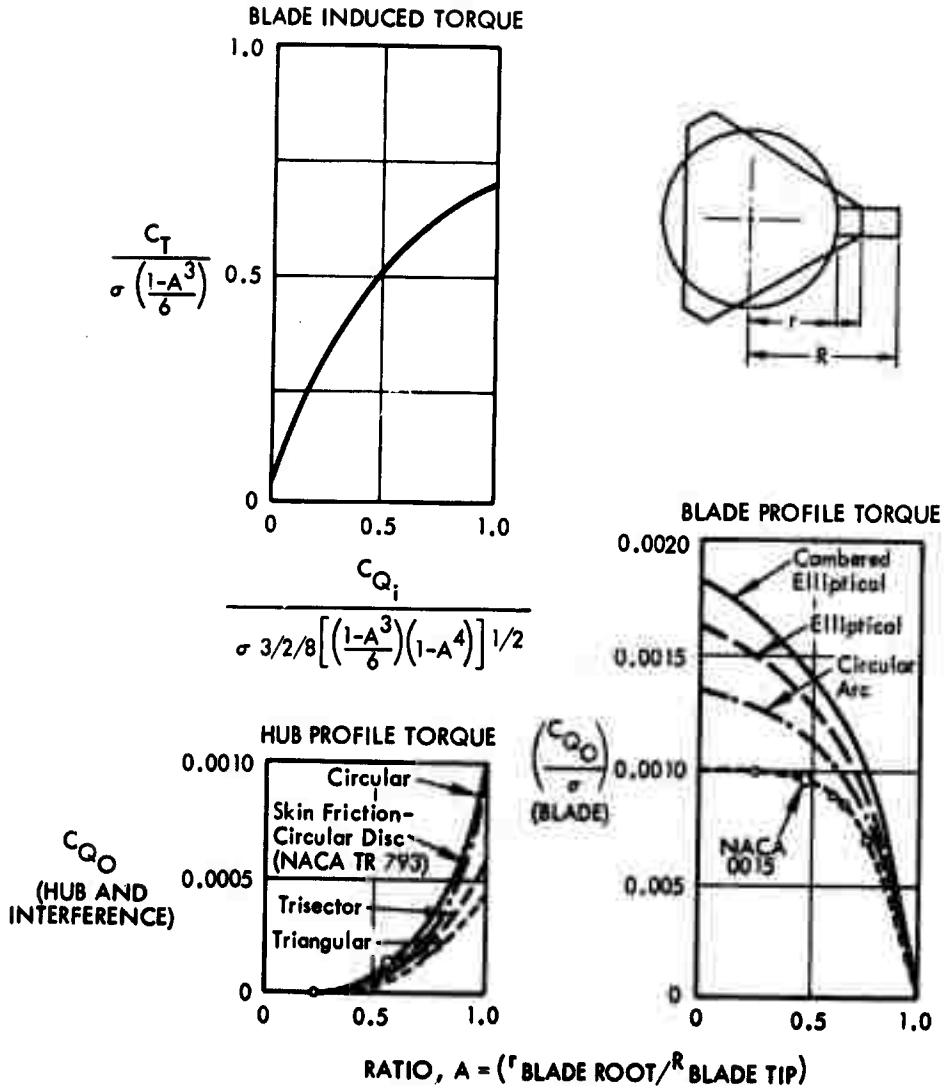

Figure D-6. Rotor/Wing Hovering Analysis

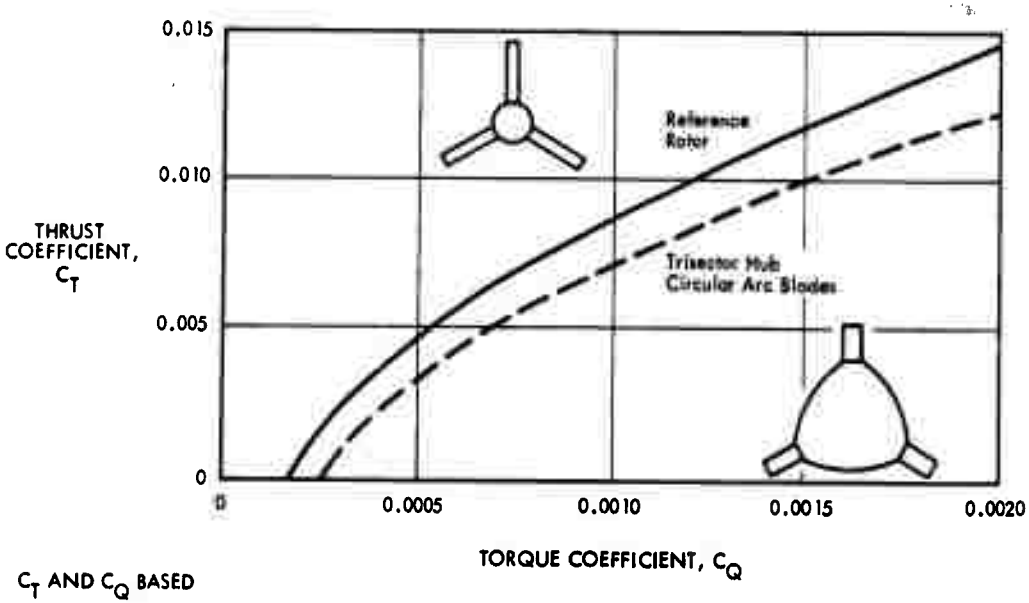

Figure D-7. Rotor/Wing Hovering Performance

APPENDIX E

ROTOR/WING ALONE WIND TUNNEL TEST RESULTS

APPENDIX E

ROTOR/WING ALONE WIND TUNNEL TEST RESULTS

The Series I wind tunnel tests conducted in the 8- by 10-foot subsonic wind tunnel at the David Taylor Model Basin Aerodynamics Laboratory for the purpose of obtaining early data on the aerodynamic characteristics of the Rotor/Wing in its stopped-rotor mode. These tests were conducted by BUWEPS, using models supplied by Hughes. The models used were the triangular and circular hubs with elliptical blades of constant 15-percent thickness and 6.66-inch chord; NACA 0015 blades were used with the triangular hub for a few tests. Figure E-1 shows these components, and Figure E-2 shows the models installed in the wind tunnel.

Hub-alone data for the circular and triangular hubs are given in Figure E-3. Data for the hubs, plus elliptical blades, may be seen in Figure E-4. Limited tests were made to show the roll effectiveness of the two rotor blades used as ailerons; Figures E-5 and E-6 indicate the rolling effectiveness. In all these plots, the coefficients are based on the total Rotor/Wing disc area and the blade tip radius; that is:

$$\text{Force coefficient} = \left(\frac{\text{force}}{q\pi R^2}\right)$$

$$\text{Moment coefficient} = \left(\frac{\text{moment}}{q\pi R^3}\right)$$

Where R, the rotor blade tip radius, equals 40 inches, and q is the tunnel dynamic pressure.

As an interesting aside, the circular hub curves of Figure E-3 represent a major contribution to the store of published data on circular wings.

The aileron effectiveness shown in Figures E-5 and E-6 is for the configuration of one blade forward and two swept back. The forward blade is kept at zero incidence and the other two are deflected. The $\Delta \delta_A$ value is numerically equivalent to two times the collective pitch setting, θ. The data show that the longer blades on the circular hub are more effective than the short blades on the triangular hub. There is little to choose between the elliptical and NACA 0015 blades on the triangular hub.

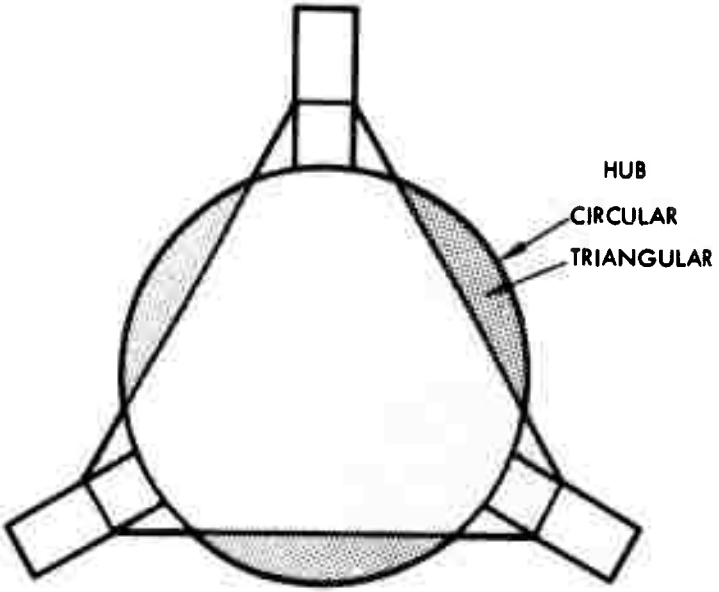

BLADE AIRFOIL SECTIONS

15% ELLIPSE

NACA 0015

Figure E-1. Rotor/Wing Model Configurations Series I Wind Tunnel Test

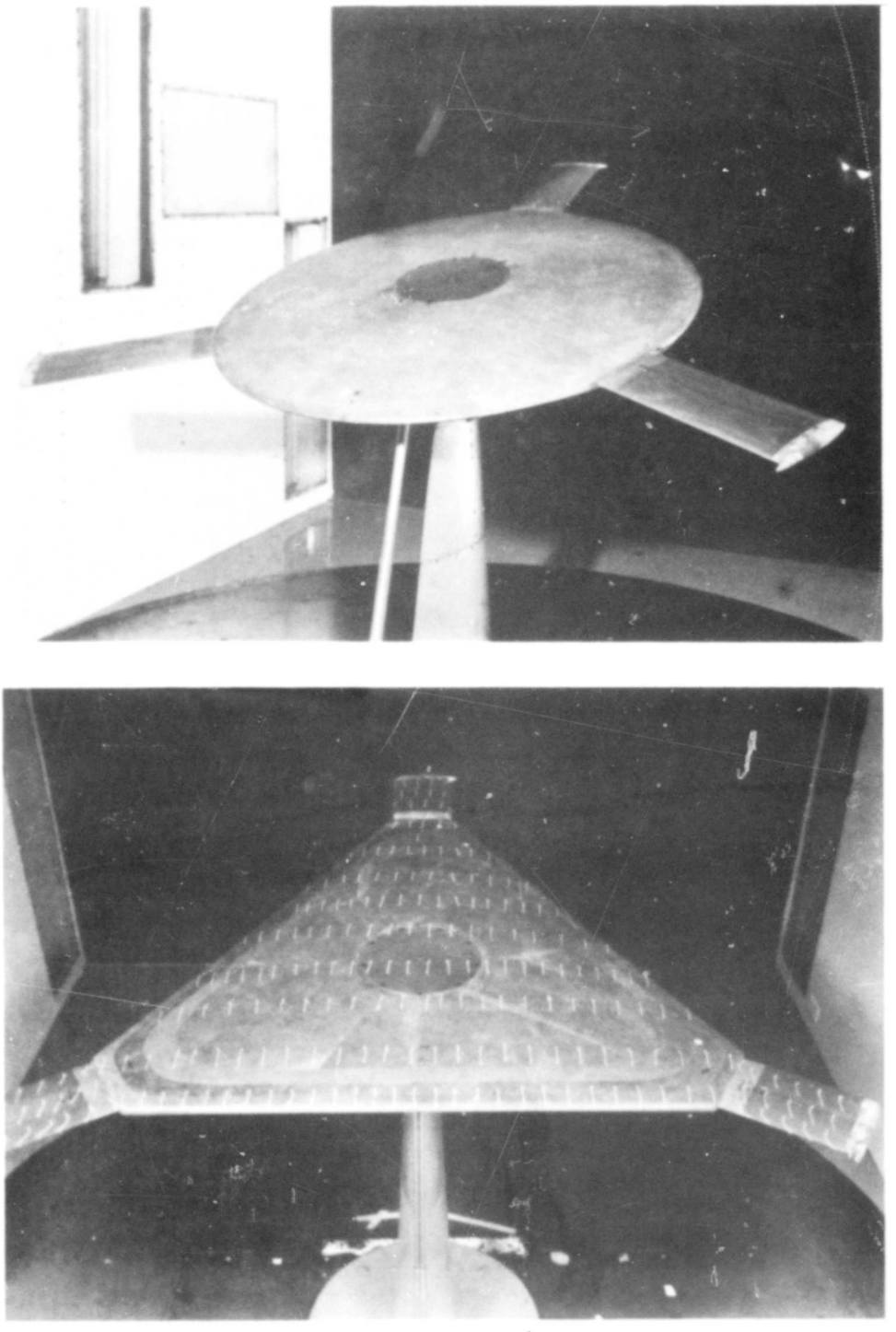

Figure E-2. Rotor/Wing Wind Tunnel Tests, Series I - David Taylor Model Basin

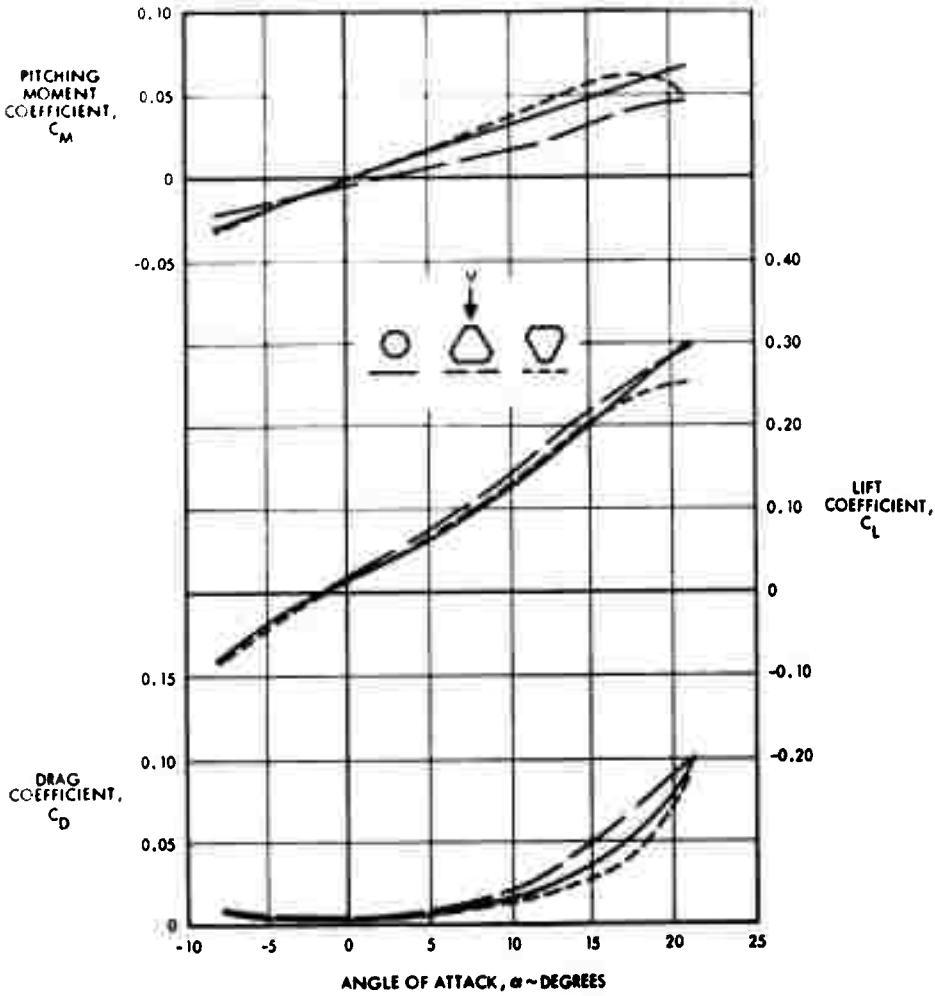

Figure E-3. Rotor Hub Aerodynamic Characteristics

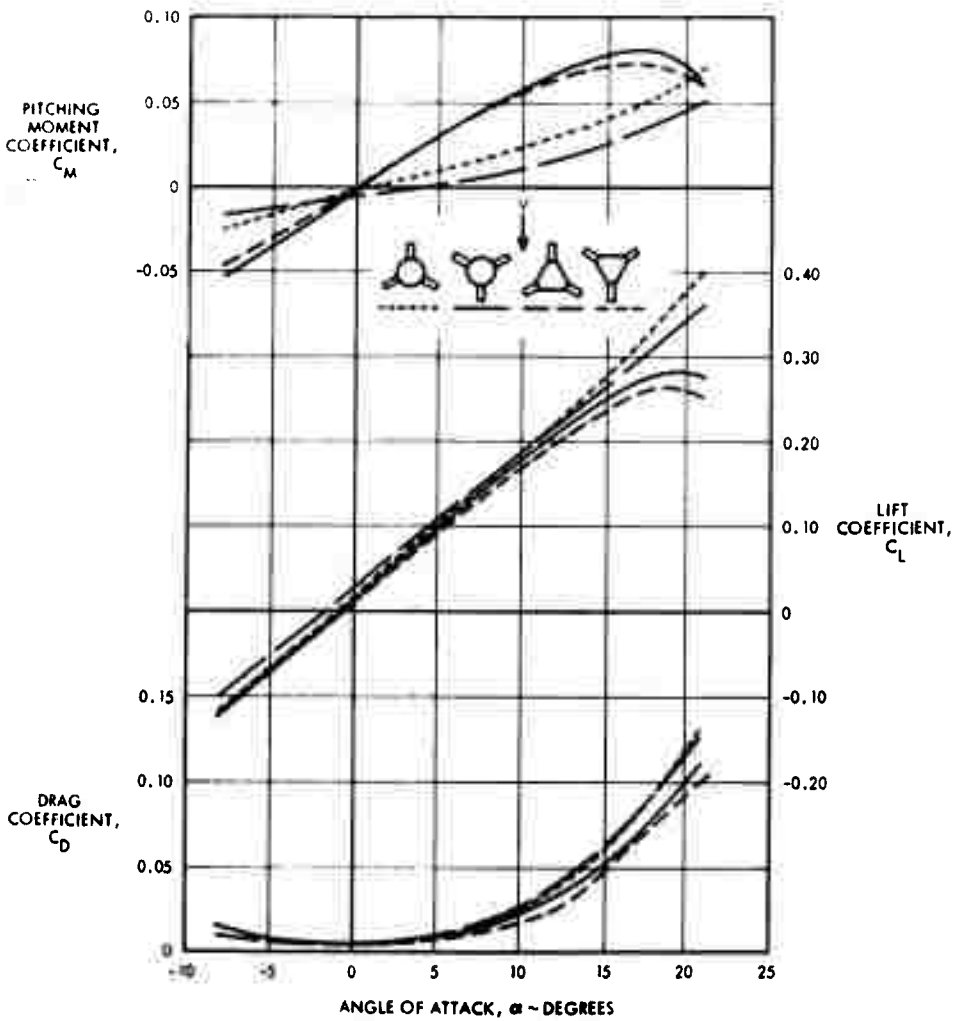

Figure E-4. Rotor/Wing Aerodynamic Characteristics

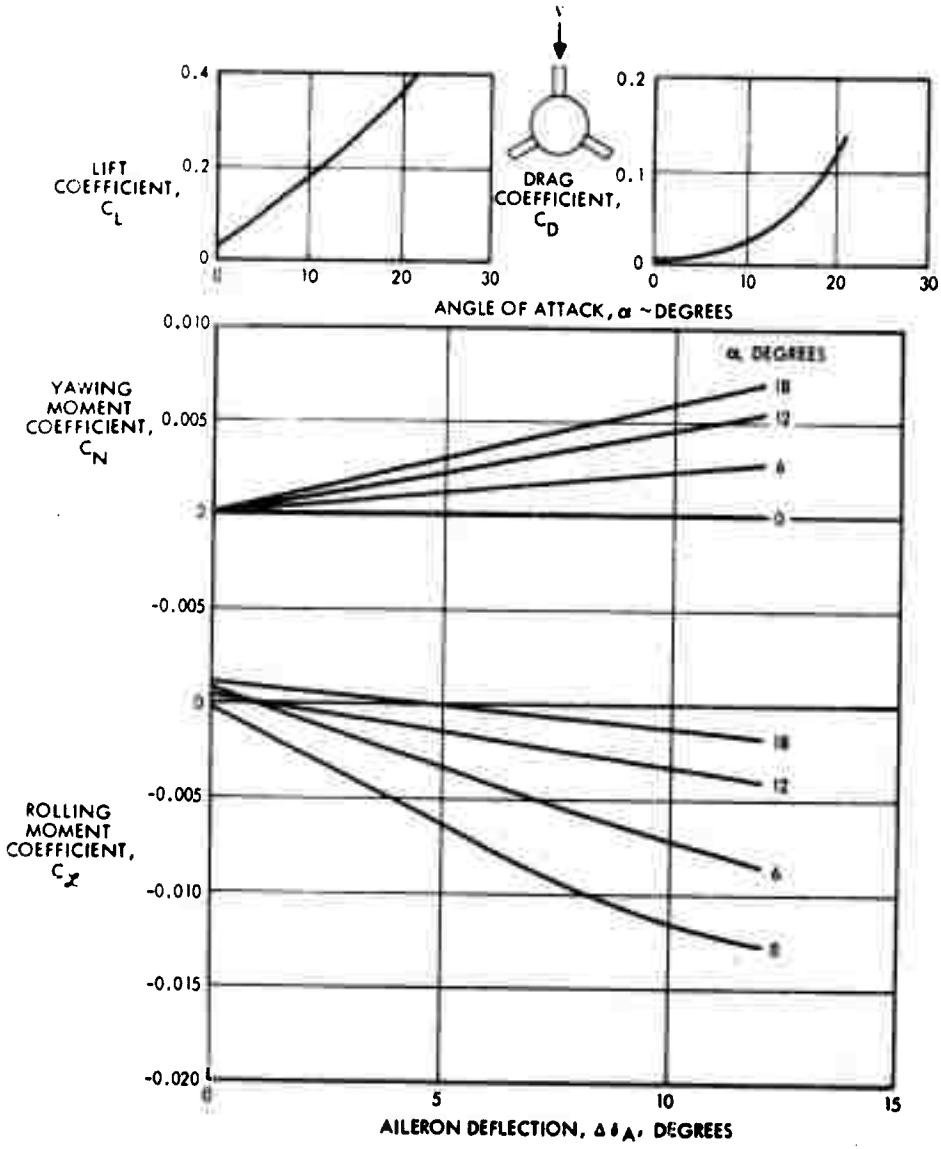

COEFFICIENTS BASED ON ROTOR DISC AREA AND RADIUS, MOMENTS ABOUT ROTOR CENTER

Figure E-5. Aileron Effectiveness – Circular Hub

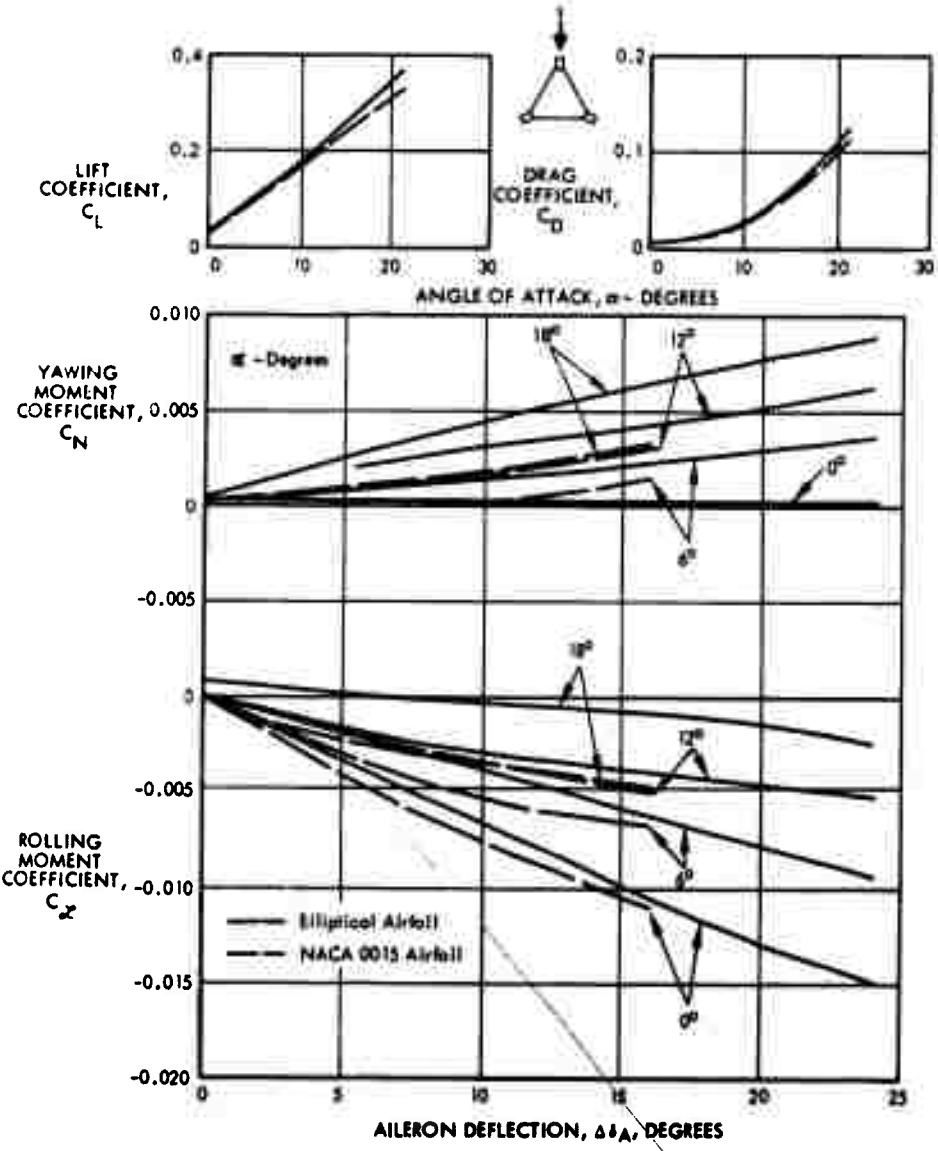

COEFFICIENTS BASED ON ROTOR DISC AREA AND RADIUS, MOMENTS ABOUT ROTOR CENTER

Figure E-6. Aileron Effectiveness - Triangular Hub

APPENDIX F

COMPLETE MODEL WIND TUNNEL TEST RESULTS

APPENDIX F

COMPLETE MODEL WIND TUNNEL TEST RESULTS

The primary purpose of these tests was to establish the feasibility of starting and stopping the Rotor/Wing in flight, for without this capability the Rotor/Wing concept would be meaningless. The second purpose was to evaluate the aerodynamic characteristics of the Rotor/Wing in the powered-rotor helicopter phase, autorotating-rotor transition phase, and the stopped-rotor airplane phase. The third purpose was to establish trends of the structural dynamics characteristics. The dynamics of the model could only indicate trends, because no attempt was made to achieve dynamic similarity with any full-scale aircraft.

The model was tested during two test series, designated Series II and Series III, in the 8- by 10-foot subsonic wind tunnel at the David Taylor Basin Aerodynamics Laboratory in March and June of 1965. Figure F-1 shows the layout of the model, and Figures F-2 through F-5 show the model and its associated equipment in the tunnel. Table F-1 is the run schedule for both series of tests, and Tables F-2 and F-3 define, respectively the configuration symbols and the coefficients used in these tests.

The test data are then presented in four groups.

Powered-Rotor
Autorotating Rotor
Conversion
Stopped-Rotor

As in the case of the Rotor/Wing alone (Appendix E), the aerodynamic coefficients are based on the total disc area and blade tip radius:

$$\text{Force coefficient} = \left(\frac{\text{force}}{q\pi R^2}\right)$$

$$\text{Moment coefficient} = \left(\frac{\text{moment}}{q\pi R^3}\right)$$

where R, the tip radius, equals 42.95 inches and q is the wind tunnel dynamic pressure. All moments are measured about a point on the rotor shaft 8.5 percent of the blade tip radius below the plane of the blade spars.

Bending moment data measured in the rotor shaft and at the blade roots are made nondimensional by dividing by the Rotor/Wing lift force and the tip radius; these nondimensional moments are designated $\pm\bar{\bar{M}}$. The significance of the $\pm$ is that the moments plotted are equal to one-half the peak-to-peak moments; thus:

without attempt to harmonically analyze the record, except in a few limited cases in which the actual harmonic content is given.

TABLE F-1

WIND TUNNEL TEST SCHEDULE

Test Series	Run No.	Configuration	Type
II	1-P	FN_1HBLC	Tail-off pitch
	2-Y		Tail-off yaw
	3-Y		Tail-off yaw
	4-P	$FN_1HBLCVS_o$	Tail effectiveness in pitch
	5-P		
	6-P		
	7-P		
	8-P		
	9-P		
	10-P		
	11-P		
	12-P		
	13-Y		Tail-on yaw
	14-Y		Tail-on yaw
	15-P		Rotor blade roll effectiveness
	16-P		Rotor blade roll effectiveness
	17-P		Horizontal tail roll effectiveness
	18-P		Horizontal tail roll effectiveness
	19-P	$FN_3HBLCVS_o$	Tail effectiveness in pitch
	20-P		
	21-P		
	22-P		
	23-P		
	24-P		
	25-P	FN_3HBLC	Tail-off pitch
	26-Y		Tail-off yaw
	27-Y	$FN_3HBLCVS_o$	Tail-on yaw
	28-P	$FN_2HBL*VS_oZ$	Pitch test, open fairings
	29-P	$FN_1HBLCVS_oZ$	Tare run for stiffening struts
	30-P	FN_2HBZ	Dynamic
	31-P		Helicopter, Tail-Off, μ = .25
	32-P		Helicopter, Tail-Off, μ = 0
	33-P		Helicopter, Tail-Off, μ = .15
	34 A-P		Helicopter, Tail-Off, μ = .15
	35-P		Helicopter, Tail-Off, μ = .35
	35 A-P		Helicopter, Tail-Off, μ = .35
	36-P	FN_2HBVS_oZ	Helicopter, Tail-On, μ = .15 → .35
	37-P		Helicopter, Tail-On, μ = .15 → .35
	38-P		Helicopter, Tail-On, μ = .15 → .35
	39-P		Helicopter, Tail-On, μ = .25
	40-P	FN_2HBZ	Helicopter, Tail-Off, μ = .25
	41-P		Conversion
	42-P		Autogyro, Tail-Off
	43-P		Autogyro, Tail-Off
	44-P	FN_2HBVS_oZ	Autogyro, Tail-On
	45-P		Autogyro, Tail-On
II	46-P	FN_2HBVS_oZ	Autogyro, Tail-On

TABLE F-2 (Continued)

Test Series	Run No.	Configuration	Type
II	47-P	$FN_3H(2B)LCVS_0Z$	Airplane, Tail-On, 2 Blades, $i_{bl} = 0°$
	48-P	$FN_3H(2B)LCZ$	Airplane, Tail-Off, 2 Blades, $i_{bl} = 0°$
	49-P		Airplane, Tail-Off, 2 Blades, $i_{bl} = -5°$
	50-P	$FN_3H(2B)LCVS_0Z$	Airplane, Tail-On, 2 Blades, $i_{bl} = -5°$
	51-P	FN_3HCVS_0Z	Airplane, Tail-On, Blades-Off
	52-P	FN_3HCZ	Airplane, Tail-On, Blades-Off
	53-P	$FN_1HBLCVS_0$	Repeat Basic Configuration
II	54-P	$FN_1HBLCVS_0$	Hydraulic Lines Off
III	55-P	FN_1H_1BLC	Tail-Off Pitch
	56-Y		Tail-Off Yaw
	57-Y		Tail-Off Yaw
	58-P	$FN_1H_1BLCV_1S_1$	Tail-On Pitch
	59-P		
	60-P		
	61-P		
	62-P		
	62 A-P		
	63-P		
	64-P		
	65-P		Tail rolling effectiveness
	66-P		Tail rolling effectiveness
	67-Y	$FN_1H_1BLCV_2S_1$	Tail-On yaw
	68-Y		
	69-Y		
	70-Y		
	71-Y		
	72-Y		
	73-P	$FN_2H_3BV_1S_1Z$	Automatic Conversion, $A_2 = 0°$
	74-P	FN_2H_2BZ	Pseudo-Conversion, Powered $A_2 = 5°$
	75-P		Hover performance, $A_2 = 5°$
	76-P		Hover control power, $A_2 = 5°$
	77-P		Hover control power, $A_2 = 5°$
	78-P		Helicopter performance, $\mu = .25$, $A_2 = 5°$
	79-P		Helicopter control power, $\mu = .25$, $A_2 = 5°$
	80-P		Helicopter performance, $\mu = .35$, $A_2 = 5°$
	81-P	$FN_2H_2BV_1S_1Z$	Automatic Conversion, $A_2 = 5°$
	82-P		Automatic Conversion, $A_2 = 5°$
	83-P	FN_2H_2BZ	Autogyro, Tail-Off
	84-P	$FN_2H_2BV_1S_1Z$	Autogyro, Tail effectiveness, $A_2 = 5°$
	85-P		Autogyro, Tail effectiveness, $A_2 = 5°$
	86-P		Autogyro, Tail effectiveness, $A_2 = 5°$
	87-P		Helicopter, Tail effectiveness, $A_2 = 5°$
	88-P		Helicopter, Tail effectiveness, $A_2 = 5°$
	89-P		Helicopter, Tail effectiveness, $A_2 = 5°$
	90-P	FN_2H_2Z	Helicopter, Blades Off, Tail Off, $\mu = .15$
	91-P		Helicopter, Blades Off, Tail Off, $\mu = .25$
III	92-P	FN_2H_2Z	Helicopter, Blades Off, Tail Off, $\mu = .35$

TABLE F-2 (Continued)

Test Series	Run No.	Configuration	Type
III	93-P	$FN_2H_3BV_1S_1Z$	Automatic Conversion, $A_2 = 0°$
	94-P	FN_2H_3BXZ	Pseudo-Conversion, Powered, A_2=0°, Spoilers
	94 A-P		Pseudo-Conversion, Powered, A_2=0°
	95-P	FN_2H_1BZ	Pseudo-Conversion, Powered, A_2=3.5°
	95 A-P		Pseudo-Conversion, Powered, A_2=3.5°
	96-P	$FN_2H_1BV_1S_1Z$	Automatic Conversion, $A_2 = 3.5°$
	97-P	FN_1H_1BLCY	Stall Fence Test
	98-P	$FN_1H_1BLCV_1S_1$	Pitch test, Aft Blades, i = -10°
	99-P	FN_3H_1BLC	Pitch Test, Fwd Blade, i = 90°, Aft Blades, i = -10°
	100-Y	FN_3H_1BLC	Yaw Test, Fwd Blade, i = 90°, Aft Blades, i = -10°
	101-Y	FN_3H_1BLC	Yaw Test, Fwd Blade, i = 90°, Aft Blades, i = -10°
	102-P	$FN_3H_1BLCV_1S_1$	Pitch Test, Fwd Blade, i = 90°, Aft Blades, i = -10°
	103-Y	$FN_3H_1BLCV_1S_1$	Yaw Test, Fwd Blade, i = 90°, Aft Blades, i = -10°
	104-Y	$FN_3H_1BLCV_1S_1$	Yaw Test, Fwd Blade, i = 90°, Aft Blades, i = -10°
	105-P	$FN_1H_1B_1LCV_1S_1$	Pitch test, 2.5" Blade Extension
	106-P	$FN_1H_1B_1LC$	Pitch test, 2.5" Blade Extension
	107-P	$FN_1H_1B_2LC$	Pitch test, 5" Blade Extension
	108-P	$FN_1H_1B_2LCV_1S_1$	Pitch test, 5" Blade Extension
III	109-P	$FN_2H_3BX_1Z$	Pseudo-Conversion, Powered, $A_2 = 0°$, Short Spoilers

TABLE F-2

CONFIGURATION SYMBOLS

F	fuselage
N_1	long nose, sealed to rotor
N_2	long nose, open for rotor clearance
N_3	short nose
H	trisector rotor hub (Series II)
H_1	trisector hub, second harmonic swashplate, A_2=3.5° (Series III)
H_2	trisector hub, second harmonic swashplate, A_2=5° (Series III)
H_3	trisector hub, second harmonic swashplate, A_2=0° (Series III)
B	circular arc blades
L	rotor locked (all gaps sealed)
L*	rotor locked (all gaps open)
C	turtleback fairing
V	vertical tail (Series II)
V_1	vertical tail (Series III)
V_2	vertical tail, added span (Series III)
S_o	horizontal tail (Series II)
S_1	horizontal tail (Series III)
X	blade spoilers at 50-% chord, 0.05 C high, full span
X_1	blade spoilers at 50-% chord, 0.05 C high, partial span
Y	stall fences on hub
Z	strut-stiffening braces

TABLE F-2 (Continued)

MODEL SYMBOLS

A_1	rotor longitudinal cyclic pitch angle
B_1	rotor lateral cyclic pitch angle
i_s	horizontal stabilizer incidence
Δi_s	differential stabilizer incidence
N_R	rotor speed
q	tunnel dynamic pressure
α	model angle of attack
β	yaw angle
θ	rotor collective pitch angle
μ	rotor advance ratio
ρ	air density in tunnel
ψ	rotor azimuth angle

TABLE F-3

DEFINITION OF COEFFICIENTS

Lift coefficient	C_L	=	$\frac{L}{q\pi R^2}$
Drag coefficient	C_D	=	$\frac{D}{q\pi R^2}$
Side force coefficient	C_Y	=	$\frac{Y}{q\pi R^2}$
Rolling moment coefficient	$C_{\mathscr{L}}$	=	$\frac{\mathscr{L}}{q\pi R^3}$
Pitching moment coefficient	C_M	=	$\frac{M}{q\pi R^3}$
Yawing moment coefficient	C_N	=	$\frac{N}{q\pi R^3}$
Thrust coefficient	C_T	=	$\left(\frac{\mu^2}{2}\right) C_L$
Torque coefficient	C_Q	=	$\frac{\mu^2 Q}{2q\pi R^3}$
Bending moment coefficient	$\pm \bar{M}$	=	$\frac{\pm M}{LR}$

L	=	lift
D	=	drag
Y	=	side force
$\mathscr{L}$	=	rolling moment
M	=	pitching moment
N	=	yawing moment
Q	=	rotor torque
R	=	rotor radius

ROTOR/WING

Diameter	85.90 in.
Disc area	40.30 sq ft
Solidity ratio	0.149
Wing area	13.87 sq ft (hub + 2 blades), 14.68 sq ft (hub + 3 blades)
Aspect ratio	2.98 (hub + 2 blades), 2.82 (hub + 3 blades)
Collective pitch	-10 to +20 deg
Cyclic pitch	
Lateral	±15 deg
Longitudinal	±15 deg
Blade chord	6.66 in.
Blade thickness ratio	15 percent
Blade airfoil section	Modified circular arc

HORIZONTAL TAIL	SERIES II	SERIES III
Span	39.40 in.	54.00 in.
Area	3.61 sq ft	4.17 sq ft
Root chord (theoretical)	16.50 in.	12.00 in.
Aspect ratio	3.00	4.50
Taper ratio	0.60	0.83
Leading edge sweepback	25 deg	20 deg
Tail length (to ℄ rotor)	50.00 in.	52.41 in.
Airfoil section		
Root	NACA 0015	NACA 0015
Tip	NACA 0012	NACA 0012

VERTICAL TAIL

Span	19.60 in.	25.00 in.
Area	2.10 sq ft	2.88 sq ft
Root chord	21.20 in.	21.20 in.
Aspect ratio	1.27	1.50
Taper ratio	0.46	0.57
Leading edge sweepback	6 deg	5 deg
Tail length (to ℄ rotor)	50.30 in.	50.57 in.
Airfoil section		
Root	NACA 0019	NACA 0019
Tip	NACA 0009	NACA 0012

FUSELAGE

1. Tandem cockpit forward of blade tip, leading blade faired into fuselage
2. Tandem cockpit forward of blade tip, fuselage fairings open for blade clearance
3. Tandem cockpit beneath blade, leading blade not faired into fuselage

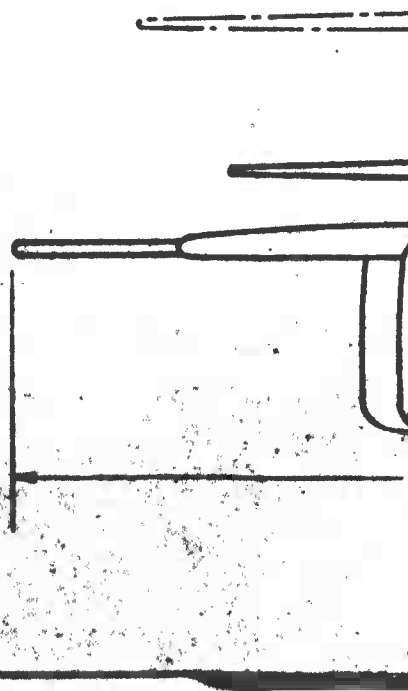

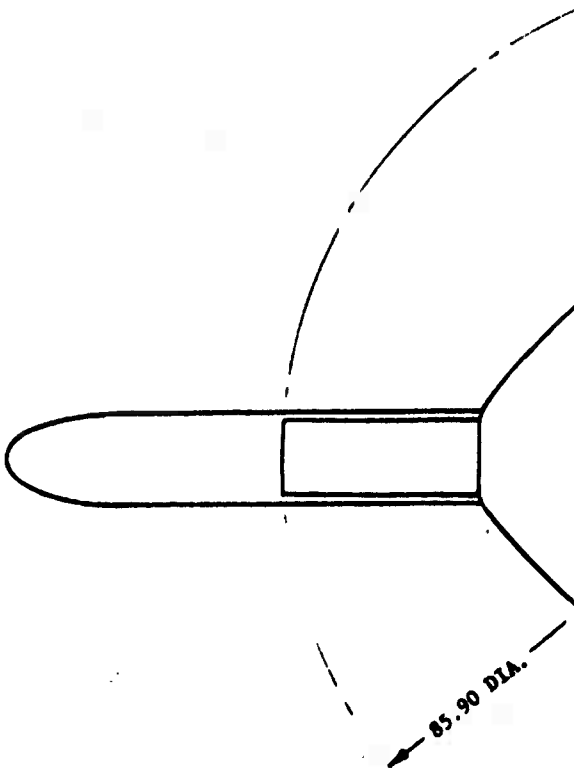
85.90 DIA.

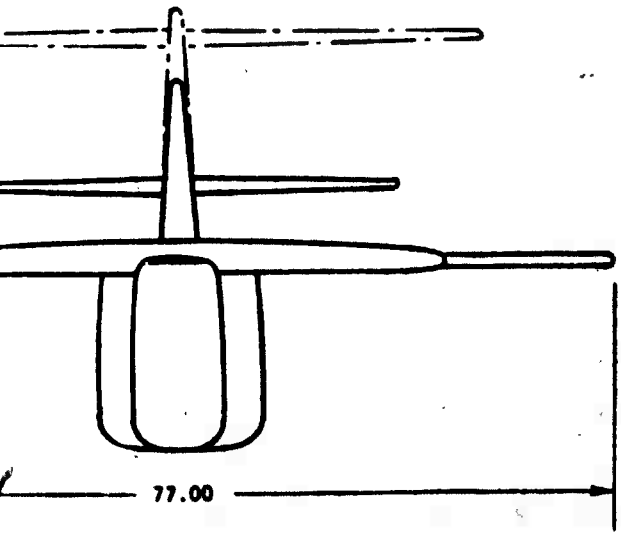
77.00

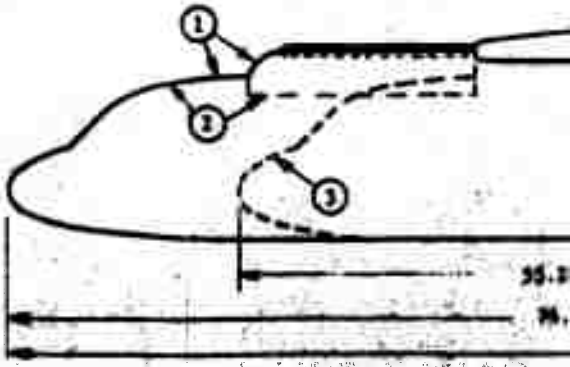
1
2
3

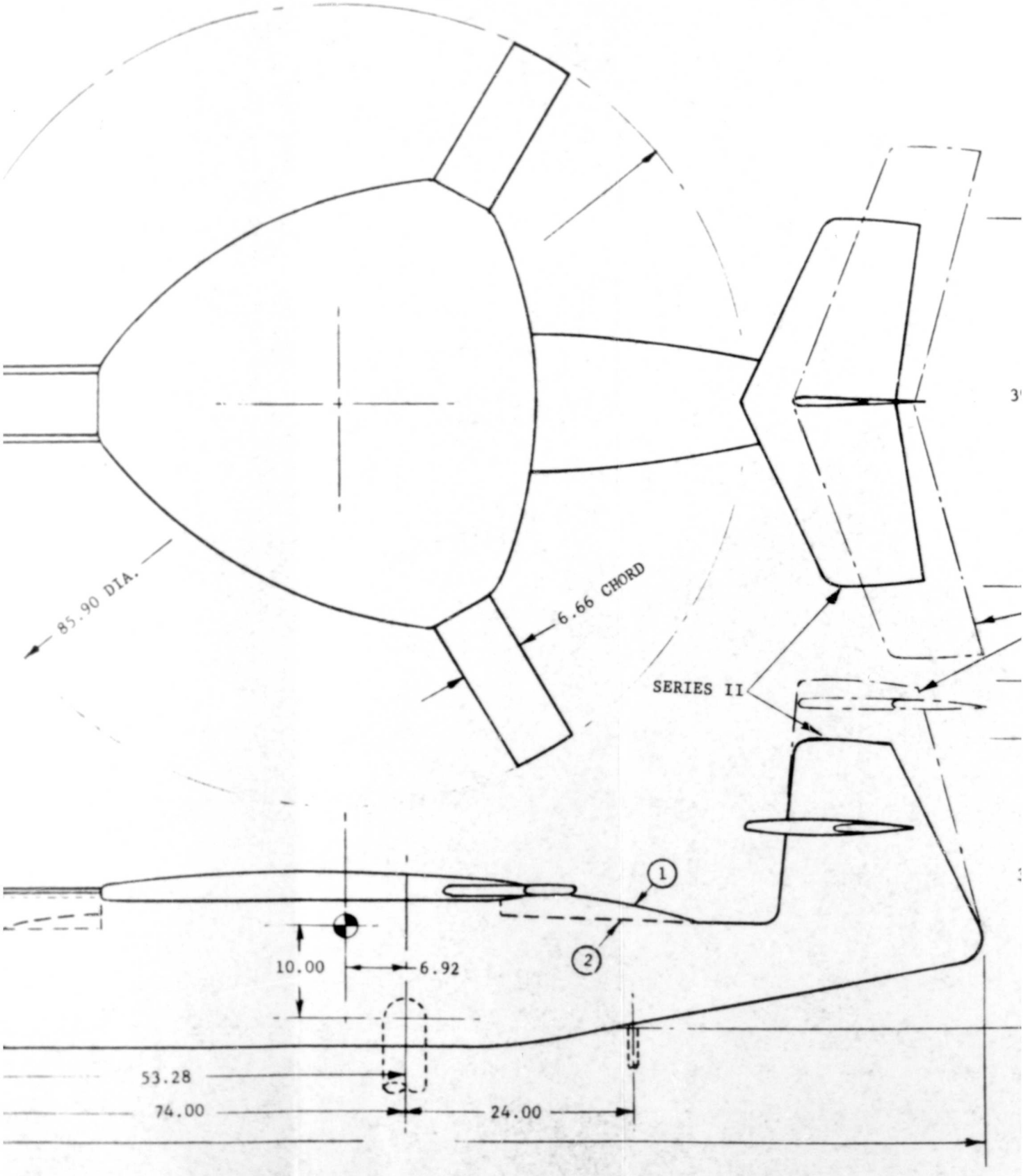

Figure F-1. General Arrangement, Rotor/Wing Wind Tunnel Model

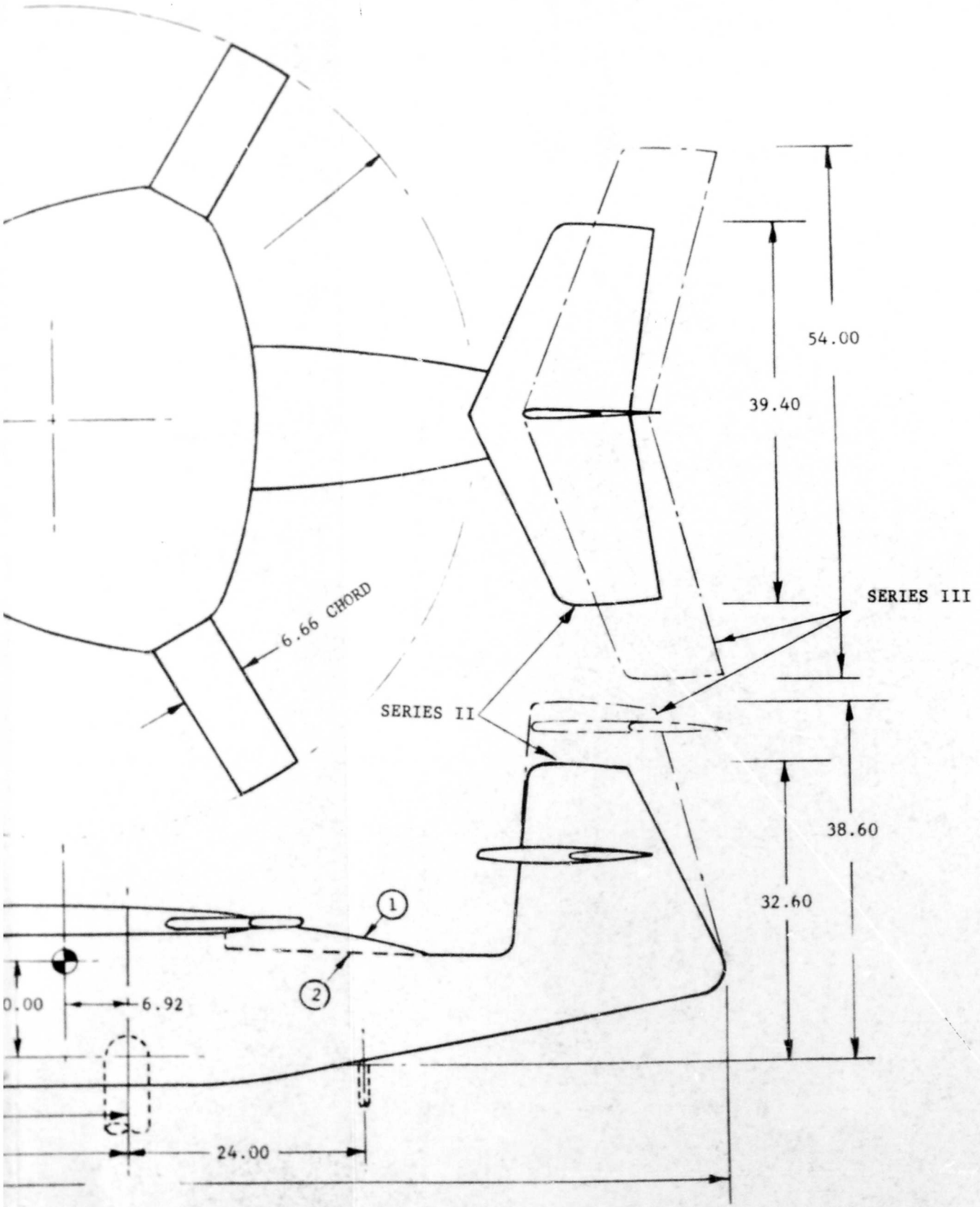

Figure F-1. General Arrangement, Rotor/Wing Wind Tunnel Model

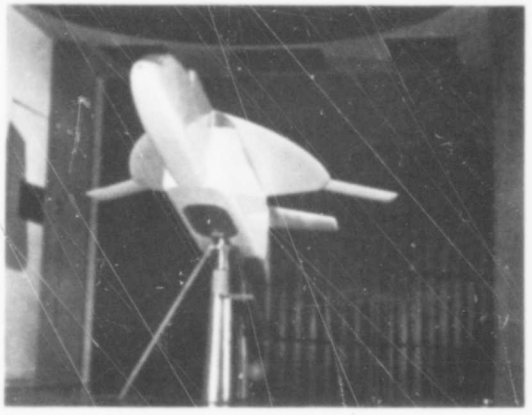

Stopped-Rotor Configuration,
Series II

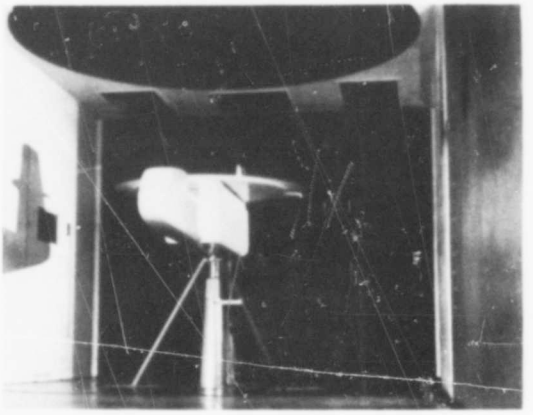

Running-Rotor Configuration,
Series II

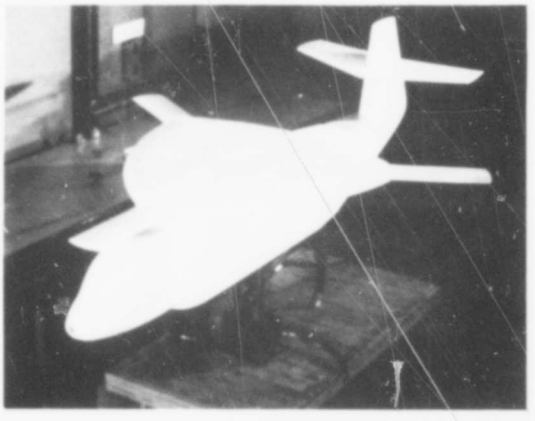

Stopped-Rotor Configuration,
Series II

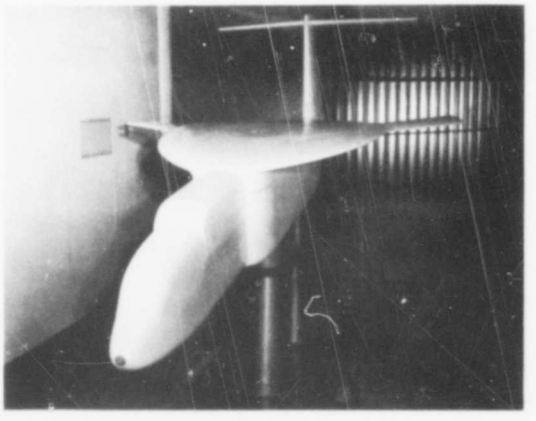

Stopped-Rotor Configuration,
Series III

Figure F-2. Rotor/Wing Wind Tunnel Model

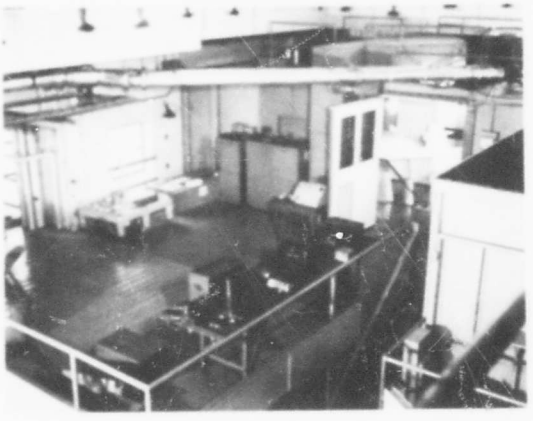

Overall View of Wind Tunnel

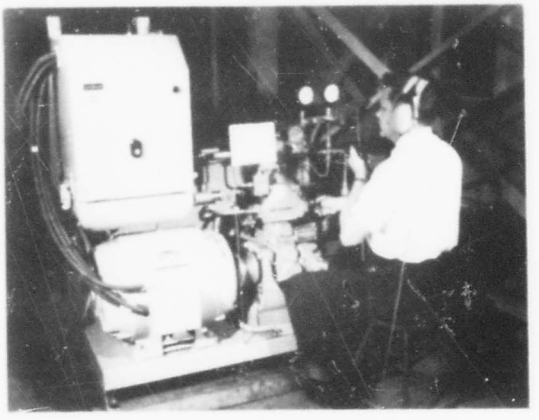

Hydraulic Power Supply Unit

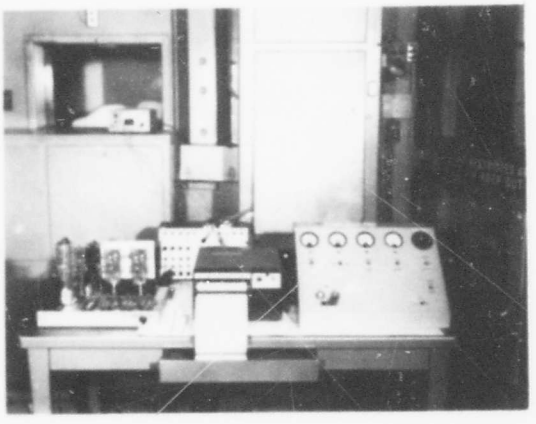

Model Instrumentation

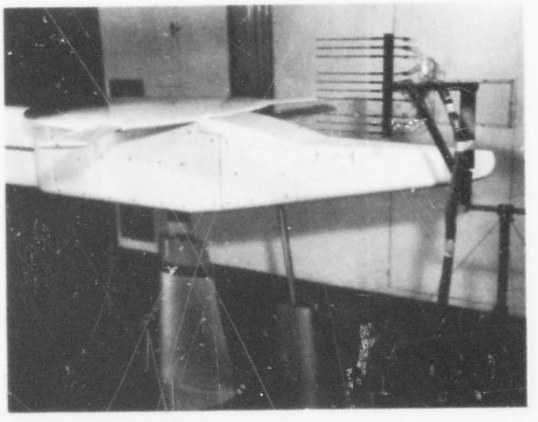

Pressure Survey Rake

Figure F-3. Rotor/Wing Model Installation

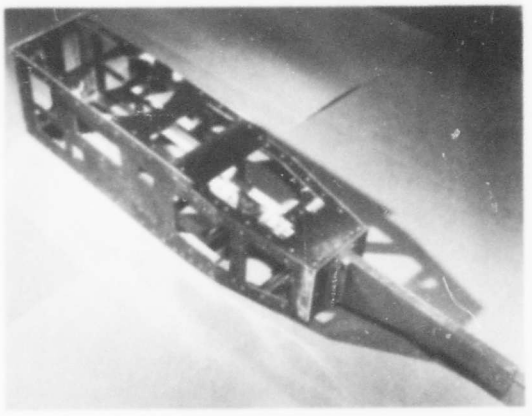

Model Structural Box

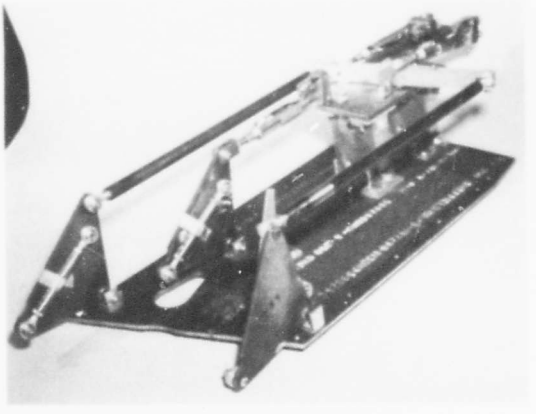

Cyclic and Collective
Control System

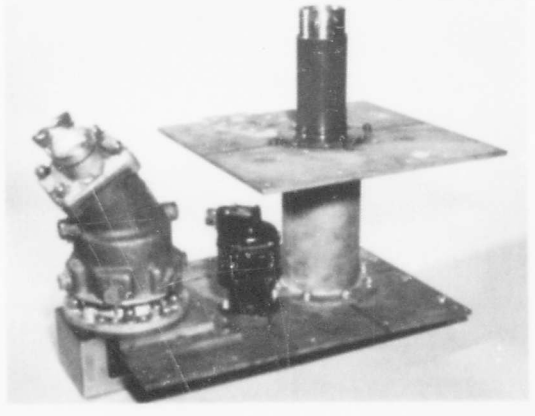

Rotor Mast and Drive Motor

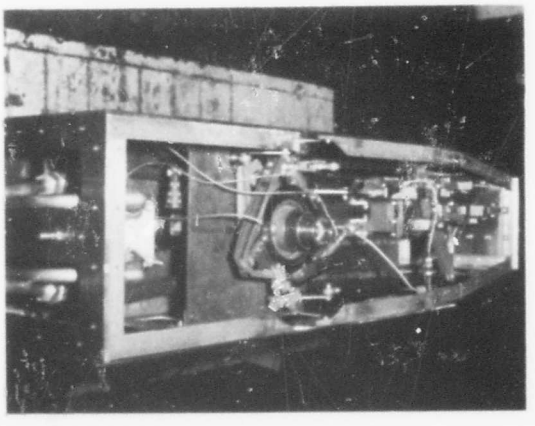

Fuselage Assembly

Figure F-4. Model Components

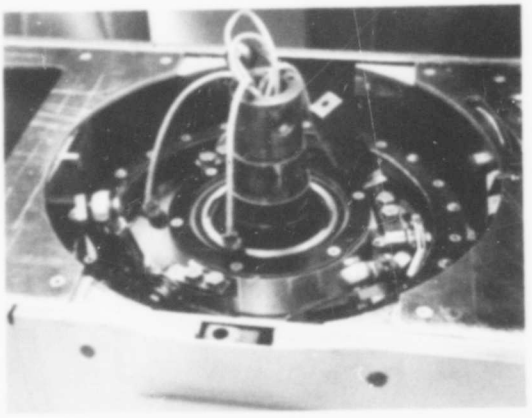

Two-Per-Rev Swashplate Assembly

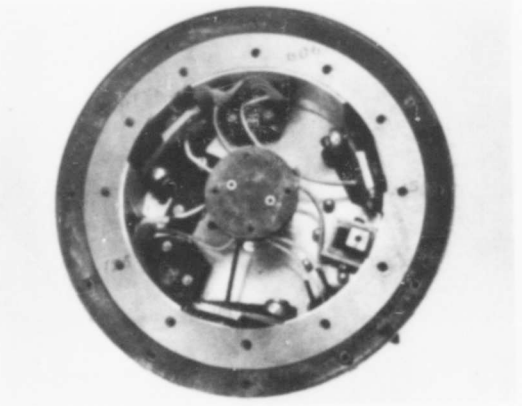

Hub Interior

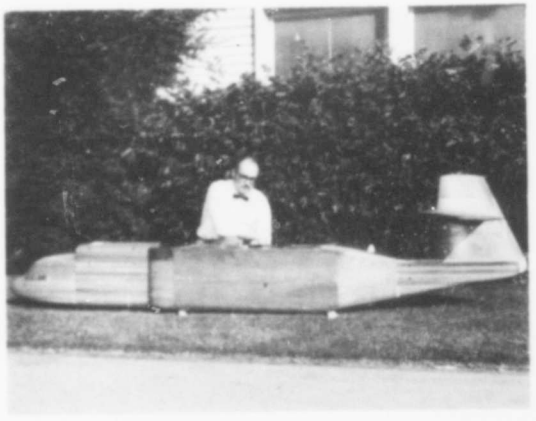

Fuselage and Tail

Rotor Blade Airfoil Section

Figure F-5. Model Components

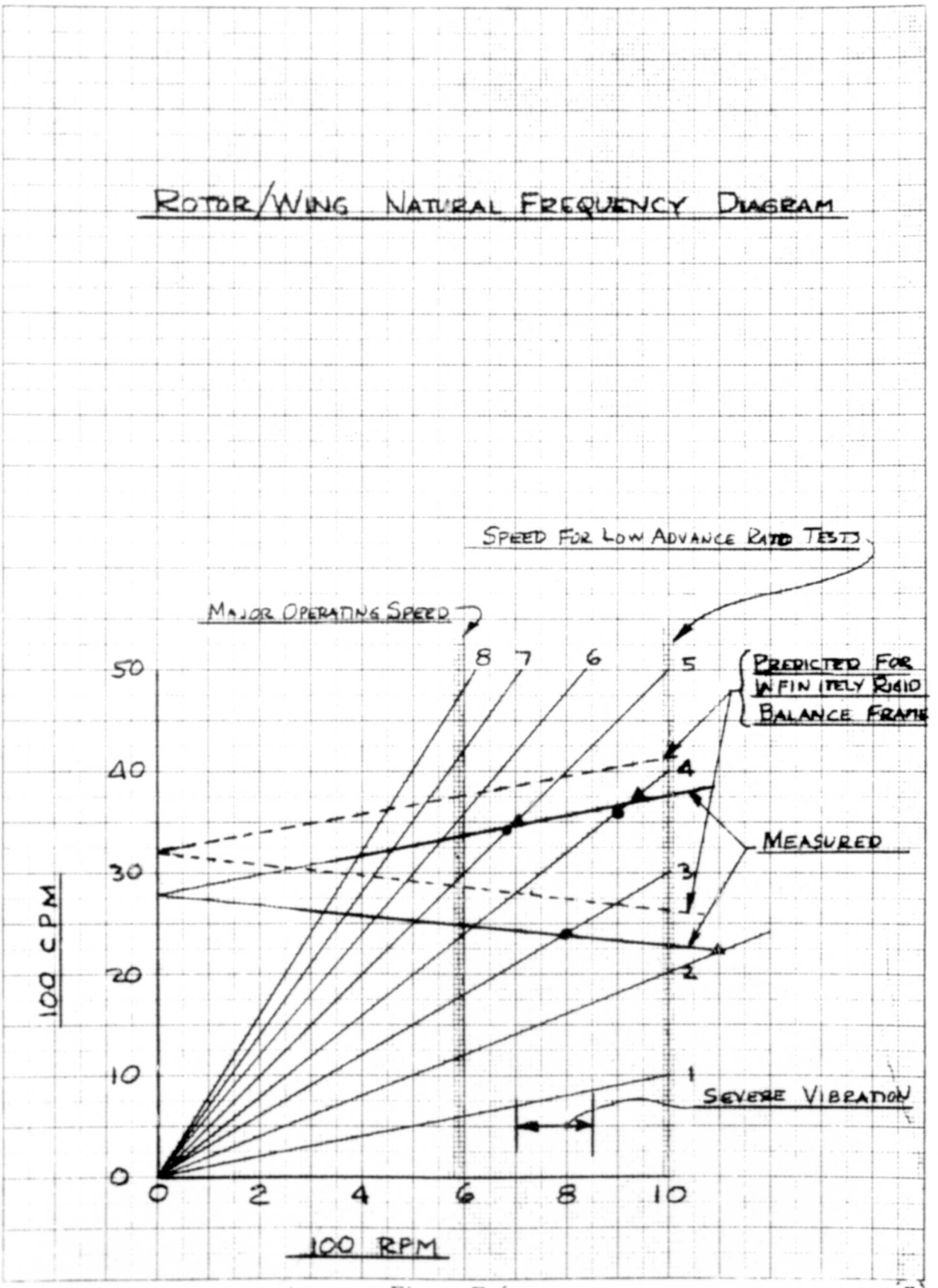
ROTOR/WING NATURAL FREQUENCY DIAGRAM
SPEED FOR LOW ADVANCE RATIO TESTS
MAJOR OPERATING SPEED
8
7
6
5
PREDICTED FOR INFINITELY RIGID BALANCE FRAME
4
MEASURED
3
2
1
SEVERE VIBRATION
50
40
30
20
10
0
100 CPM
0
2
4
6
8
10
100 RPM

Figure F-6

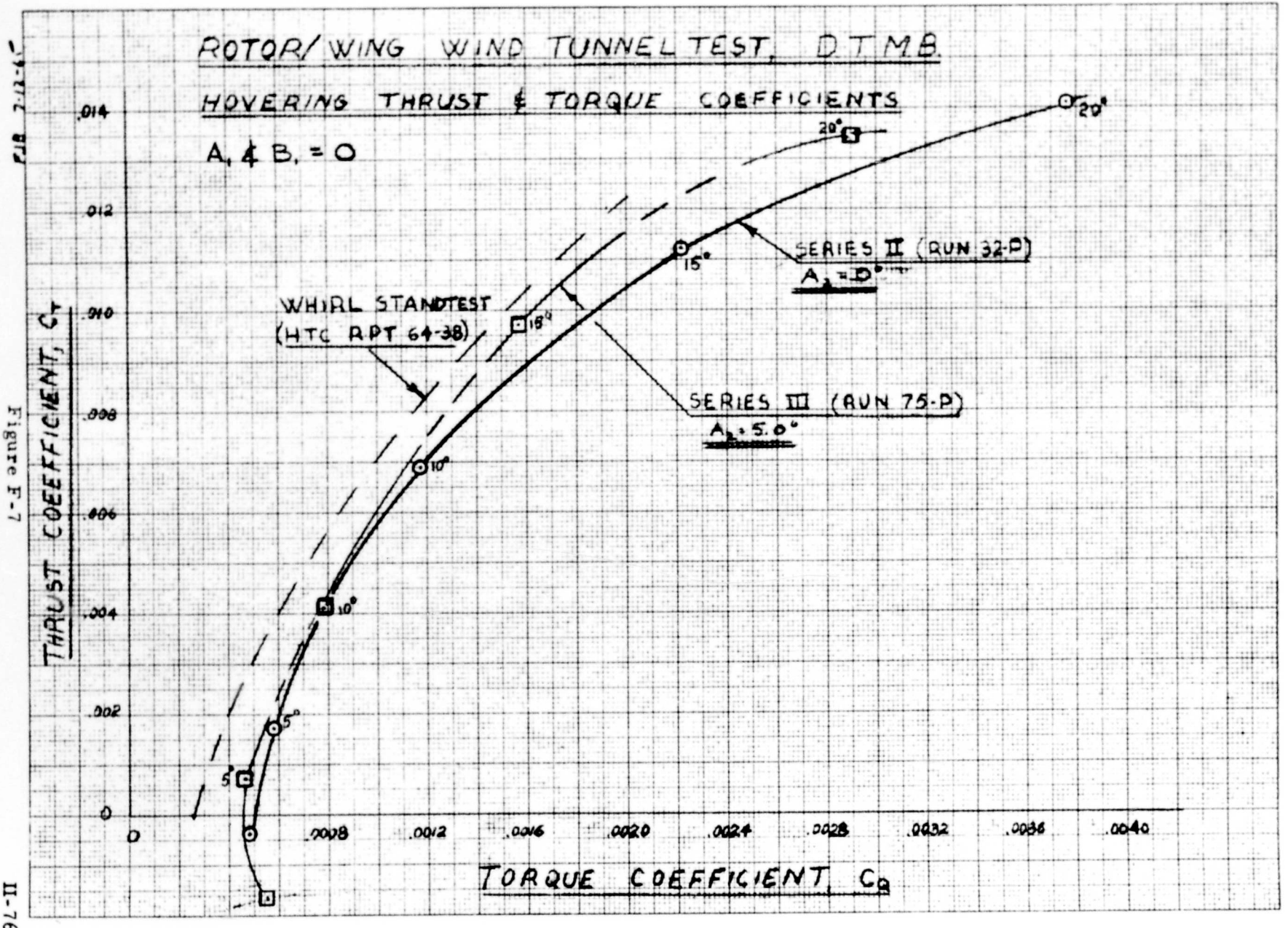
ROTOR/WING WIND TUNNEL TEST, D.T.M.B.
HOVERING THRUST & TORQUE COEFFICIENTS
A, & B, = 0
SERIES II (RUN 32-P)
A1 = 0°
SERIES III (RUN 75-P)
A1 = 5.0°
WHIRL STAND TEST
(HTC RPT 64-38)
THRUST COEFFICIENT, CT
TORQUE COEFFICIENT, CQ
.014
.012
.010
.008
.006
.004
.002
0
.0008
.0012
.0016
.0020
.0024
.0028
.0032
.0036
.0040
5°
10°
15°
18°
20°

Figure F-7

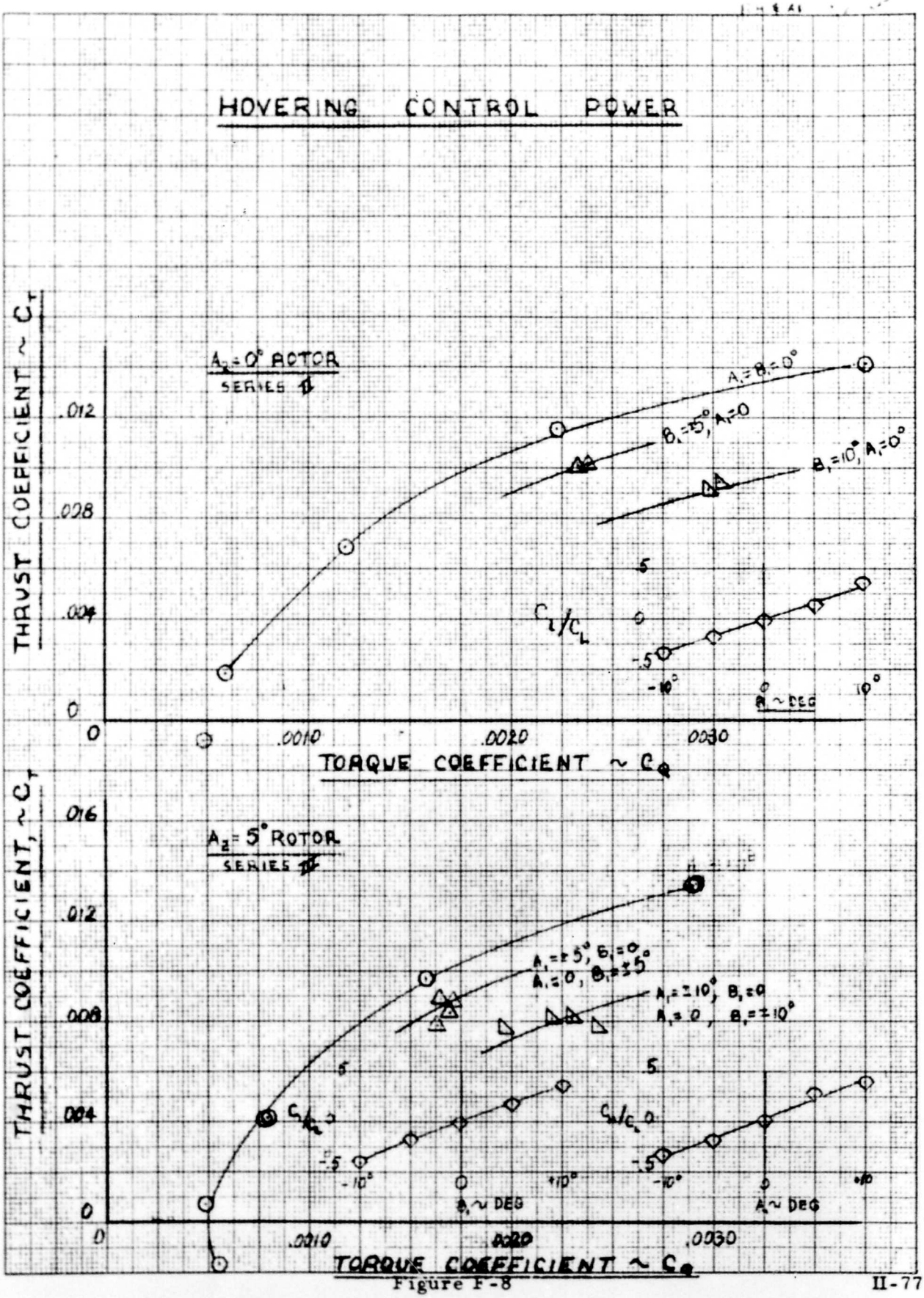
HOVERING CONTROL POWER
THRUST COEFFICIENT ~ C_T
A_2 = 0° ROTOR
SERIES 1
.012
.008
.004
0
$A_1 = B_1 = 0°$
$B_1 = 5°, A_1 = 0$
$B_1 = 10°, A_1 = 0°$
C_L/C_L
5
0
-5
-10°
θ ~ DEG
10°
0
.0010
.0020
.0030
TORQUE COEFFICIENT ~ C_Q
THRUST COEFFICIENT, ~ C_T
A_2 = 5° ROTOR
SERIES 1
.016
.012
.008
.004
0
$A_1 = \pm 5°, B_1 = 0°$
$A_1 = 0, B_1 = \pm 5°$
$A_1 = \pm 10°, B_1 = 0$
$A_1 = 0, B_1 = \pm 10°$
C_L/C_L
B_1 ~ DEG
A_1 ~ DEG
0
.0010
.0020
.0030
TORQUE COEFFICIENT ~ C_Q

Figure F-8

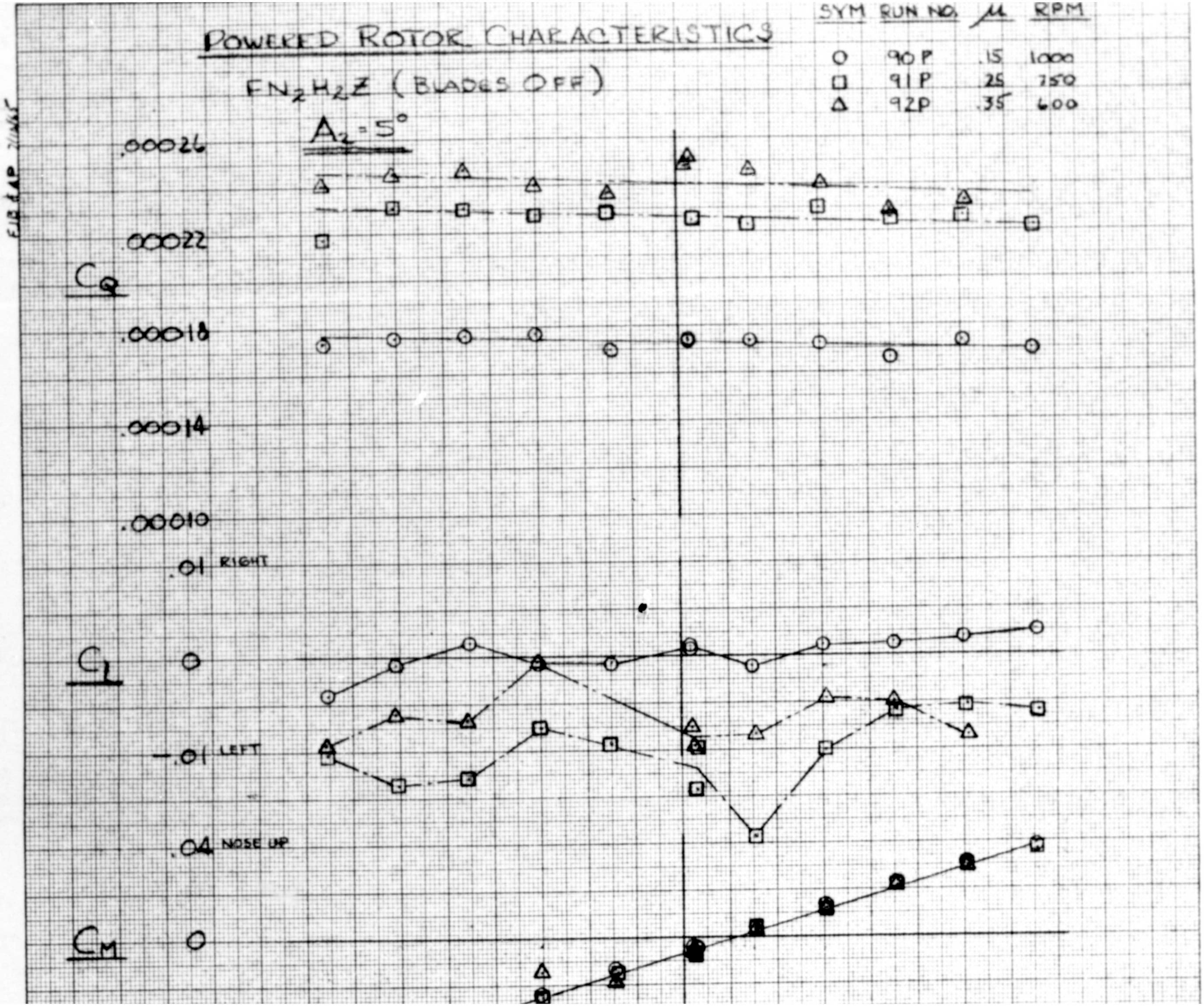

POWERED ROTOR CHARACTERISTICS
FN2H2Z (BLADES OFF)
A2 = 5°
SYM RUN NO. μ RPM
○ 90P .15 1000
□ 91P .25 750
△ 92P .35 600
.00026
.00022
.00018
.00014
.00010
CQ
.01 RIGHT
CL
0
-.01 LEFT
.04 NOSE UP
CM
0

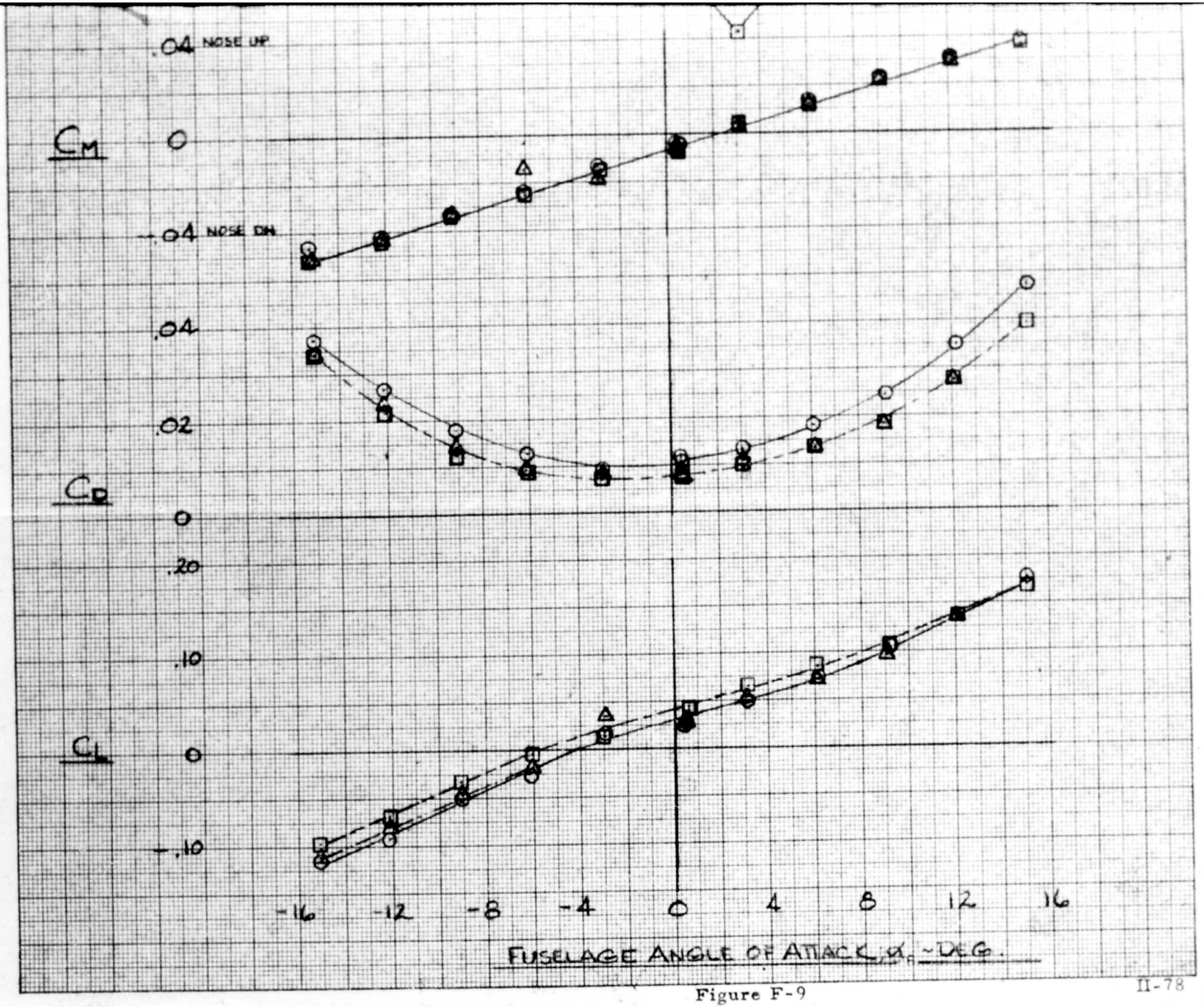

Figure F-9

II-78

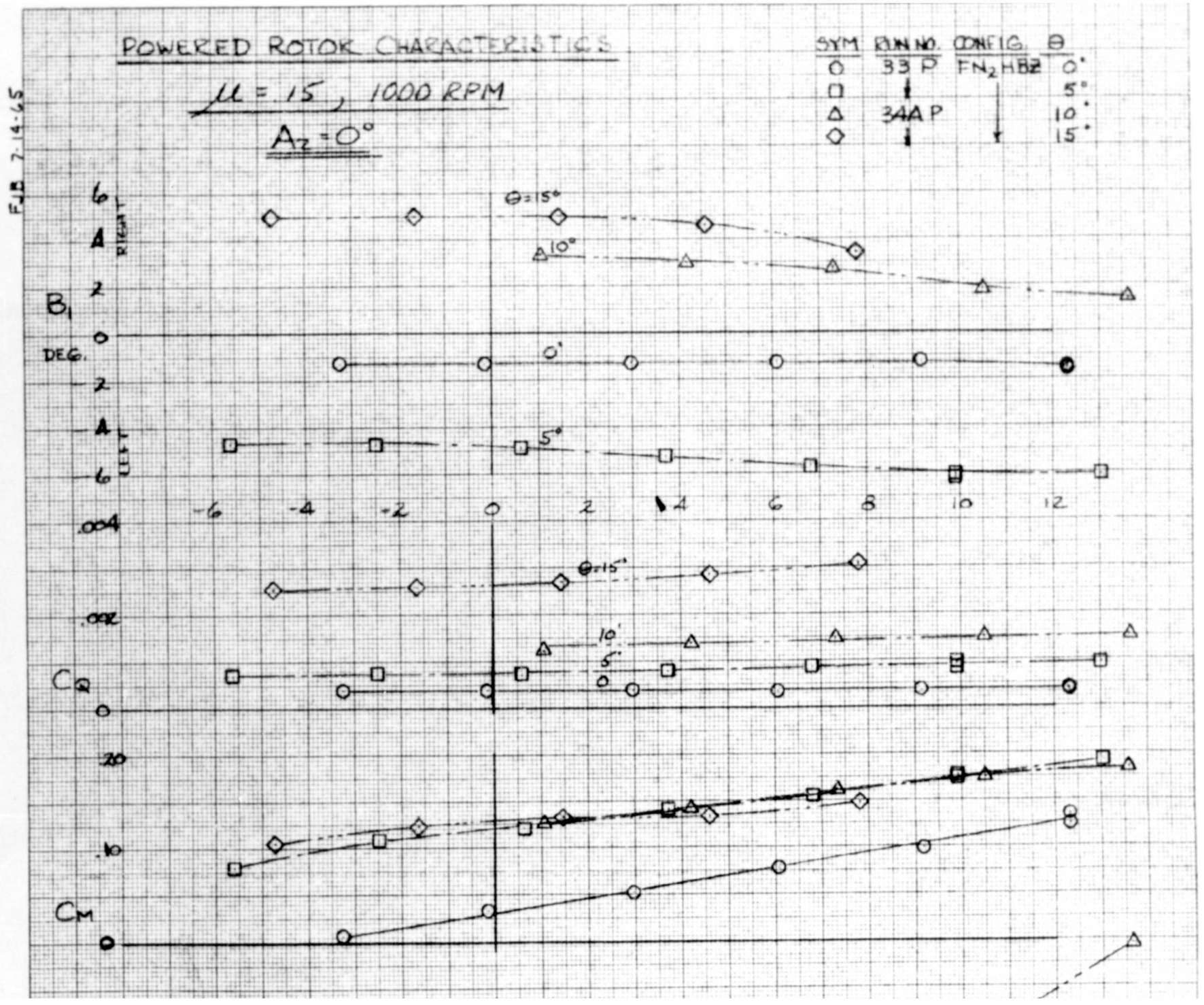
POWERED ROTOR CHARACTERISTICS
μ = .15, 1000 RPM
A_z = 0°
SYM RUN NO. CONFIG. θ
33 P FN2 HB2 0°
5°
34A P 10°
15°
FJB 7-14-45
B_1 DEG.
RIGHT
LEFT
θ=15°
10°
0°
5°
C_Q
C_M
-6 -4 -2 0 2 4 6 8 10 12
.004
.002
0
.20
.10
0

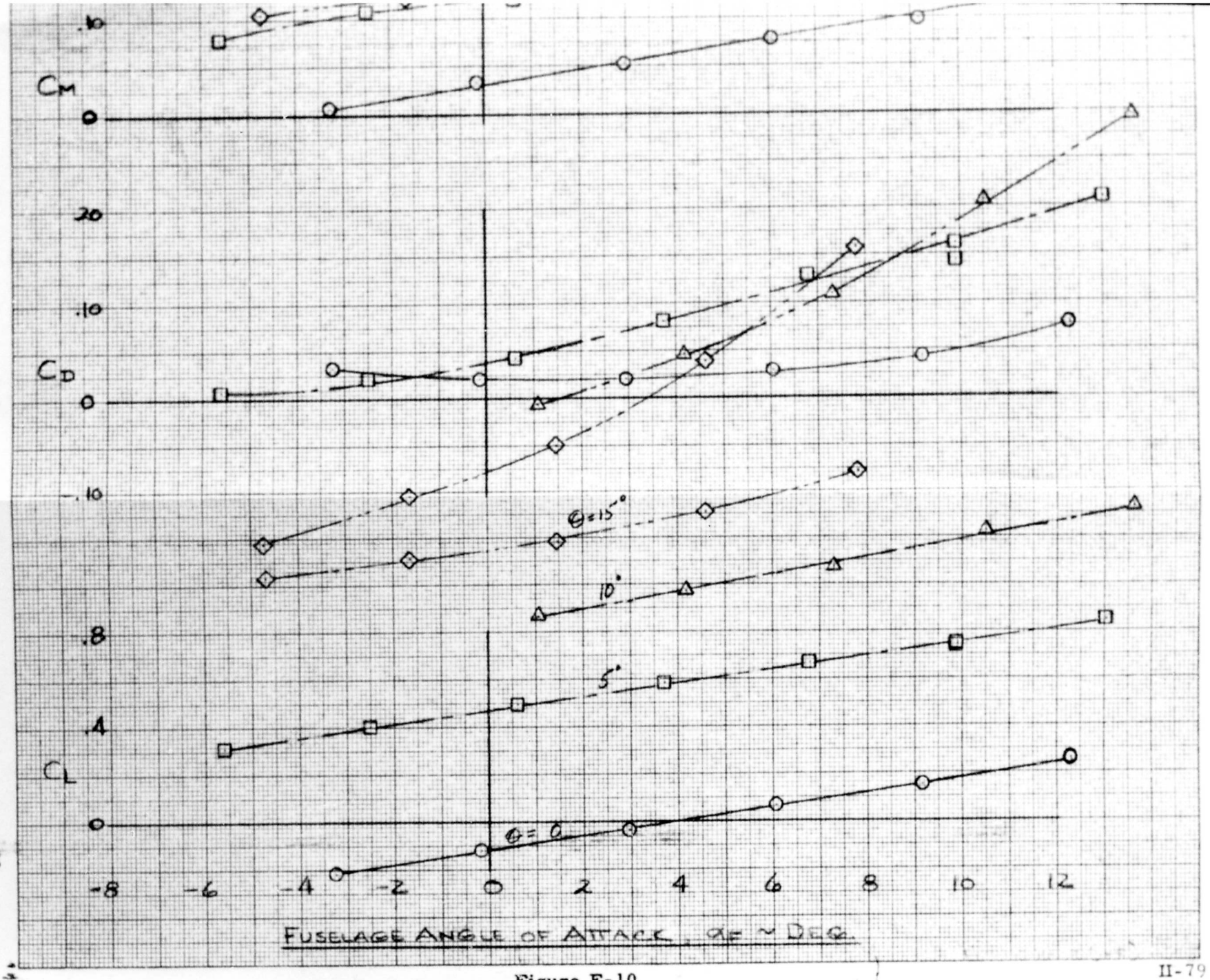
.10
C_M
0
.20
.10
C_D
0
-.10
Θ=15°
10°
.8
5°
.4
C_L
0
Θ=0
-8
-6
-4
-2
0
2
4
6
8
10
12
FUSELAGE ANGLE OF ATTACK, α_F ~ DEG.

Figure F-10

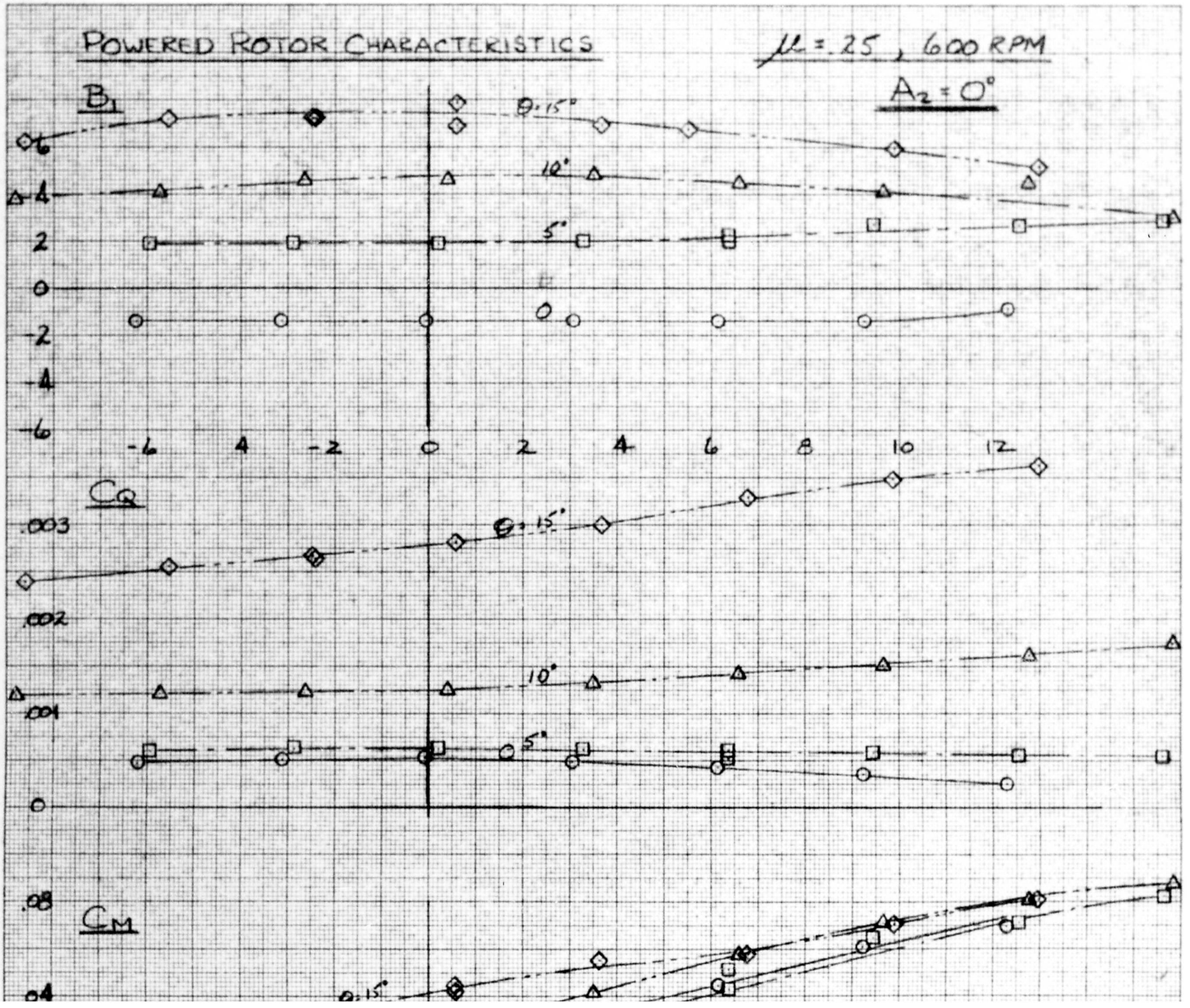
POWERED ROTOR CHARACTERISTICS
μ = .25 , 600 RPM
$A_2 = 0°$
B_1
θ 15°
10°
5°
0
6
4
2
0
-2
-4
-6
-6
-4
-2
0
2
4
6
8
10
12
C_Q
.003
.002
.001
0
15°
10°
5°
.08
C_M
.04
15°

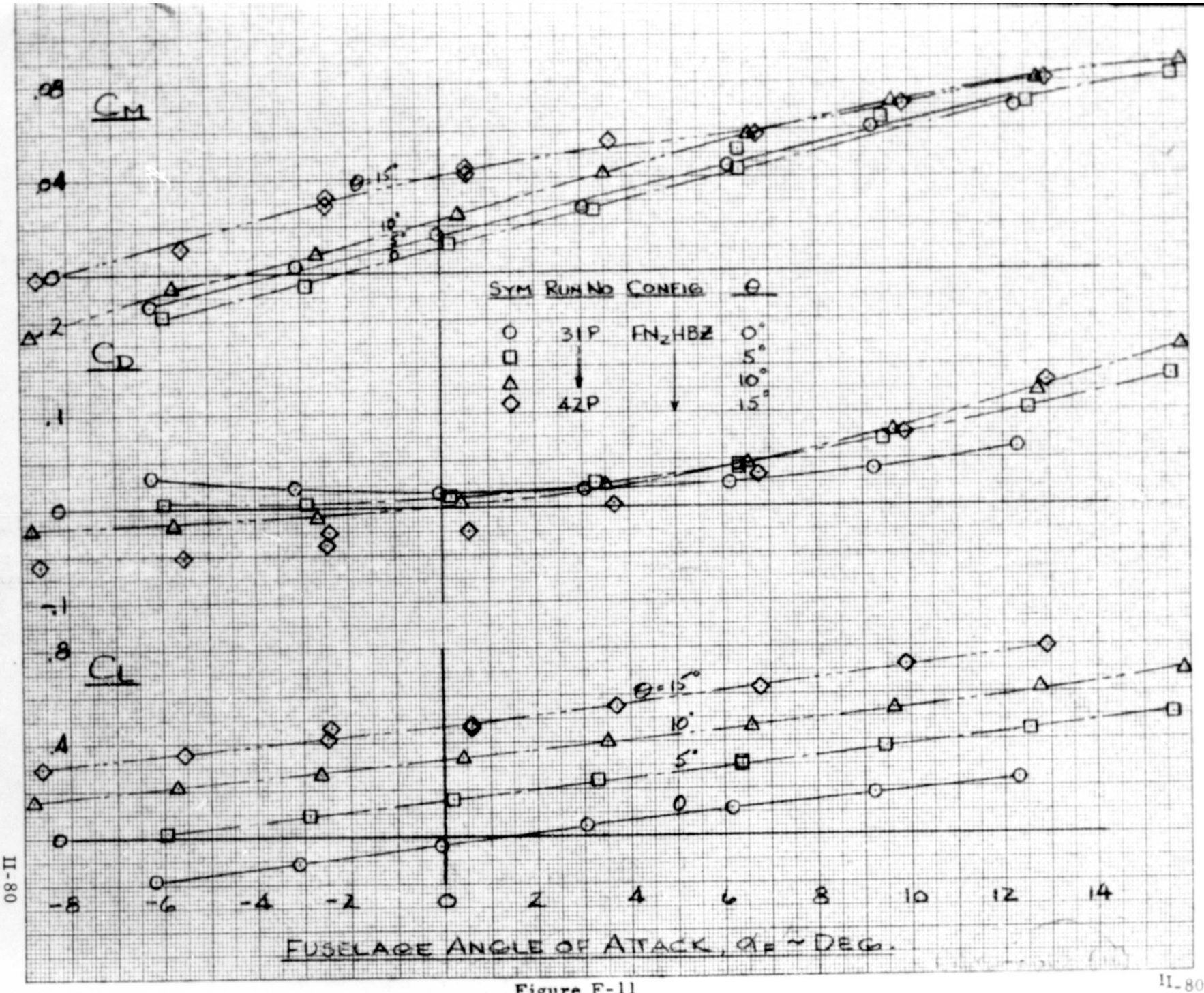

Figure F-11

II-80

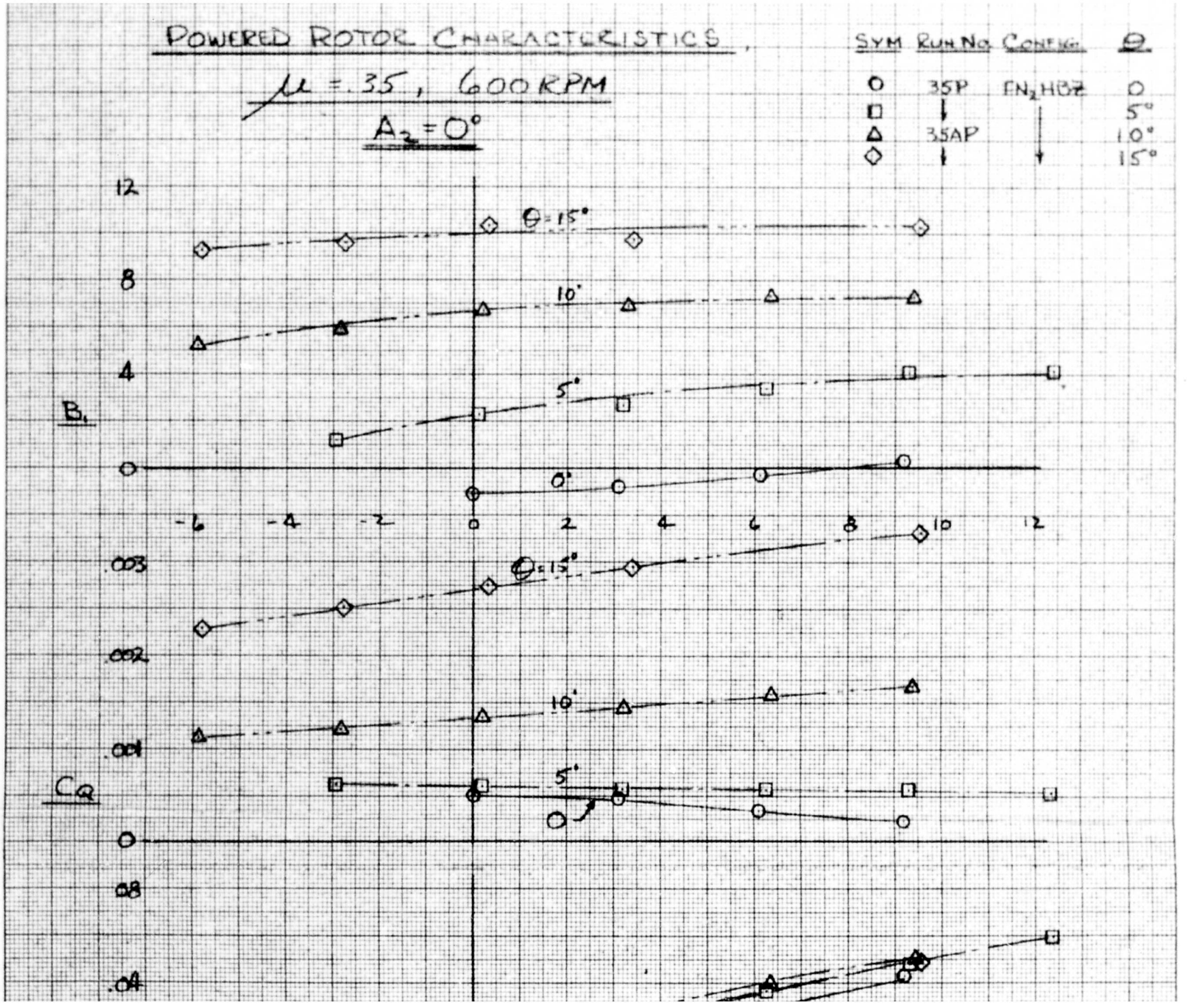
POWERED ROTOR CHARACTERISTICS
μ = .35, 600 RPM
A₂ = 0°
SYM RUN NO CONFIG θ
35P EN₂HBZ
35AP
0
5°
10°
15°
B₁
θ=15°
10°
5°
0°
12
8
4
0
-6
-4
-2
0
2
4
6
8
10
12
CQ
.003
.002
.001
0
.08
.04

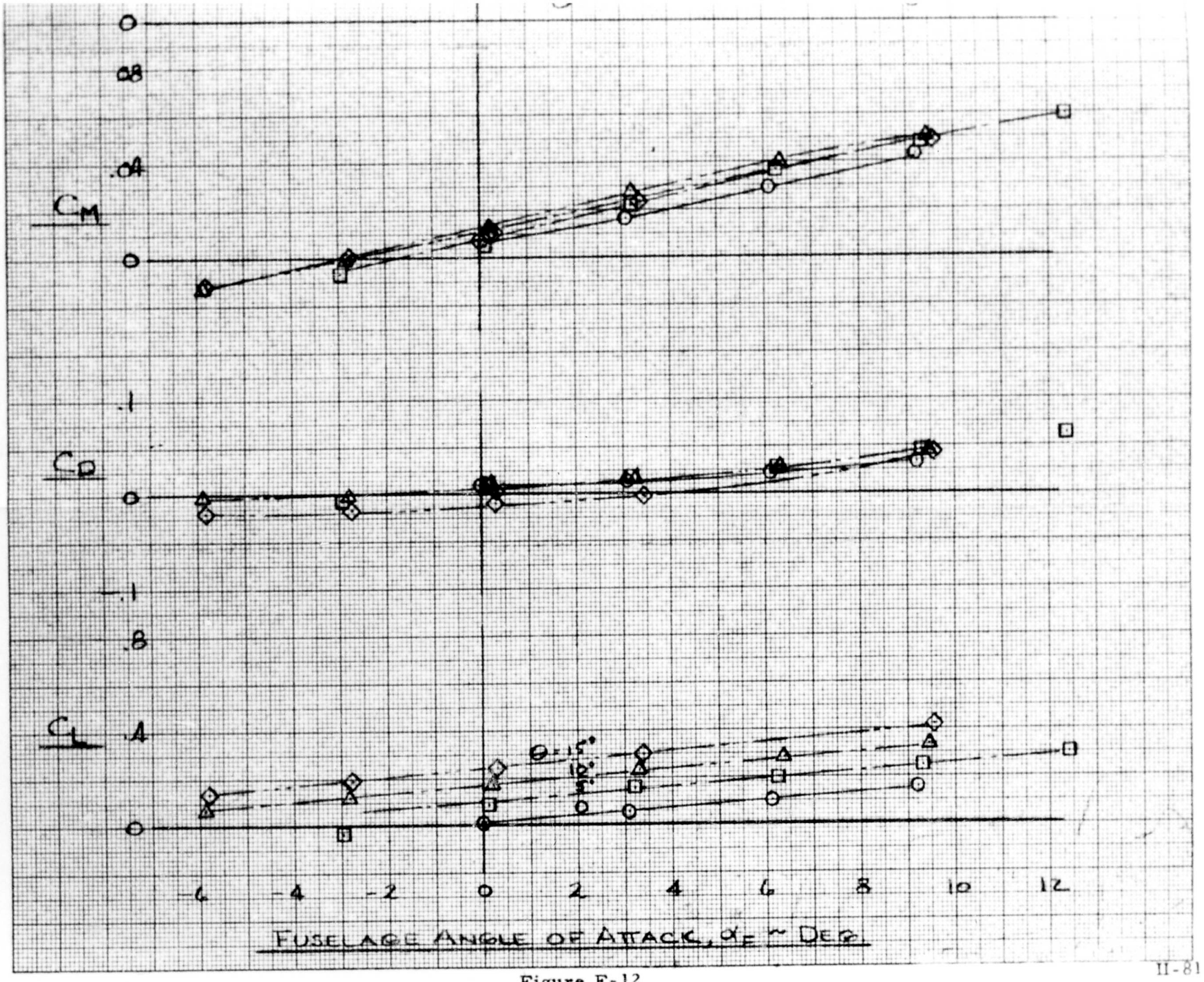

Figure F-12

II-81

POWER ROTOR CHARACTERISTICS

LATERAL CONTROL POWER AVAILABLE

FTR & AP 7/23/65

$\mu = .25$
600 RPM
$\theta = 10°$

$A_2 = 0°$

SYM	CONFIG	RUN NO	COMMENT
△	FN_2HBVS_2	39P	TAIL ON $i_t = 15°$
□	FN_2HB	40P	TAIL OFF

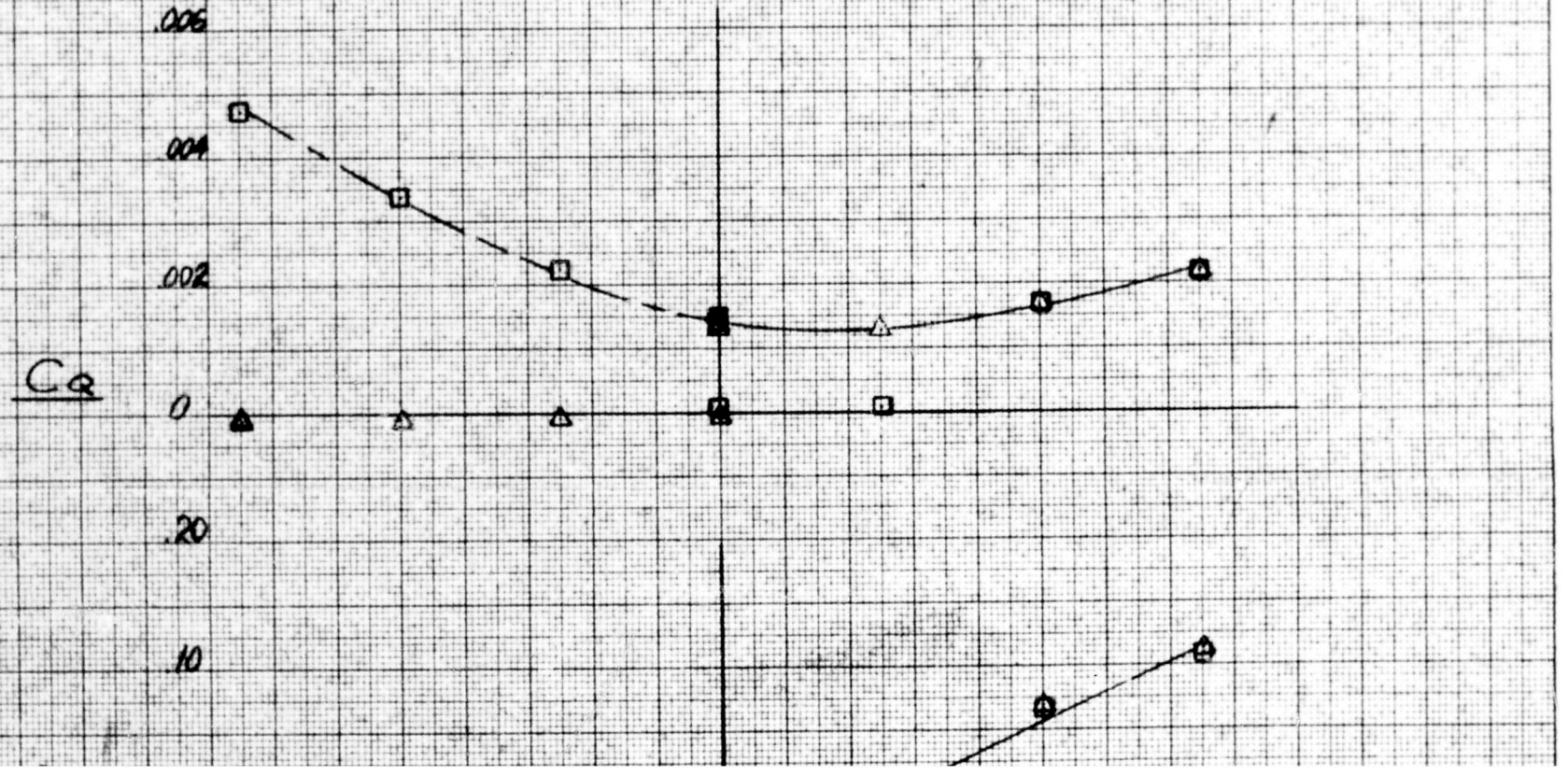

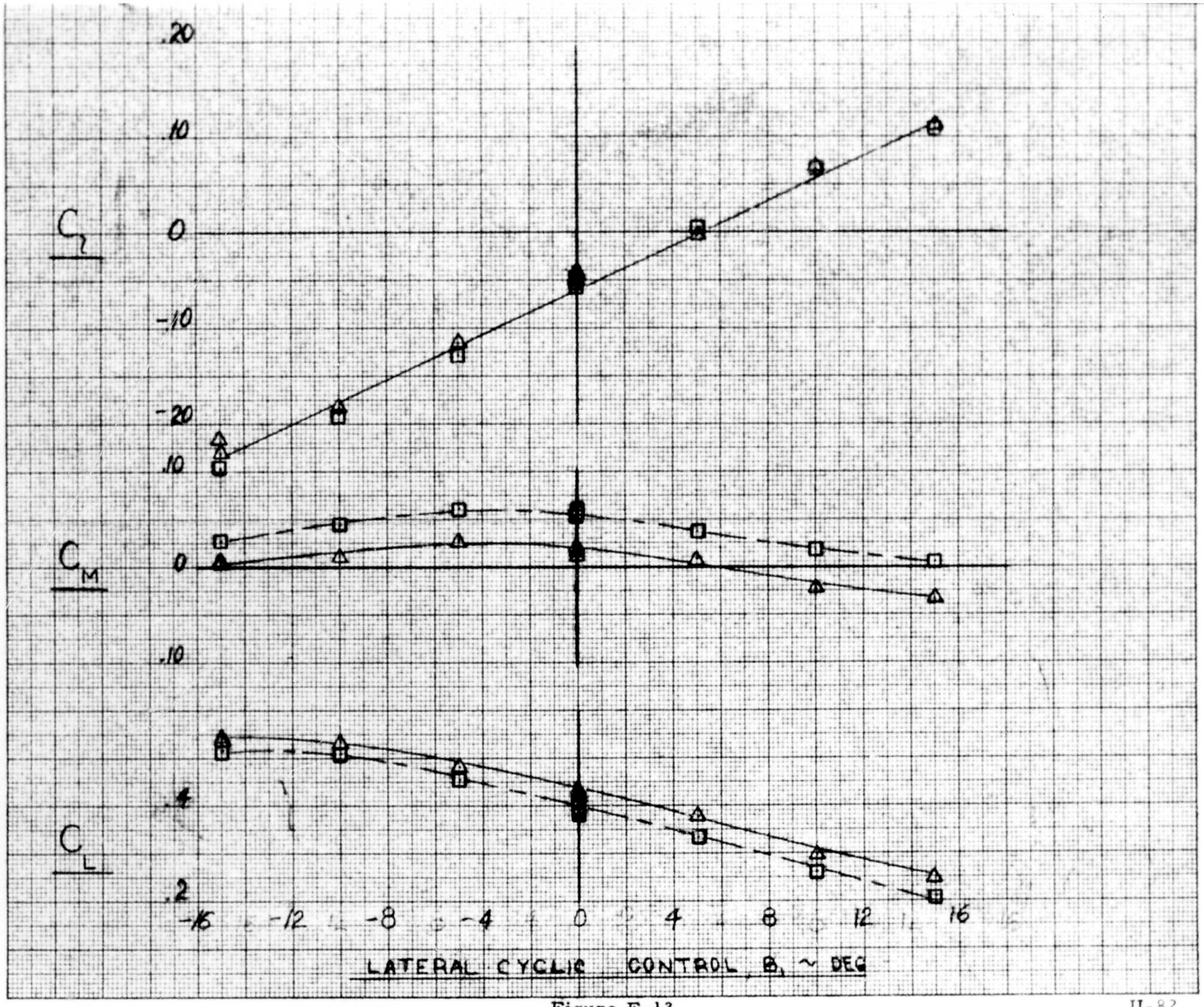

Figure F-13

II-82

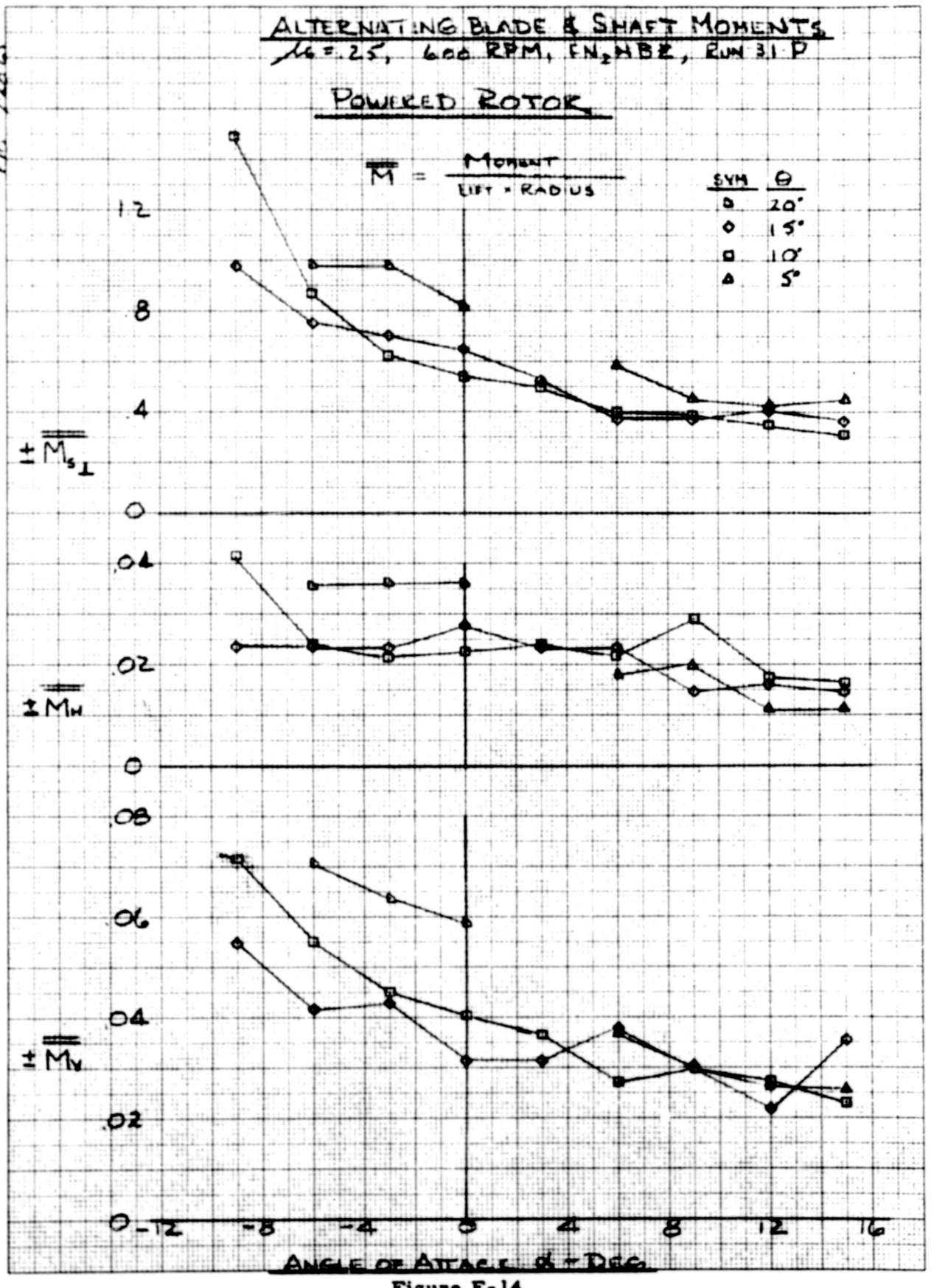

Figure F-14
(Sheet 1 of 2)

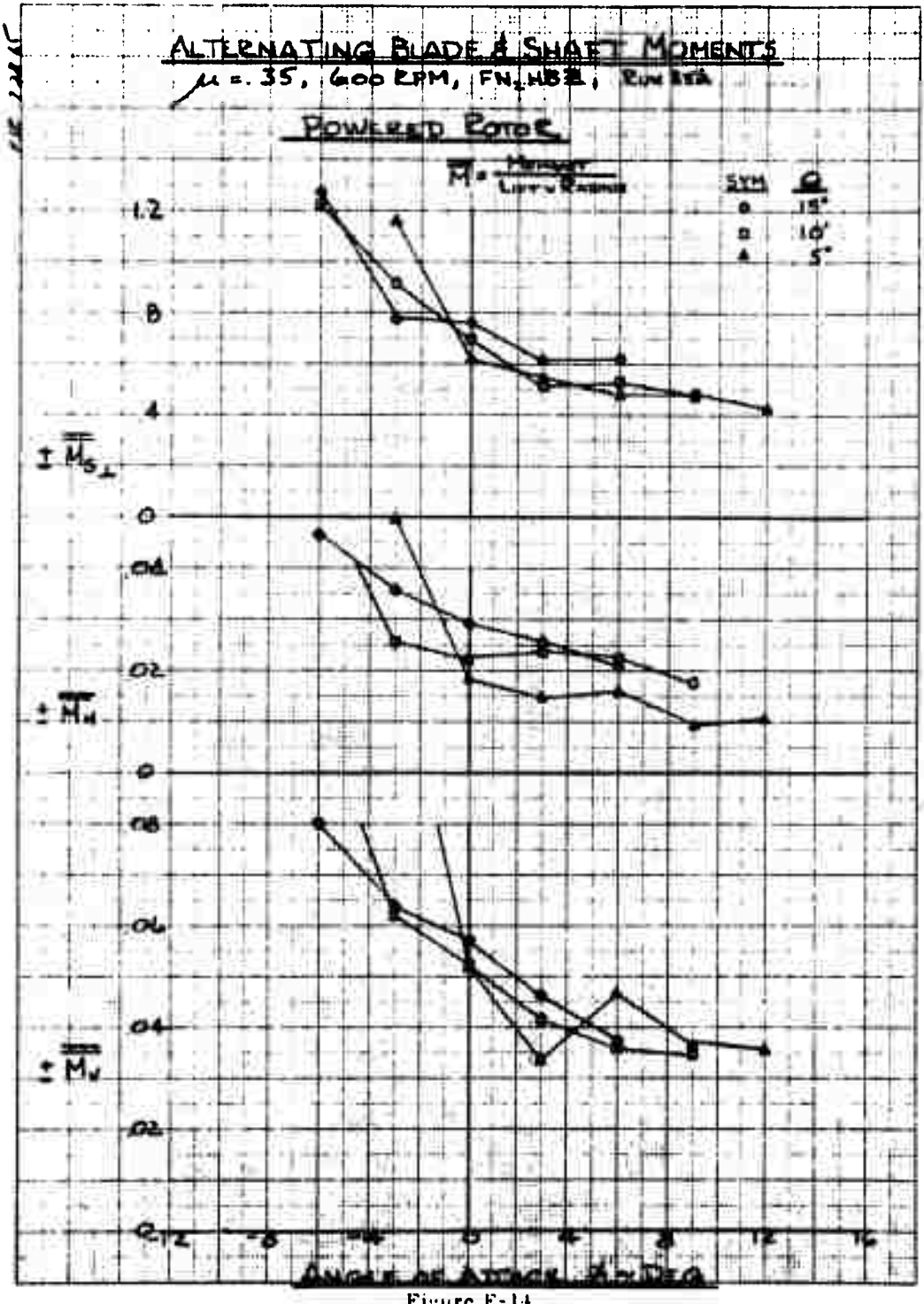

Figure F-14
(Sheet 2 of 2)

F.J.B. 4.8° 2/22/65

HORIZONTAL TAIL EFFECTIVENESS WITH POWERED ROTOR

$\mu = .15$
$\theta = 10°$

$A_2 = 0°$

SYM	RUN NO	CONFIG	i_t
○	36 P	$FN_2HBVS_{.2}$	$-5°$
△	37 P	↓	$+5°$
□	36 P	↓	$+15°$
×	31 P	FN_2HBZ	OFF

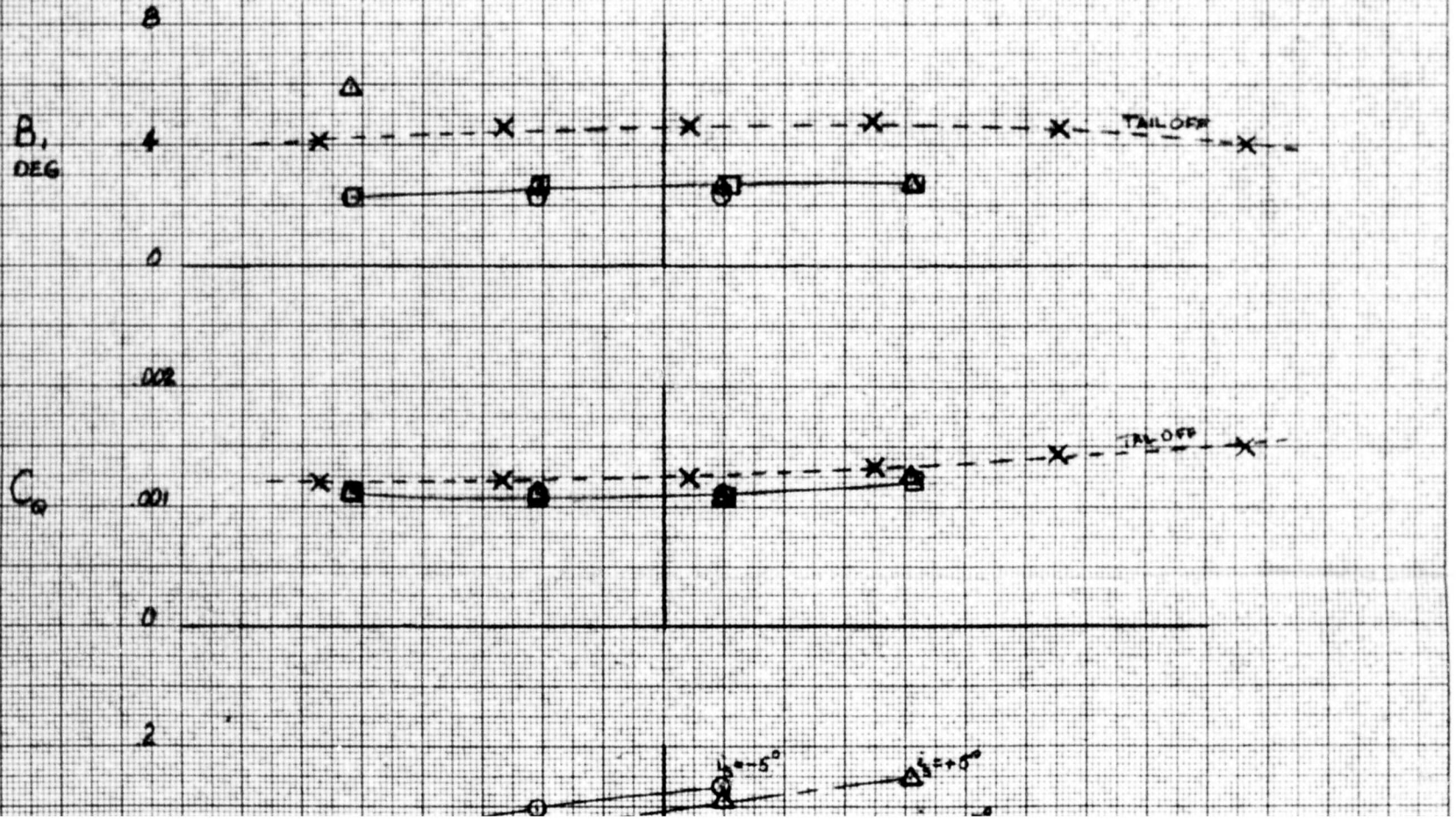

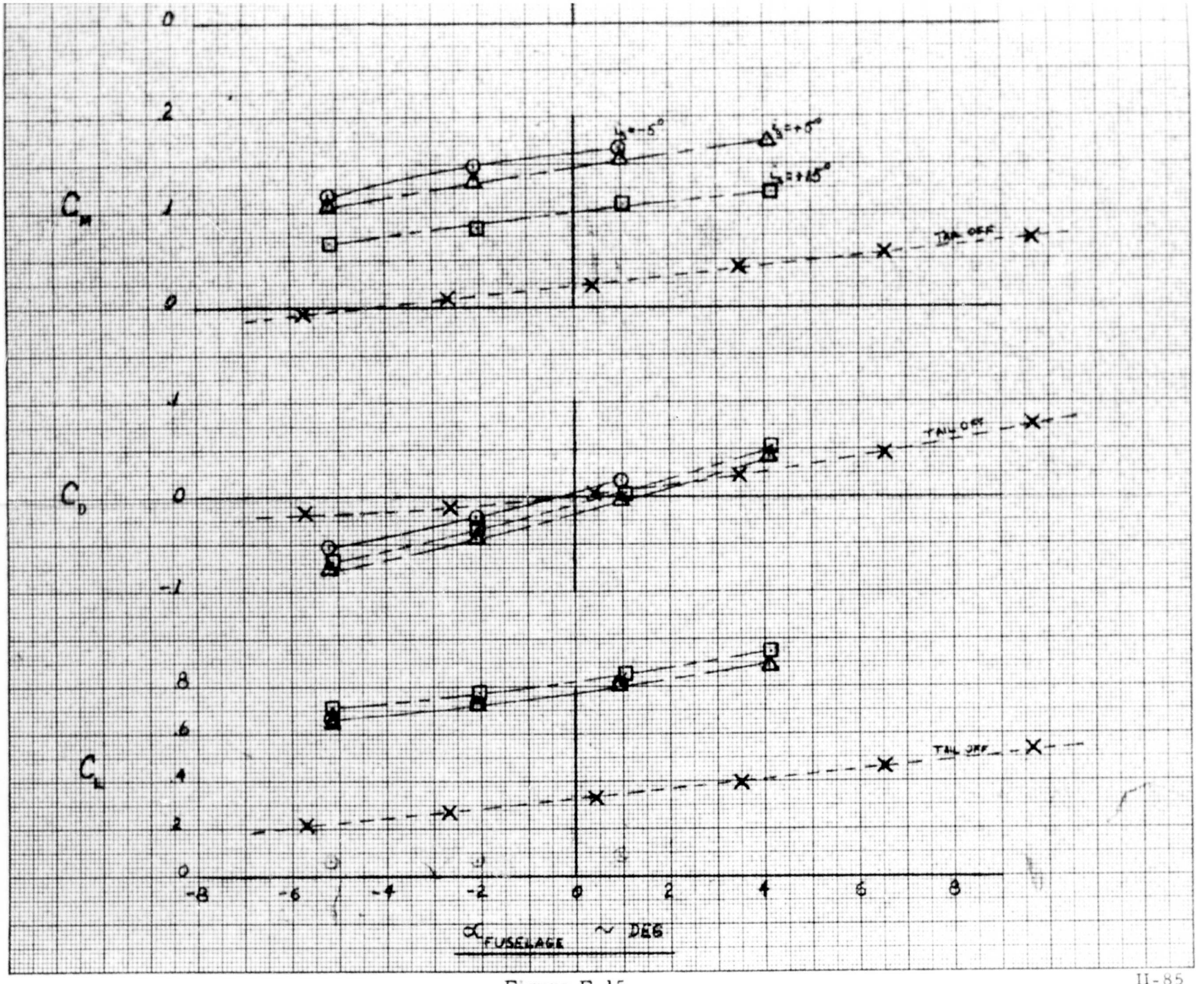
C_M
C_D
C_L
δ_E=-5°
δ_E=+5°
δ_E=+15°
TAIL OFF
TAIL OFF
TAIL OFF
$\alpha_{FUSELAGE}$ ~ DEG

Figure F-15

HORIZONTAL TAIL EFFECTIVENESS WITH POWERED ROTOR

$\mu = 2.5$
$\Theta = 10°$

$A_z = 0°$

SYM	RUN NO	CONFIG	i_t
○	36 P	$FN_2HBV_{5.2}Z$	$-5°$
△	37 P	↓	$+5°$
□	38 P	↓	$+15°$
✕	34A P	FN_2HBZ	OFF

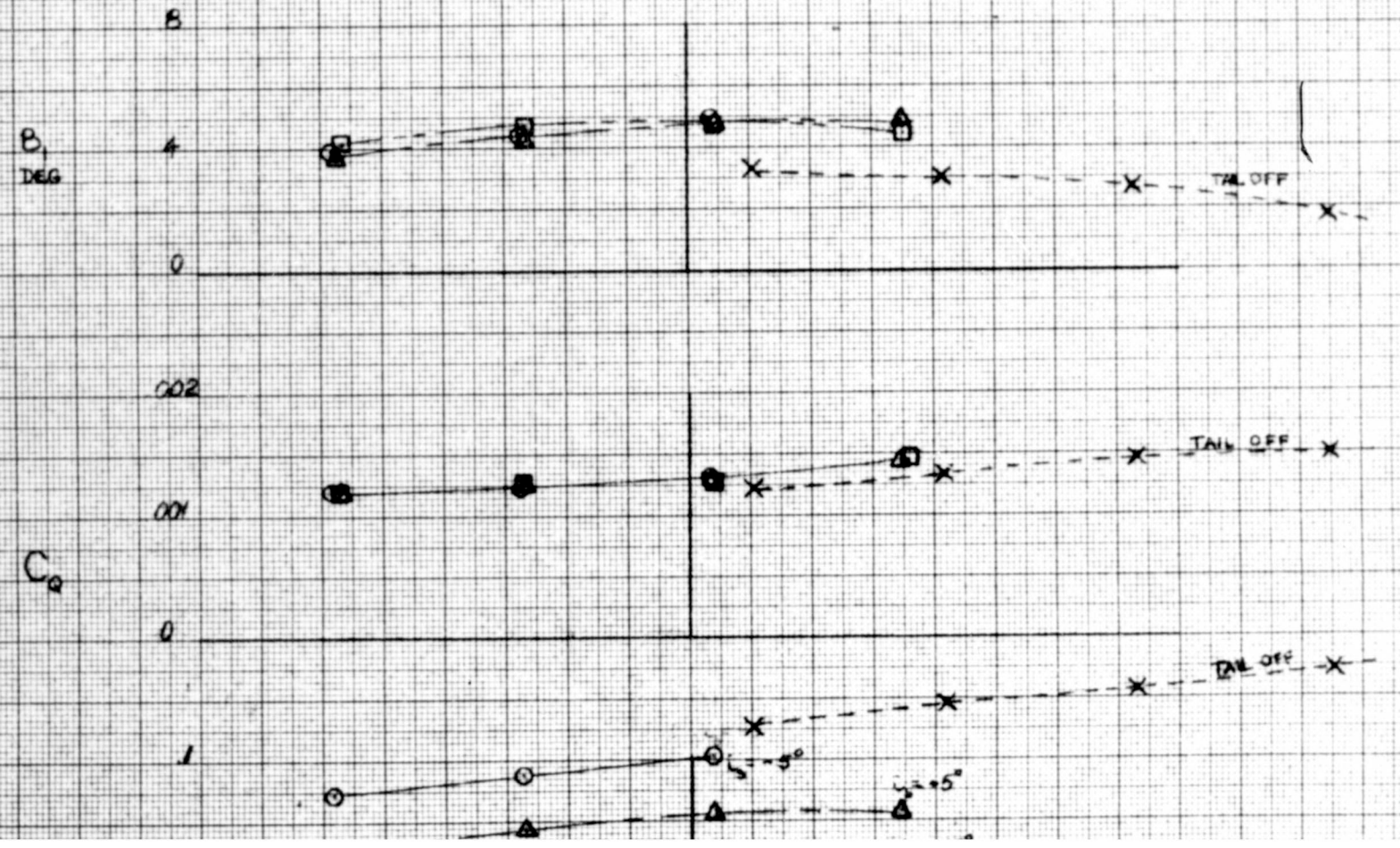

E.S.R. & AP 7/22/65

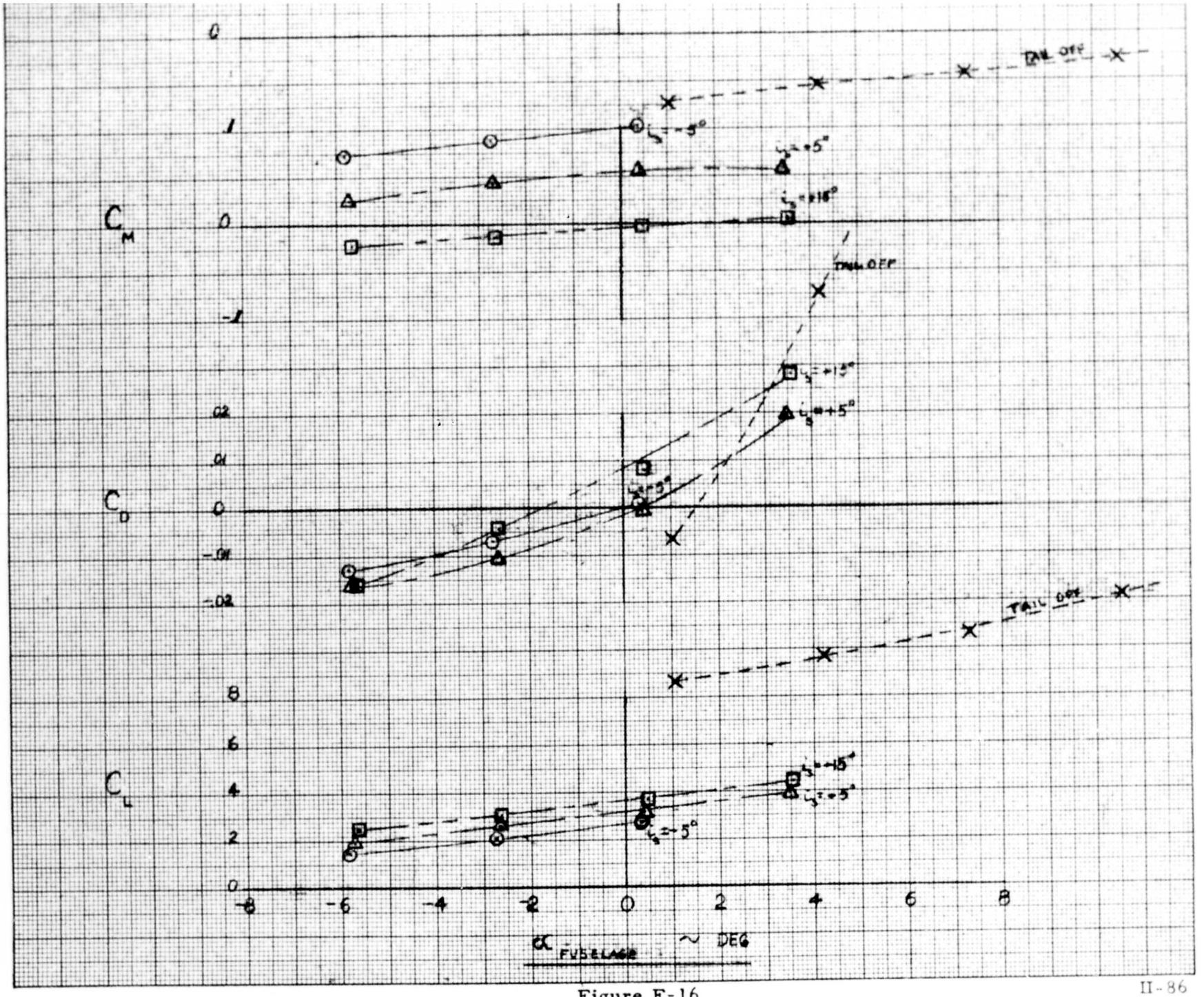

Figure F-16

II-86

HORIZONTAL TAIL EFFECTIVENESS WITH POWERED ROTOR

$\mu = .35$
$\beta = 10°$

SYM	RUN NO	CONFIG	i_T
○	36 P	$FN_2HBVS_{.2}$	-5°
△	37 P	↓	+5°
□	38 P	↓	+15°
X	35A-P	FN_2HB_2	OFF

$A_{1_S} = 0°$

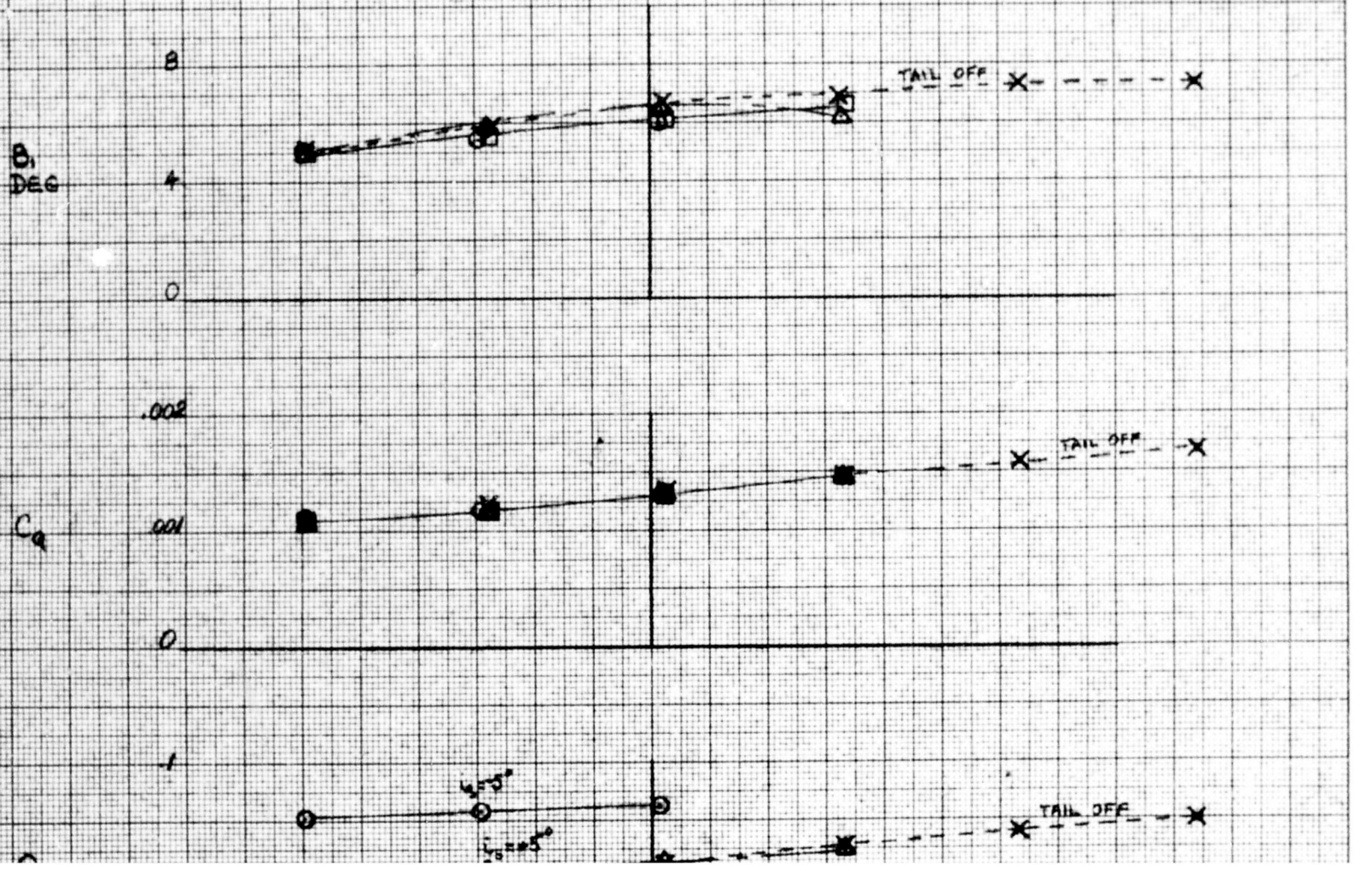

FJB & AP 7/21/65

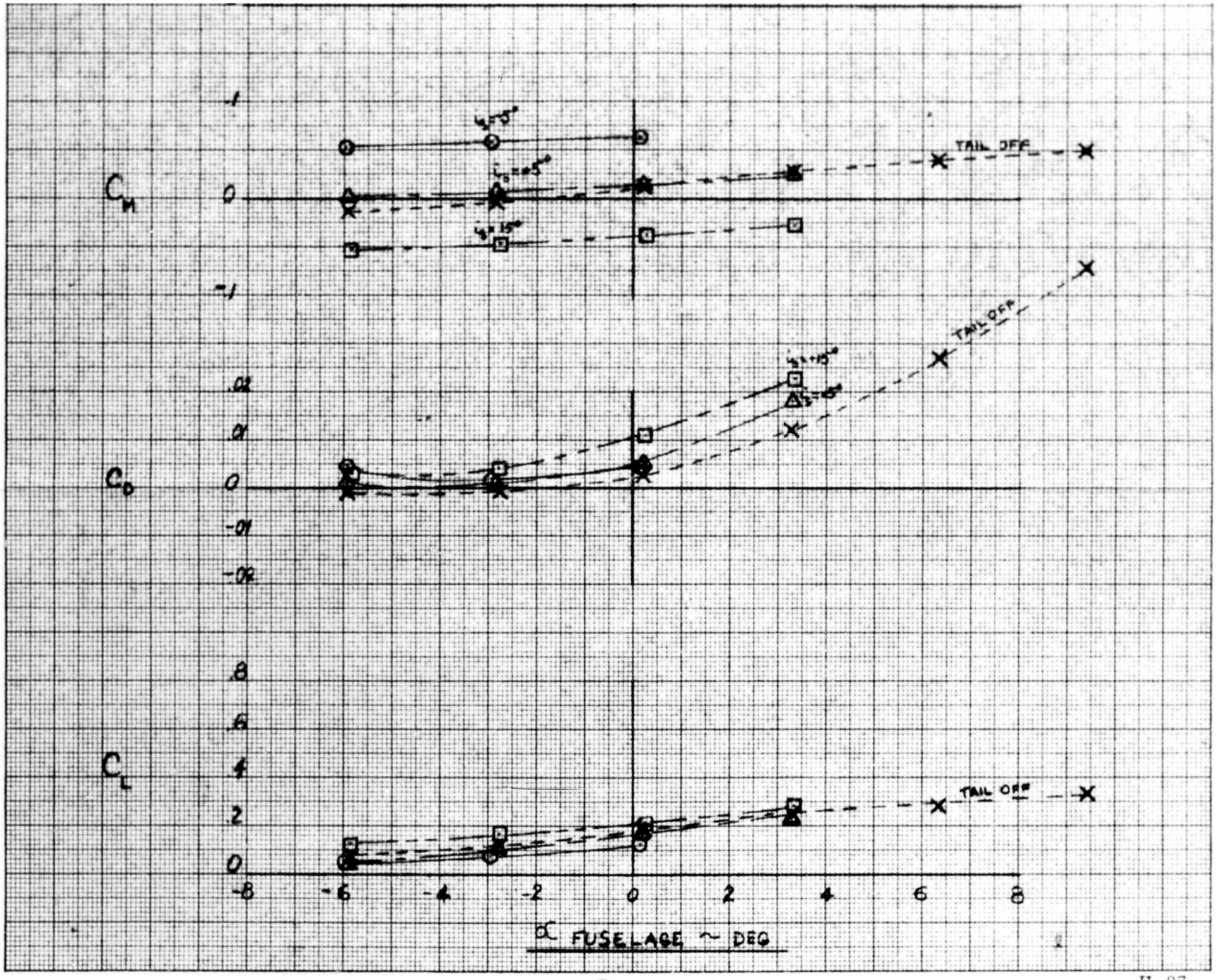

Figure F-17

II-87

POWERED ROTOR CHARACTERISTICS

$\mu = .25$ FN_2H_2BZ (TAIL-OFF)
COLLECTIVE PITCH VARIATION

$A_2 = 5°$

RUN No. 78 P

SYM	Θ
□	5°
△	10°
○	15°
◇	20°

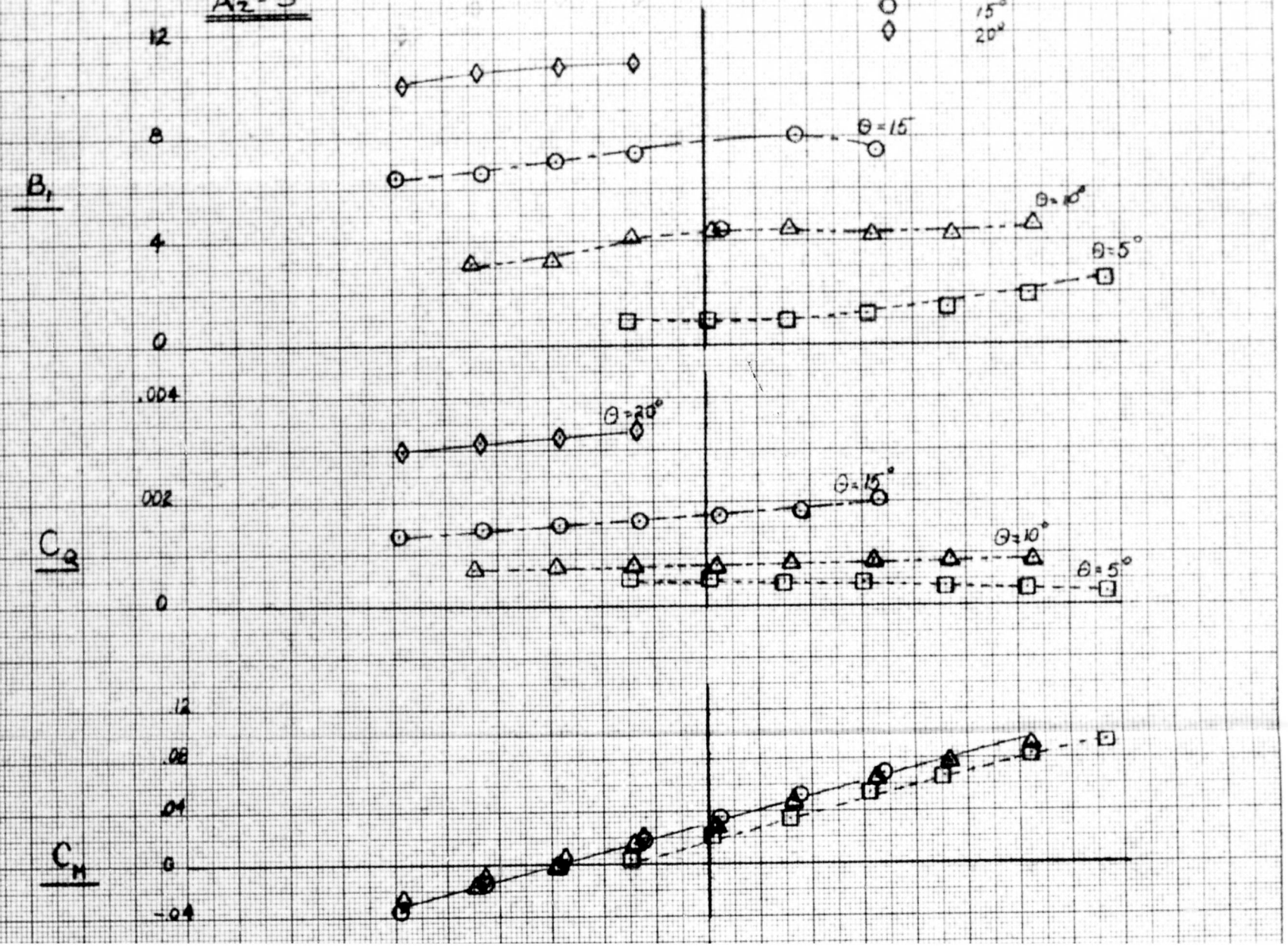

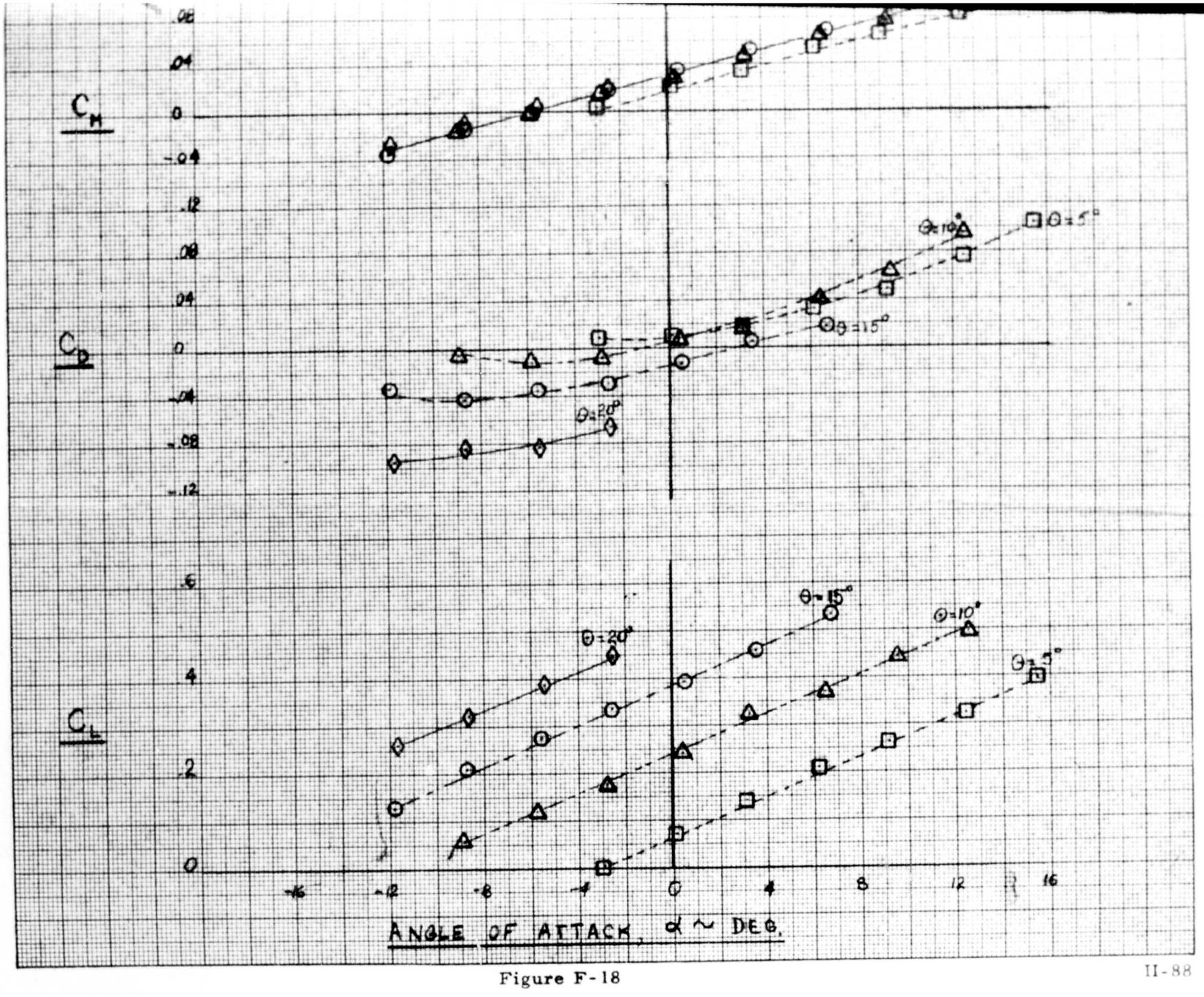

Figure F-18

II-88

POWERED ROTOR CHARACTERISTICS

$\mu = .35$ FN_2H_2BZ (TAIL OFF)

COLLECTIVE PITCH VARIATION

$A_2 = 5°$

RUN No. 80 P

SYM	θ
□	5°
△	10°
○	15°

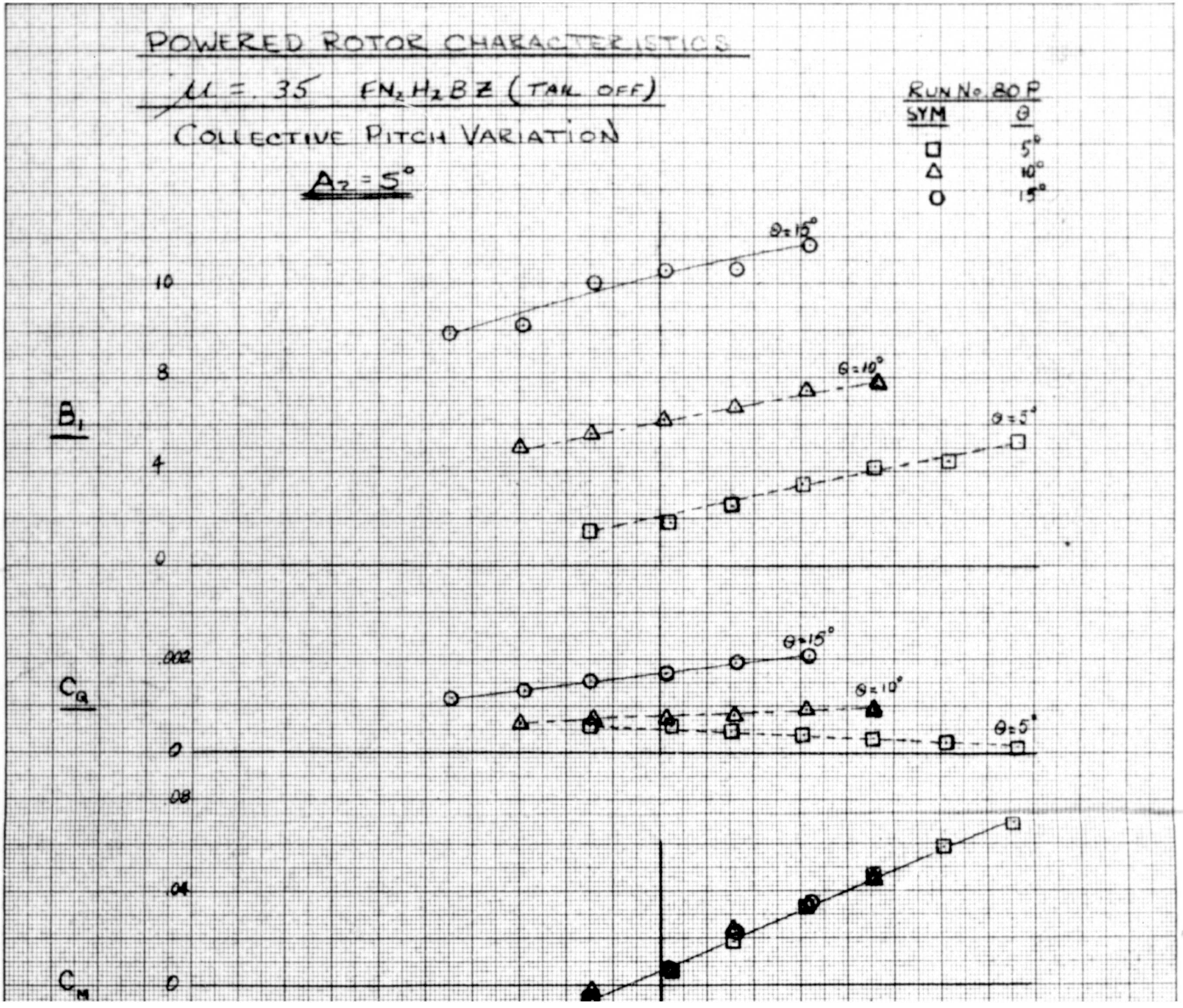

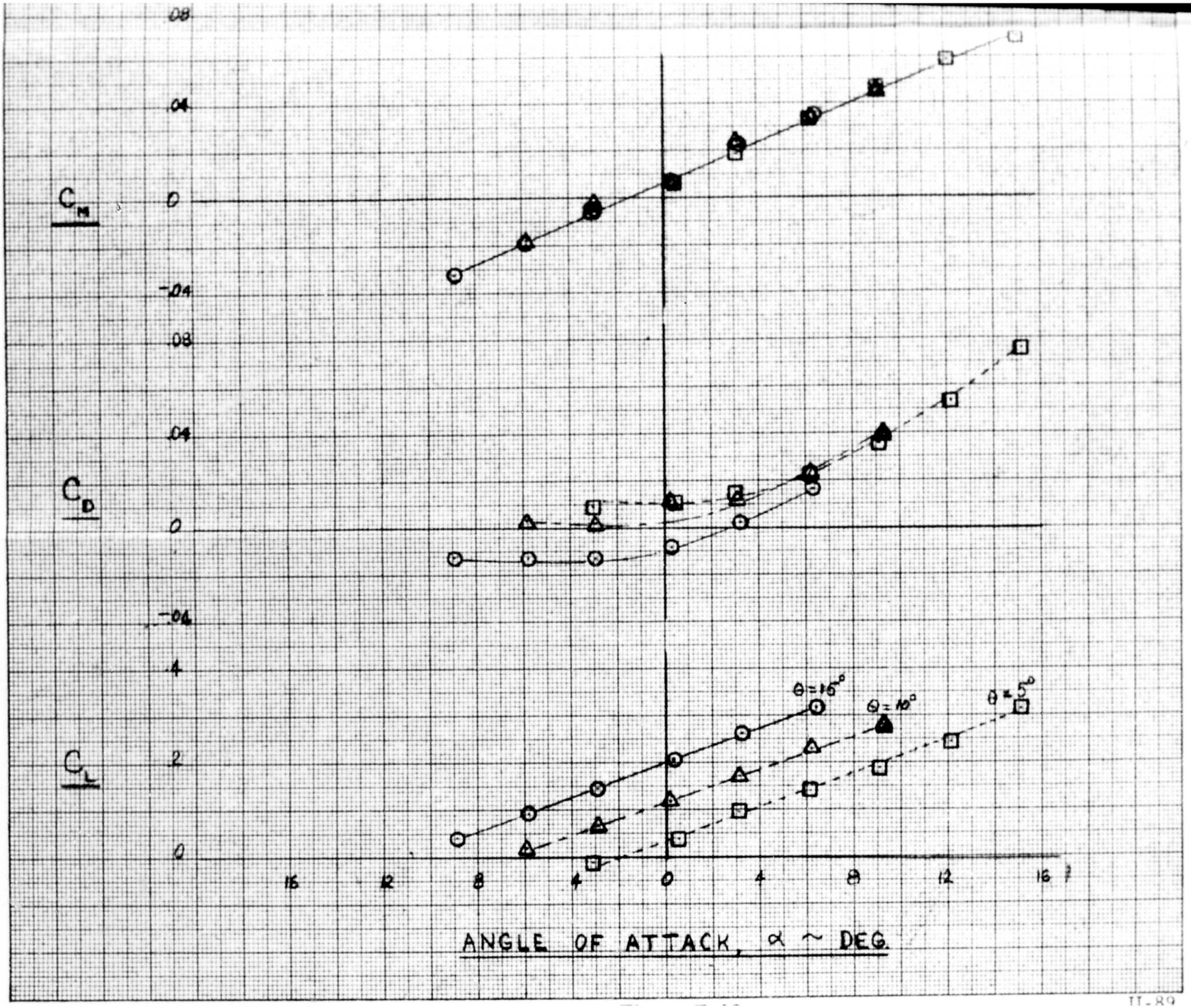
.08
.04
0
-.04
-.08
.04
0
-.04
.4
.2
0
C_m
C_D
C_L
θ = 15°
θ = 10°
θ = 5°
15
12
8
4
0
4
8
12
16
ANGLE OF ATTACK, α ~ DEG.

POWERED ROTOR CHARACTERISTICS

CONTROL POWER AVAILABLE

$\mu = .25$
600 RPM

CONFIG	RUN NO	Θ
FN_2H_2BZ	79P	10°

$A_2 = 5°$

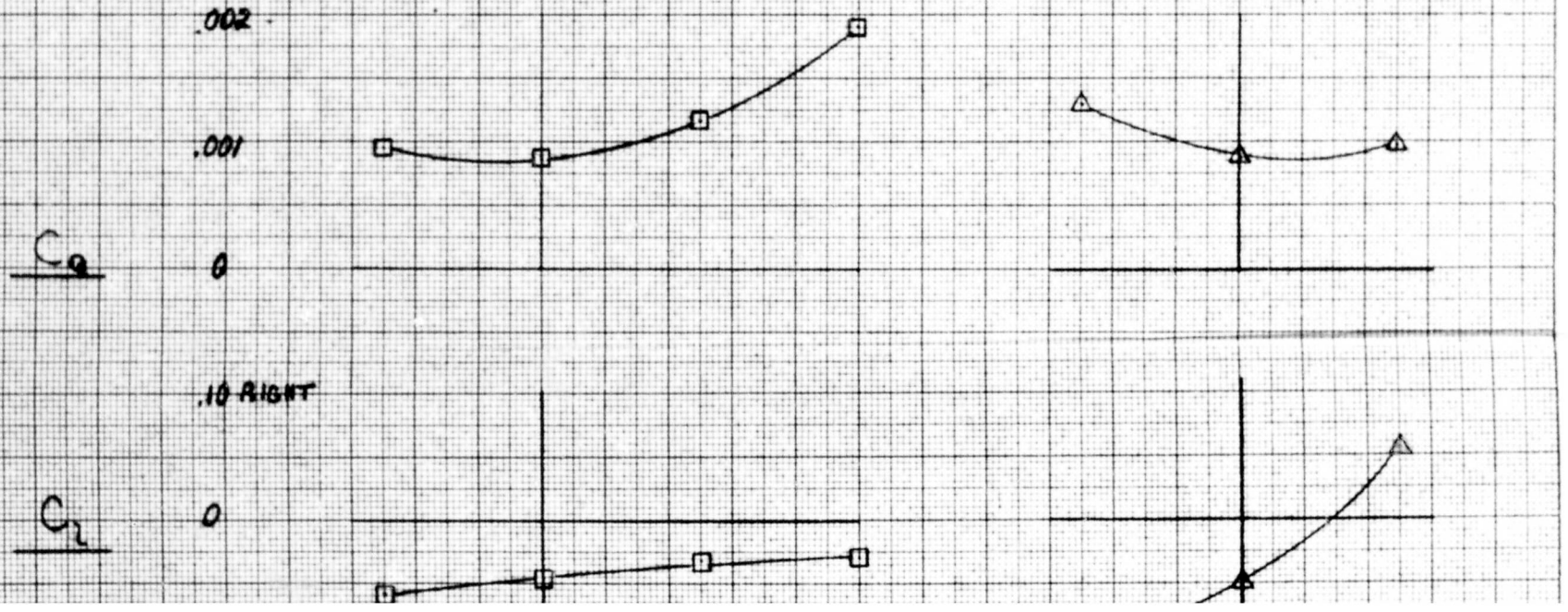

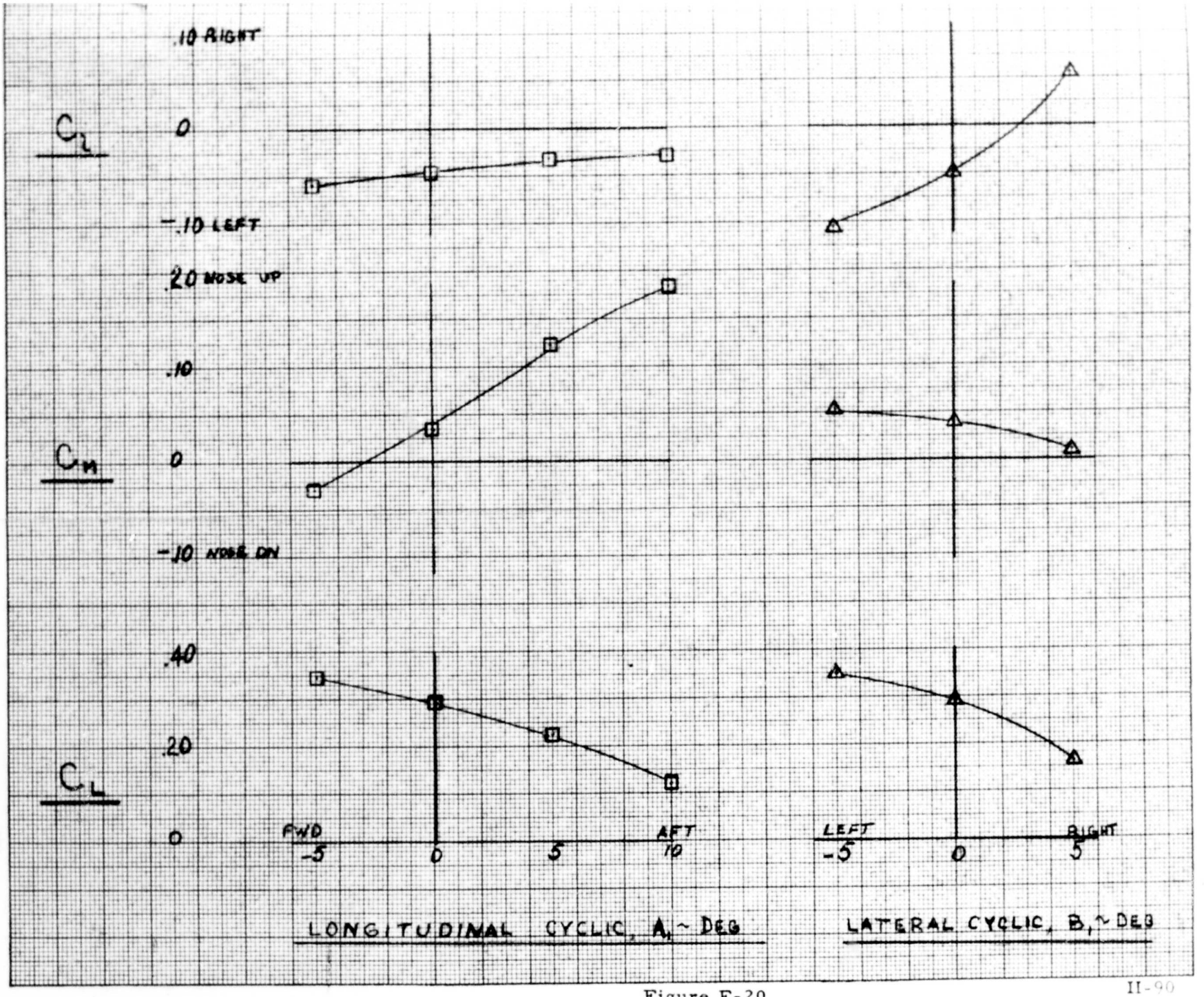
.10 RIGHT
C_l
0
-.10 LEFT
.20 NOSE UP
.10
C_m
0
-.10 NOSE DN
.40
.20
C_L
0
FWD
AFT
-5
0
5
10
LONGITUDINAL CYCLIC, A_1 ~ DEG
LEFT
RIGHT
-5
0
5
LATERAL CYCLIC, B_1 ~ DEG

Figure F-20

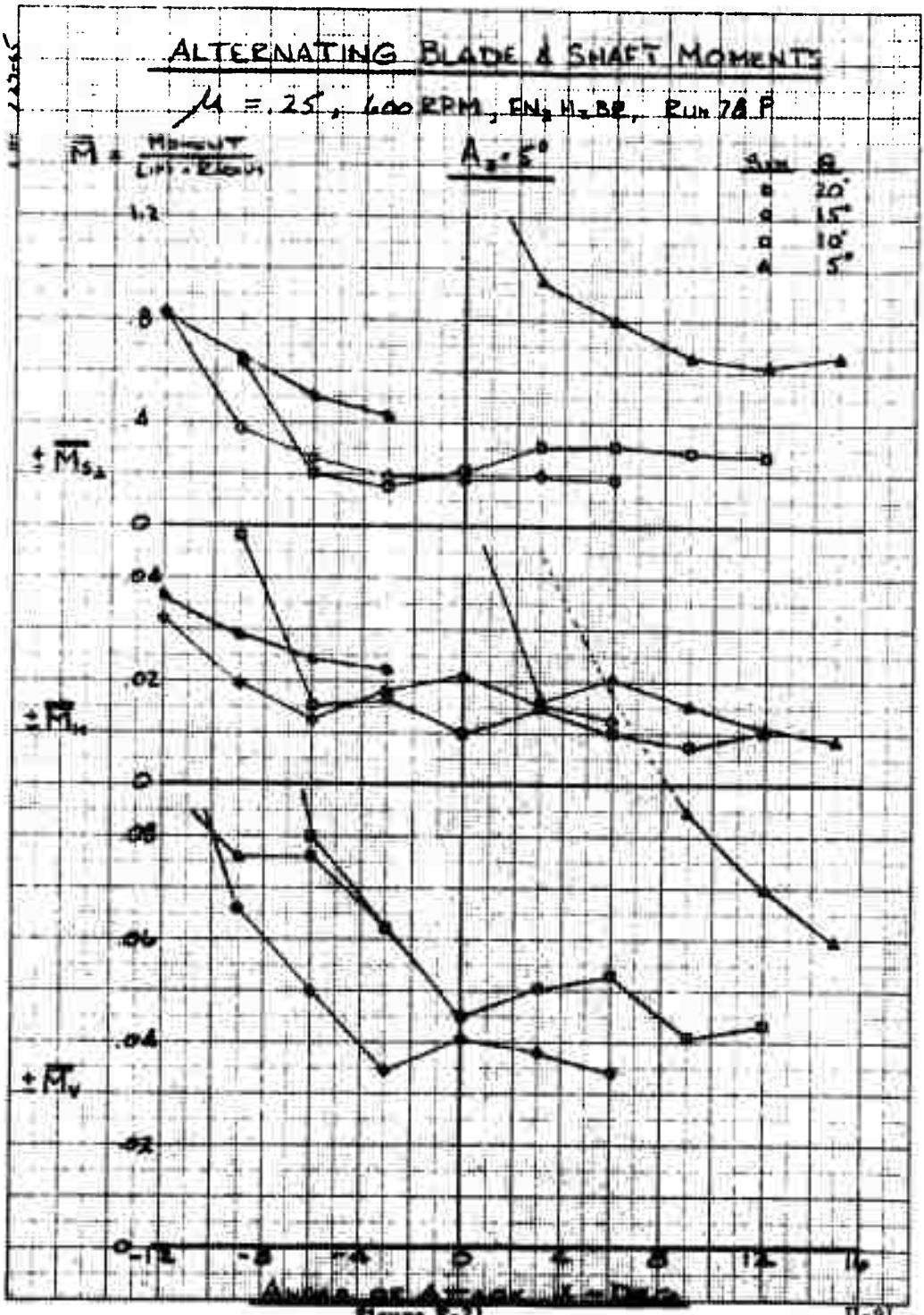
ALTERNATING BLADE & SHAFT MOMENTS
μ = .25, 600 RPM, EN, H-82, RUN 78 F
$\bar{M} = \frac{\text{MOMENT}}{\text{LIFT} \cdot \text{RADIUS}}$
$A_s = 5°$
SYM θ
20°
15°
10°
5°
1.2
.8
.4
$\pm \bar{M}_{S_A}$
0
.04
.02
$\pm \bar{M}_H$
0
-.08
-.06
-.04
$\pm \bar{M}_V$
-.02
0
-12
-8
-4
0
4
8
12
16
ANGLE OF ATTACK, α - DEG.

Figure F-21

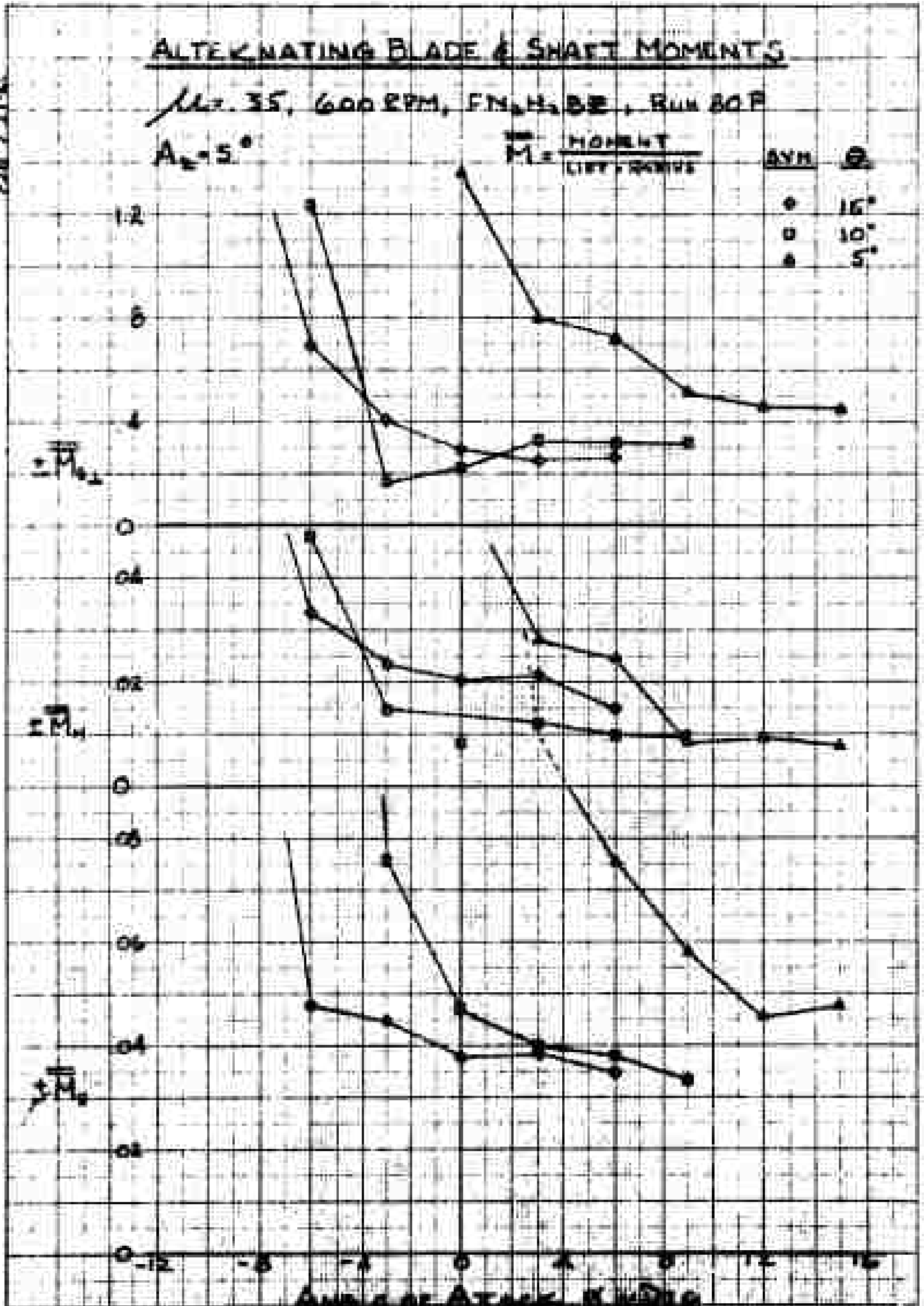
ALTERNATING BLADE & SHAFT MOMENTS
μ = .35, 600 RPM, FN2H2B2, RUN 80P
1.2
.8
.4
0
.04
.02
0
.08
.06
.04
.02
0
-12
-8
-4
0
4
8
12
16

Figure F-22

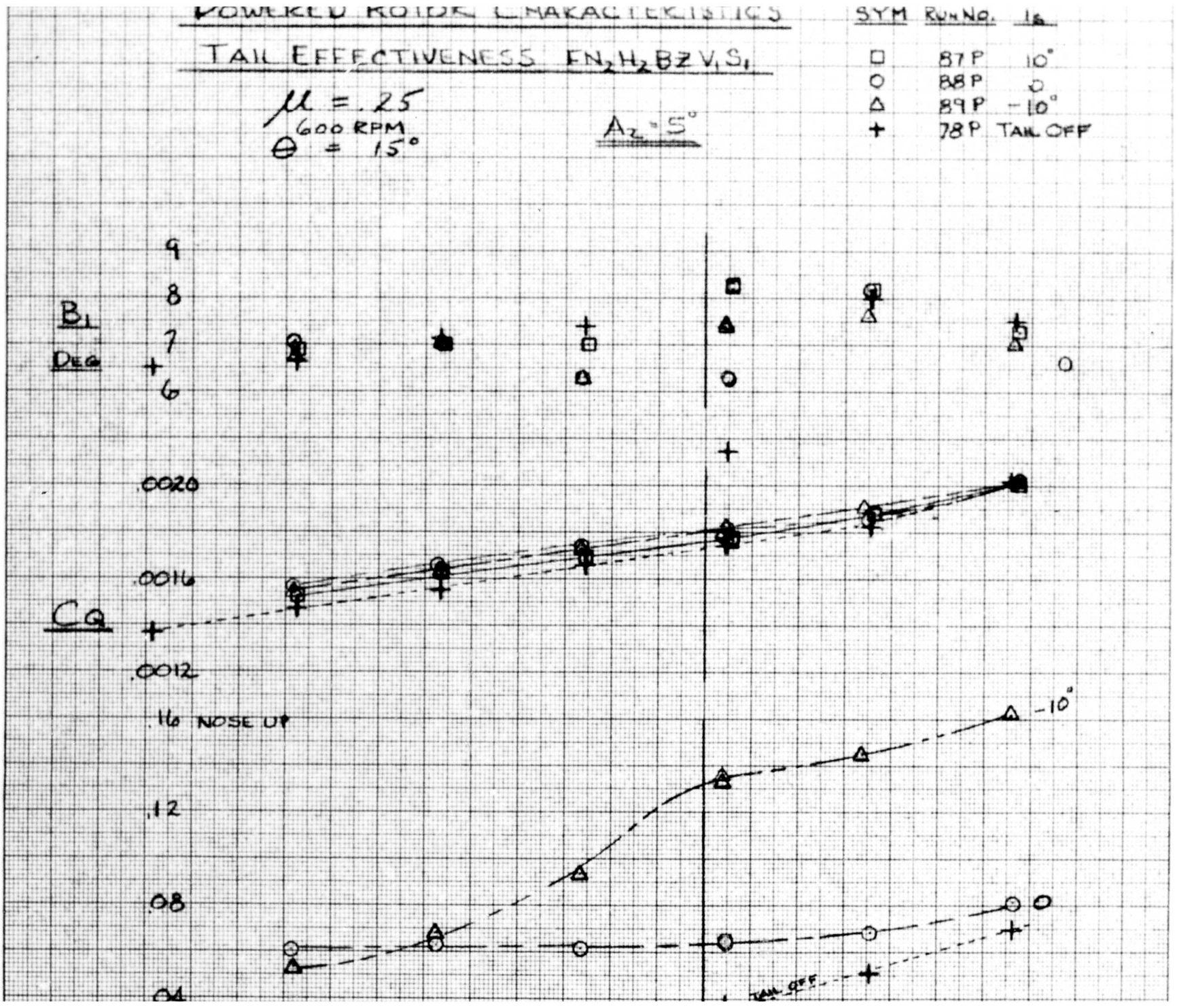
POWERED ROTOR CHARACTERISTICS
TAIL EFFECTIVENESS FN2H2BZV1S1
μ = .25
600 RPM
θ = 15°
Az = 5°
SYM RUN NO. 16
87P 10°
88P 0°
89P -10°
78P TAIL OFF
B1 DEG
9
8
7
6
CQ
.0020
.0016
.0012
.16 NOSE UP
.12
.08
.04
-10°
0
TAIL OFF

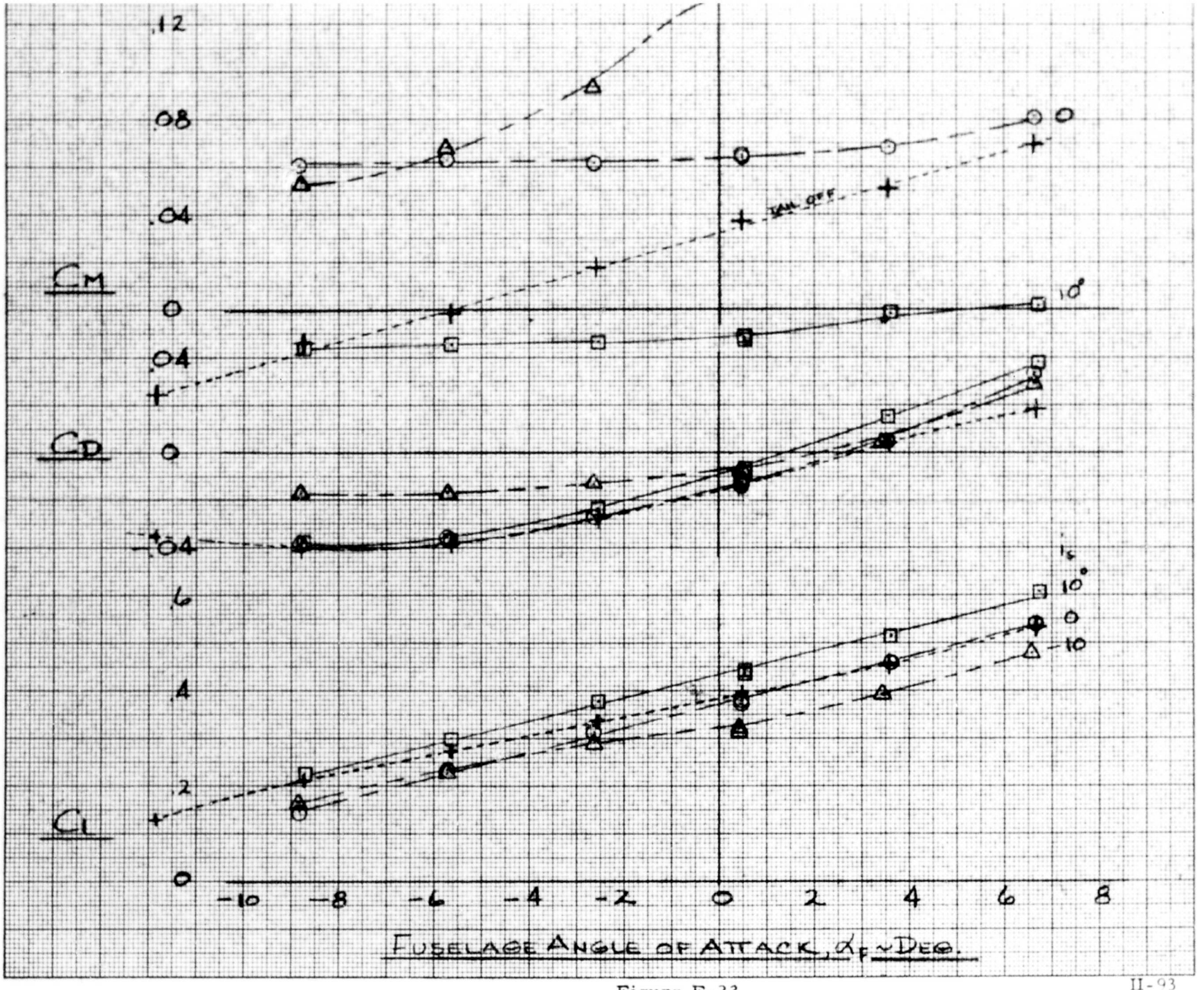

Figure F-23

II-93

AUTOROTATING ROTOR CHARACTERISTICS

$A_2 = 0°$

SYM	RUN	θ	CONFIGURATION
○	43-P	0°	FN_2 HBZ
△	↓	-4.5°	↓
□	↓	-5.0°	↓

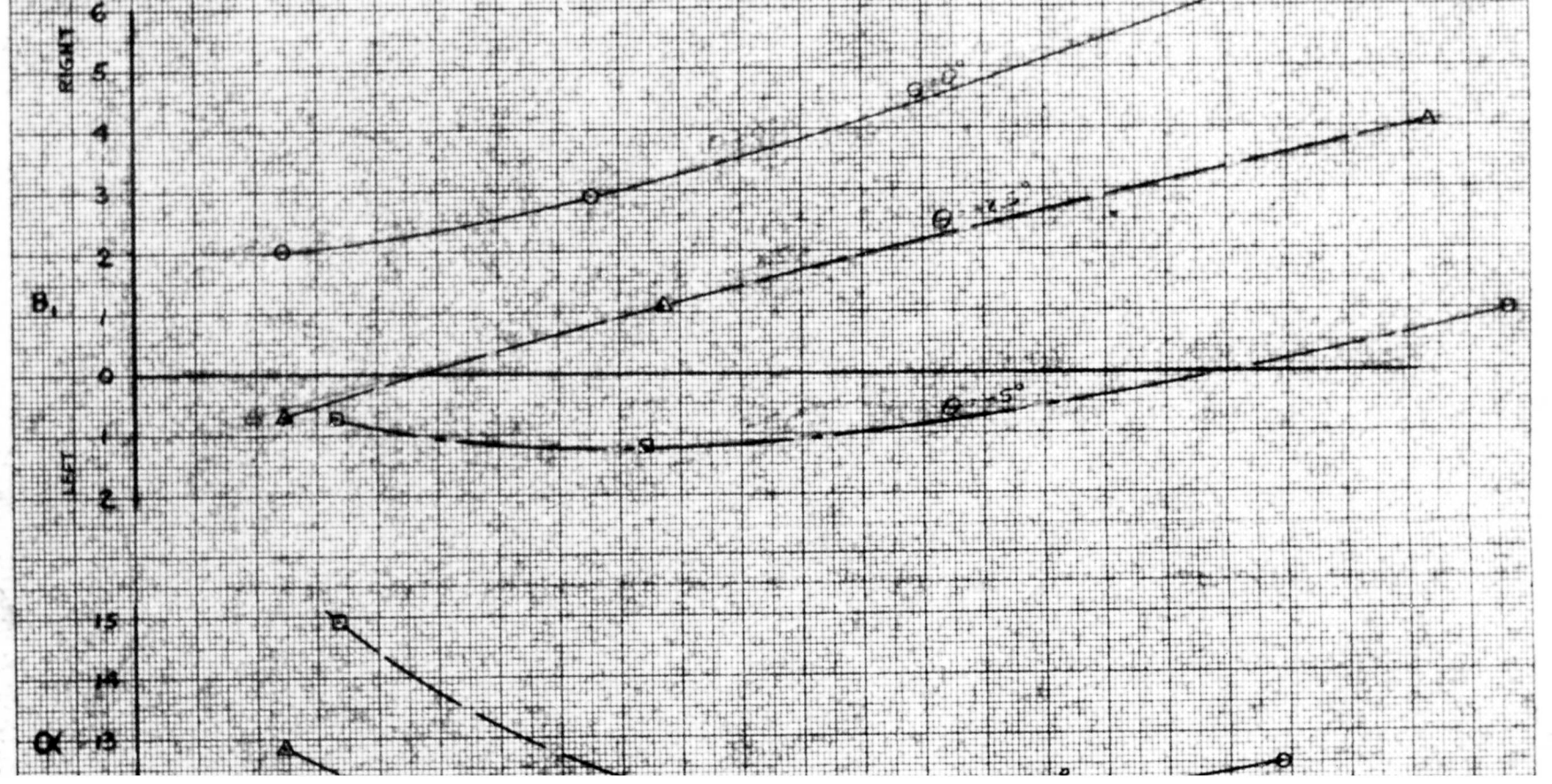

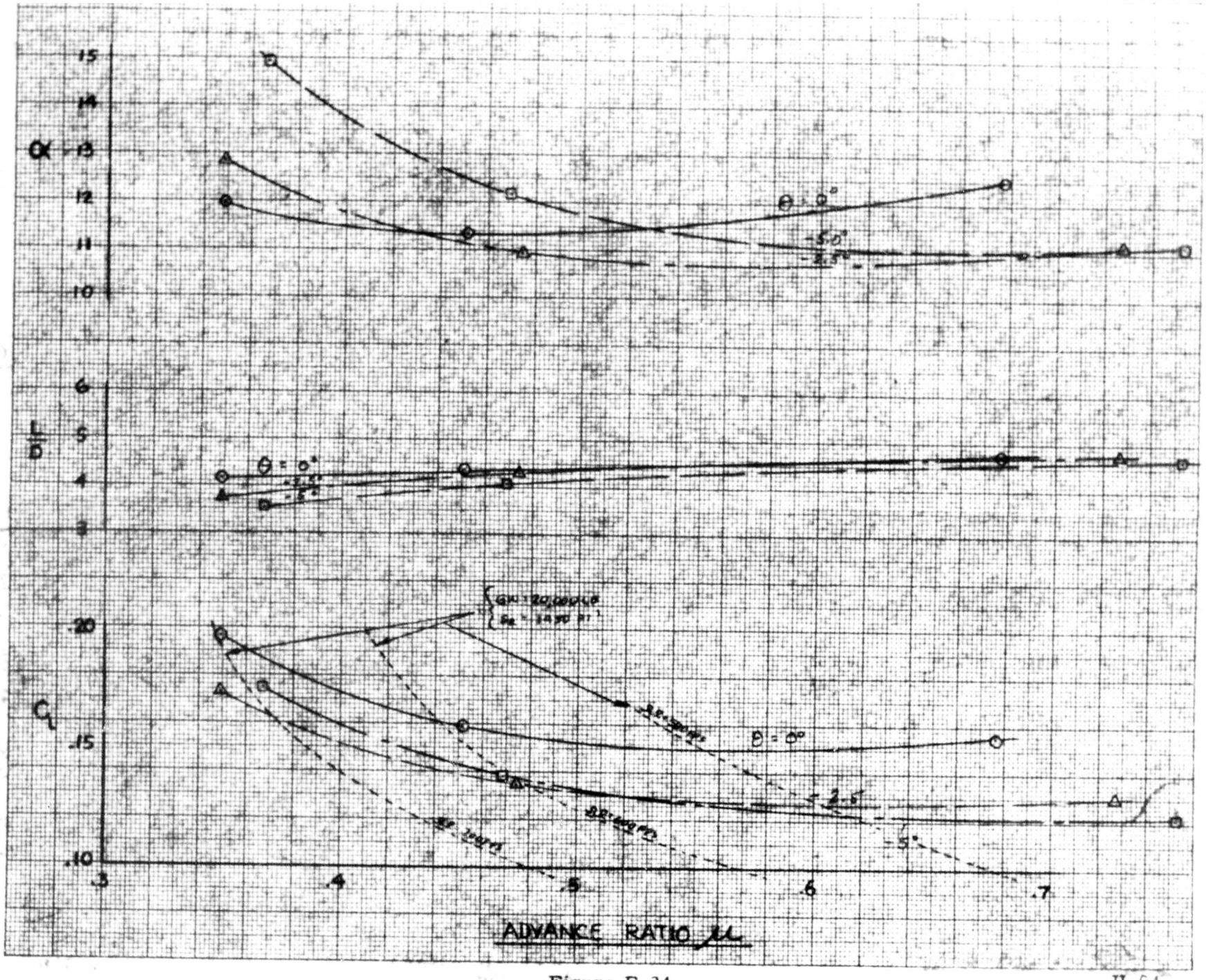

Figure F-24

II-94

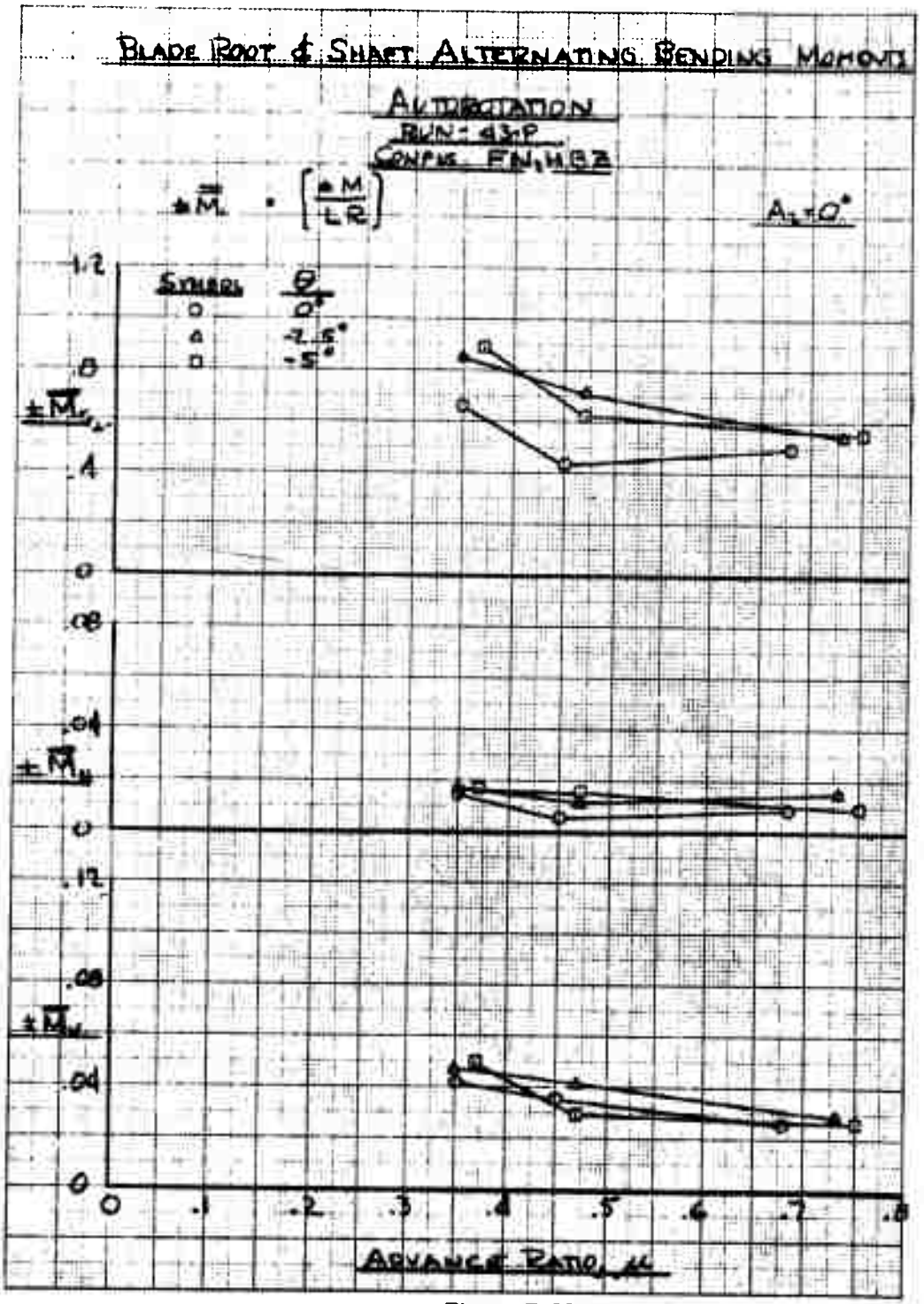
BLADE ROOT & SHAFT ALTERNATING BENDING MOMENTS
ALTERNATION
RUN: 43-P
CONFIG. FN, HB2
$\pm\bar{M}_L = \left[\frac{\pm M}{LR}\right]$
$A_1 = 0°$
SYMBOL
θ_0
0°
-2.5°
-5°
$\pm\bar{M}_{L_{1c}}$
$\pm\bar{M}_{H}$
$\pm\bar{M}_{H_{1c}}$
1.2
.8
.4
0
.08
.04
0
.12
.08
.04
0
0
.1
.2
.3
.4
.5
.6
.7
.8
ADVANCE RATIO, μ

Figure F-25

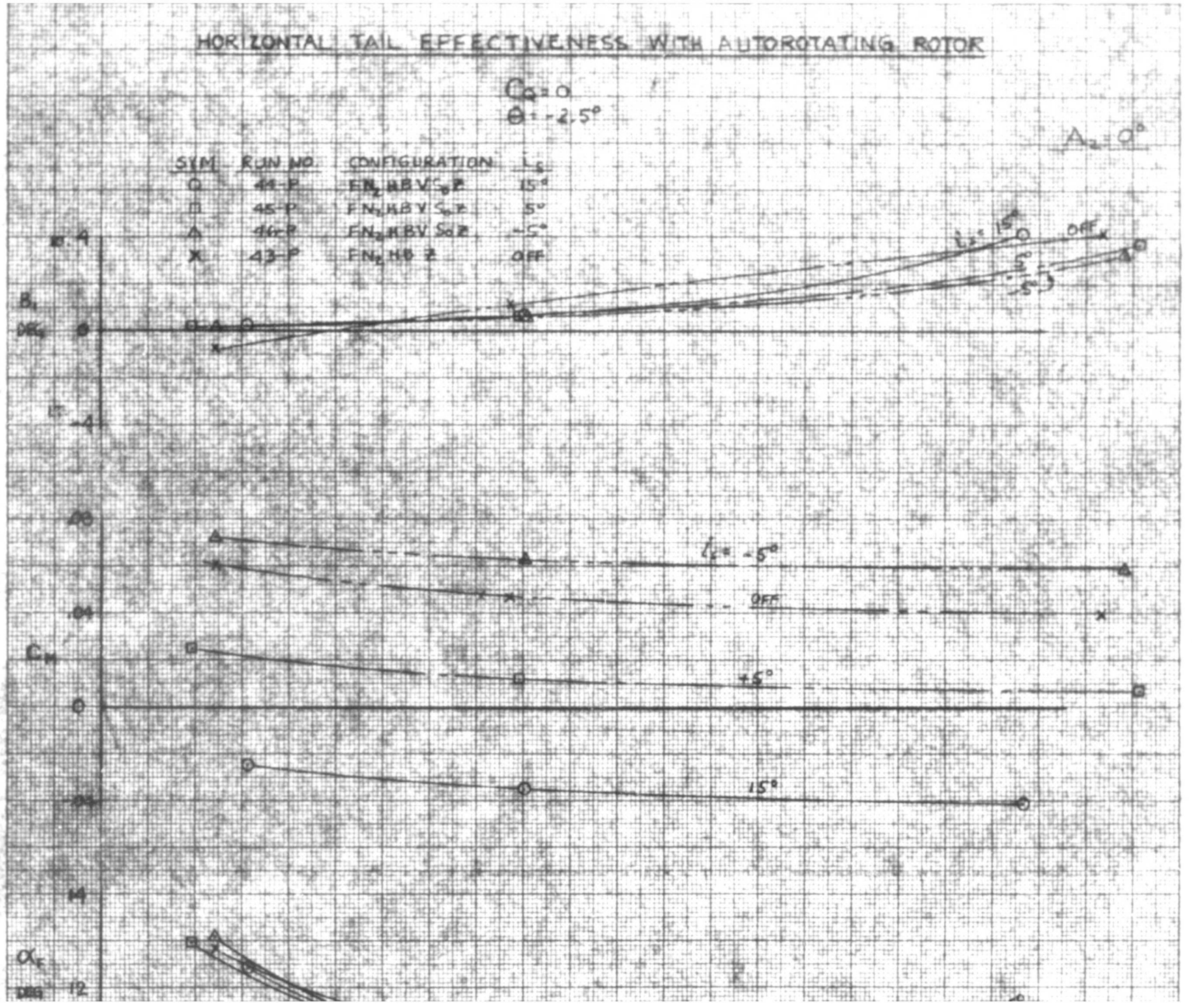
HORIZONTAL TAIL EFFECTIVENESS WITH AUTOROTATING ROTOR
$C_Q = 0$
$\theta = -2.5°$
$A_s = 0°$
SYM RUN NO. CONFIGURATION i_t
□ 44-P FN_2HBVS_0P 15°
□ 45-P FN_2HBVS_0P 5°
△ 46-P FN_2HBVS_0P -5°
× 43-P FN_2HB2 OFF
i_t = 15°
OFF
5°
-5°
C_H
i_t = -5°
OFF
+5°
15°
α_s DEG

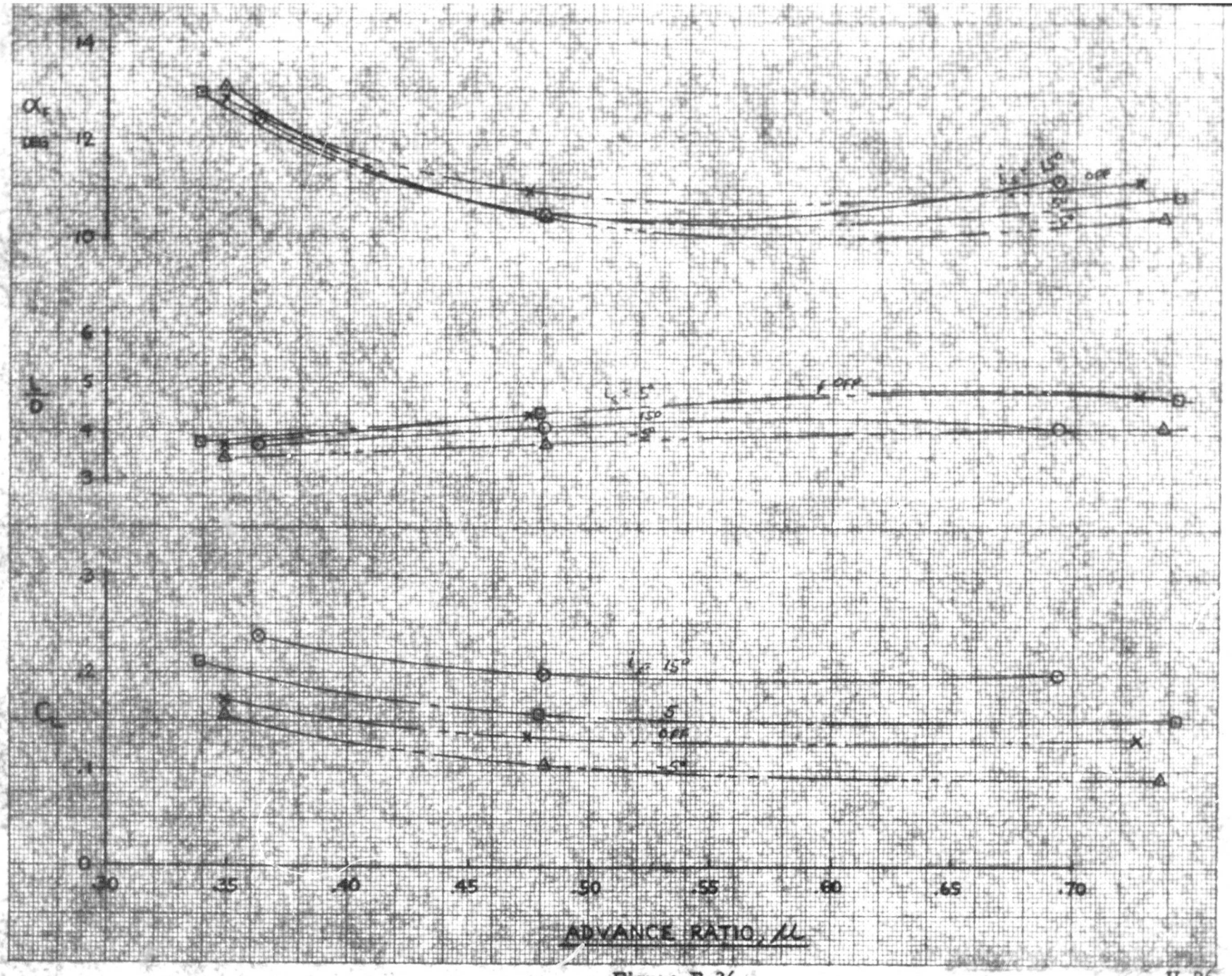

Figure F-26

II-96

AR AEDB 7/16/65

AUTOROTATION

HORIZONTAL TAIL EFFECTIVENESS

$\theta = 2^\circ$

SYM	RUN	CONFIGURATION
X	83-P	FN2H2B2 (TAIL OFF).
◇	84-P	V.S. $i_s = -10^\circ$
○	85-P	V.S. $i_s = 0$
□	86-P	V.S. $i_s = 10^\circ$

$A_z = 5^\circ$

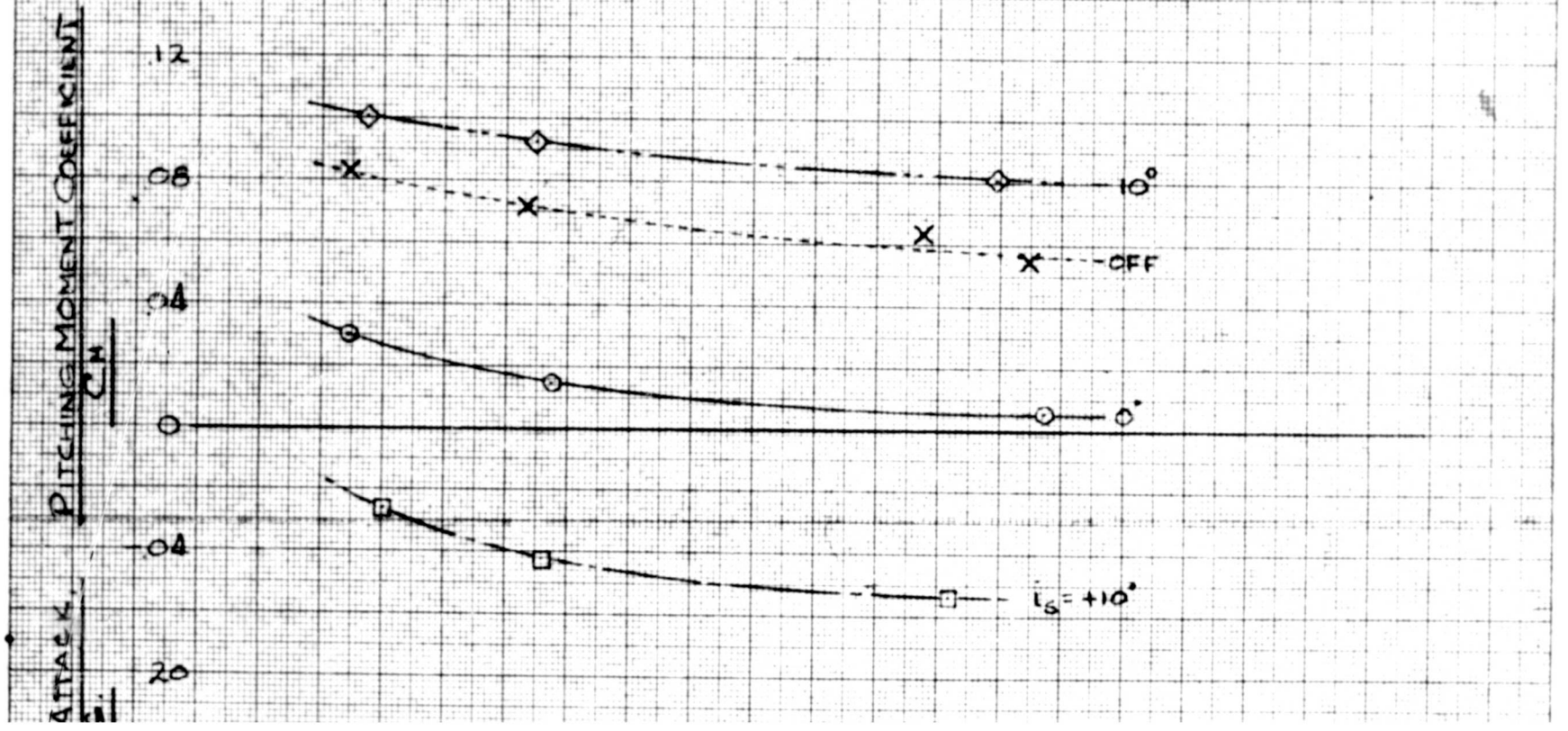

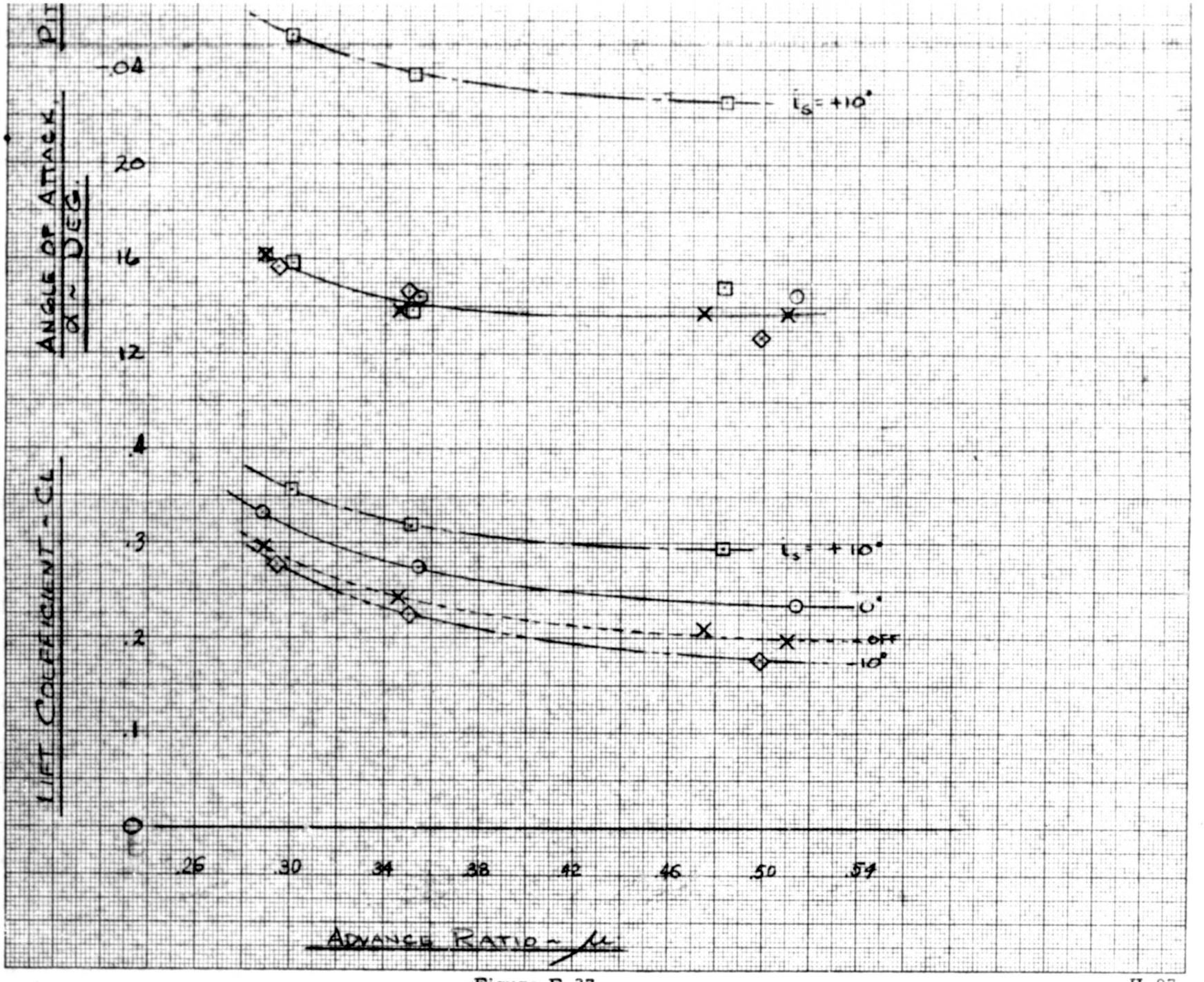

Figure F-27

II-97

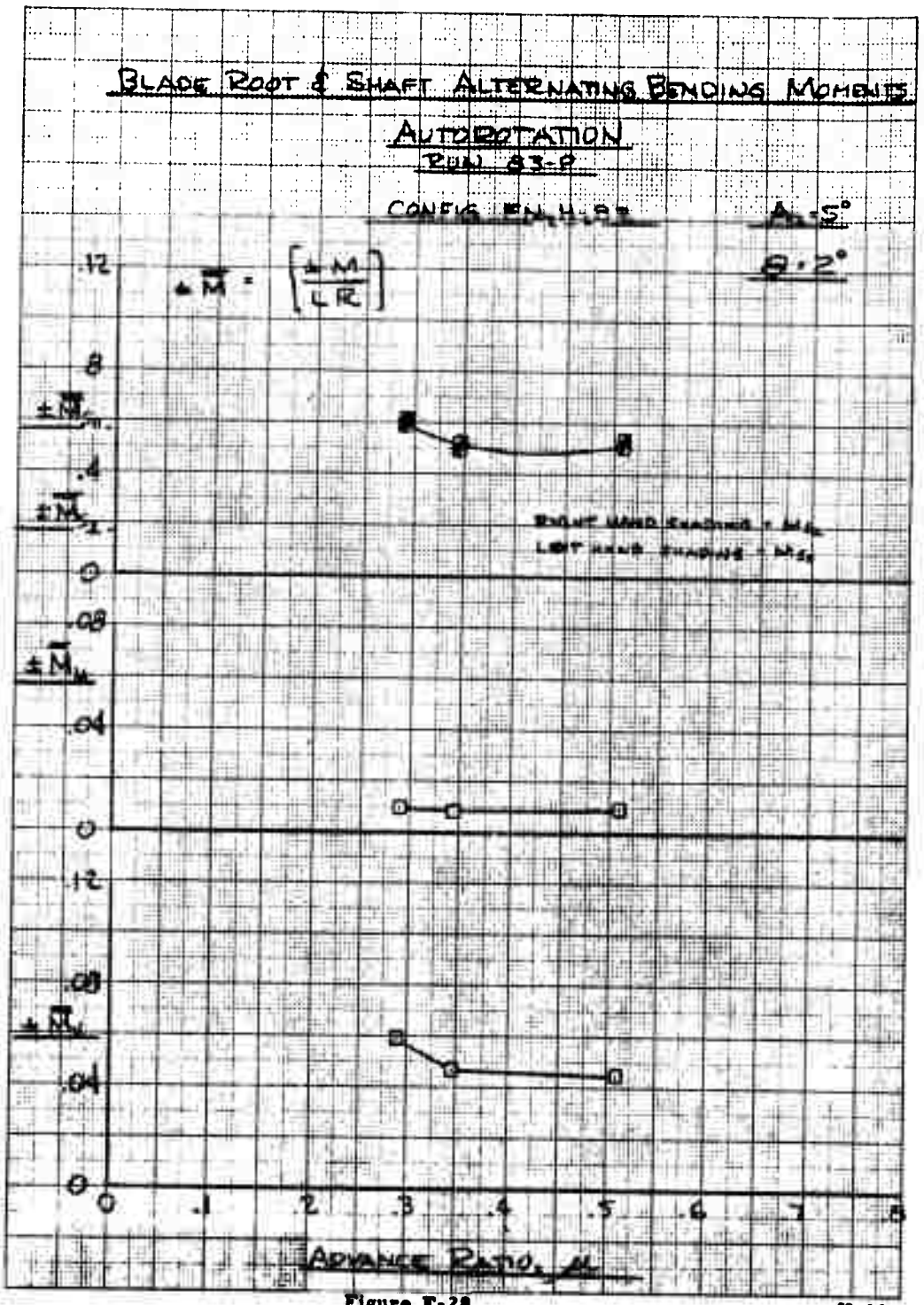
BLADE ROOT & SHAFT ALTERNATING BENDING MOMENTS
AUTOROTATION
RUN 83-P
CONFIG. FM-4-83
A_s -5°
θ .2°
$\pm\bar{M} = \left[\frac{\pm M}{\rho R^2}\right]$
$\pm\bar{M}_{FP}$
$\pm\bar{M}_{X}$
$\pm\bar{M}_{M}$
$\pm\bar{M}_{Y}$
RIGHT HAND READING = M_R
LEFT HAND READING = M_L
0 .1 .2 .3 .4 .5 .6 .7 .8
ADVANCE RATIO, μ

Figure F-28

CONVERSION TEST

RUN 41P
CONFIG. FN, HBZ

$A_2 = 0°$

LIFT ≈ 50 LBS
ROLLING MOMENT = 0 FT-LBS
LONG. CYCLIC PITCH = 0 DEG.
DYNAMIC PRESSURE = 2.3 LB/FT²

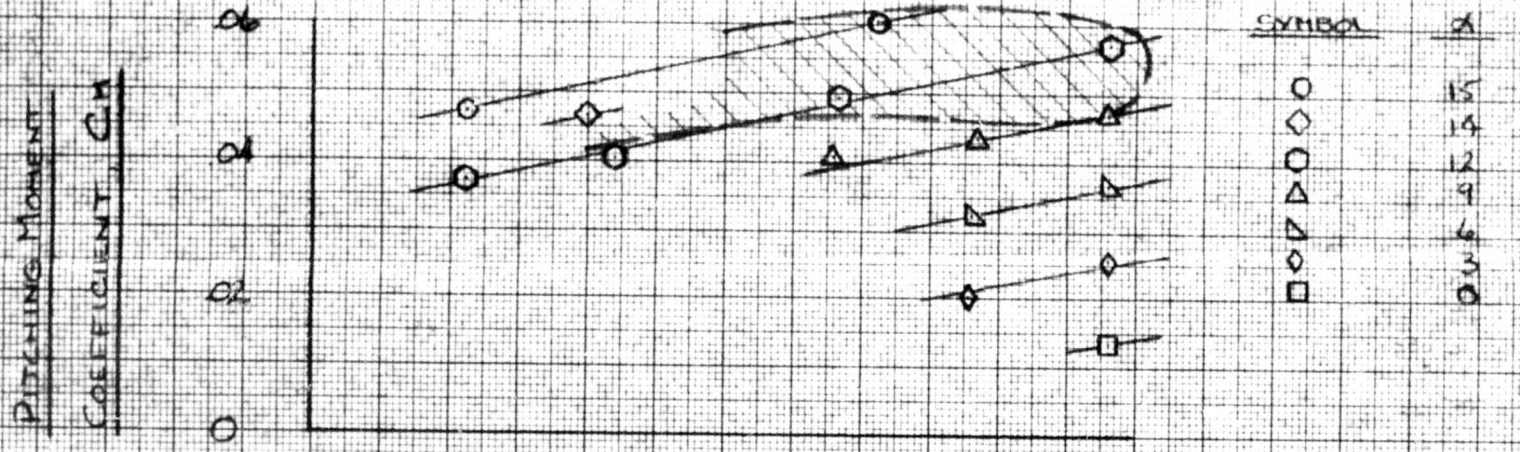

ROTOR ACCELERATION WITHIN CROSS HATCHED AREAS
ROTOR DECELERATION OUTSIDE CROSS HATCHED AREAS

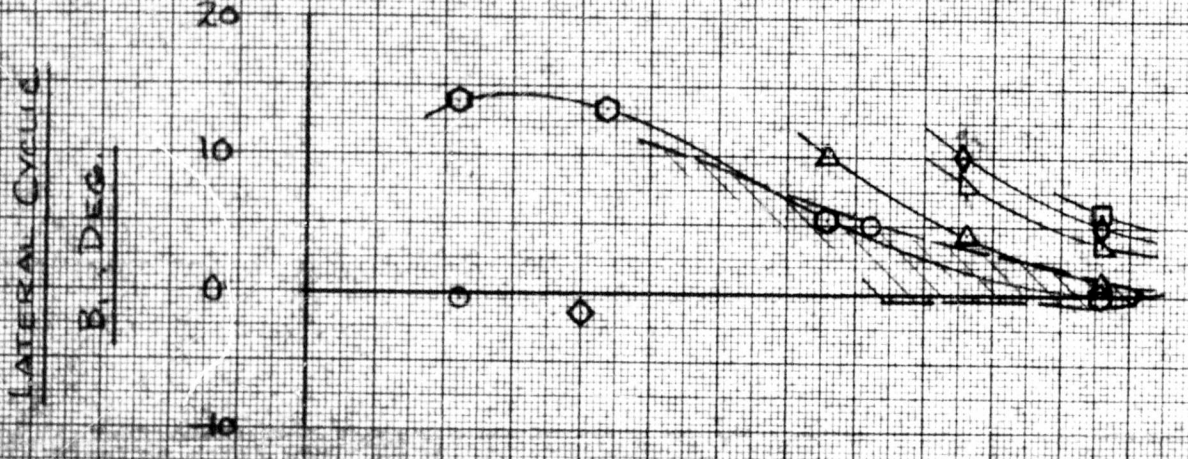

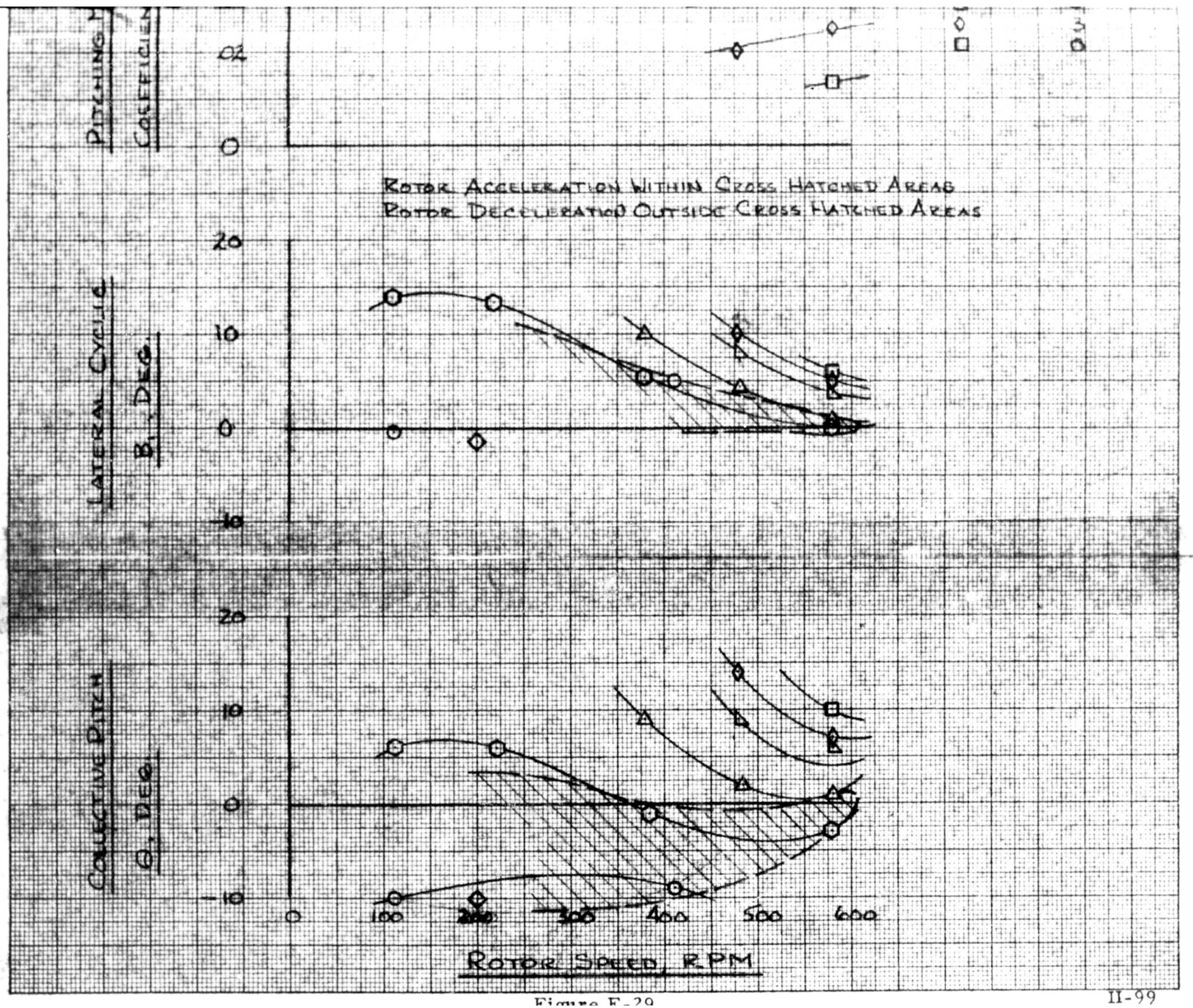
Pitching M
Coefficien
0.2
0
Rotor Acceleration Within Cross Hatched Areas
Rotor Deceleration Outside Cross Hatched Areas
Lateral Cyclic
B1, Deg.
20
10
0
-10
Collective Pitch
θ, Deg.
20
10
0
-10
0
100
200
300
400
500
600
Rotor Speed, RPM

Figure F-29

CONVERSION TEST

RUNS 95 & 95A

CONFIG. FN, H, BZX

LIFT ≈ 50 LBS.
ROLLING MOMENT = 0 FT-LBS
LONG. CYCLIC PITCH = 0 DEG.
DYNAMIC PRESSURE = 7.3 P.S.F

$A_1 = 3.5°$

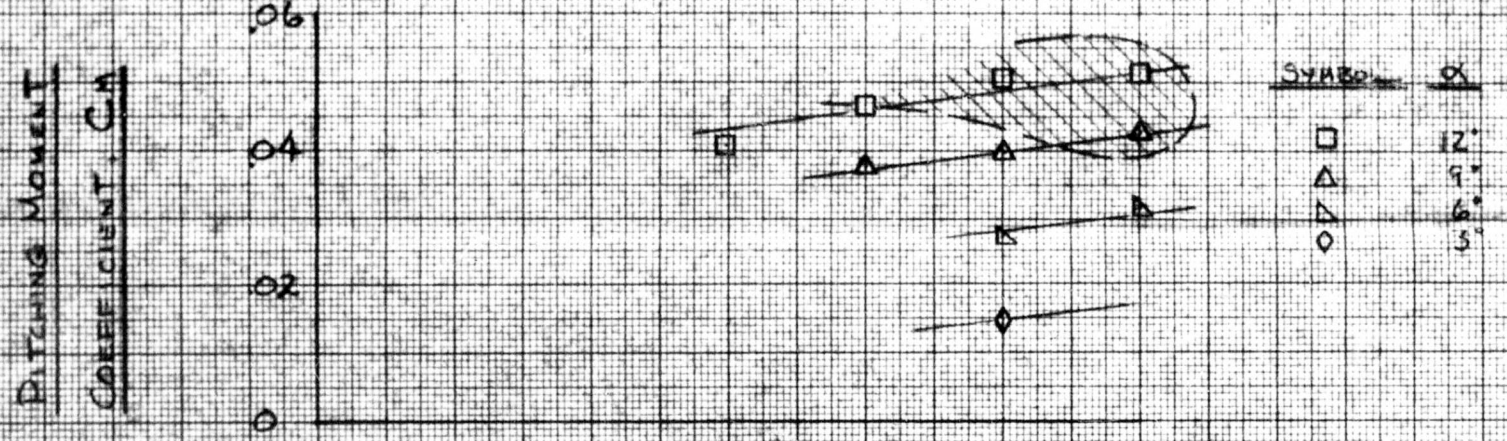

ROTOR ACCELERATION WITHIN CROSS HATCHED AREAS

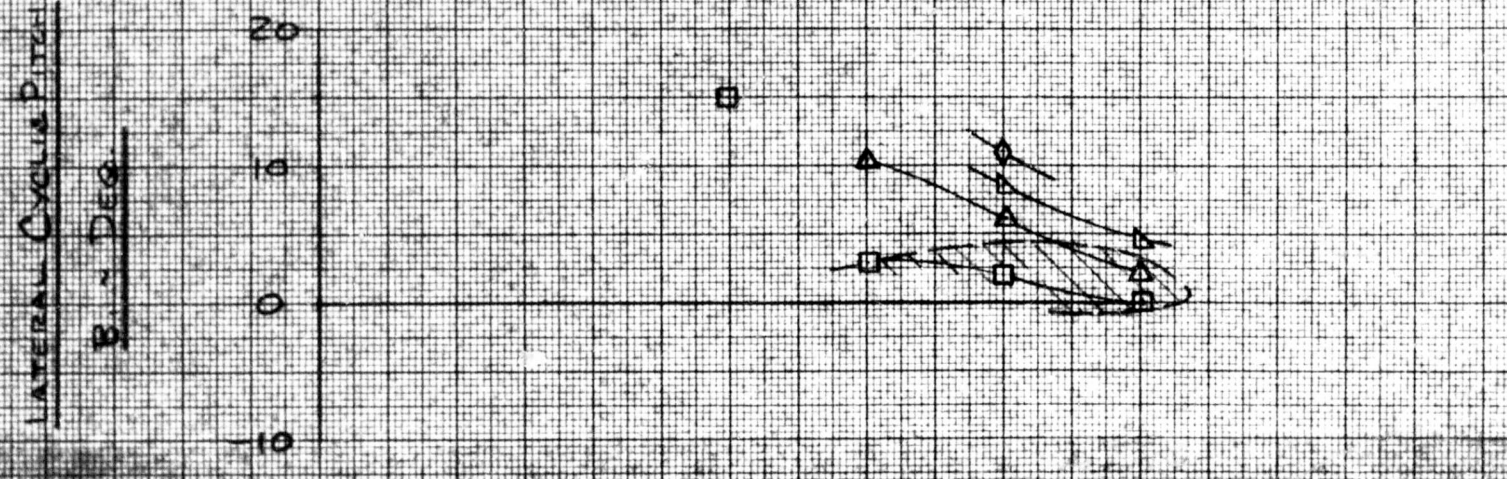

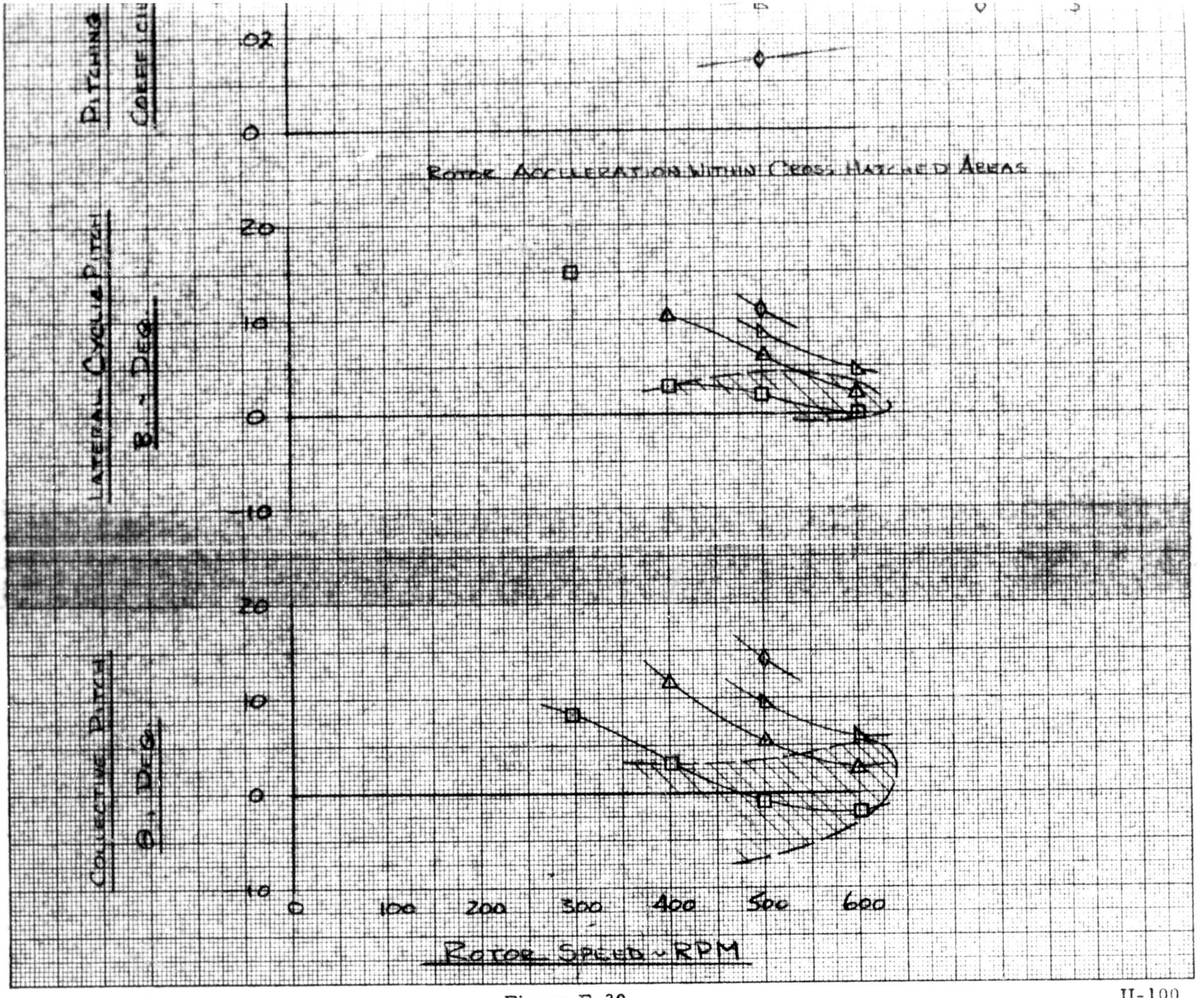

Figure F-30

II-100

CONVERSION TEST

RUNS 74P & 74AP

CONFIG. FN_2H_2BZ

$A_2 = 5°$

LIFT ≈ 50 LBS
ROLLING MOMENT = 0 FT-LBS
LONG. CYCLIC PITCH = 0 DEG
DYNAMIC PRESSURE = 7.3 PSF

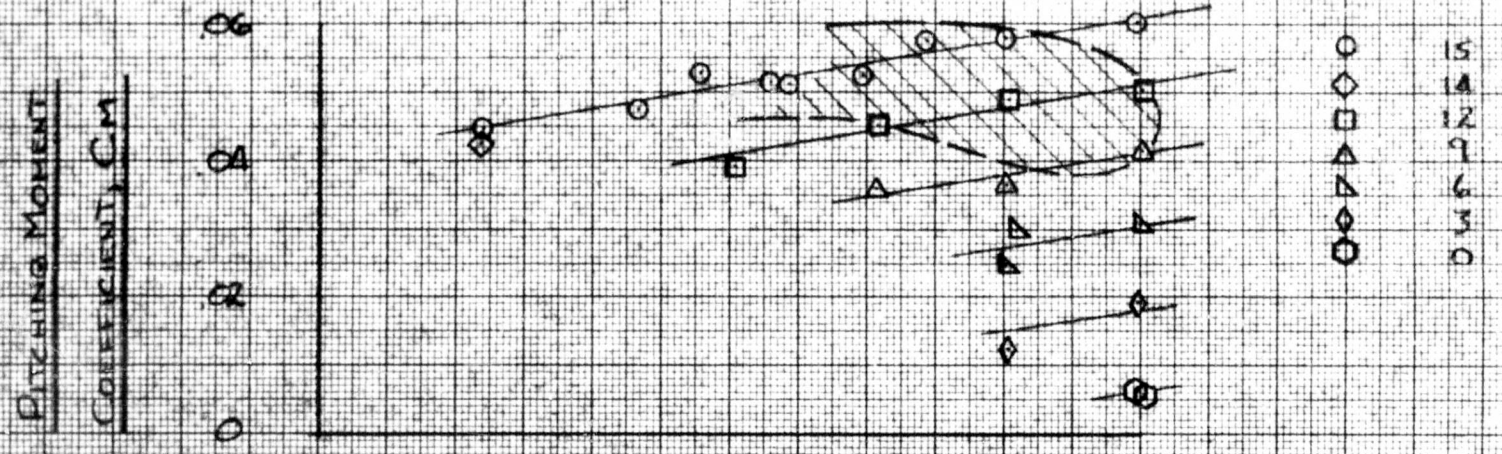

ROTOR ACCELERATION WITH CROSS HATCHED AREAS
ROTOR DECELERATION OUTSIDE CROSS HATCHED AREAS

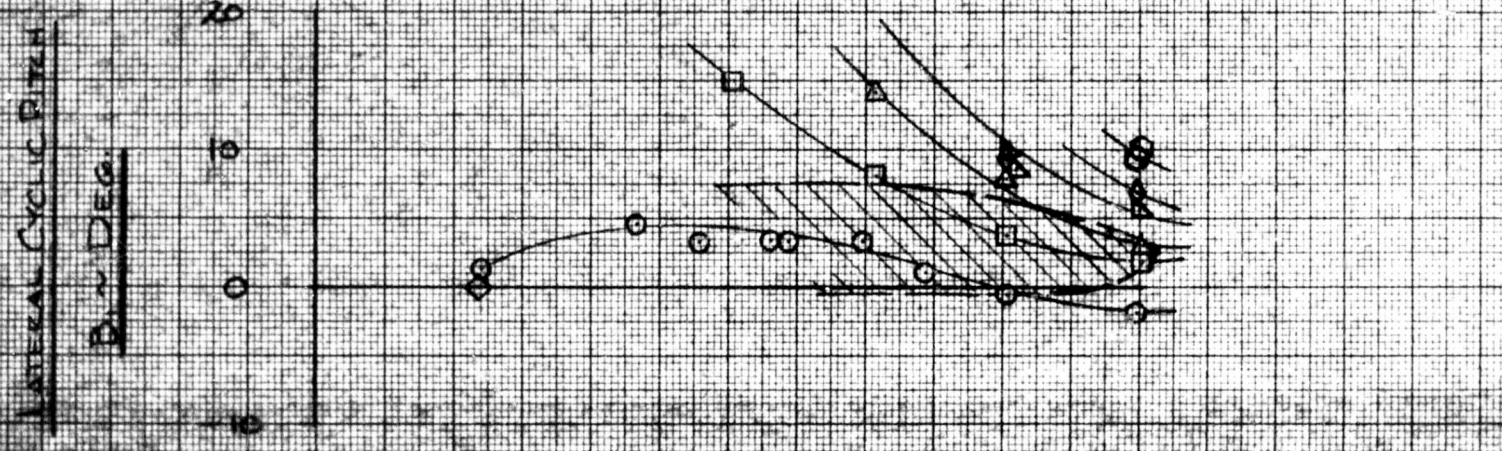

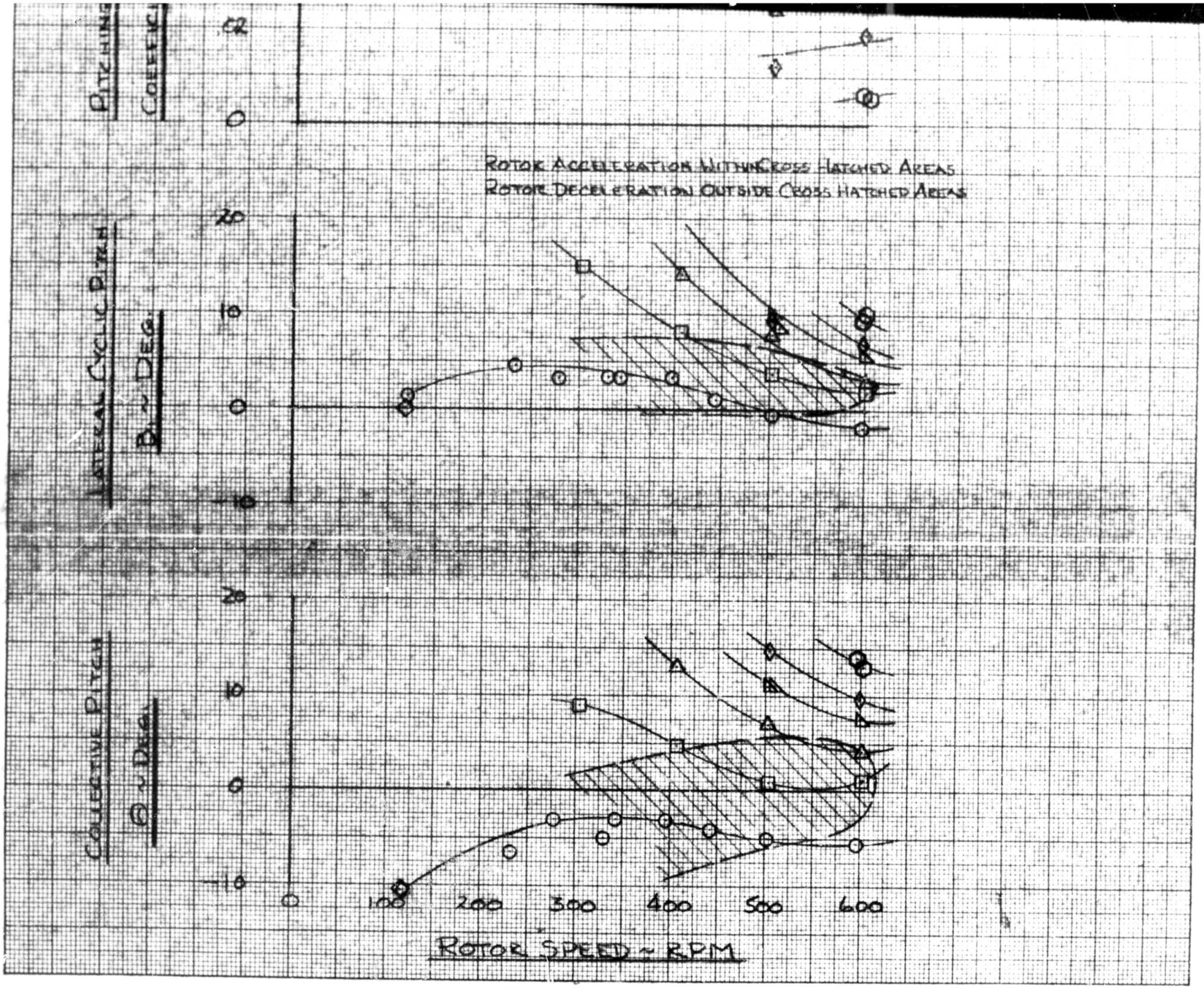

Figure F-31

II-101

AP & FIB 7-26-65

CONVERSION TEST

RUNS 94P & 94AP

CONFIG. FN_2H_3BZX

LIFT = 50 LBS.
ROLLING MOMENT = 0 FT-LBS
LONG. CYCLIC PITCH = 0 DEG.
DYNAMIC PRESSURE = 7.3 LBS/FT.^{2}

NOTE: ALL TEST PTS. SHOWN FOR DECELERATION, IE, POSITIVE C_R

$A_2 = 0°$
LONG SPOILERS

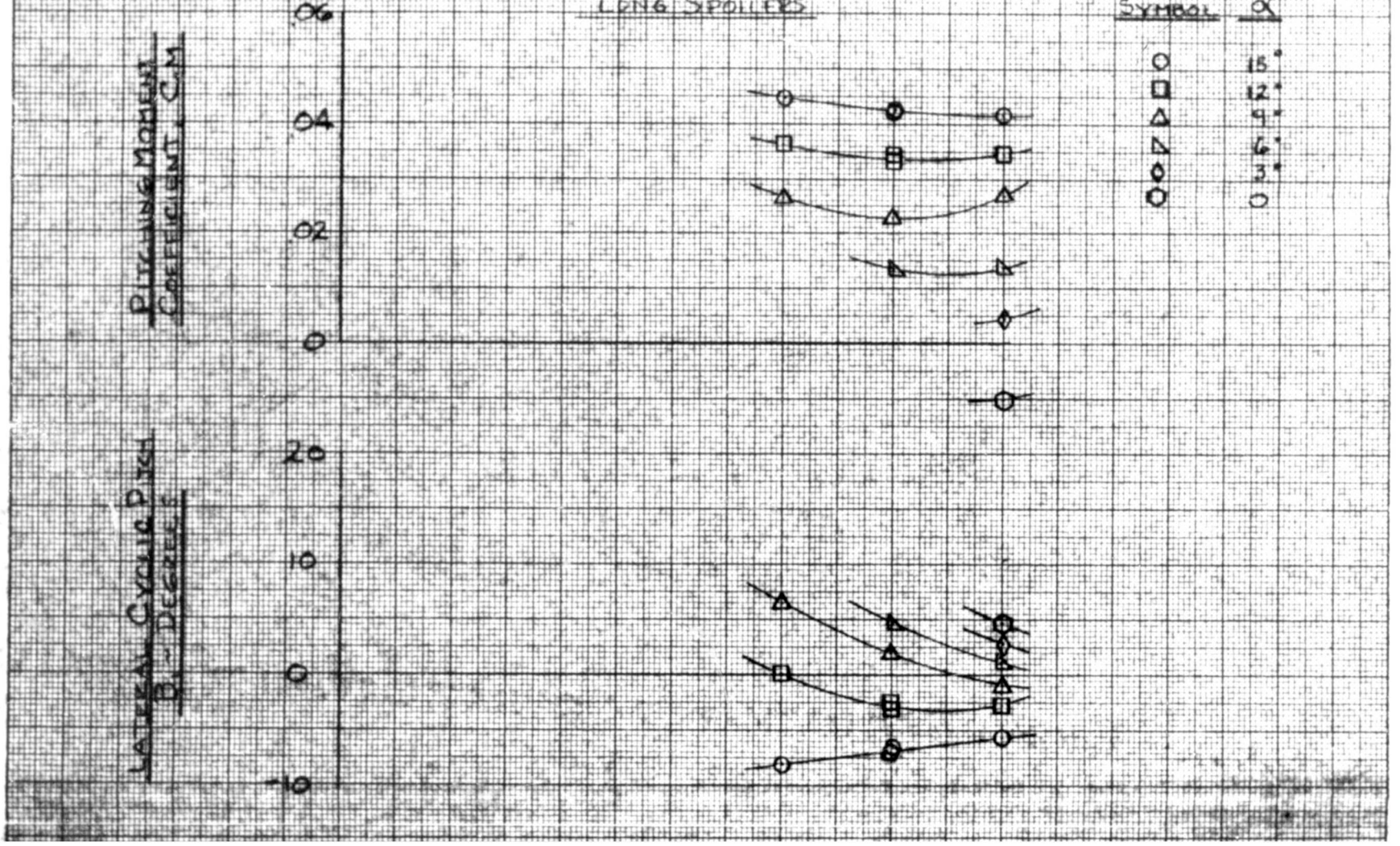

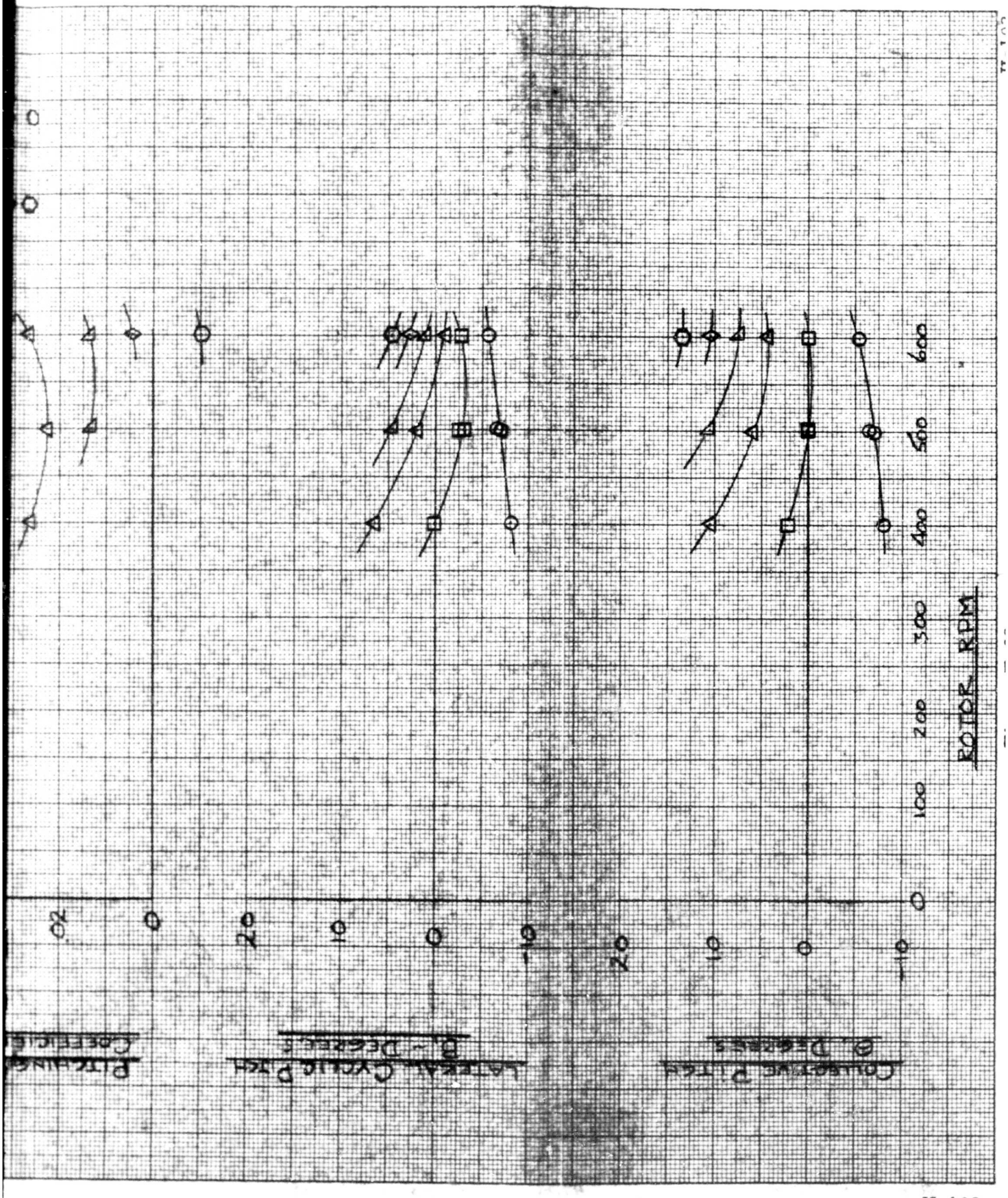
ROTOR RPM
100
200
300
400
500
600
0
Collective Pitch
θ₀ Degrees
Lateral Cyclic Pitch
B₁ - Degrees
Pitching
Coefficie

CONVERSION TEST

RUN 109P

CONFIG FN, H, BZX,

LIFT = 50 LBS.
ROLLING MOMENT = 0 FT LBS.
LONG. CYCLIC PITCH = 0 DEG

NOTE: ALL TEST PTS. SHOWN FOR DECELERATION, IE. POSITIVE C_M

$A_z = 0°$

SHORT SPOILERS

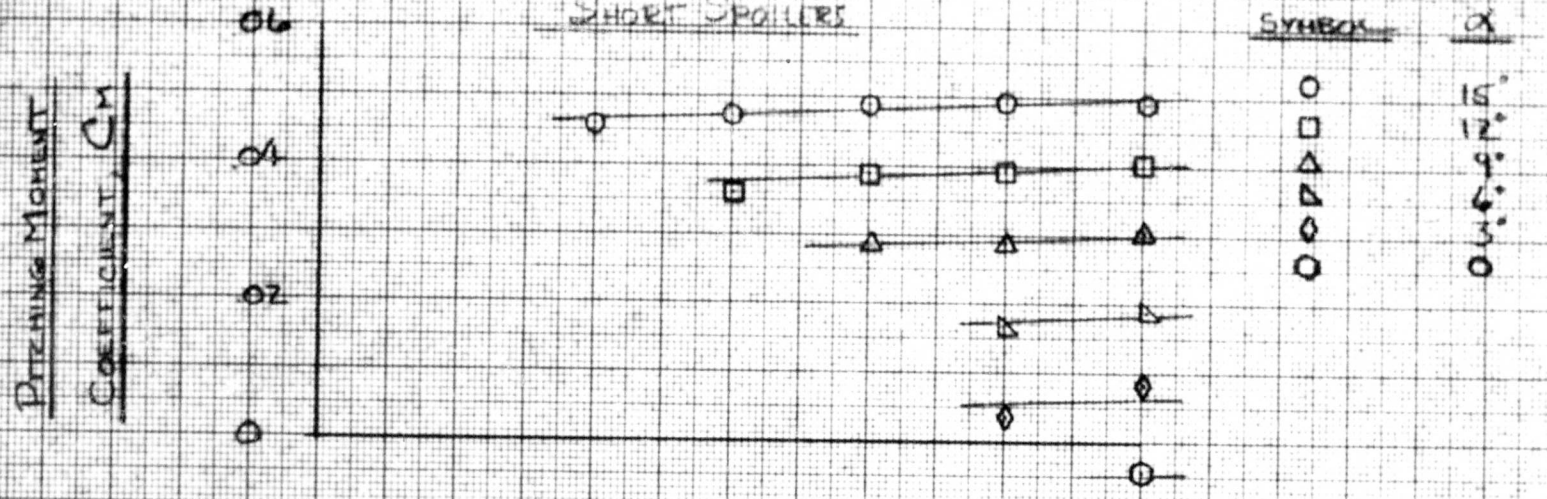

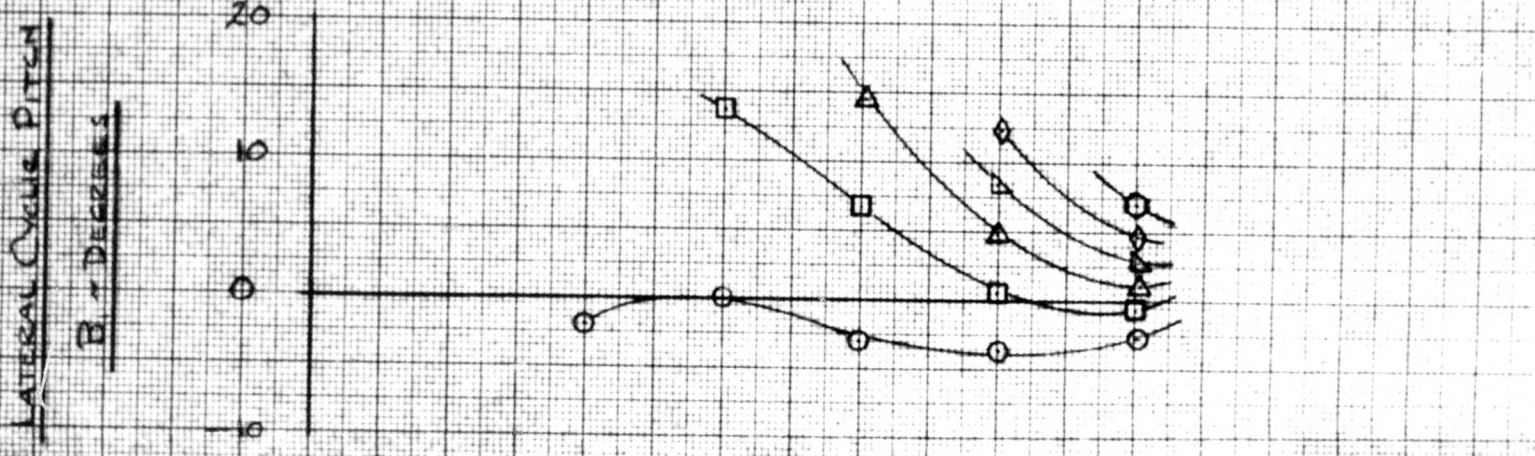

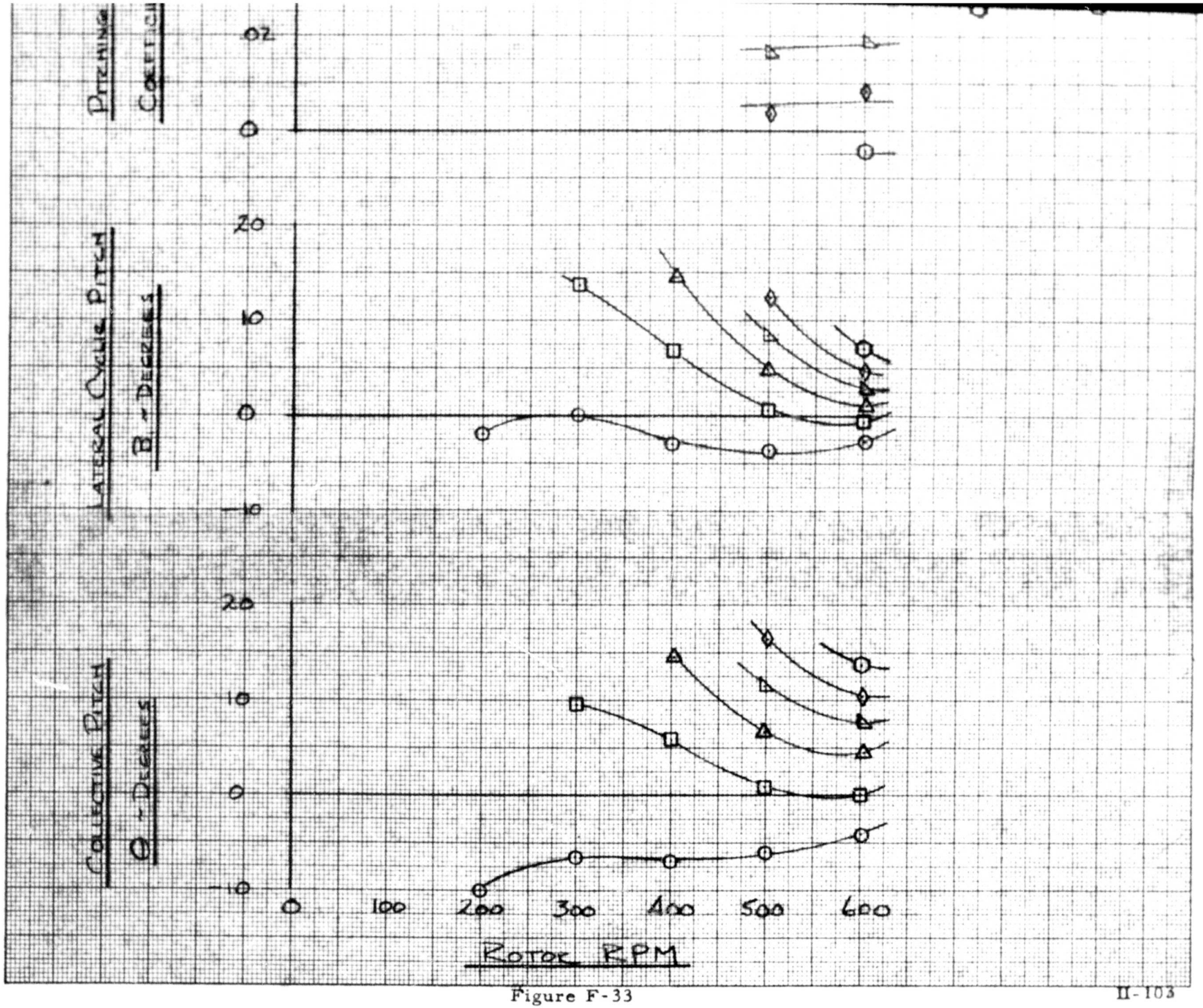

Figure F-33

II-103

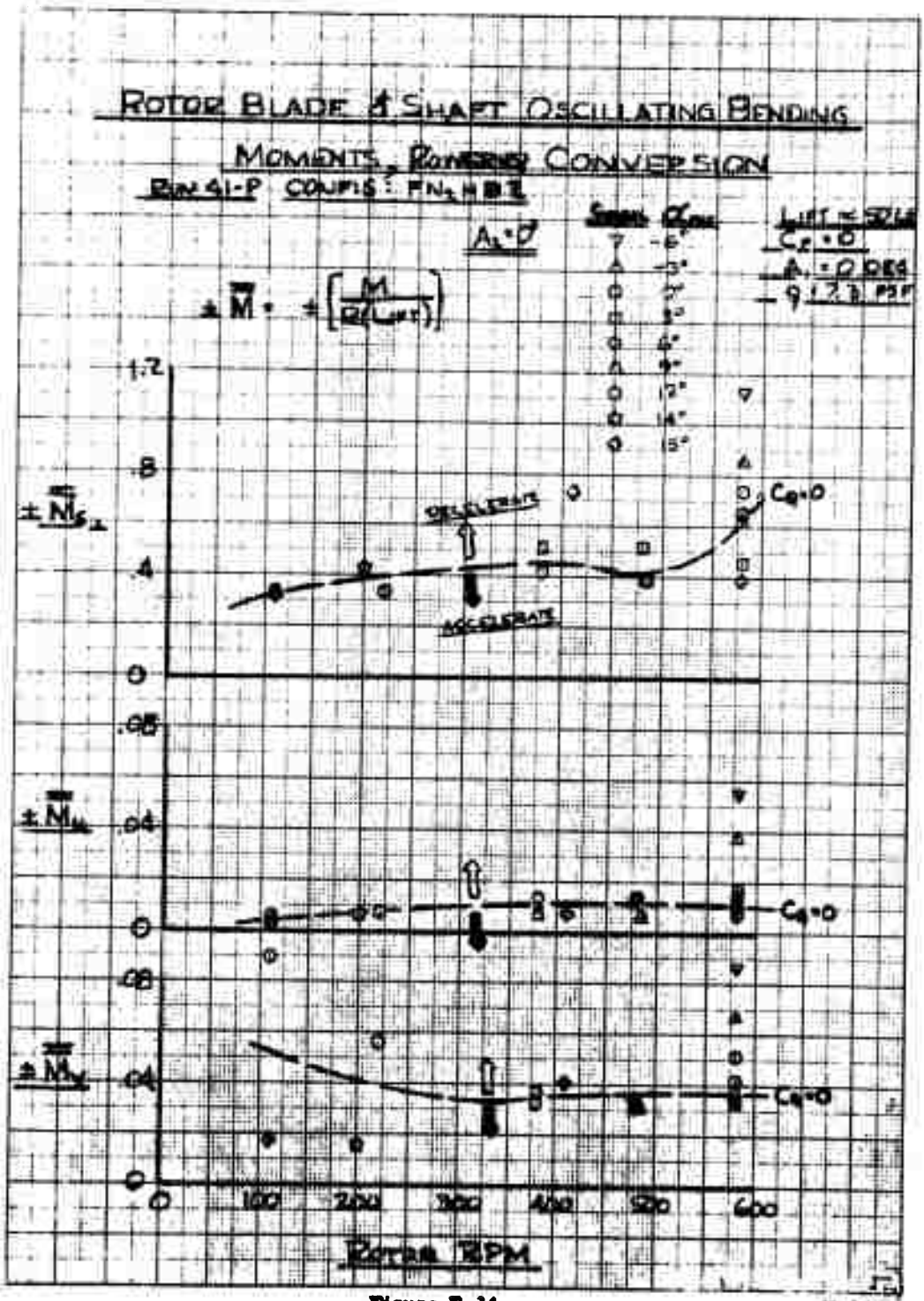
ROTOR BLADE & SHAFT OSCILLATING BENDING
MOMENTS, POWERED CONVERSION
RON 41-P CONFIG: FN, HBT
$A_s = 0$
$\pm \bar{M} = \pm \left[\frac{M}{qR(C_{MT})} \right]$
$C_T = 0$
$\mu = 0$ DES
q 123 PSF
$\pm \bar{M}_{S_{1/2}}$
$\pm \bar{M}_{H_{1/2}}$
$\pm \bar{M}_{H_{3/4}}$
$C_T = 0$
DECELERATE
ACCELERATE
1.2
.8
.4
0
.08
.04
0
.08
.04
0
100
200
300
400
500
600
ROTOR RPM

Figure F-34

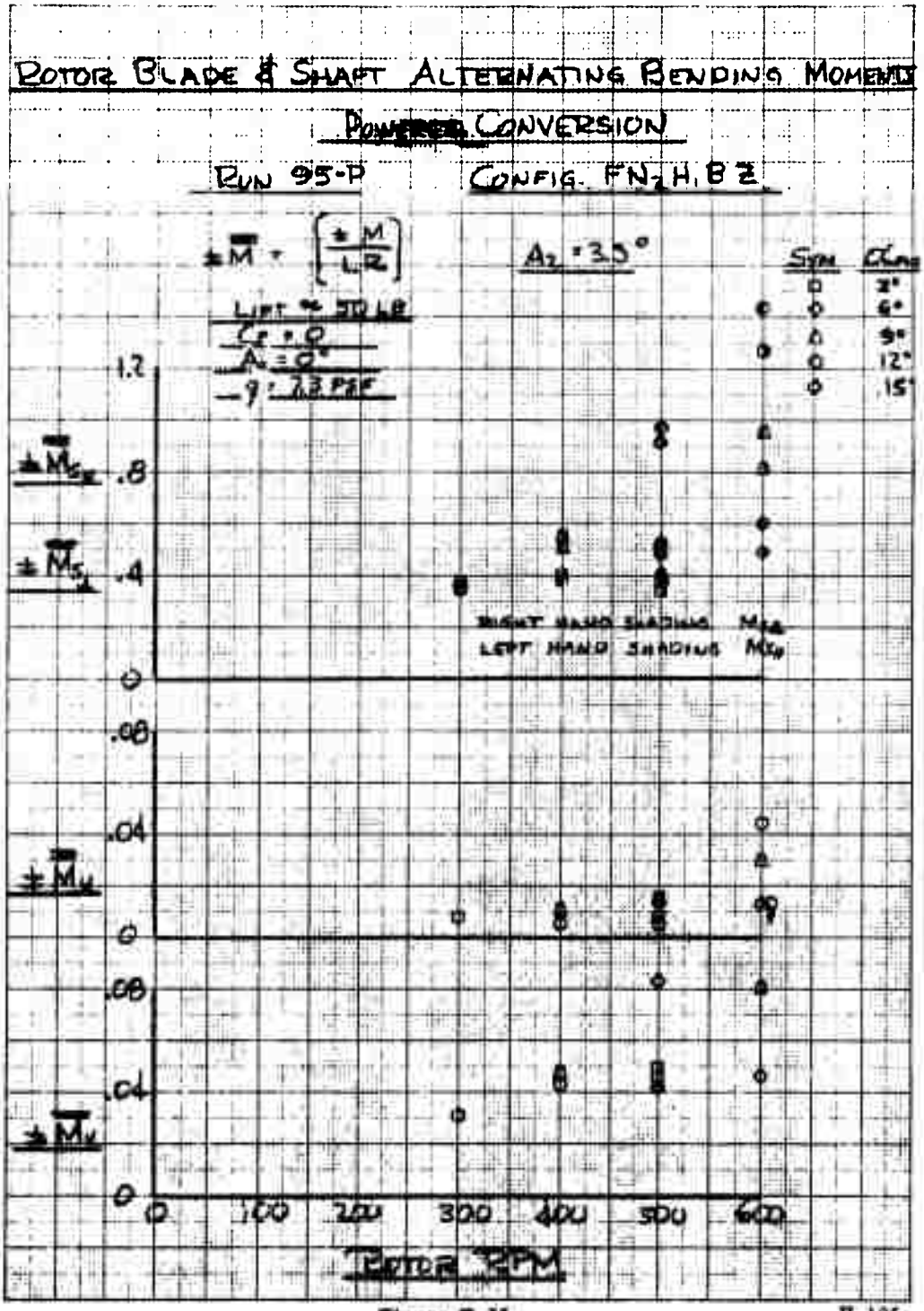
ROTOR BLADE & SHAFT ALTERNATING BENDING MOMENTS
POWER CONVERSION
RUN 95-P
CONFIG. FN-2, H, B 2
$\pm\overline{M} = \left[\frac{\pm M}{LR}\right]$
LIFT = 370 LB
$C_T = .0$
$A_1 = 0°$
$-9 = 23$ PSF
$A_2 = 3.5°$
SYM
$\alpha_{0.75R}$
2°
6°
9°
12°
15°
$\pm\overline{M}_{S_X}$
$\pm\overline{M}_{S_Y}$
$\pm\overline{M}_X$
$\pm\overline{M}_Y$
1.2
.8
.4
0
.08
.04
0
.08
.04
0
RIGHT HAND SHADING M_{X_R}
LEFT HAND SHADING M_{X_L}
0
100
200
300
400
500
600
ROTOR RPM

Figure F-35

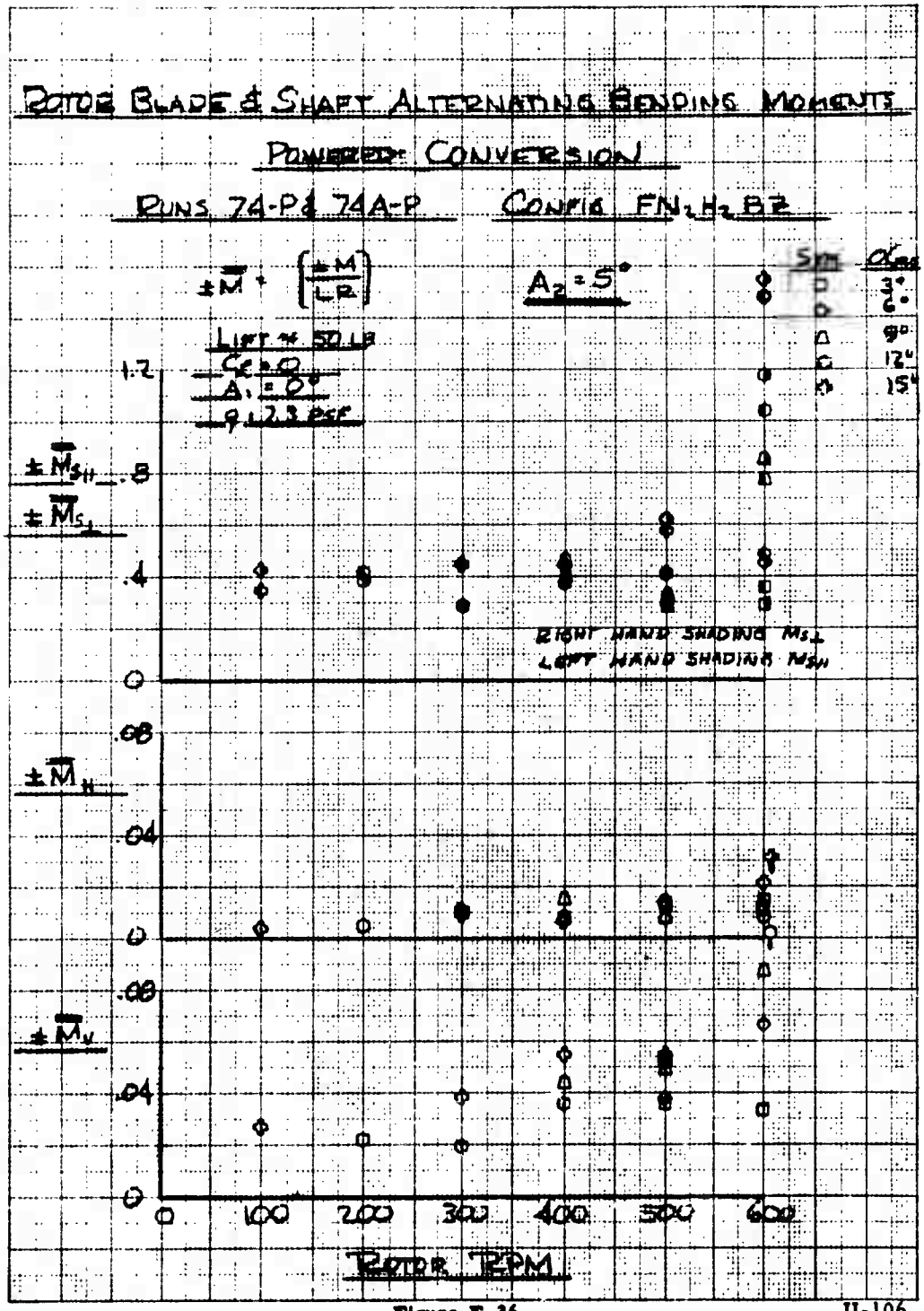
ROTOR BLADE & SHAFT ALTERNATING BENDING MOMENTS
POWERED CONVERSION
RUNS 74-P & 74A-P
CONFIG FN, H2 B2
$\pm\bar{M} = \left[\frac{\pm M}{LR}\right]$
$A_2 = 5°$
LIFT = 50 LB
$C_T = 0$
$A_1 = 0°$
$q = 2.3$ PSF
$\pm\bar{M}_{S_{II}}$
$\pm\bar{M}_{S_\perp}$
$\pm\bar{M}_{II}$
$\pm\bar{M}_\perp$
1.2
.8
.4
0
.08
.04
0
.08
.04
0
0
100
200
300
400
500
600
ROTOR RPM
RIGHT HAND SHADING $M_{S_\perp}$
LEFT HAND SHADING $M_{S_{II}}$
S/M
α_{TPP}
3°
6°
9°
12°
15°

Figure F-36

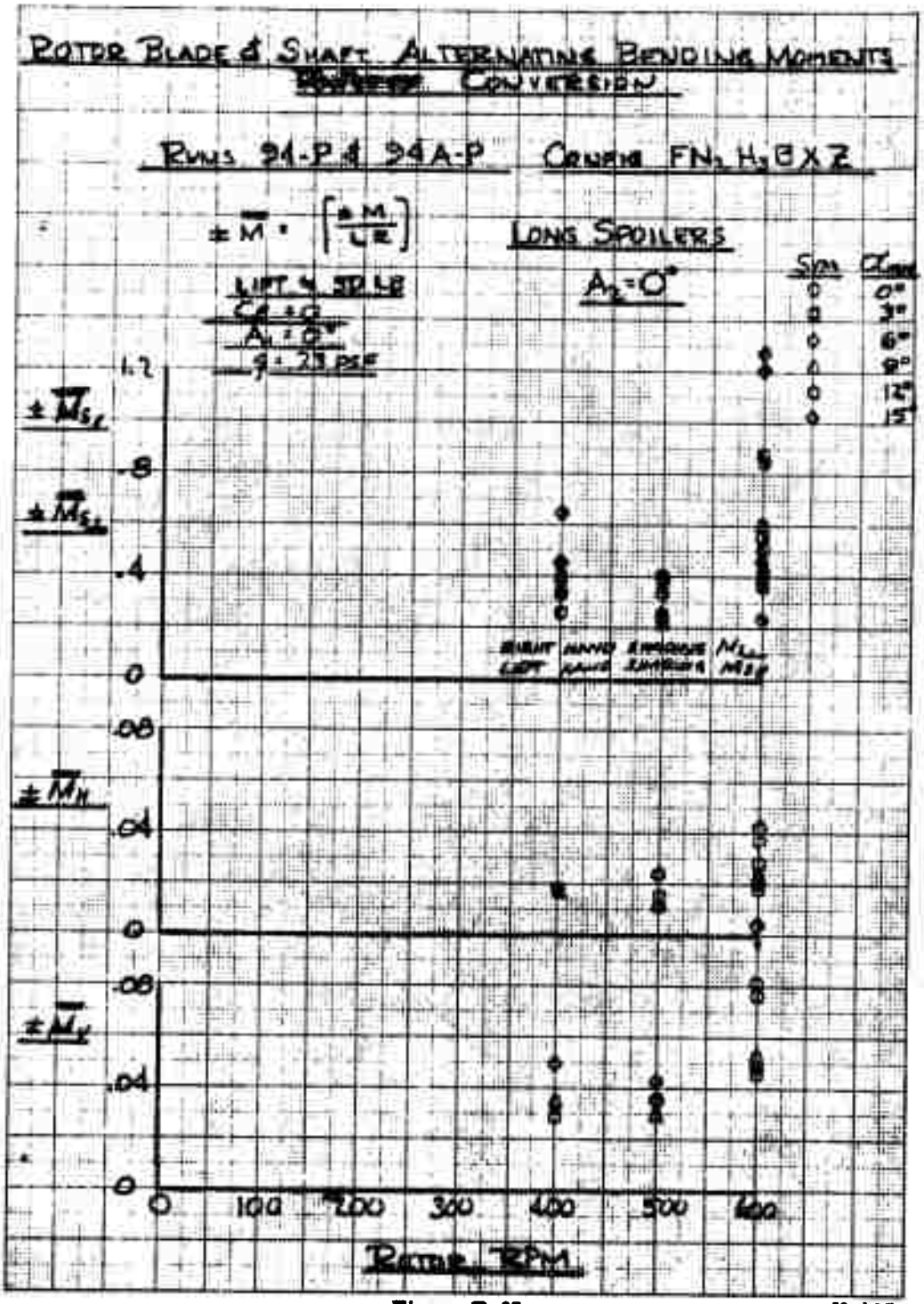
ROTOR BLADE & SHAFT ALTERNATING BENDING MOMENTS
RUNS 91-P & 94A-P
CONFIG FN, H, B X Z
LONG SPOILERS
$A_2 = 0°$
LIFT = 32,000 LB
$C_{\bar{M}} = 0$
$A_1 = 0°$
$q = 23$ PSF
$\pm \bar{M}_{S_L}$
$\pm \bar{M}_{S_R}$
$\pm \bar{M}_H$
$\pm \bar{M}_V$
1.2
.8
.4
0
.08
.04
0
.08
.04
0
0
100
200
300
400
500
600
ROTOR RPM

Figure F-37

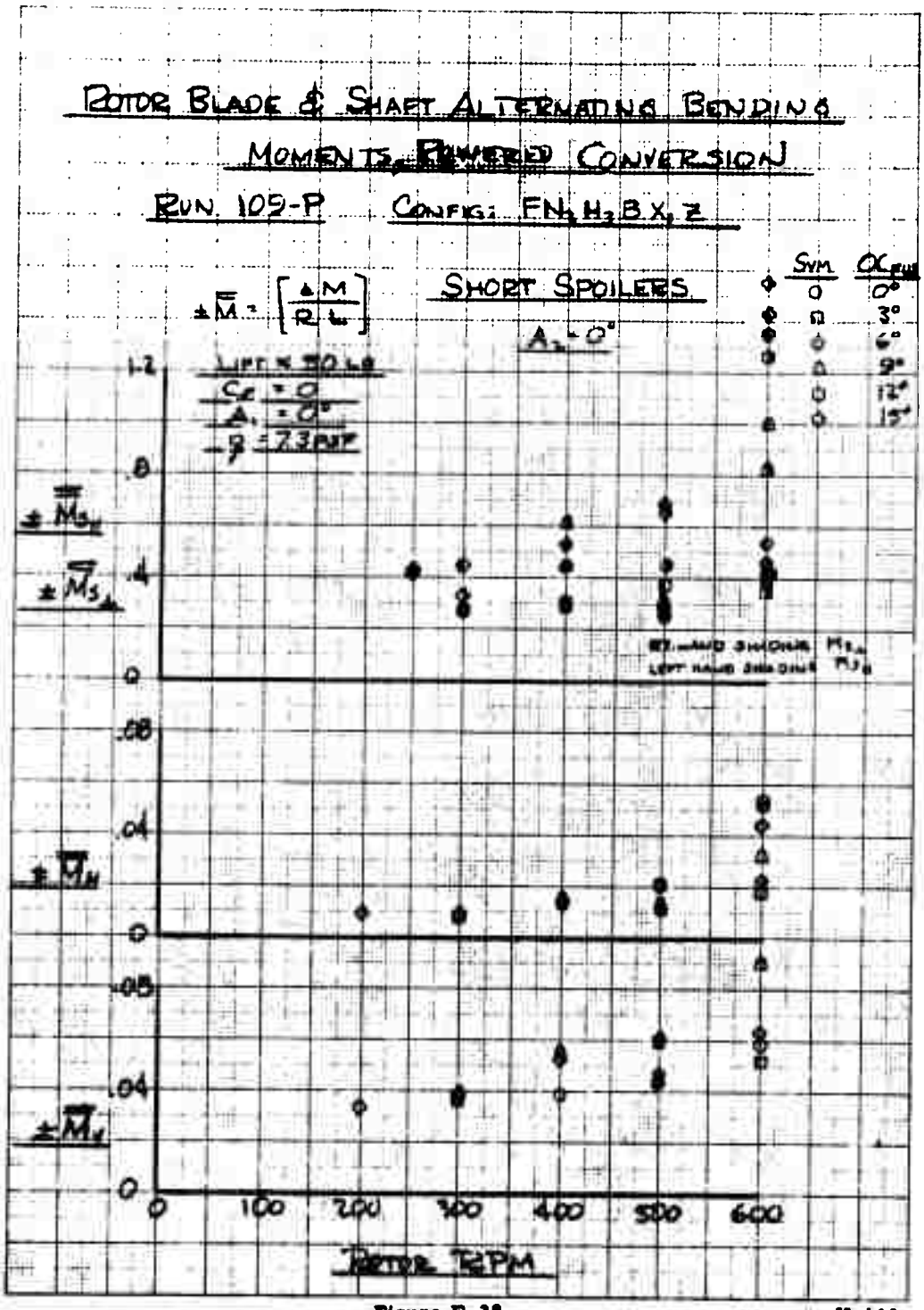
ROTOR BLADE & SHAFT ALTERNATING BENDING MOMENTS, POWERED CONVERSION
RUN 109-P CONFIG: FN2 H2 B X, Z
SHORT SPOILERS
$\pm\bar{M} = \left[\frac{\Delta M}{R L_w}\right]$
$A_2 = 0°$
LIFT = 750 LB
$C_\ell = 0$
$A_1 = 0°$
$\beta = 7.3$ DEG
SYM
OC FLAP
0°
3°
6°
9°
12°
15°
$\pm\bar{M}_{S_H}$
$\pm\bar{M}_{S_L}$
$\pm\bar{M}_H$
$\pm\bar{M}_L$
1.2
.8
.4
0
.08
.04
0
.05
.04
0
0
100
200
300
400
500
600
ROTOR RPM

Figure F-38

AUTOMATIC CONVERSION

$A_2 = 0°$

$A_1 = 0°$

RUN 93-P CONFIG F.N., H, B V, S, T

ΔC_l, $\Delta C_{(m_{c.g.})}$, ΔC_{l_r} ARE WITH RESPECT TO ZERO RPM CONDITIONS

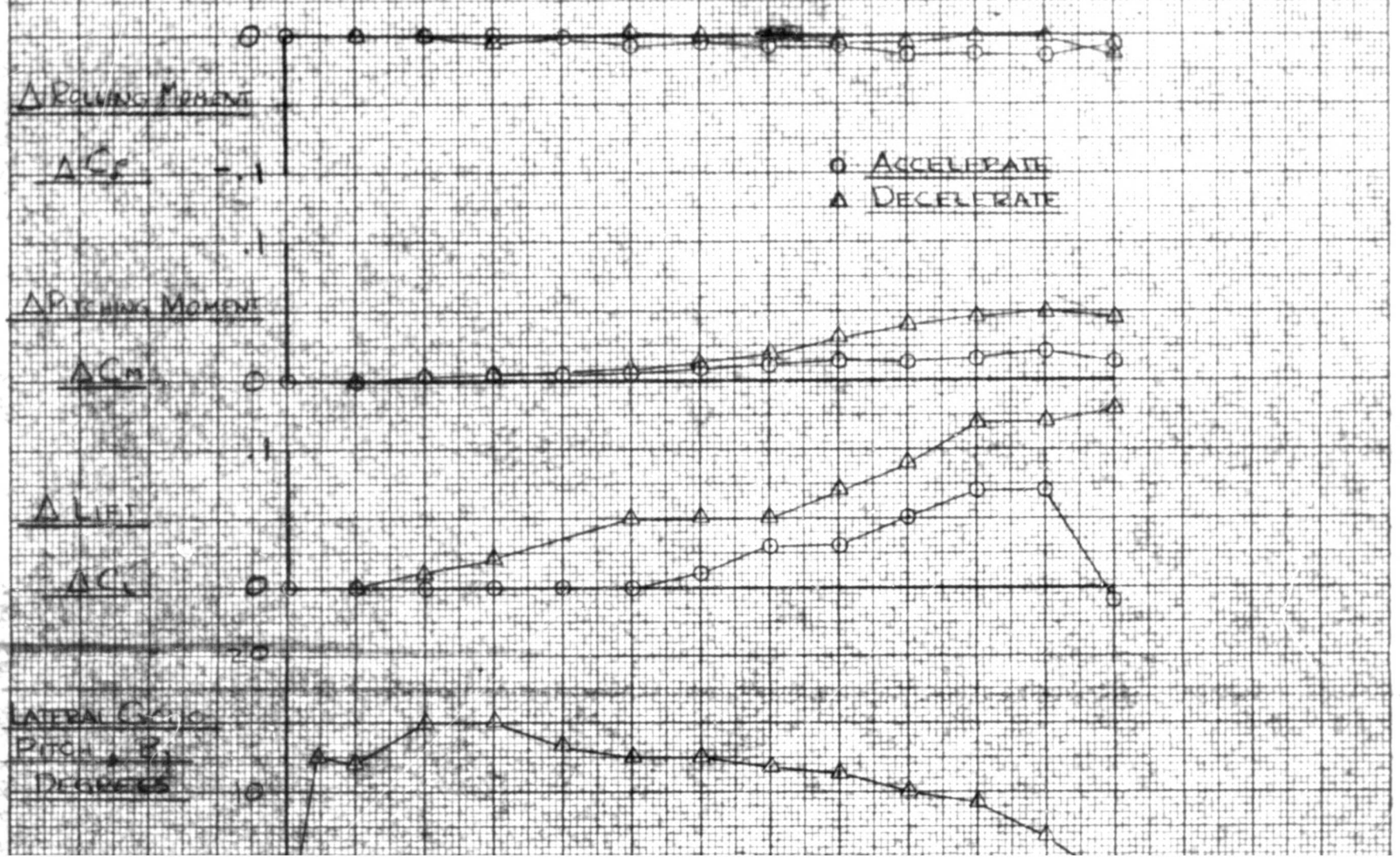

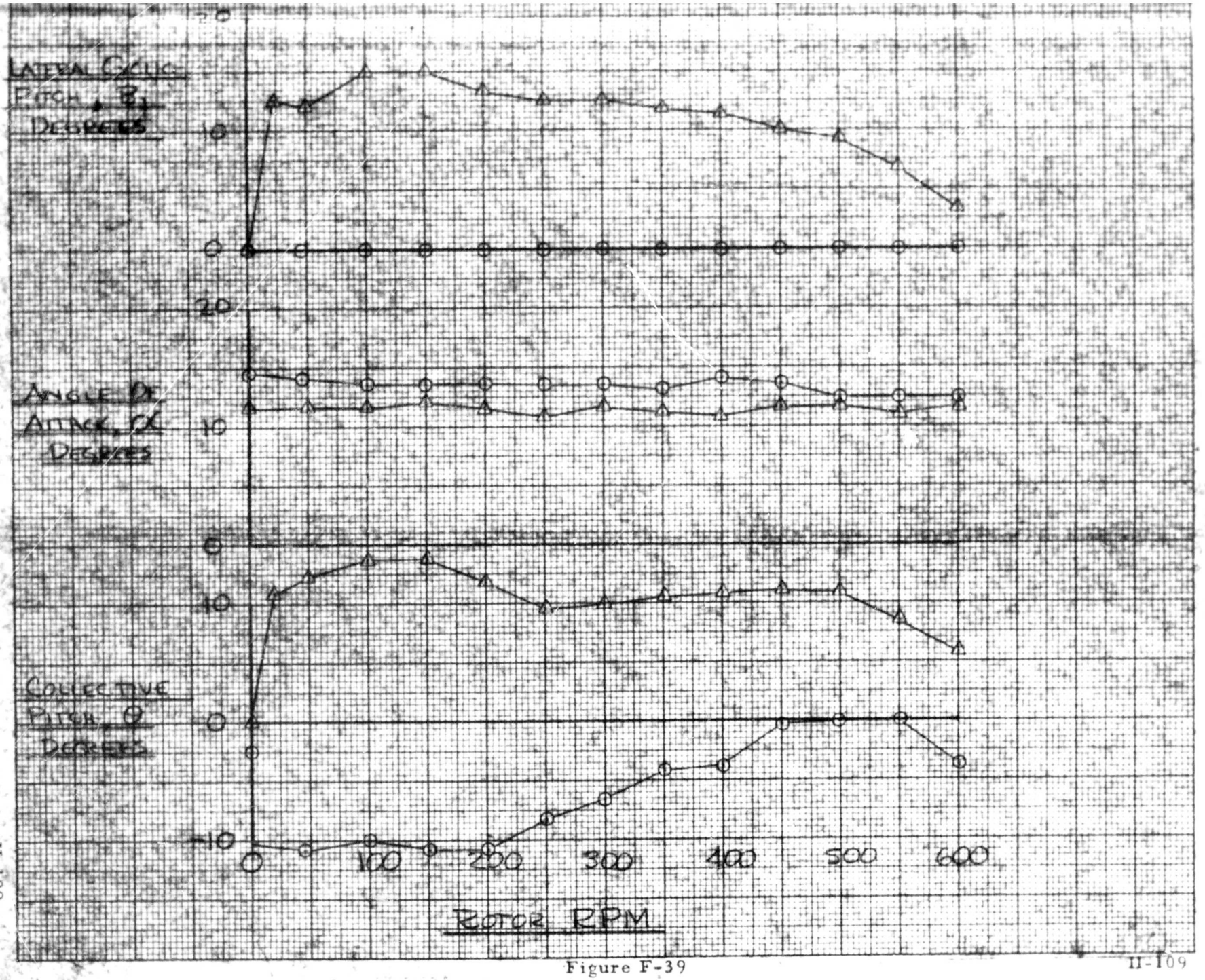

Figure F-39

II-109

AUTOMATIC CONVERSION

$A_2 = 3.5°$

$A_1 = 0°$

RUN 96C-P CONFIG. FN, H, BV, S, Z

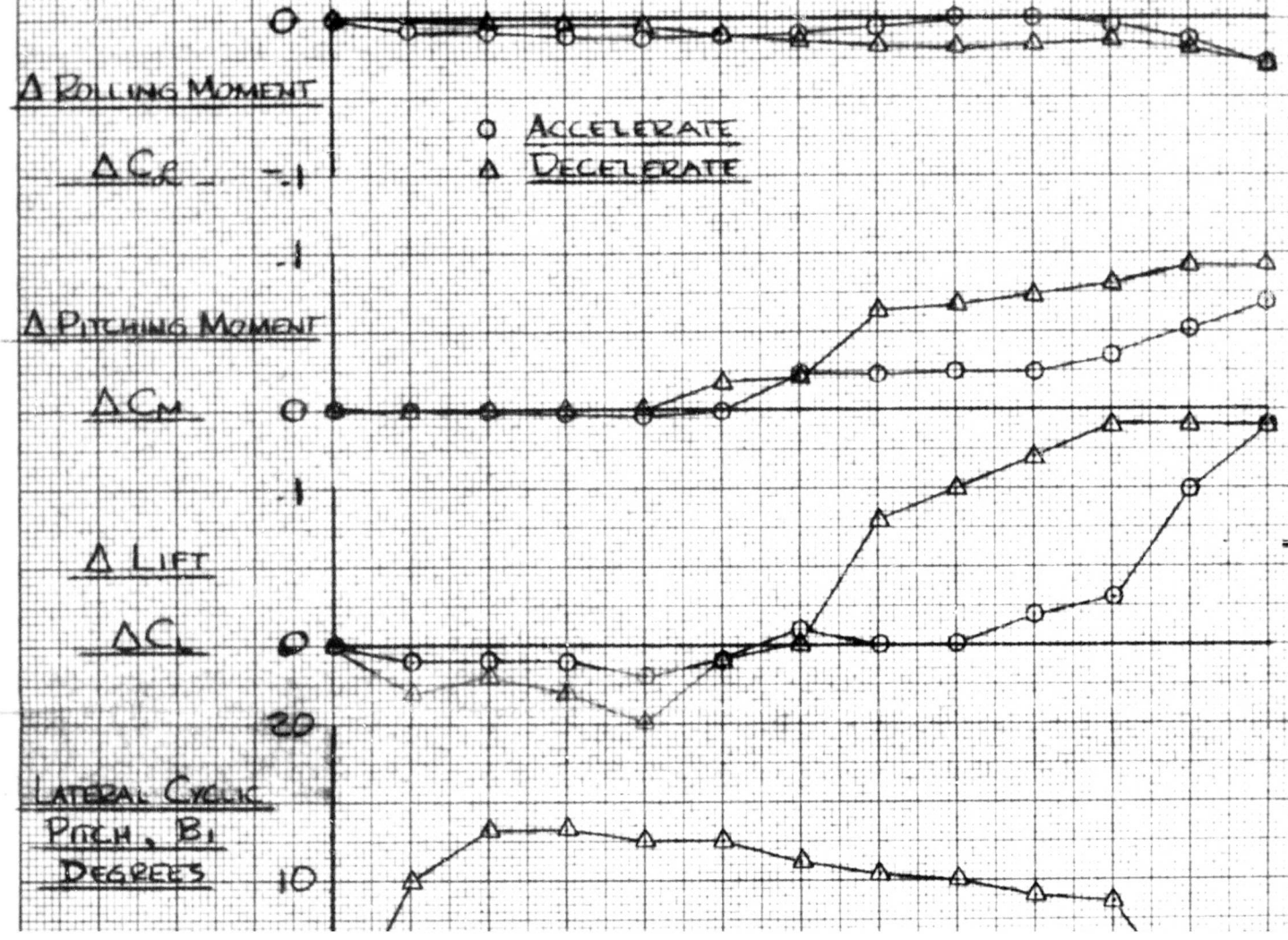

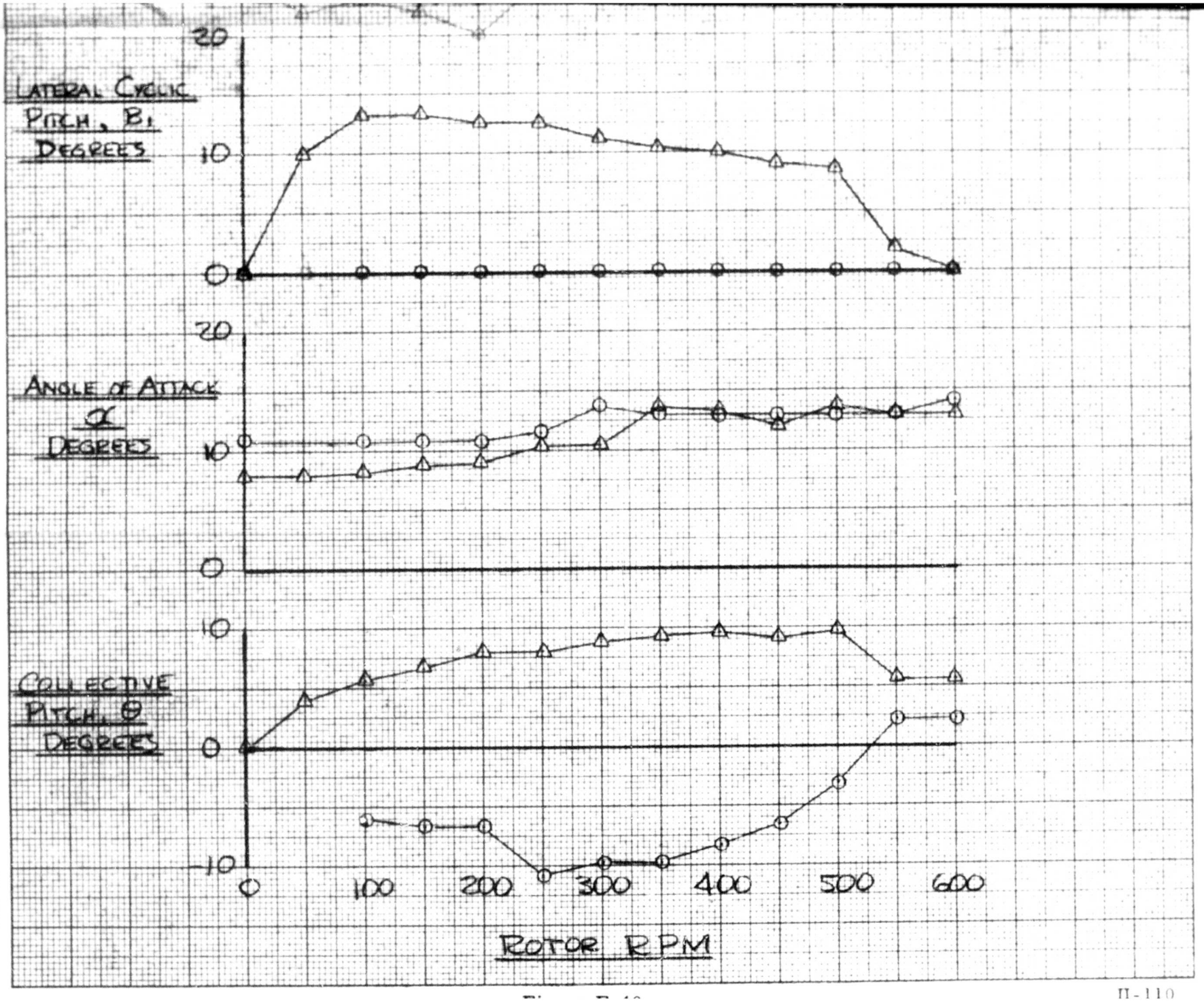

Figure II-10

II-110

Automatic Conversion

$A_1 = 5°$

$A = 0°$

Run 82-P Config. FN, H_2, BV, S, Z

ΔC_l, ΔC_m, ΔC_p Abs With Respect To Zero RPM Conditions

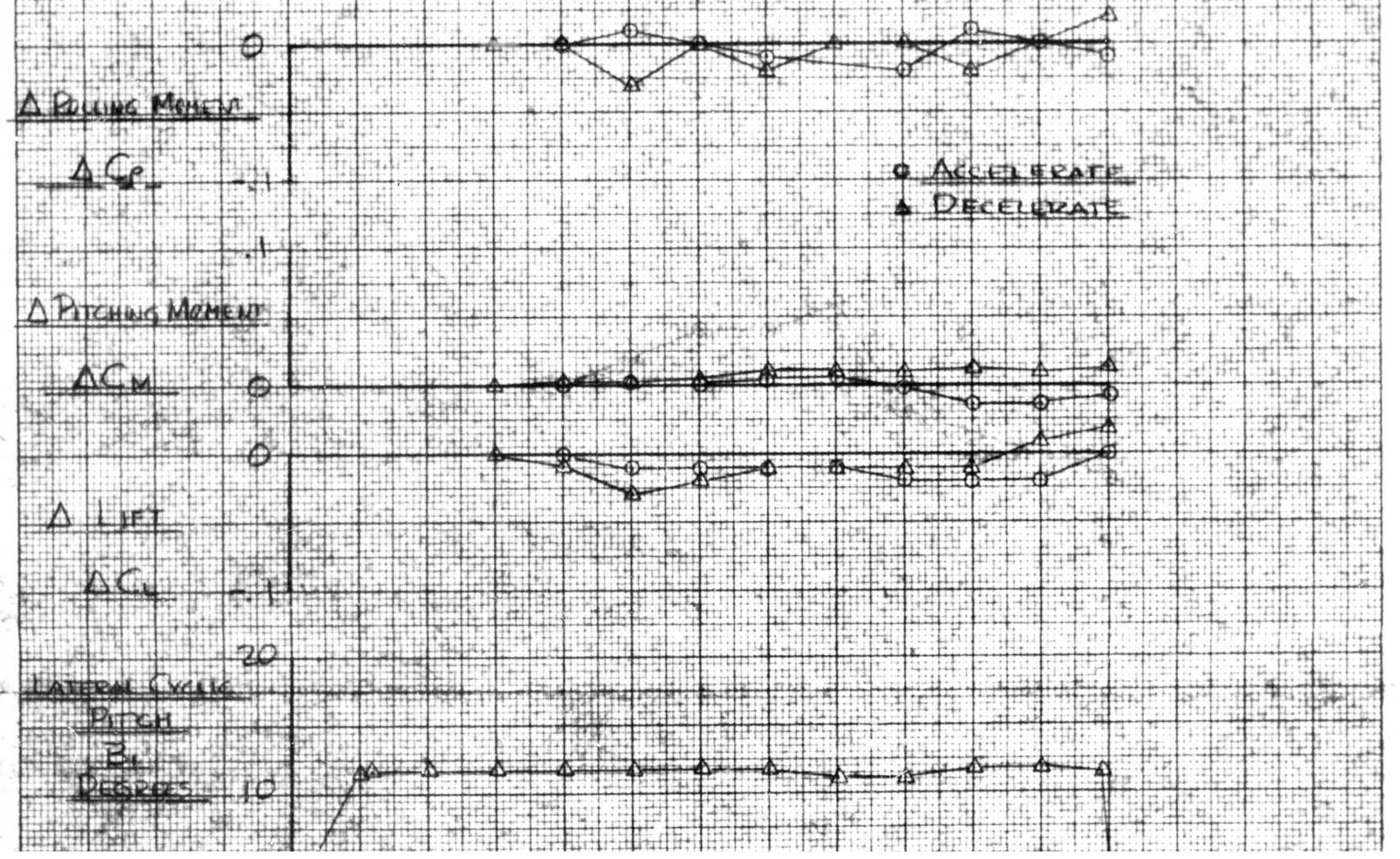

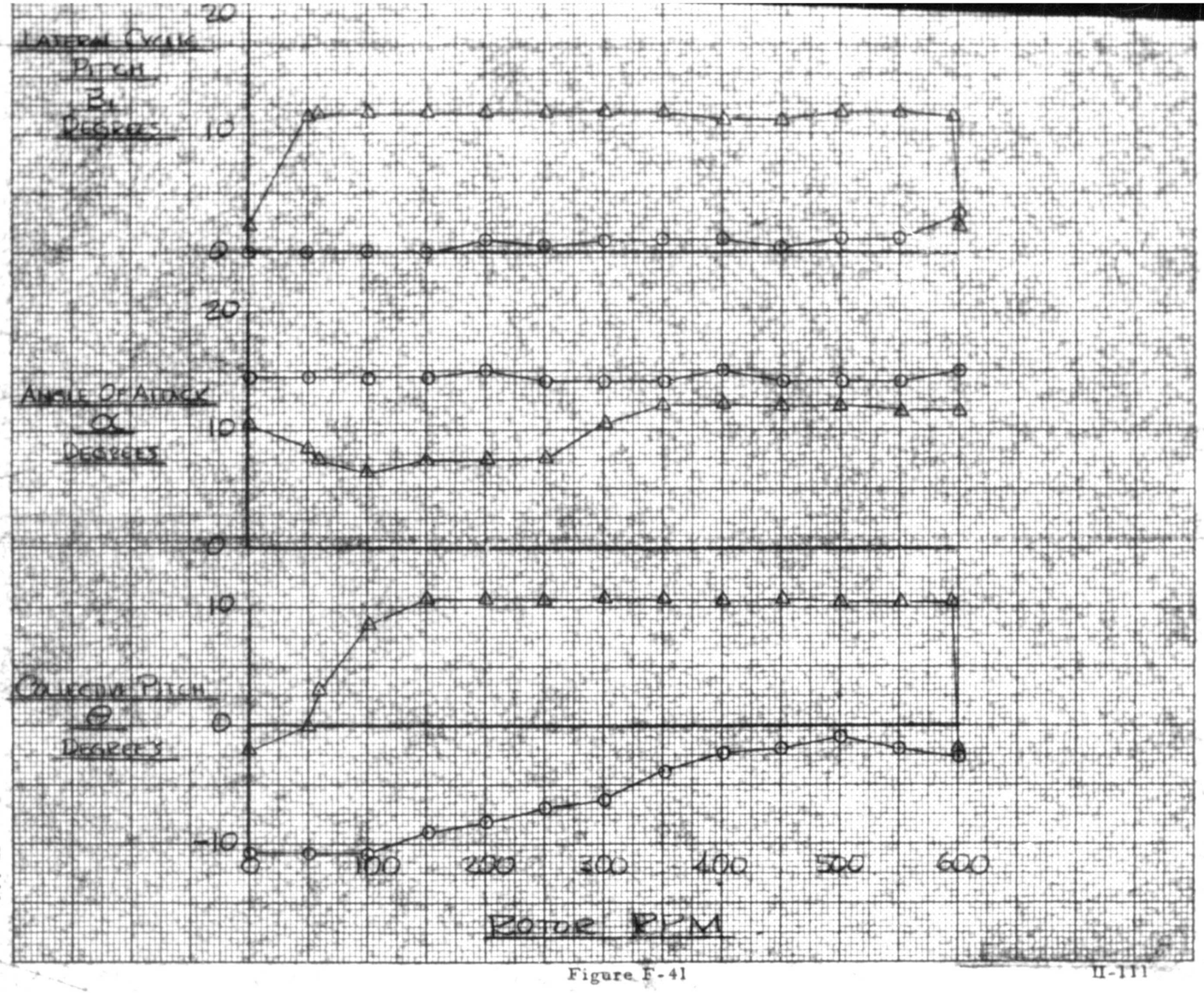

Figure F-41

II-111

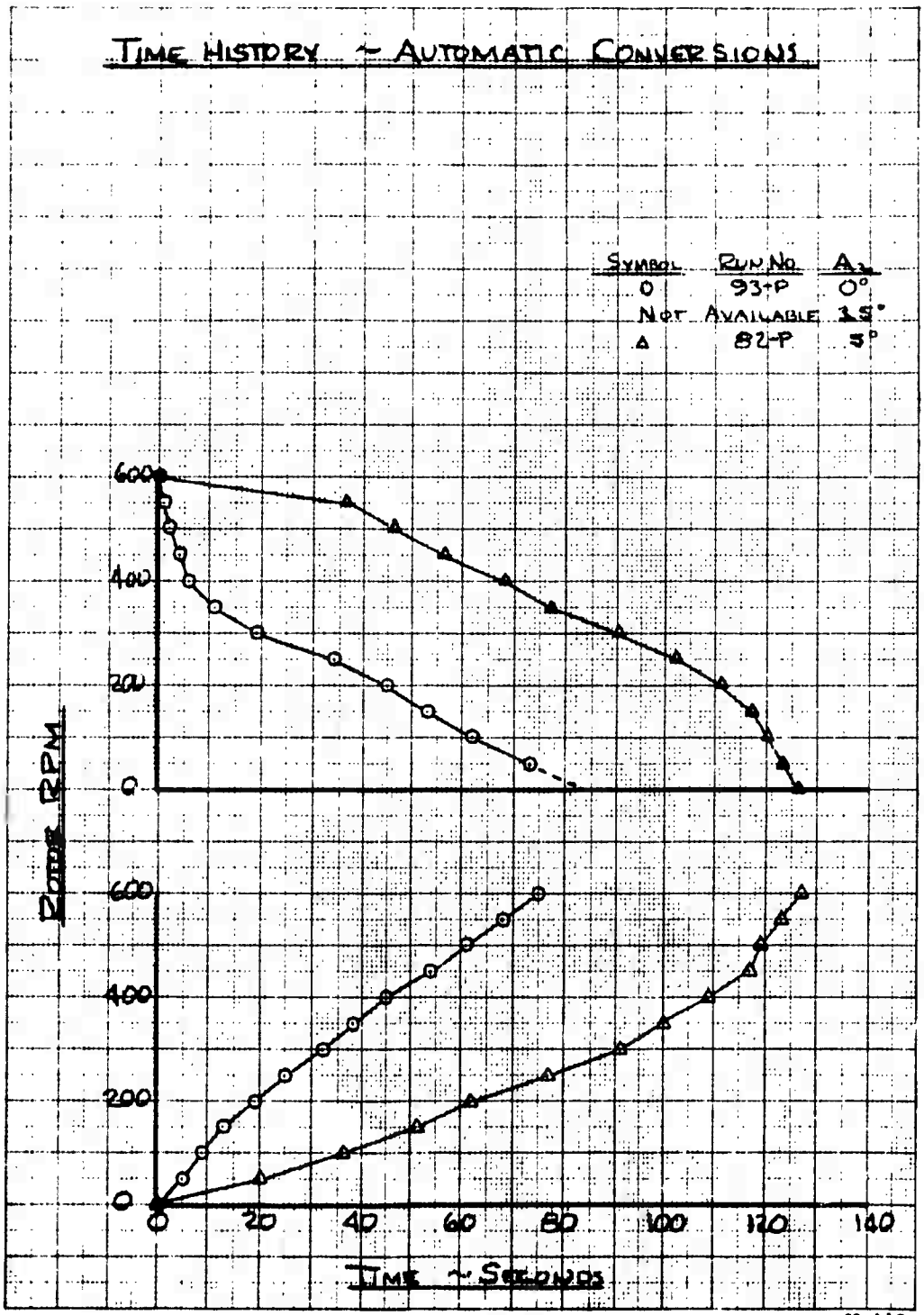
TIME HISTORY ~ AUTOMATIC CONVERSIONS
SYMBOL RUN NO. A_z
O 93+P 0°
NOT AVAILABLE 1.5°
Δ 82-P 3°
600
400
200
0
600
400
200
0
POWER RPM
0
20
40
60
80
100
120
140
TIME ~ SECONDS

Figure F-42

ALTERNATING BLADE ROOT & SHAFT BENDING MOMENTS

AUTOMATIC CONVERSION

SYMBOL	RUN	A_1
○	93-P	0°
□	96C-P	3.5°
△	82-P	5°

ACCELERATION

$$\pm\overline{M} = \left[\frac{\pm M}{LR}\right]$$

SHAFT BENDING

$\pm\overline{M}_{s_1}$ —

.6
.4
.2
0

$\pm\overline{M}_{s_2}$ —

.6
.4
.2
0
.05

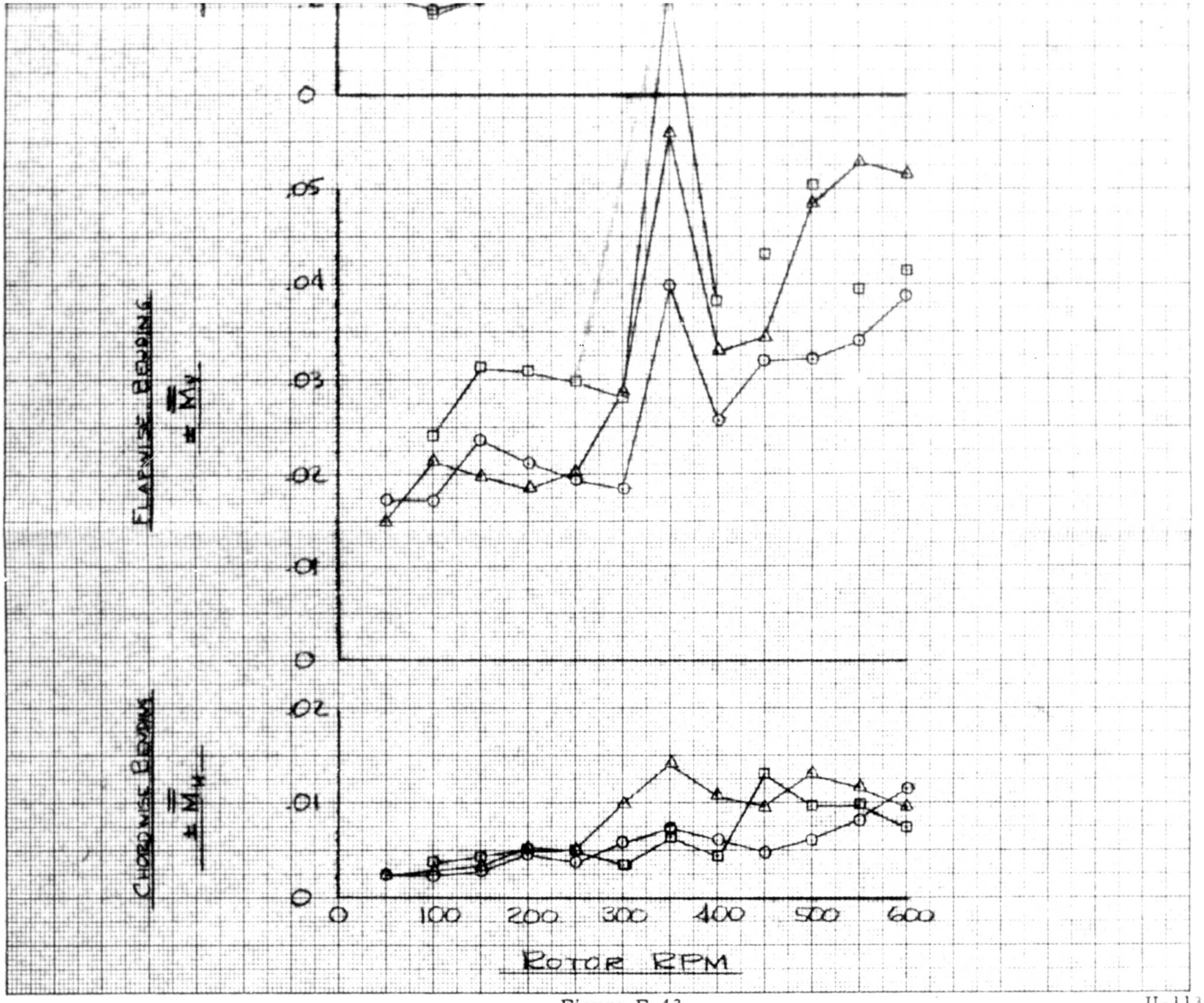

Figure F-43

II-113

ALTERNATING BLADE ROOT & SHAFT BENDING MOMENTS

AUTOMATIC CONVERSION

DECELERATION

$$\pm\bar{M} = \left[\frac{\pm M}{L R}\right]$$

SYMBOL	RUN	Δ_2
○	93-P	0°
□	96-P	2.5°
△	82-P	5°

SHAFT BENDING

$\pm\bar{M}_{s_\perp}$

.6
.4
.2
0

$\pm\bar{M}_{s_{//}}$

.6
.4
.2
0

.05

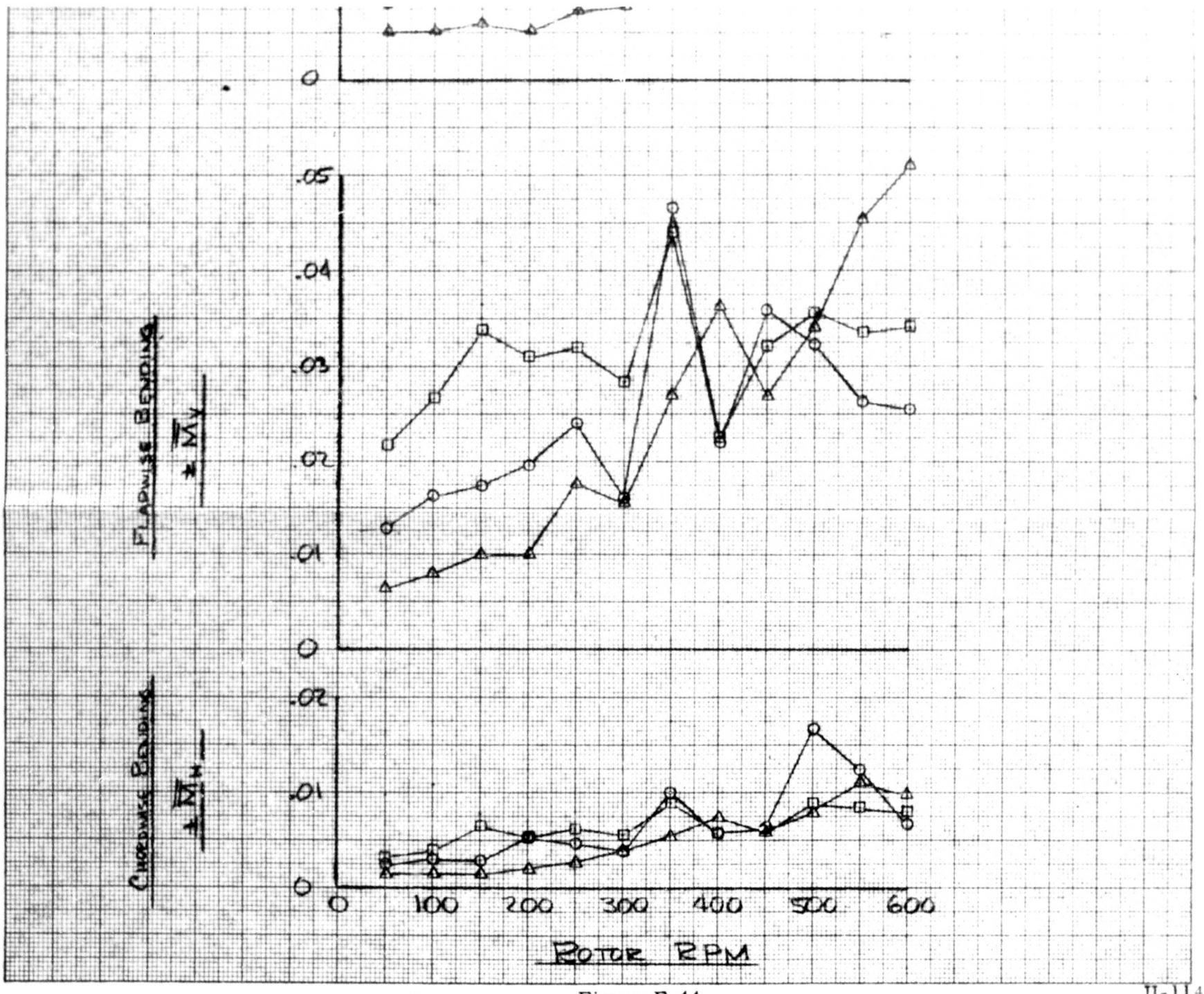

Figure F-44

II-114

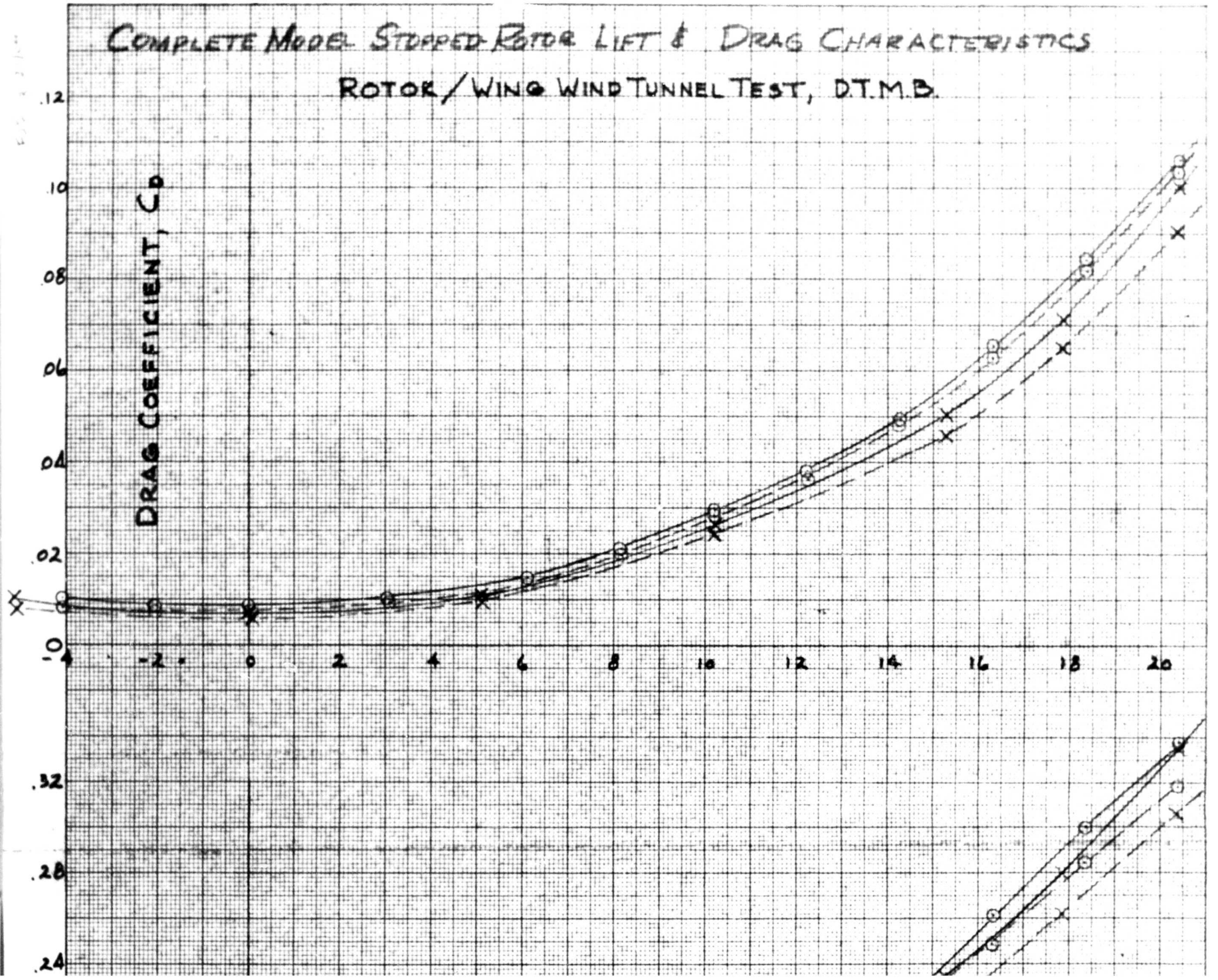
COMPLETE MODEL STOPPED ROTOR LIFT & DRAG CHARACTERISTICS
ROTOR / WING WIND TUNNEL TEST, D.T.M.B.
DRAG COEFFICIENT, C_D
.12
.10
.08
.06
.04
.02
-0
-4
-2
0
2
4
6
8
10
12
14
16
18
20
.32
.28
.24

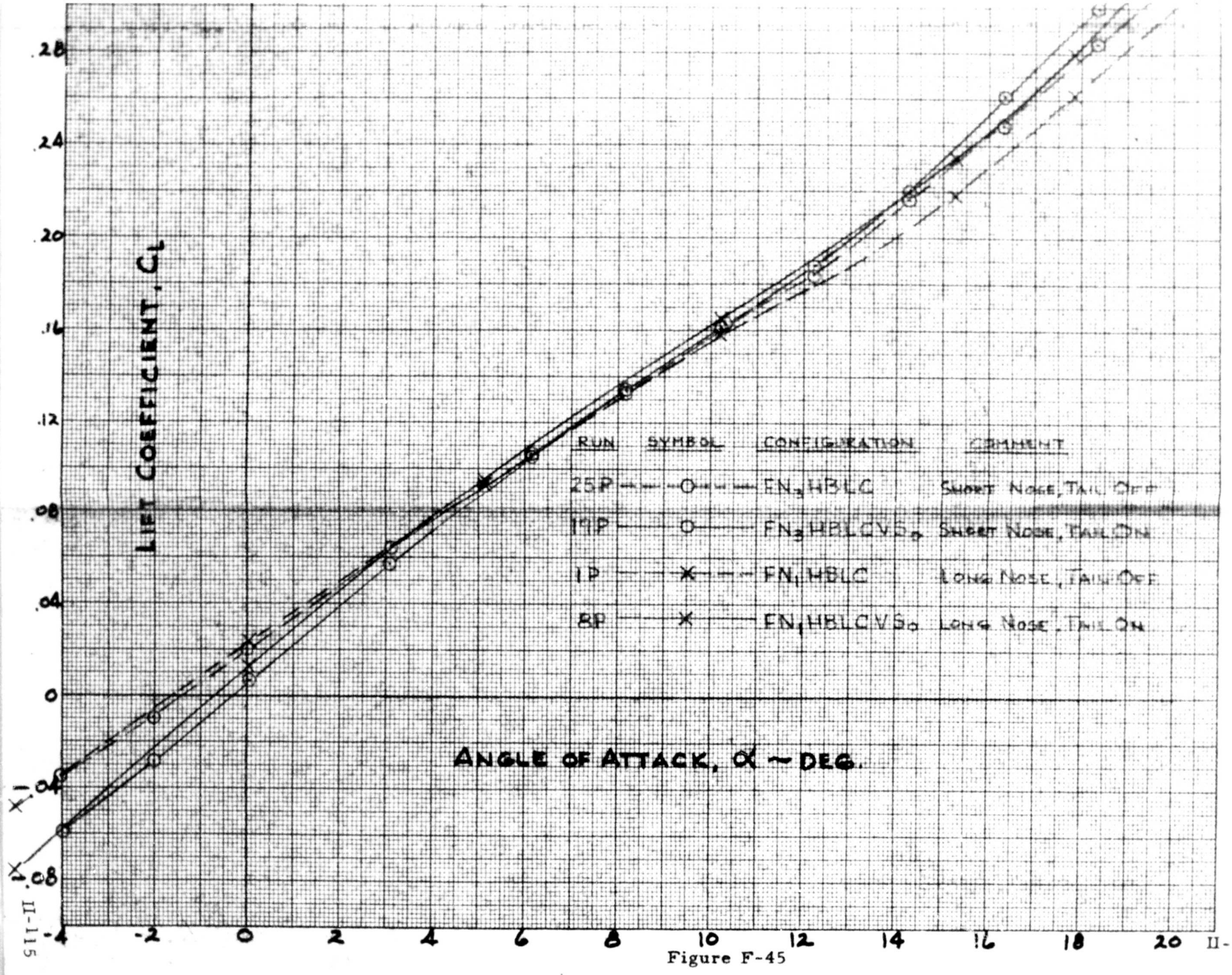
LIFT COEFFICIENT, C_L
ANGLE OF ATTACK, α ~ DEG.
.28
.24
.20
.16
.12
.08
.04
0
-.04
-.08
-4
-2
0
2
4
6
8
10
12
14
16
18
20
RUN SYMBOL CONFIGURATION COMMENT
25P FN_3HBLC SHORT NOSE, TAIL OFF
19P FN_3HBLCVS$_0$ SHORT NOSE, TAIL ON
1P FN_1HBLC LONG NOSE, TAIL OFF
8P FN_1HBLCVS$_0$ LONG NOSE, TAIL ON

Figure F-45

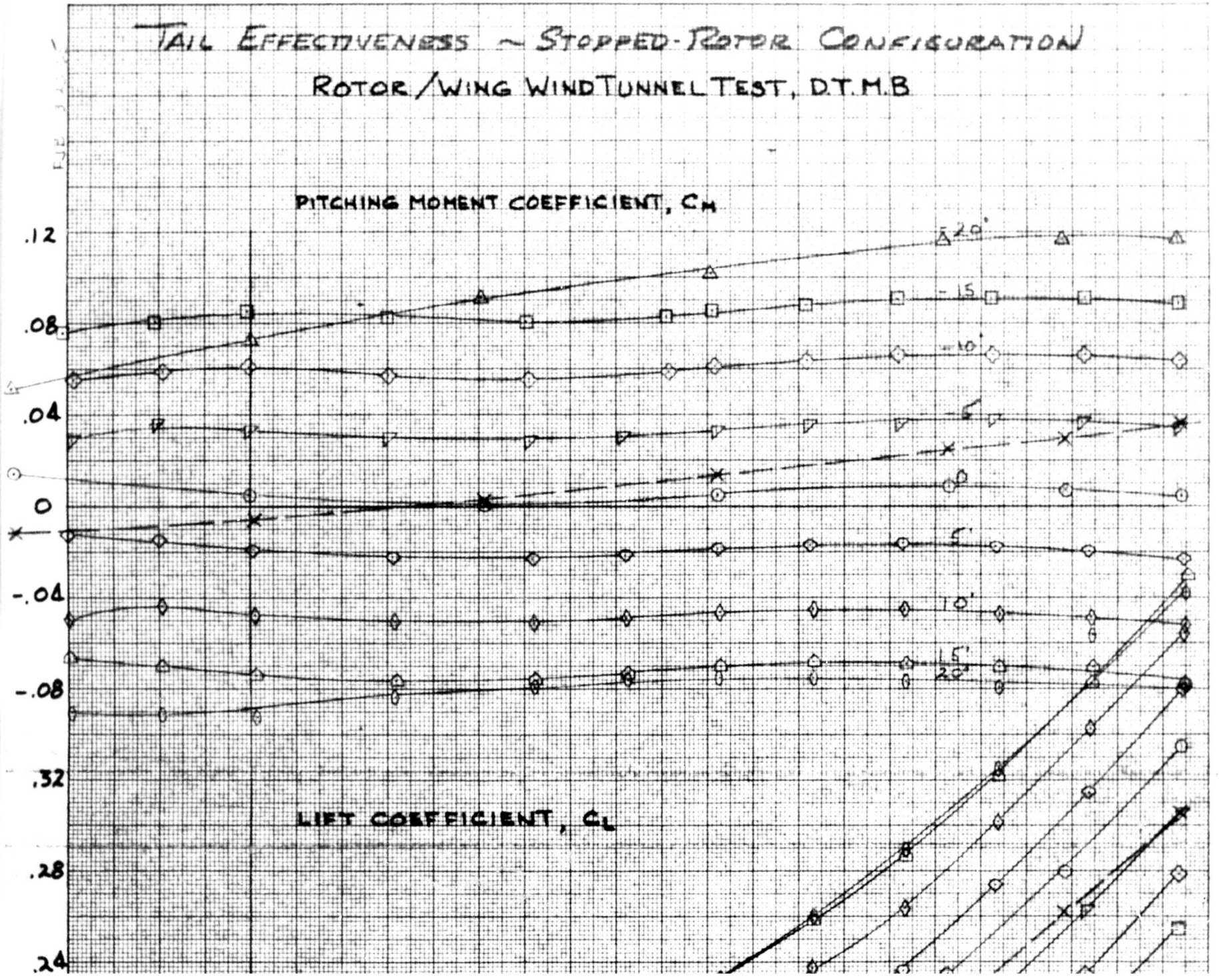
TAIL EFFECTIVENESS ~ STOPPED-ROTOR CONFIGURATION
ROTOR/WING WIND TUNNEL TEST, D.T.M.B
PITCHING MOMENT COEFFICIENT, C_M
.12
.08
.04
0
-.04
-.08
20°
15
10
5
0
-5
-10
-15
-20
LIFT COEFFICIENT, C_L
.32
.28
.24

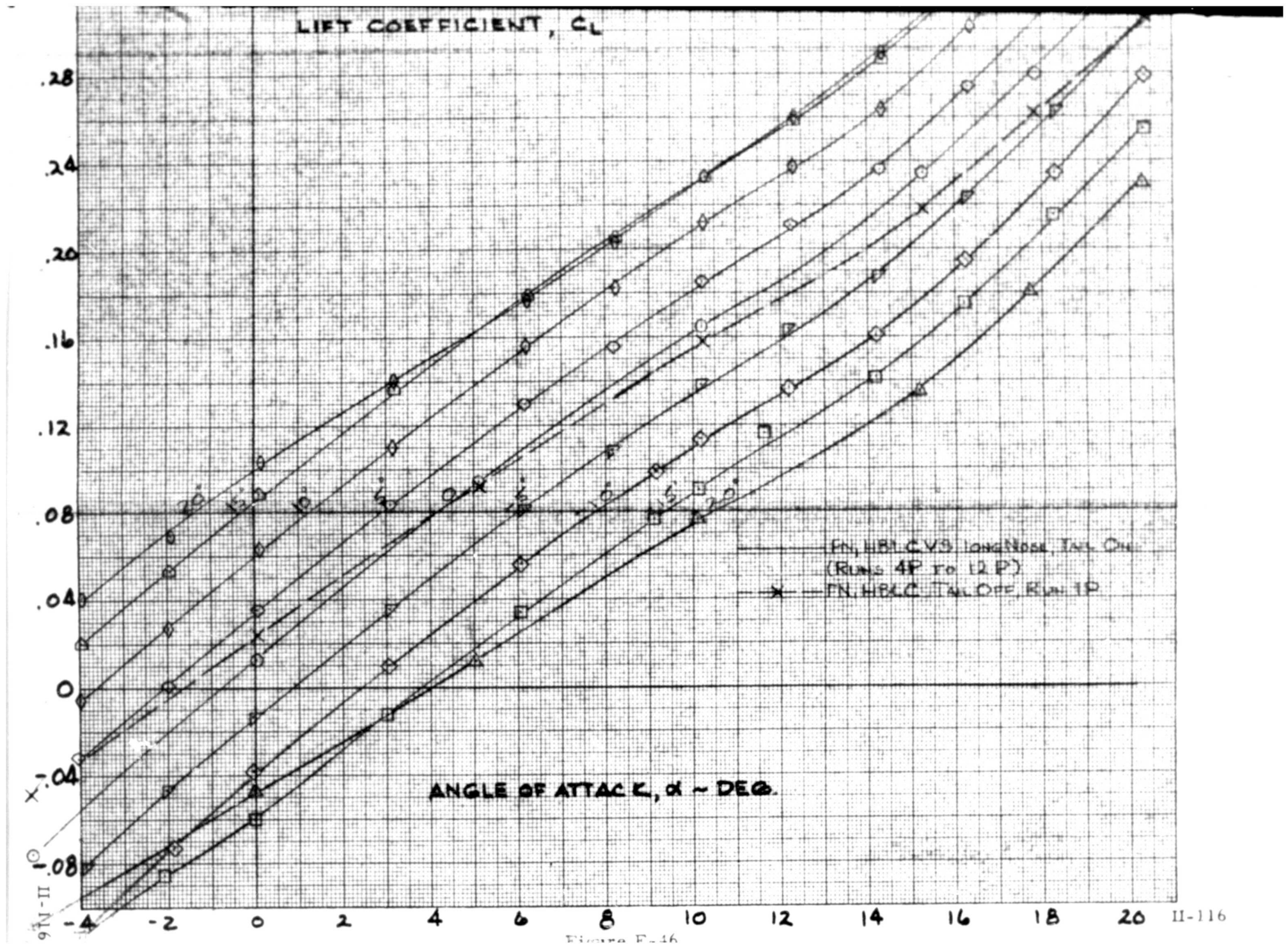
LIFT COEFFICIENT, C_L
.28
.24
.20
.16
.12
.08
.04
0
-.04
-.08
-4
-2
0
2
4
6
8
10
12
14
16
18
20
ANGLE OF ATTACK, α ~ DEG.
FN, HB1, C.V3, LONG NOSE, TAIL ON (RUNS 4P TO 12P)
FN, HB1, C, TAIL OFF, RUN 1P

Figure F-46

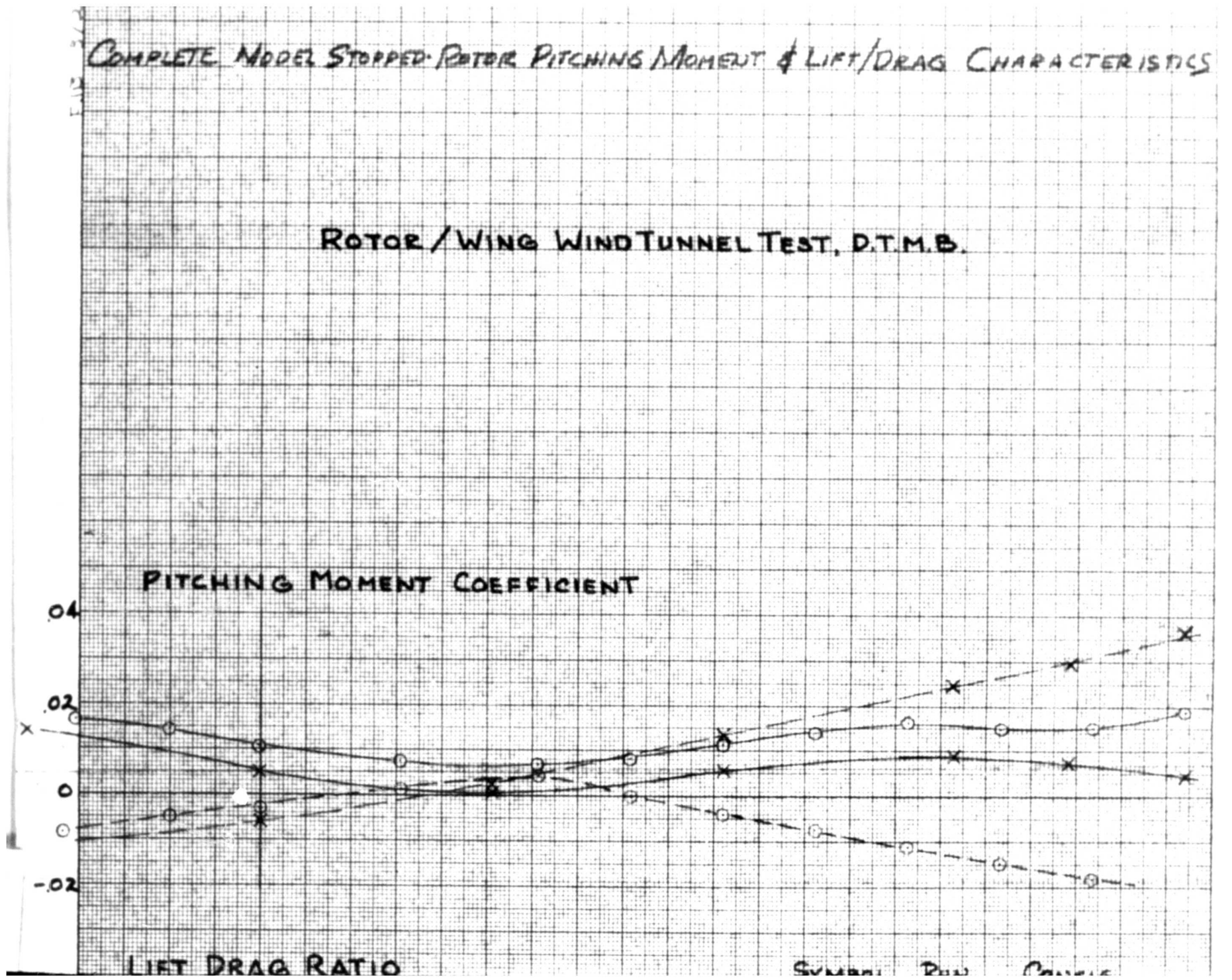
COMPLETE MODEL STOPPED ROTOR PITCHING MOMENT & LIFT/DRAG CHARACTERISTICS
ROTOR / WING WIND TUNNEL TEST, D.T.M.B.
PITCHING MOMENT COEFFICIENT
.04
.02
0
-.02
LIFT DRAG RATIO

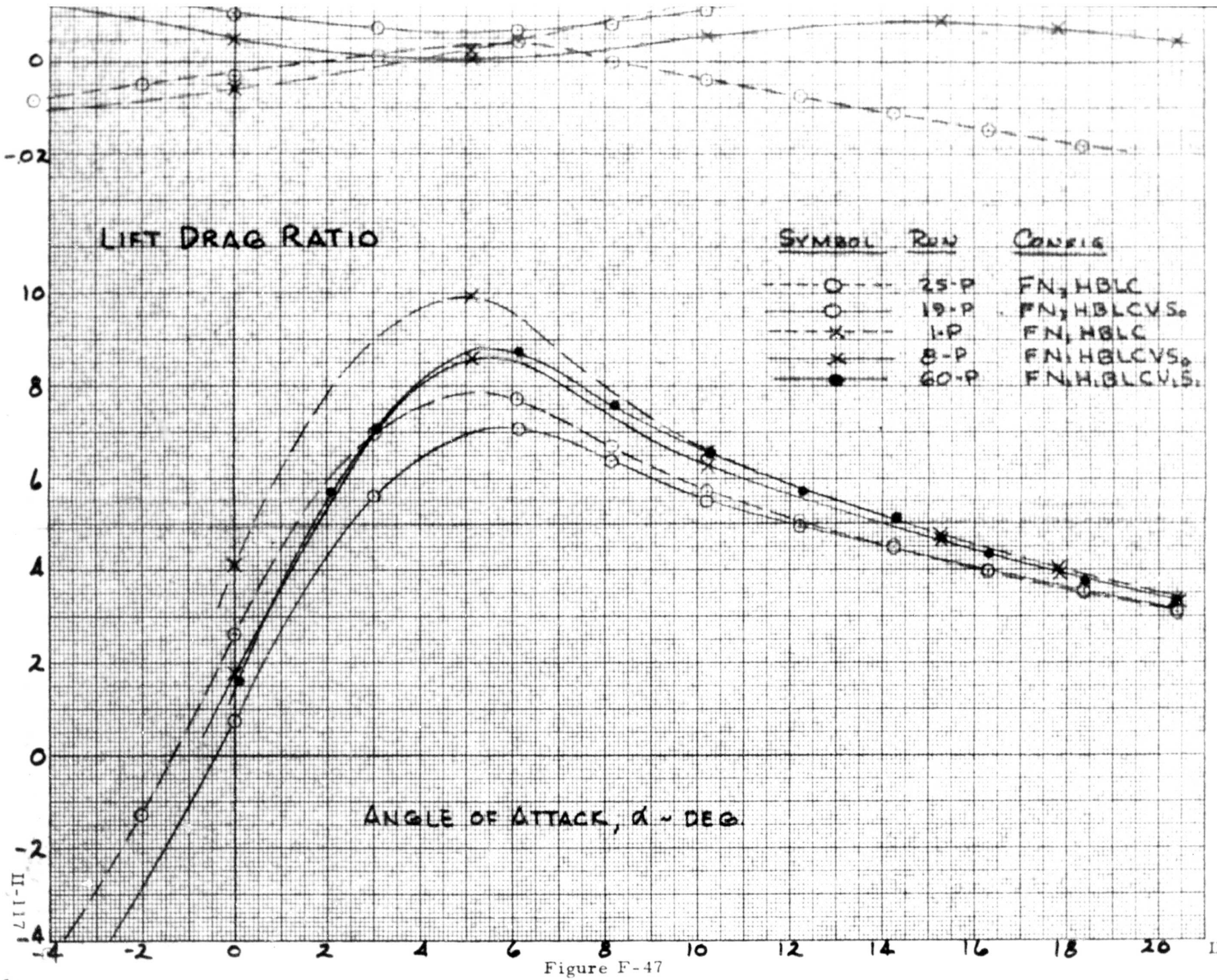

Figure F-47

II-117

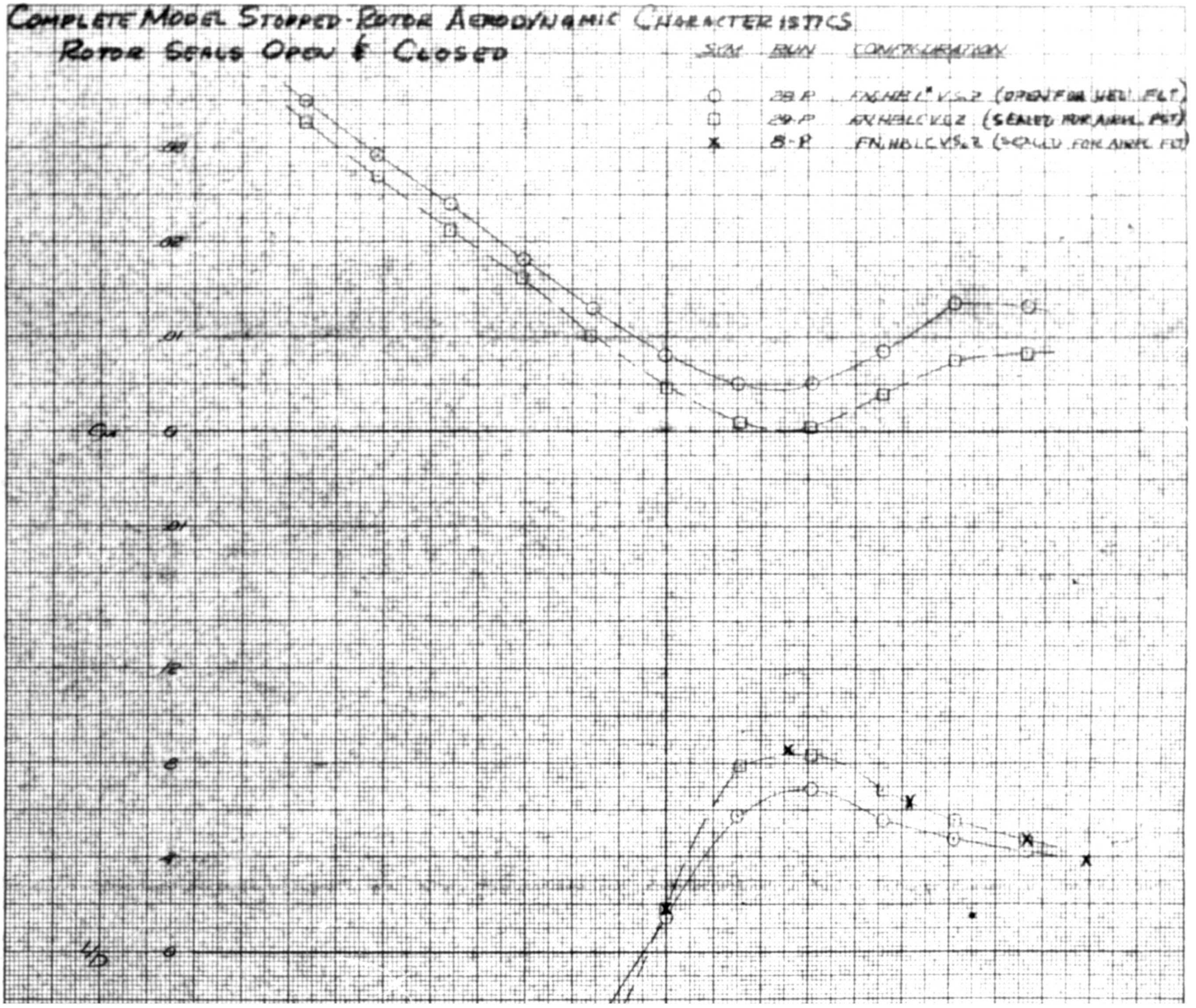
COMPLETE MODEL STOPPED-ROTOR AERODYNAMIC CHARACTERISTICS
ROTOR SEALS OPEN & CLOSED
SYM RUN CONFIGURATION
28-P FN,HBLC V=0.2 (OPEN FOR HELI. FLT.)
29-P FN,HBLC V=0.2 (SEALED FOR AIRPL. FLT.)
8-P FN,HBLC V=0.2 (SEALED FOR AIRPL. FLT.)
L/D

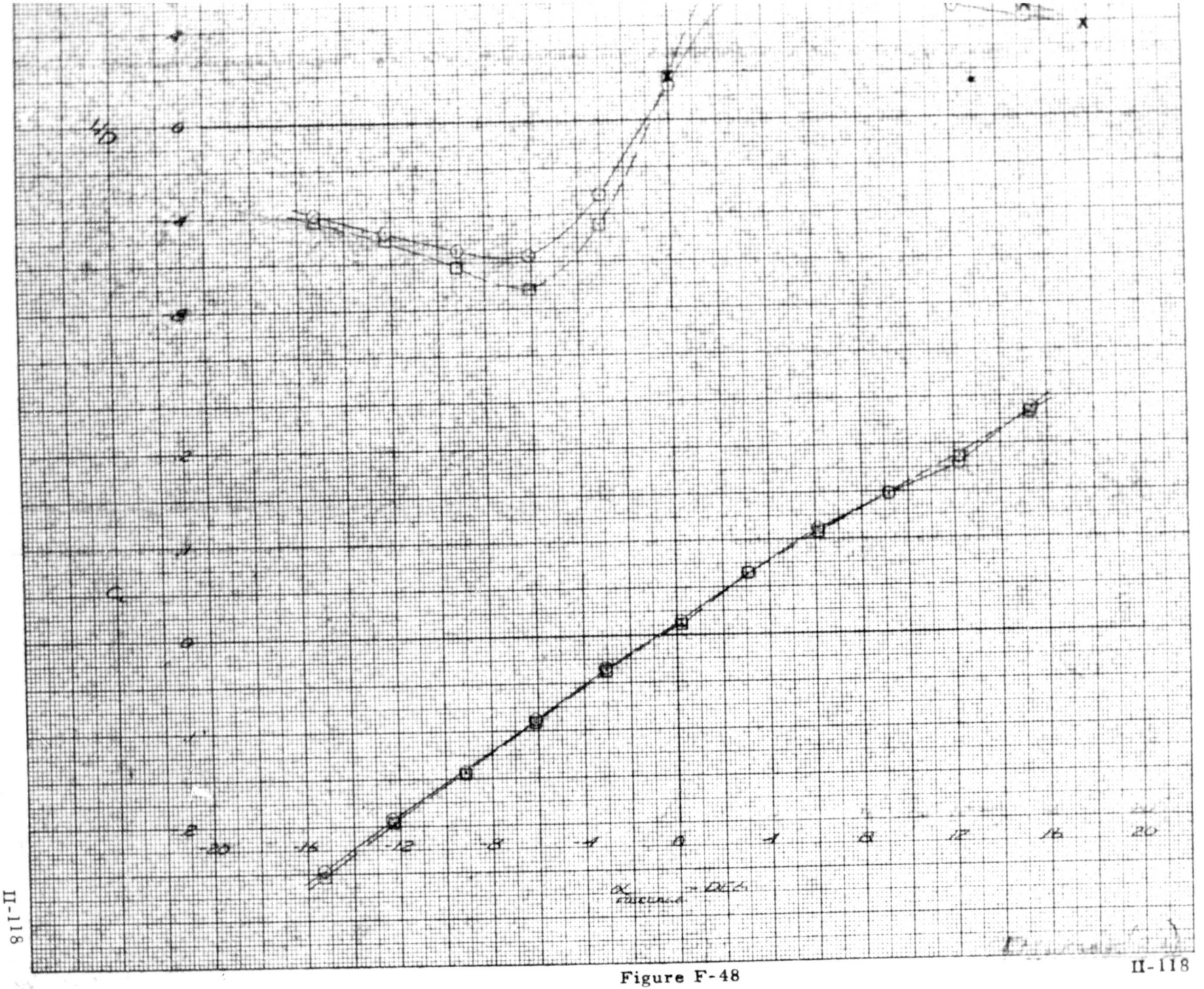

Figure F-48

II-118

COMPLETE MODEL STOPPED-ROTOR AERODYNAMIC CHARACTERISTICS

ROTOR BLADE INCIDENCE = 0° & 5°

SYM	RUN NO.	CONFIGURATION	B_1	i_s
○	47-P	FN₃H(ZB) LCVS Z	0°	0°
□	48-P	FN₃H(ZB) LC Z	0°	OFF
◇	49-P	FN₃H(ZB) LC Z	5°	OFF
△	50-P	FN₃H(ZB) LCVS Z	5°	0°
+	51-P	FN₃HCVS Z	0°	0°
☆	52-P	FN₃HC Z	0°	OFF

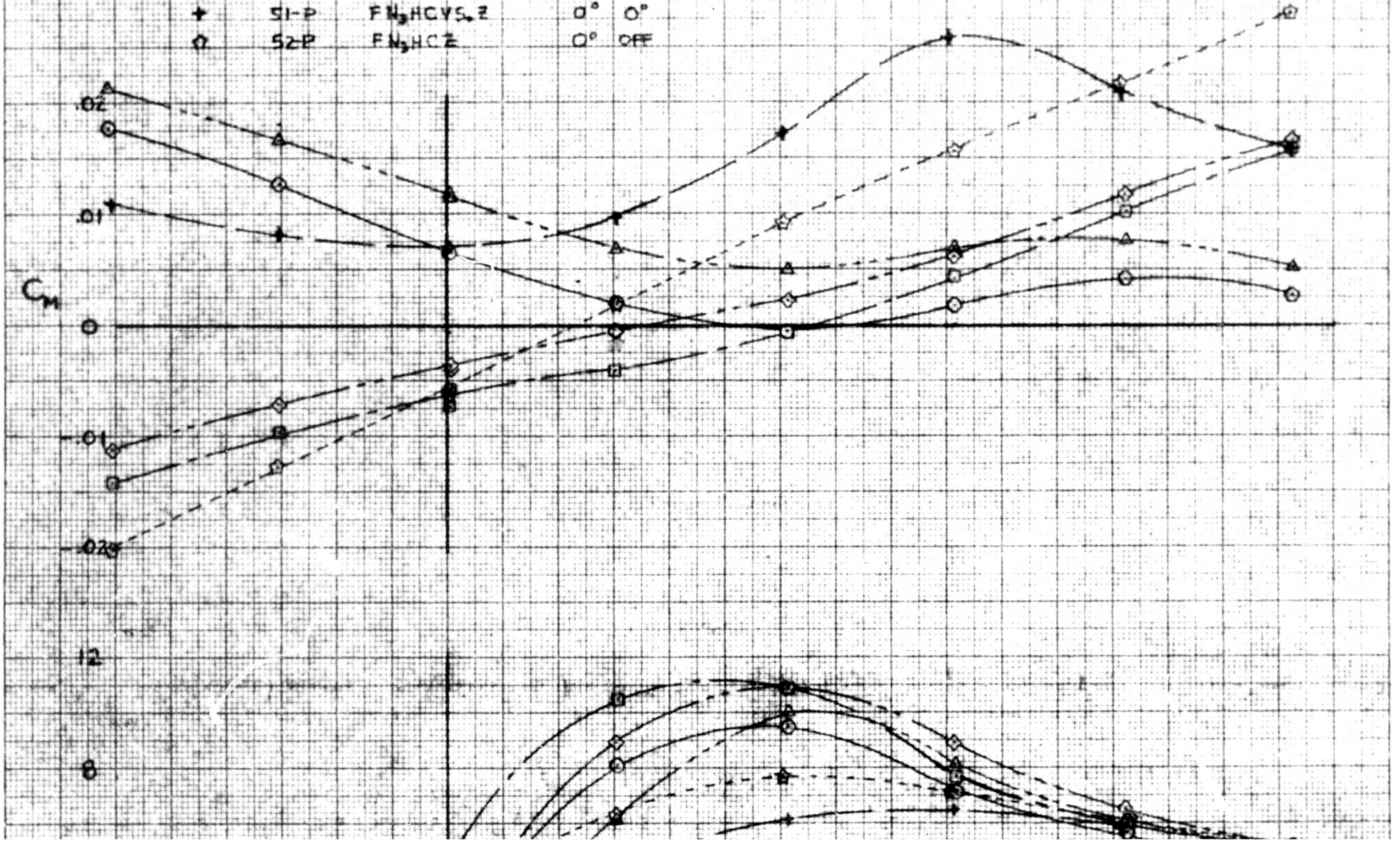

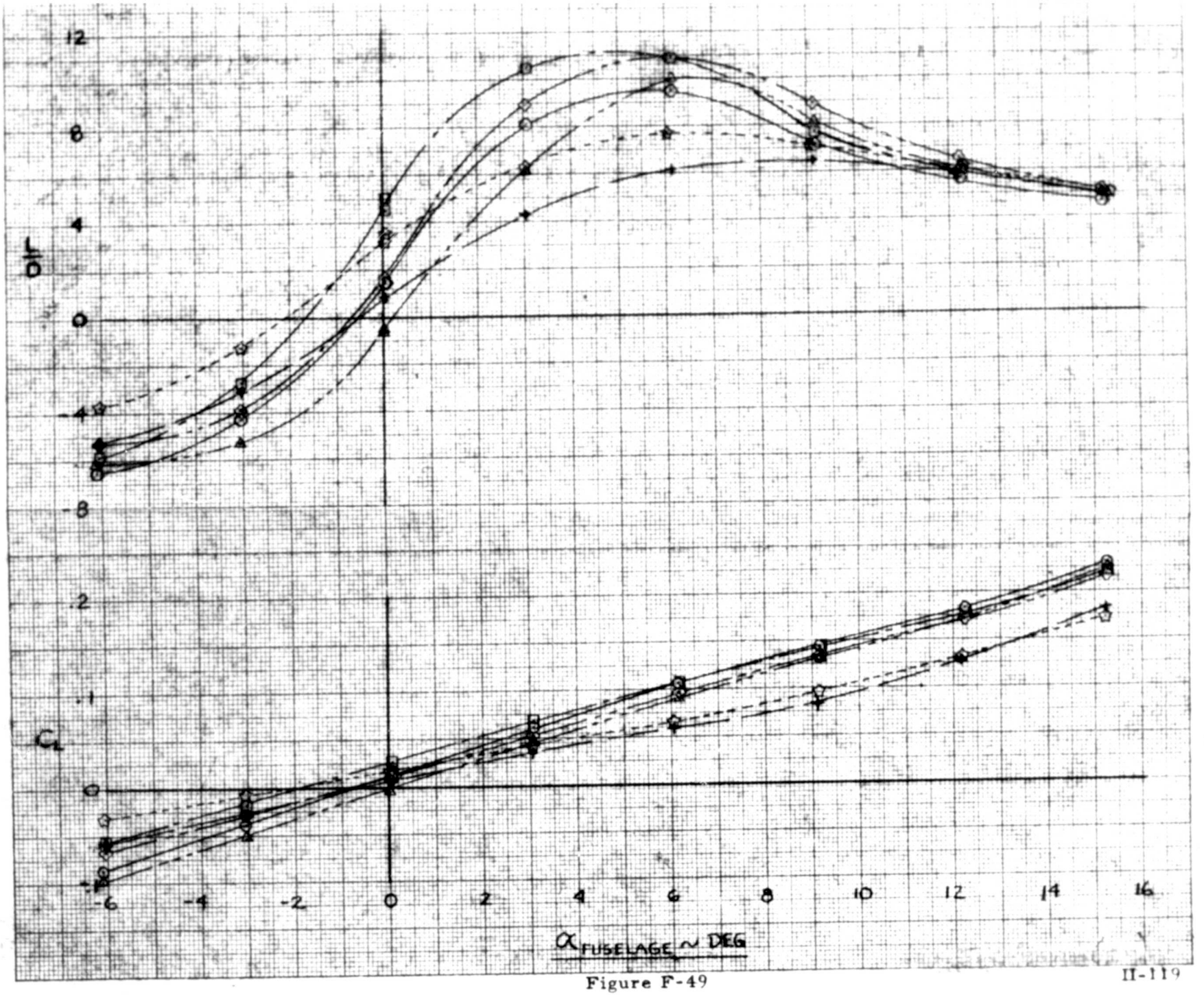

Figure F-49

II-119

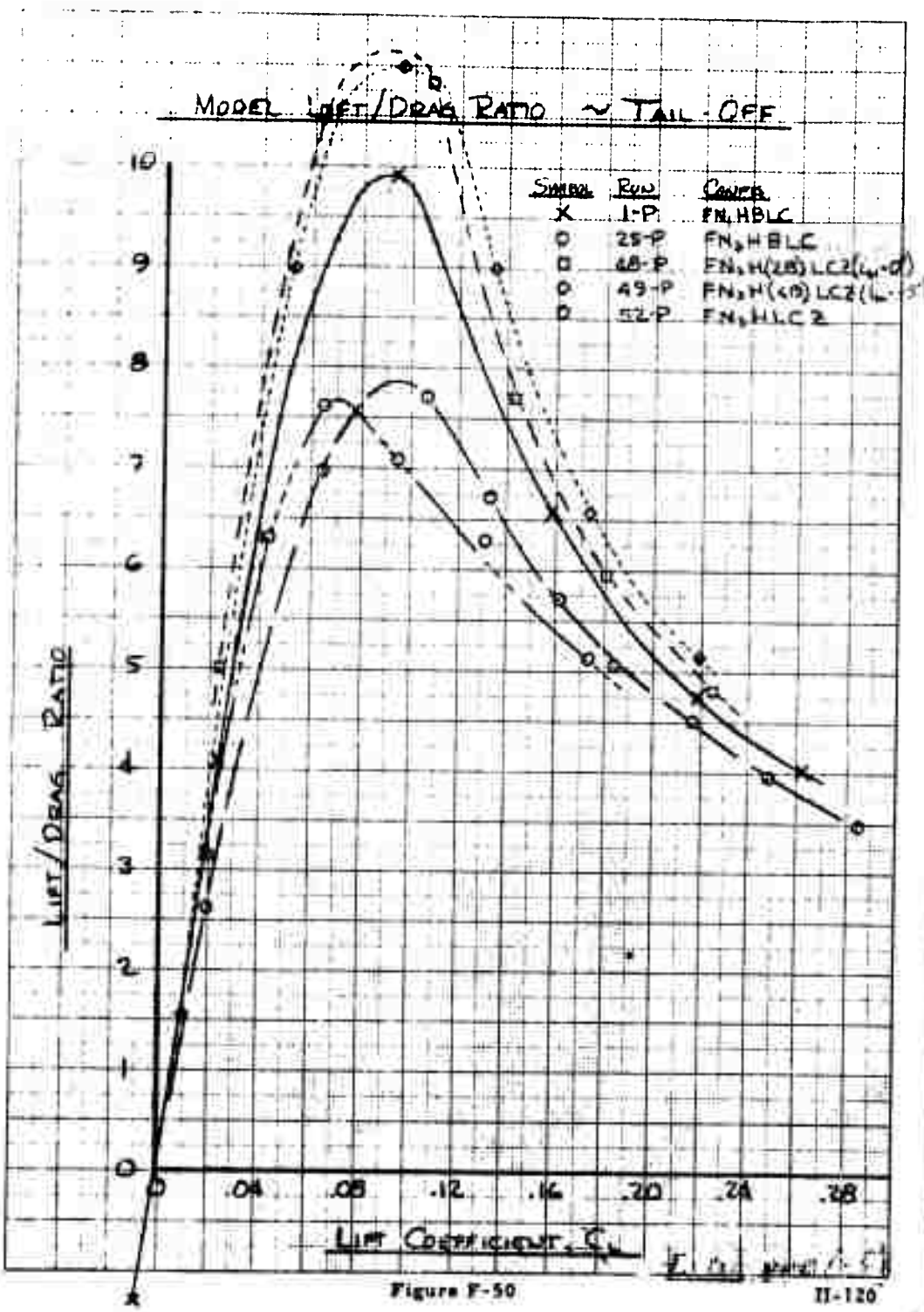
MODEL LIFT/DRAG RATIO ~ TAIL-OFF
SYMBOL RUN CONFIG.
X 1-P FN, HBLC
O 25-P FN, HBLC
□ 68-P FN, H(28) LC2(4-0)
O 49-P FN, H(-5) LC2(4-5)
O 52-P FN, HLC 2
LIFT/DRAG RATIO
LIFT COEFFICIENT, C_L
0
1
2
3
4
5
6
7
8
9
10
.04
.08
.12
.16
.20
.24
.28

Figure F-50

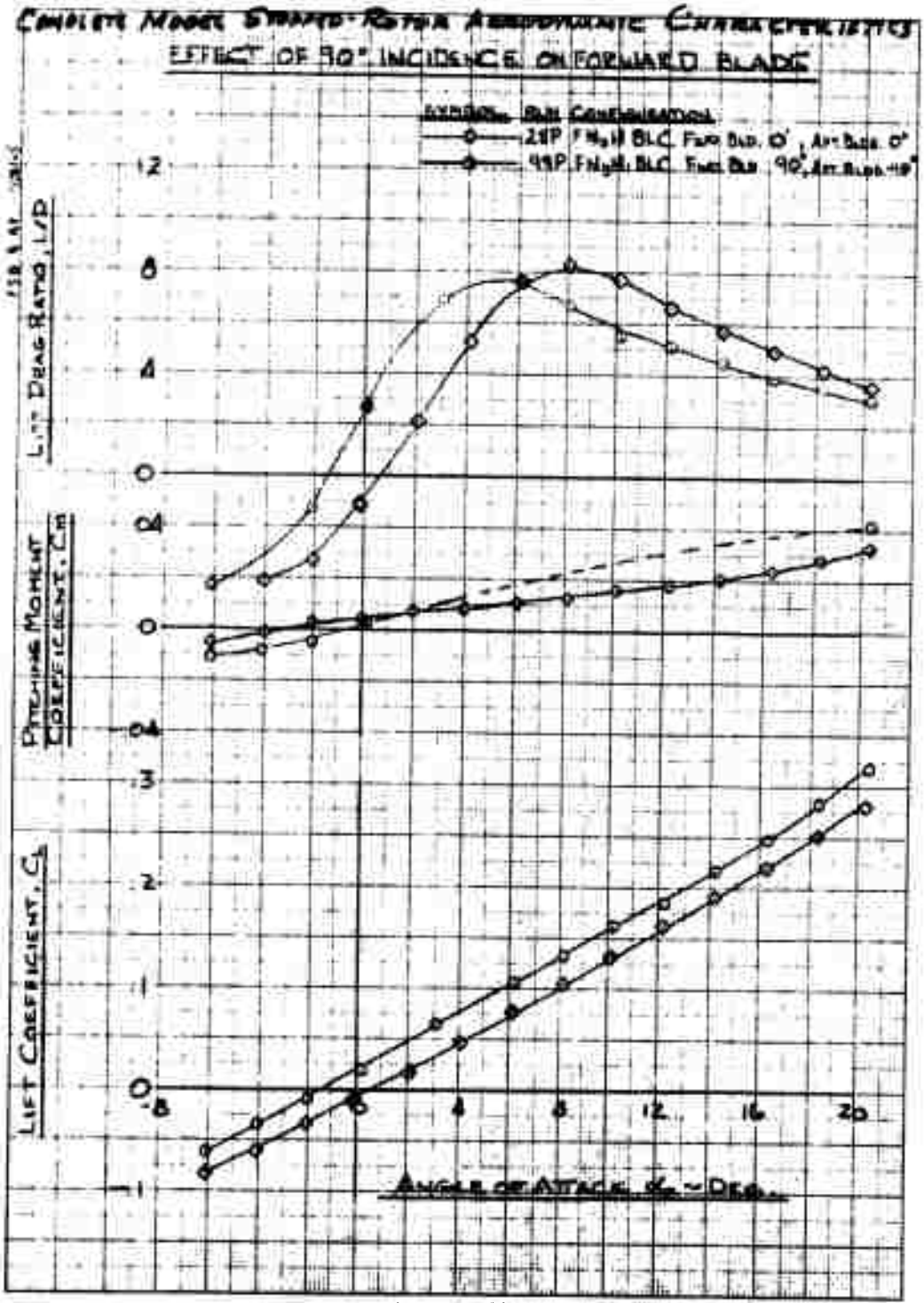
COMPLETE MODEL STRIPPED-ROTOR AERODYNAMIC CHARACTERISTICS
EFFECT OF 90° INCIDENCE ON FORWARD BLADE
LIFT DRAG RATIO, L/D
PITCHING MOMENT COEFFICIENT, Cm
LIFT COEFFICIENT, CL
ANGLE OF ATTACK, αs - DEG.

Figure F-51

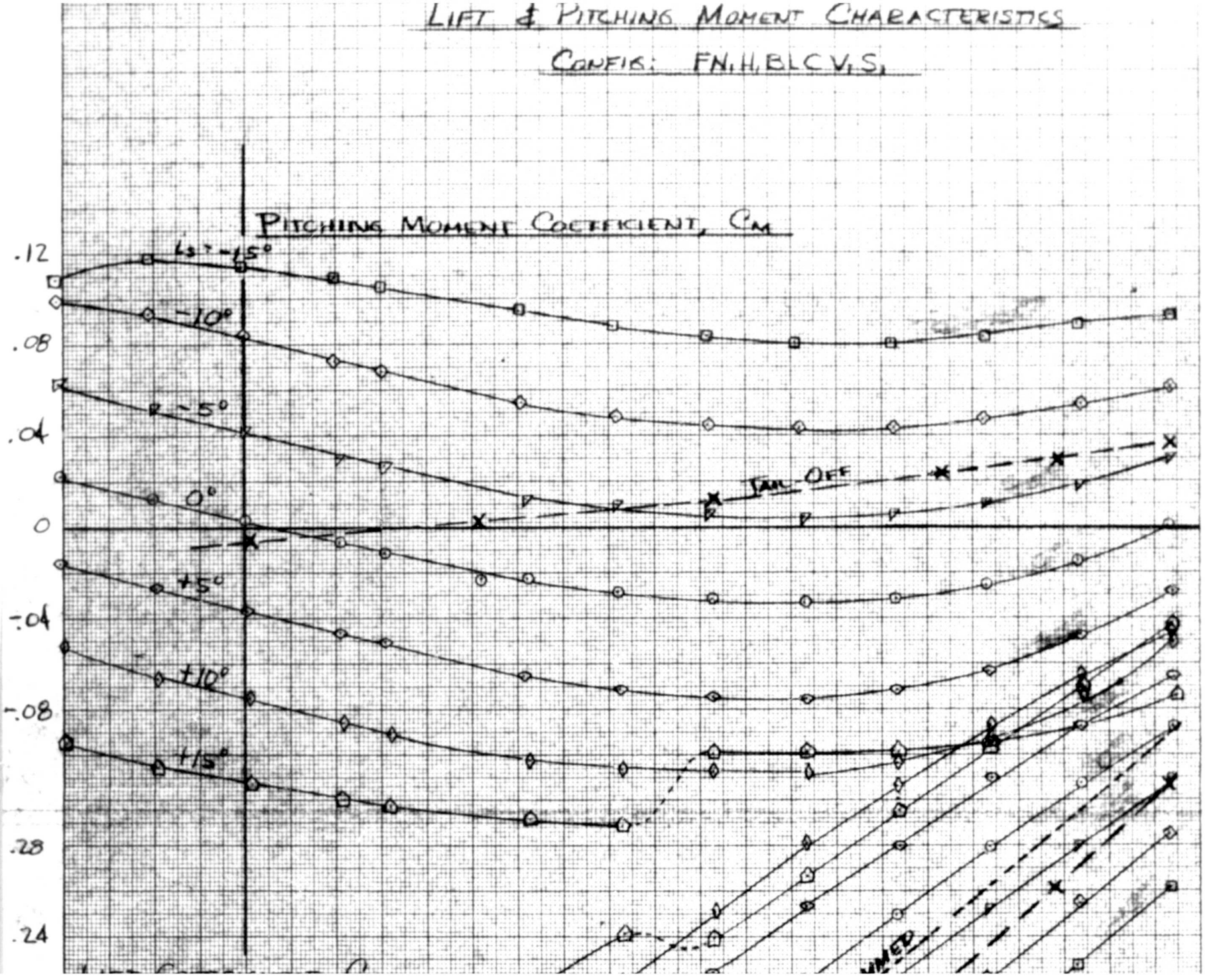
LIFT & PITCHING MOMENT CHARACTERISTICS
CONFIG: FN, H, BLC V, S,
PITCHING MOMENT COEFFICIENT, Cm
.12
.08
.04
0
-.04
-.08
.28
.24
i = -15°
-10°
-5°
0°
+5°
+10°
+15°
TAIL OFF
WING

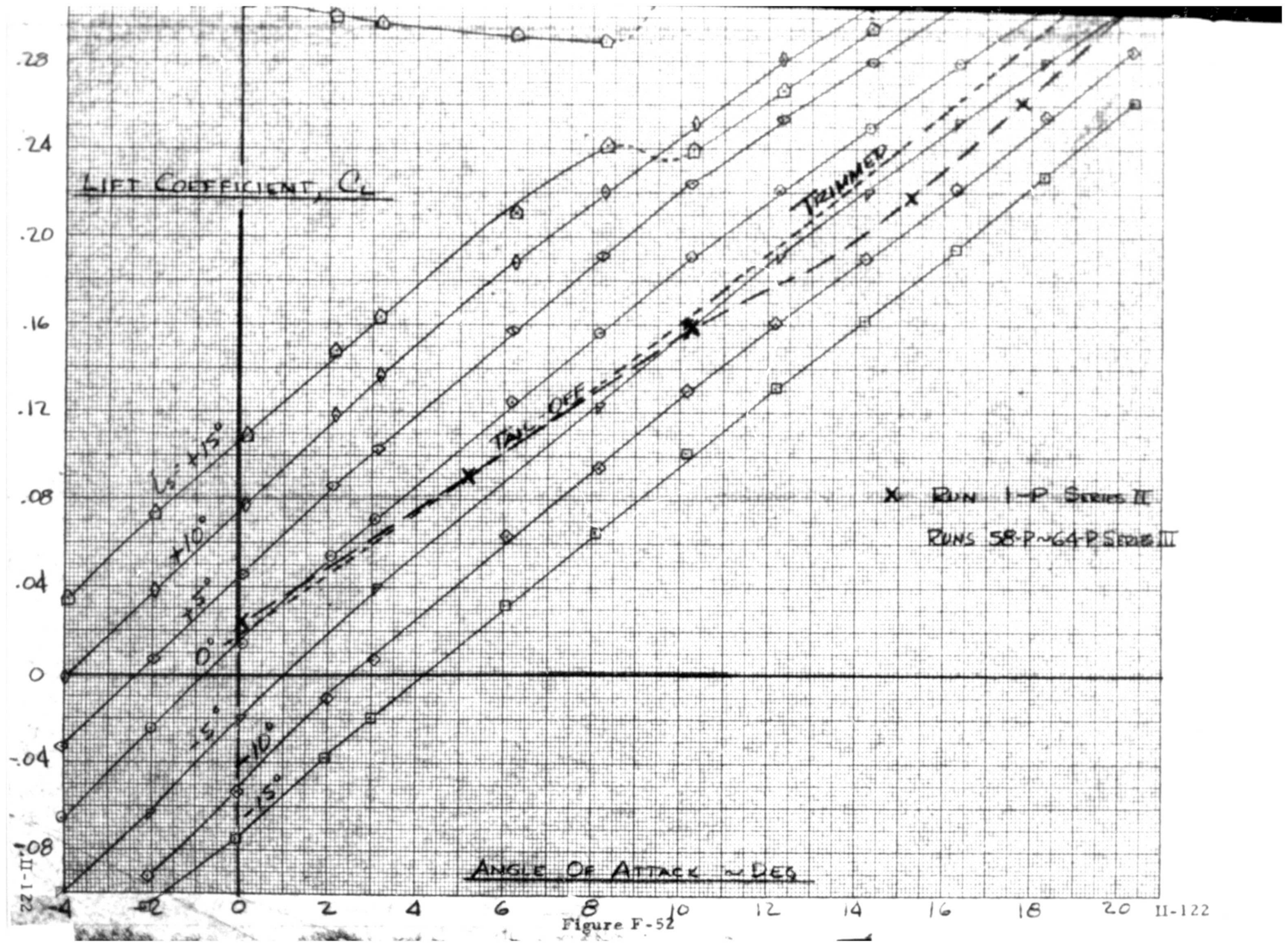
LIFT COEFFICIENT, C_L
.28
.24
.20
.16
.12
.08
.04
0
-.04
-.08
i_t = +15°
+10°
+5°
0°
-5°
-10°
-15°
TRIMMED
TAIL-OFF
X RUN 1-P SERIES II
RUNS 58-P~64-P SERIES III
ANGLE OF ATTACK ~ DEG
-4
-2
0
2
4
6
8
10
12
14
16
18
20
II-122

Figure F-52

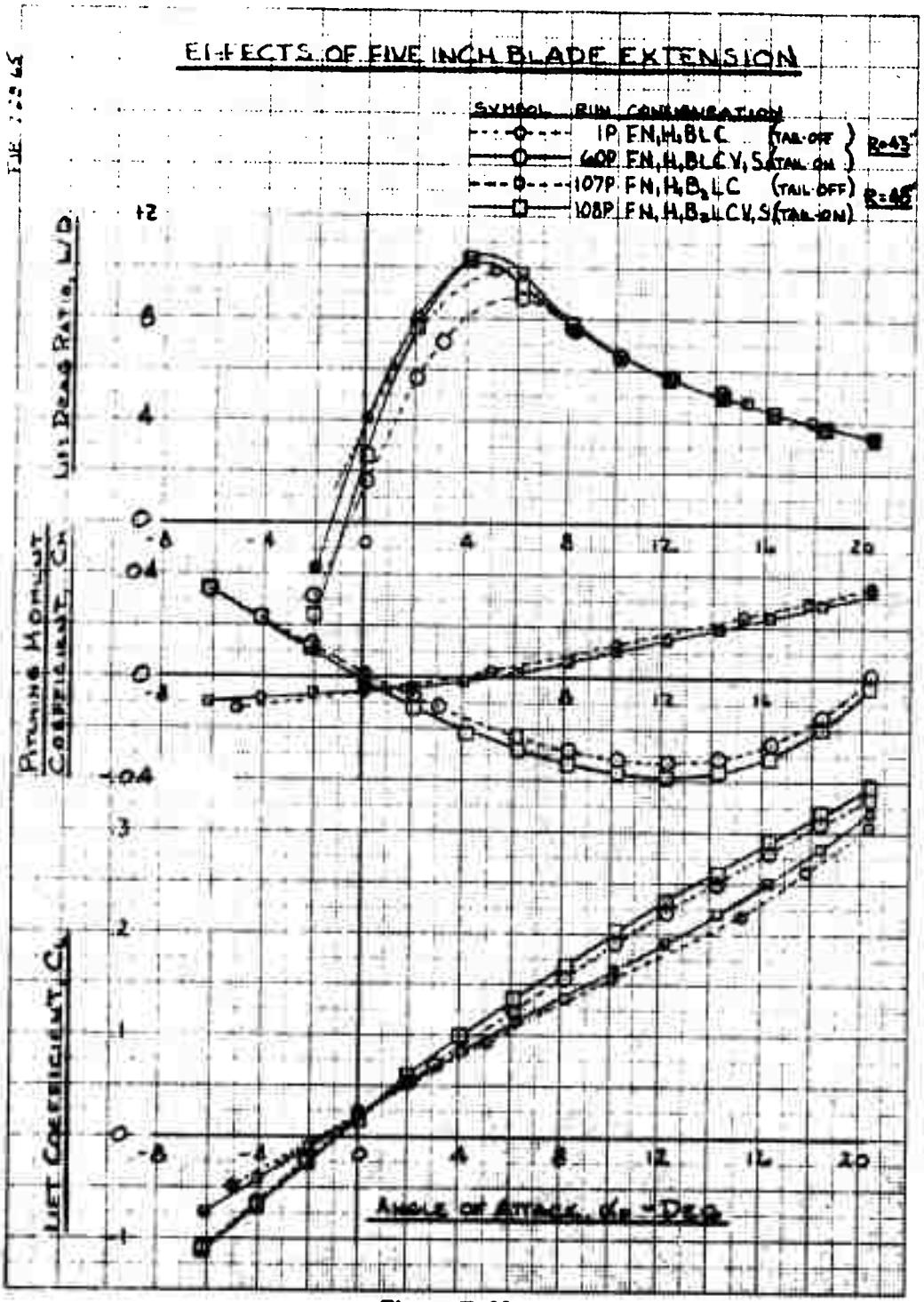
EFFECTS OF FIVE INCH BLADE EXTENSION
SYMBOL RUN CONFIGURATION
1P FN,H,BLC (TAIL-OFF) R=43"
60P FN,H,BLCV,S (TAIL-ON)
107P FN,H,B2LC (TAIL-OFF) R=46"
108P FN,H,B2LCV,S (TAIL-ON)
Lift-Drag Ratio, L/D
Pitching Moment Coefficient, Cm
Lift Coefficient, CL
Angle of Attack, α = Deg

Figure F-53

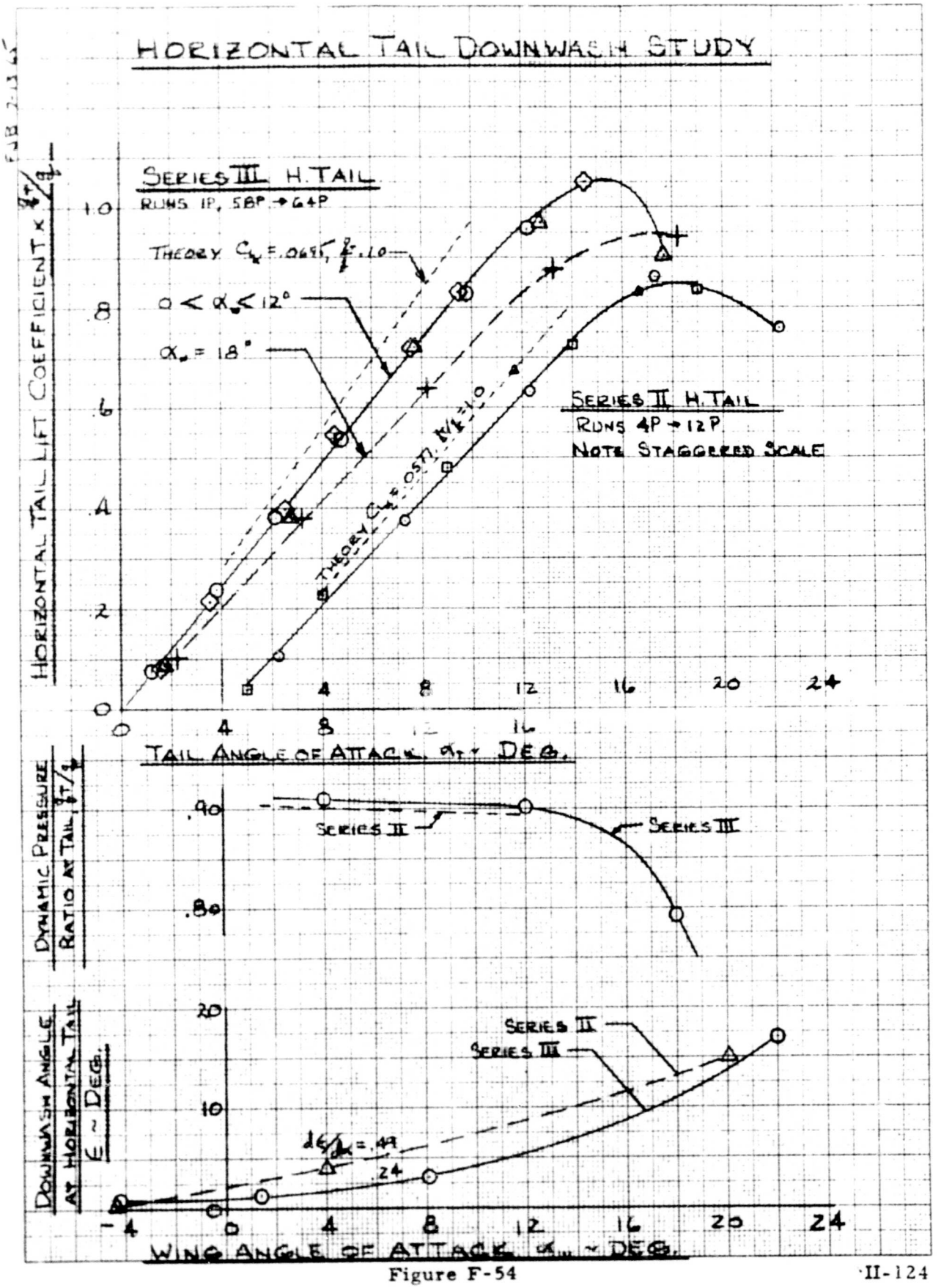
HORIZONTAL TAIL DOWNWASH STUDY
SERIES III H.TAIL
RUNS 1P, 58P → 64P
THEORY C_{L_α} = .069, $\frac{S_T}{S}$ = .10
$0 < \alpha_w < 12°$
$\alpha_w = 18°$
THEORY C_{L_α} = .057, M/L = 1.0
SERIES II H.TAIL
RUNS 4P → 12P
NOTE STAGGERED SCALE
HORIZONTAL TAIL LIFT COEFFICIENT $\times \frac{q_T}{q}$
TAIL ANGLE OF ATTACK, α_T ~ DEG.
DYNAMIC PRESSURE RATIO AT TAIL, $\frac{q_T}{q}$
SERIES II
SERIES III
DOWNWASH ANGLE AT HORIZONTAL TAIL ϵ ~ DEG.
SERIES II
SERIES III
$\frac{d\epsilon}{d\alpha} = .49$
WING ANGLE OF ATTACK α_w ~ DEG.

Figure F-54

COMPLETE MODEL STOPPED- ROTOR LATERAL- DIRECTIONAL CHARACTERISTICS

ROTOR/WING WIND TUNNEL TEST, D.T.M.B.

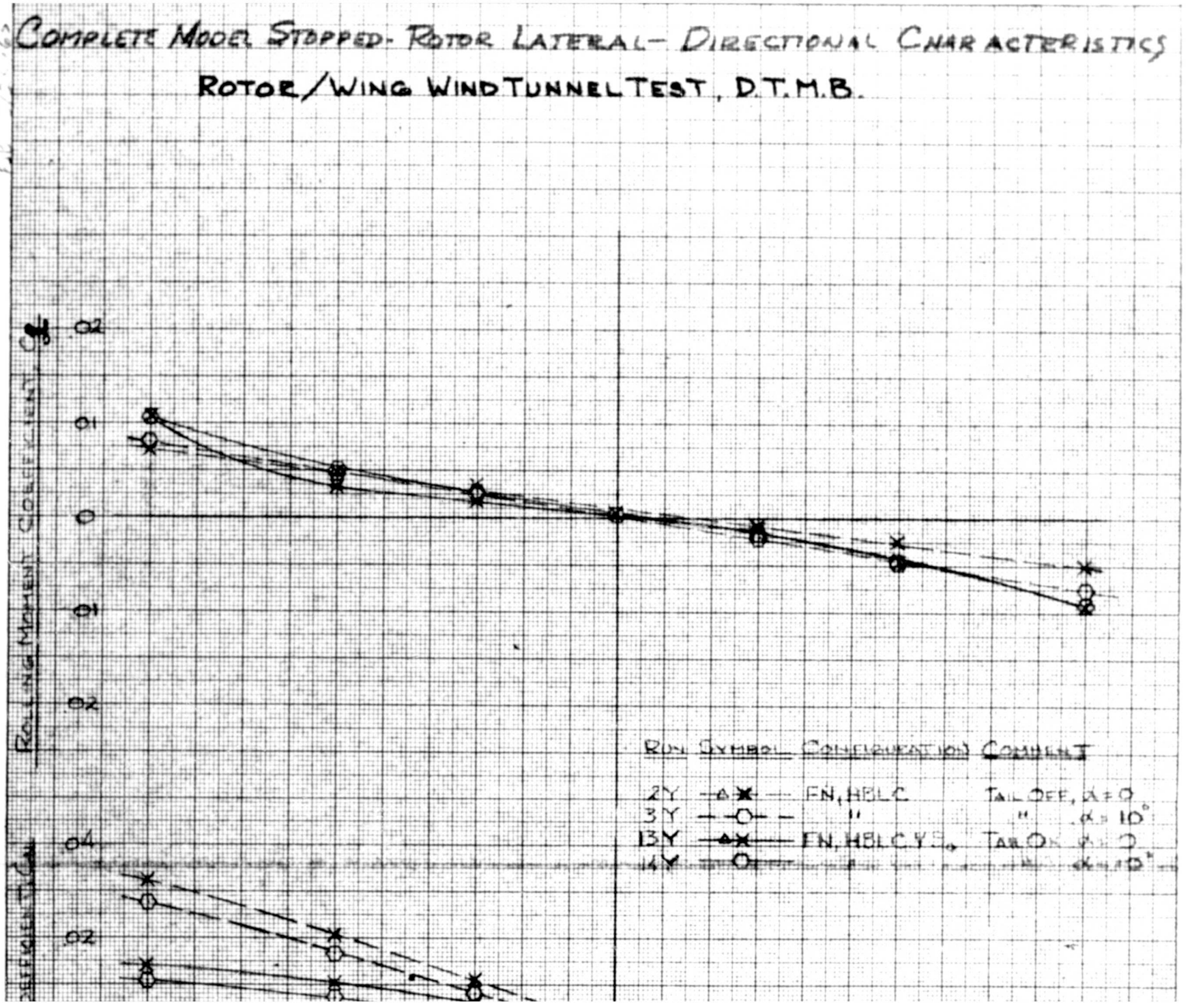

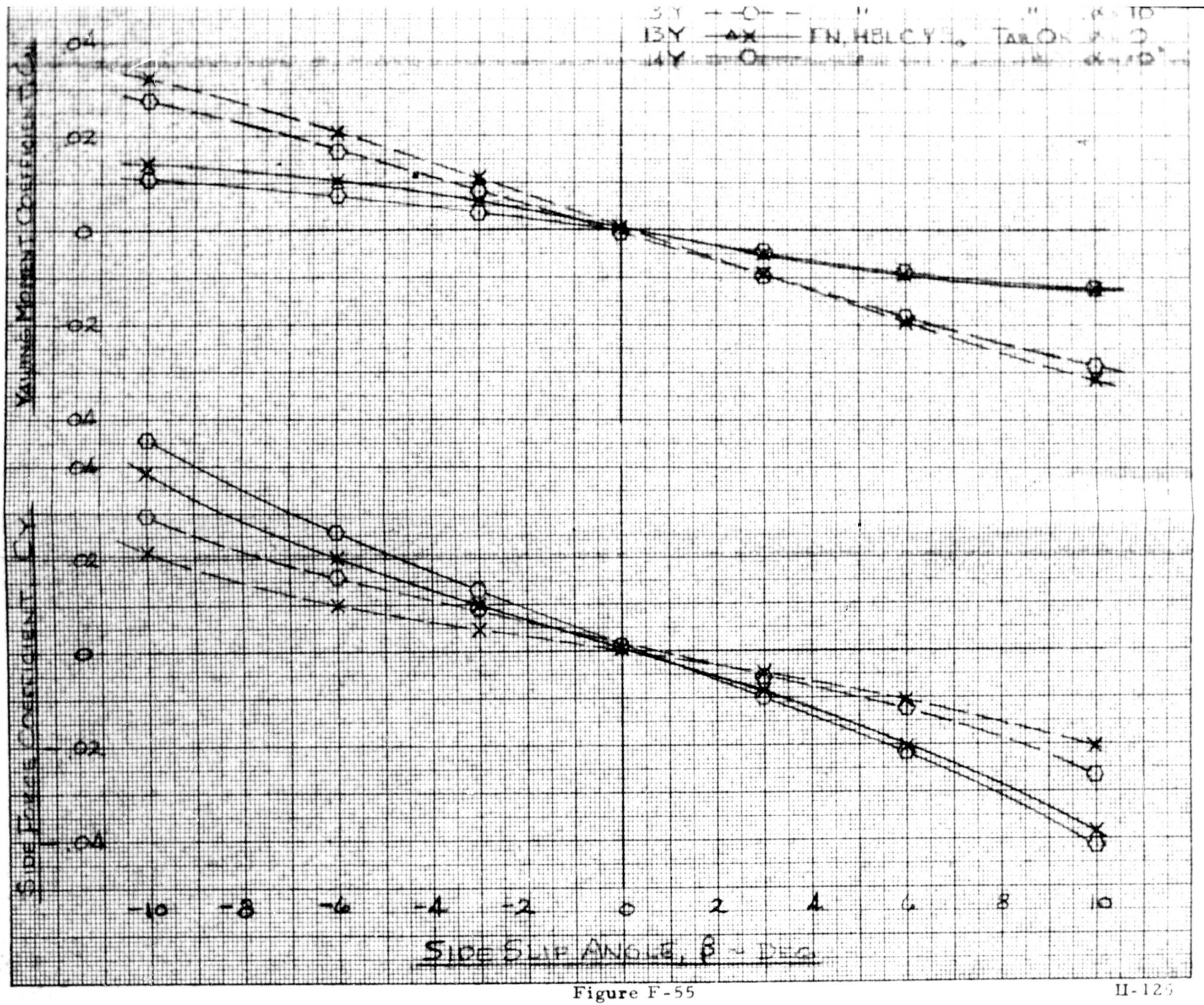

Figure F-55

II-125

Comparison Of Lateral-Directional Characteristics For Long- & Short-Nosed Foselage

Rotor/Wing Wind Tunnel Test, D.T.M.B.

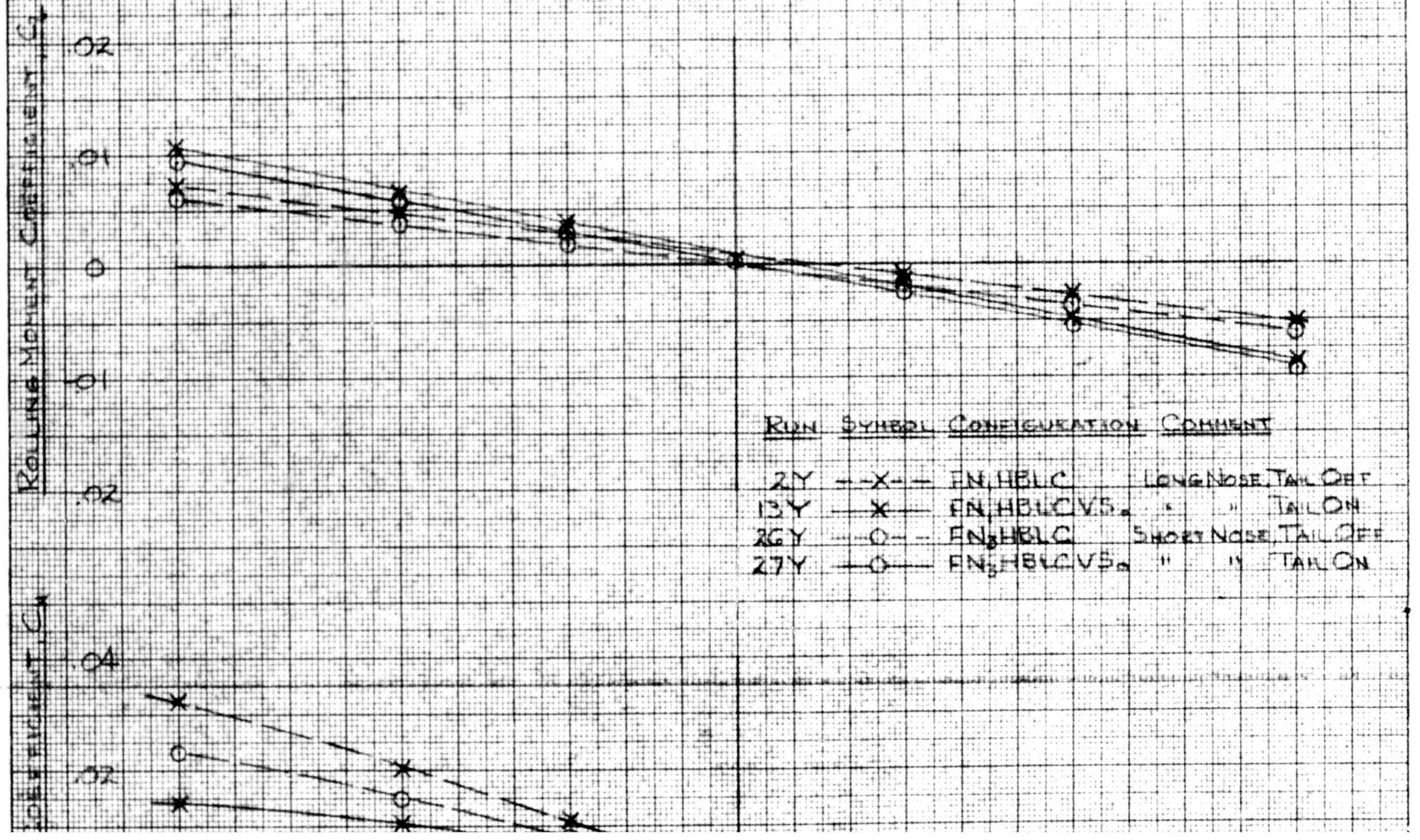

Side Slip Angle, β, Deg
10
8
6
4
2
0
-2
-4
-6
-8
-10
Side Force Coefficient, C_Y
Yawing Moment Coefficient, C_n

Figure F-56

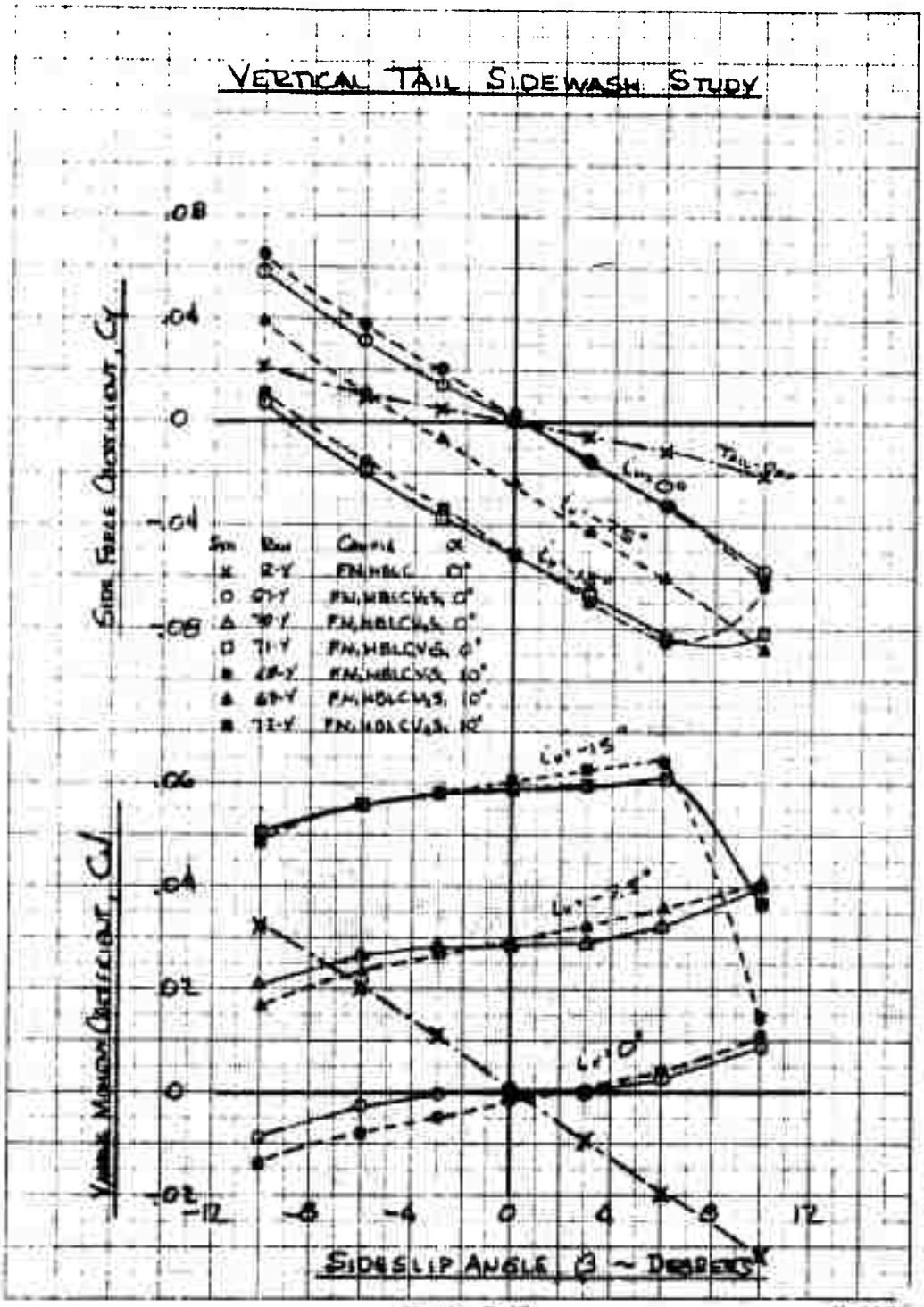
VERTICAL TAIL SIDEWASH STUDY
.08
.04
0
-.04
-.08
SIDE FORCE COEFFICIENT, C_Y
Sym Run Config α
X R-Y FN,HBLC 0°
O 69-Y FN,HBLC,VS, 0°
△ 70-Y FN,HBLC,VS, 0°
□ 71-Y FN,HBLC,VS, 0°
■ 68-Y FN,HBLC,VS, 10°
▲ 69-Y FN,HBLC,VS, 10°
■ 72-Y FN,HBLC,VS, 10°
Tail-On
i_t=0°
i_t=-7.5°
i_t=-15°
.06
.04
.02
0
-.02
YAWING MOMENT COEFFICIENT, C_n
i_t=-15°
i_t=-7.5°
i_t=0°
-12
-8
-4
0
4
8
12
SIDESLIP ANGLE, β ~ DEGREES

Figure F-57

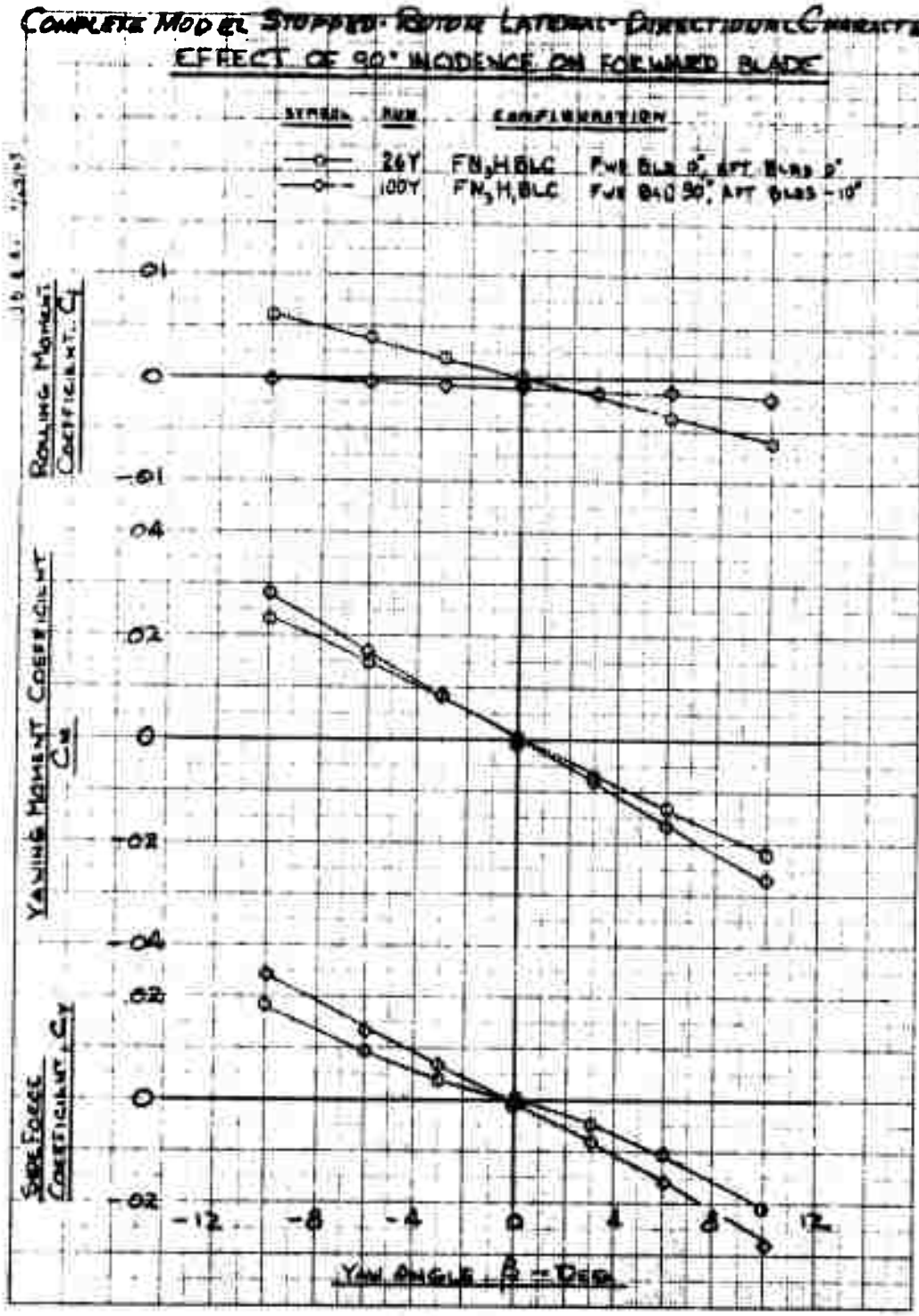
COMPLETE MODEL STOPPED ROTOR LATERAL-DIRECTIONAL CHARACTERISTICS
EFFECT OF 90° INCIDENCE ON FORWARD BLADE
SYMBOL
RUN
CONFIGURATION
26Y FN,H,BLC FWD BLDS 0°, AFT BLDS 0°
100Y FN,H,BLC FWD BLDS 90°, AFT BLDS -10°
ROLLING MOMENT COEFFICIENT, Cl
YAWING MOMENT COEFFICIENT Cn
SIDE FORCE COEFFICIENT, Cy
.01
0
-.01
.04
.02
0
-.02
-.04
.02
0
-.02
-12
-8
-4
0
4
8
12
YAW ANGLE, β = DEG.

Figure F-58

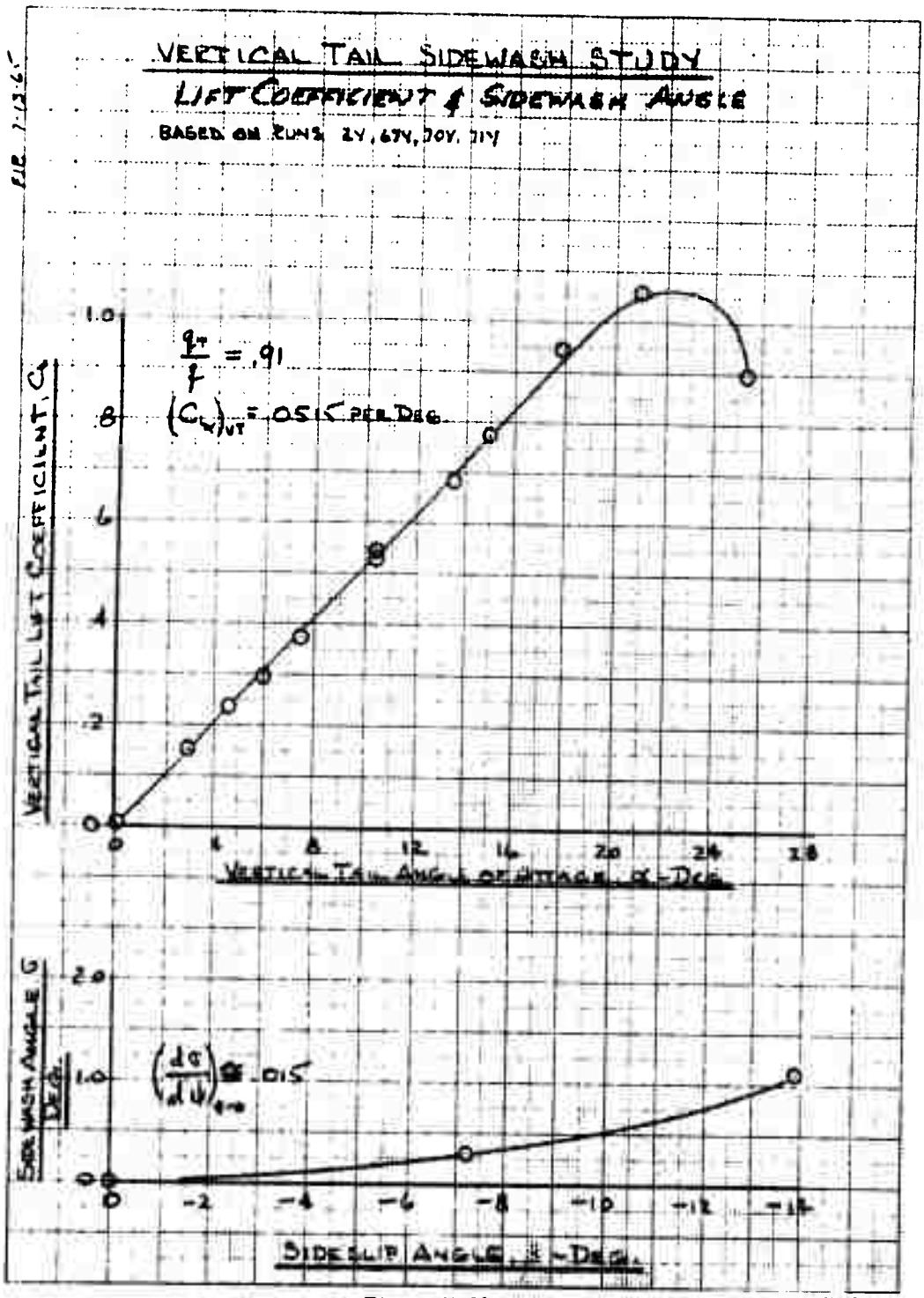
VERTICAL TAIL SIDEWASH STUDY
LIFT COEFFICIENT & SIDEWASH ANGLE
BASED ON RUNS 24, 674, 704, 714
$\frac{q_T}{q} = .91$
$(C_{L_\alpha})_{VT} = .051$ PER DEG.
VERTICAL TAIL LIFT COEFFICIENT, C_L
VERTICAL TAIL ANGLE OF ATTACK, α - DEG.
SIDEWASH ANGLE, σ DEG.
$\left(\frac{d\sigma}{d\psi}\right)_{\psi=0} = .015$
SIDESLIP ANGLE, ψ - DEG.

Figure F-59

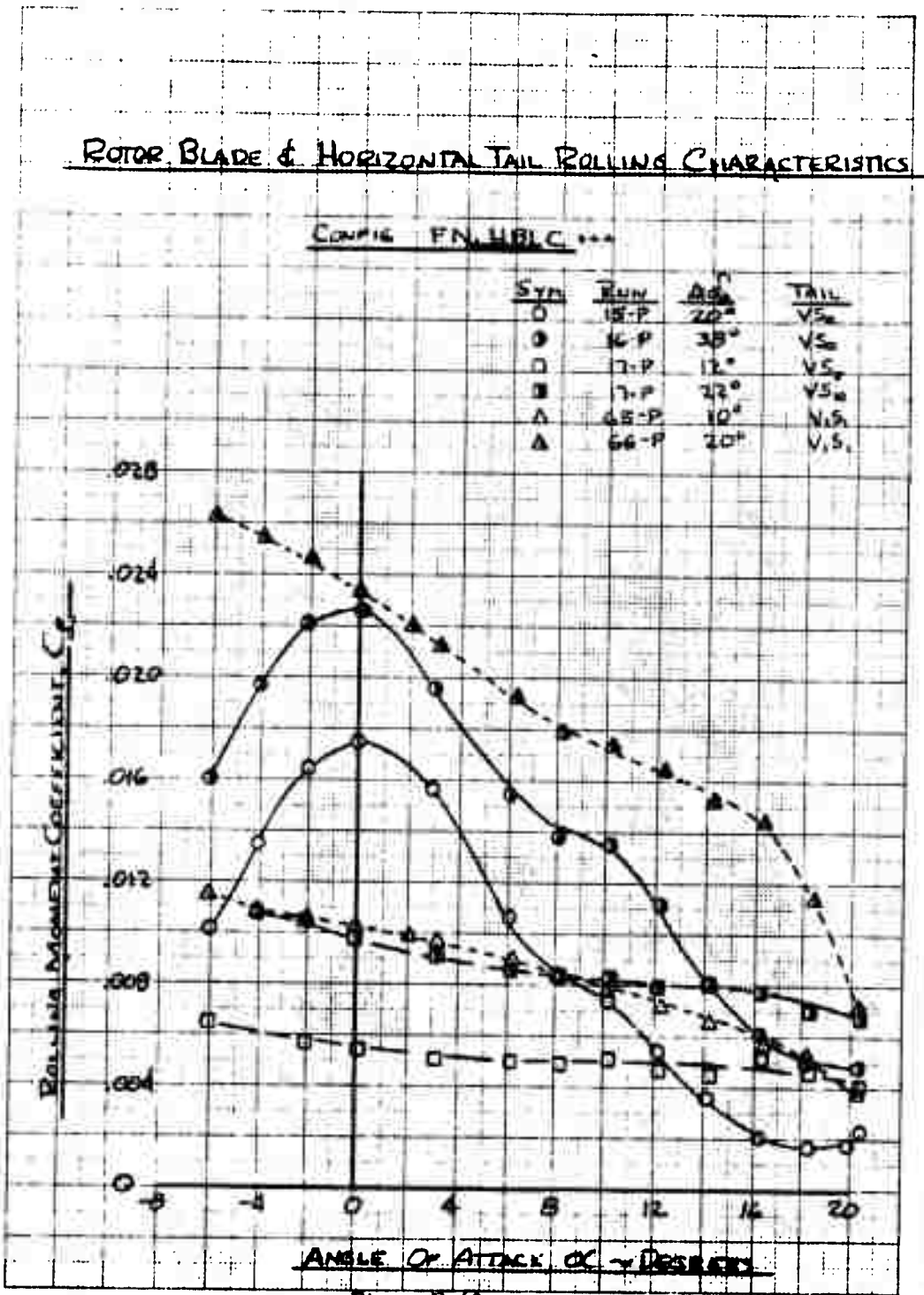
ROTOR BLADE & HORIZONTAL TAIL ROLLING CHARACTERISTICS
CONFIG FN, HBLC ...
SYM RUN AR TAIL
0 15-P 20° VSm
16-P 38° VSm
13-P 12° VSm
13-P 22° VSm
65-P 10° V,S,
66-P 20° V,S,
ROLLING MOMENT COEFFICIENT Cl
.028
.024
.020
.016
.012
.008
.004
0
-8
-4
0
4
8
12
16
20
ANGLE OF ATTACK, α, DEGREES

Figure F-60

Unclassified

Security Classification

DOCUMENT CONTROL DATA - R&D

(Security classification of title, body of abstract and indexing annotation must be entered when the overall report is classified)

1. ORIGINATING ACTIVITY (Corporate author)

Hughes Tool Company - Aircraft Division
Culver City, California

2a. REPORT SECURITY CLASSIFICATION: Unclassified

2b. GROUP: X

3. REPORT TITLE

SUMMARY TECHNICAL REPORT, ROTOR/WING CONCEPT STUDY
(Volumes I, II, and III)

4. DESCRIPTIVE NOTES (Type of report and inclusive dates)

Summary Report

5. AUTHOR(S) (Last name, first name, initial)

Head, Robert E.

6. REPORT DATE	7a. TOTAL NO. OF PAGES	7b. NO. OF REFS
September 1965		9

8a. CONTRACT OR GRANT NO.	9a. ORIGINATOR'S REPORT NUMBER(S)
Nonr-4588(00)	HTC-AD 65-15
b. PROJECT NO: NR-212-162/12-8-64	9b. OTHER REPORT NO(S) (Any other numbers that may be assigned this report): ---
c	
d	

10. AVAILABILITY/LIMITATION NOTICES

U. S. Government agencies may obtain copies of this report directly from DDC. Other qualified DDC users shall request through Air Programs, Office of Naval Research, Washington, D. C. 20360

11. SUPPLEMENTARY NOTES	12. SPONSORING MILITARY ACTIVITY
	U. S. Navy, Office of Naval Research and Bureau of Naval Weapons

13. ABSTRACT

Research work including wind tunnel and whirl test of the Rotor/Wing is described. The Rotor/Wing is a dual-purpose lifting device that is a rotor with an unusually large hub. It acts as a tip-jet powered helicopter for low-speed flight and stops in flight to become a tapered and sweptback low-aspect ratio wing for cruise. Stopping the rotor in flight removes the speed limitations of the helicopter rotor and permits flight speeds up to 500 knots. Research work was supported by the U. S. Navy Office of Naval Research and Bureau of Naval Weapons. Three series of wind tunnel tests demonstrated that the powered-rotor and autorotating-rotor characteristics are similar to those of a high-performance helicopter; that the stopped-rotor characteristics are similar to a conventional low-aspect ratio wing with sweep and taper, and maximum lift/drag ratios of 12 or more should be achievable for full-scale aircraft; and that conversion from stopped- to running- rotor and vice versa is a simple and straightforward procedure.

DD FORM 1 JAN 64 1473

Unclassified

Security Classification

14 KEY WORDS	LINK A		LINK B		LINK C	
	ROLE	WT	ROLE	WT	ROLE	WT
Rotor						
Wing						
Stopped-rotor						
Conversion						
Helicopter						
Wind tunnel test						

INSTRUCTIONS

1. ORIGINATING ACTIVITY: Enter the name and address of the contractor, subcontractor, grantee, Department of Defense activity or other organization *(corporate author)* issuing the report.

2a. REPORT SECURITY CLASSIFICATION: Enter the overall security classification of the report. Indicate whether "Restricted Data" is included. Marking is to be in accordance with appropriate security regulations.

2b. GROUP: Automatic downgrading is specified in DoD Directive 5200.10 and Armed Forces Industrial Manual. Enter the group number. Also, when applicable, show that optional markings have been used for Group 3 and Group 4 as authorized.

3. REPORT TITLE: Enter the complete report title in all capital letters. Titles in all cases should be unclassified. If a meaningful title cannot be selected without classification, show title classification in all capitals in parenthesis immediately following the title.

4. DESCRIPTIVE NOTES: If appropriate, enter the type of report, e.g., interim, progress, summary, annual, or final. Give the inclusive dates when a specific reporting period is covered.

5. AUTHOR(S): Enter the name(s) of author(s) as shown on or in the report. Enter last name, first name, middle initial. If military, show rank and branch of service. The name of the principal author is an absolute minimum requirement.

6. REPORT DATE: Enter the date of the report as day, month, year, or month, year. If more than one date appears on the report, use date of publication.

7a. TOTAL NUMBER OF PAGES: The total page count should follow normal pagination procedures, i.e., enter the number of pages containing information.

7b. NUMBER OF REFERENCES: Enter the total number of references cited in the report.

8a. CONTRACT OR GRANT NUMBER: If appropriate, enter the applicable number of the contract or grant under which the report was written.

8b, 8c, & 8d. PROJECT NUMBER: Enter the appropriate military department identification, such as project number, subproject number, system numbers, task number, etc.

9a. ORIGINATOR'S REPORT NUMBER(S): Enter the official report number by which the document will be identified and controlled by the originating activity. This number must be unique to this report.

9b. OTHER REPORT NUMBER(S): If the report has been assigned any other report numbers *(either by the originator or by the sponsor)*, also enter this number(s).

10. AVAILABILITY/LIMITATION NOTICES: Enter any limitations on further dissemination of the report, other than those imposed by security classification, using standard statements such as:

(1) "Qualified requesters may obtain copies of this report from DDC."

(2) "Foreign announcement and dissemination of this report by DDC is not authorized."

(3) "U. S. Government agencies may obtain copies of this report directly from DDC. Other qualified DDC users shall request through _____."

(4) "U. S. military agencies may obtain copies of this report directly from DDC. Other qualified users shall request through _____."

(5) "All distribution of this report is controlled. Qualified DDC users shall request through _____."

If the report has been furnished to the Office of Technical Services, Department of Commerce, for sale to the public, indicate this fact and enter the price, if known.

11. SUPPLEMENTARY NOTES: Use for additional explanatory notes.

12. SPONSORING MILITARY ACTIVITY: Enter the name of the departmental project office or laboratory sponsoring *(paying for)* the research and development. Include address.

13. ABSTRACT: Enter an abstract giving a brief and factual summary of the document indicative of the report, even though it may also appear elsewhere in the body of the technical report. If additional space is required, a continuation sheet shall be attached.

It is highly desirable that the abstract of classified reports be unclassified. Each paragraph of the abstract shall end with an indication of the military security classification of the information in the paragraph, represented as *(TS), (S), (C), or (U)*.

There is no limitation on the length of the abstract. However, the suggested length is from 150 to 225 words.

14. KEY WORDS: Key words are technically meaningful terms or short phrases that characterize a report and may be used as index entries for cataloging the report. Key words must be selected so that no security classification is required. Identifiers, such as equipment model designation, trade name, military project code name, geographic location, may be used as key words but will be followed by an indication of technical context. The assignment of links, rules, and weights is optional.